WEARABLE ANTENNAS FOR PERSONAL WIRELESS NETWORKS

Shaozhen Zhu

A Thesis Submitted to the University of Sheffield for the Degree of Doctor of Philosophy in Electronic and Electrical Engineering

January 2008

Abstract

In this study, we mainly characterize the wearable antenna system for off-body communications with respect to two conventional wireless communication systems as, cellular mobile systems (PCS, GSM and UMTS) and wireless local area networks (WLAN). Unlike antennas embedded in portable devices, the complicated body-centric environment has emerged with special requirements for wearable antennas design, like compact dimensions, light weight and flexible structure, hidden or water proofing, and most importantly, capable of providing certain radiation shielding into the human body. This thesis aims to find an optimum solution to meet the particular requirements of wearable antenna design.

The first part is primarily concerned with characterising the electromagnetic properties of some textile and leather materials. Both insulating and conducting materials are investigated for using as substrate and radiating elements of high performance textile antennas. Then a few of new antenna designs are proposed in the second part. These antennas are made out of textile and leather materials. They are low profile, planar in geometry, and most importantly, they are capable to provide multi-operations with considerable wide bandwidth.

An electromagnetic band gap structure is studied as it can provide a high impedance ground plane for low profile antennas. The EBG plane can provide a perfect shielding layer for the body, and reduce the radiation toward the body significantly. Furthermore, the EBG plane is able to reduce the detuning of the antenna when placing near the body without serious bandwidth reduction, increase antenna gain and reduce mutual coupling from other devices.

The final part carries out a series of experiments which can represent the body-centric environment. These include bending, washing, wearing, coupling and SAR investigations. Antenna and EBG performances under body worn environment are tested and discussed in this thesis.

Acknowledgements

I would like to express my heartfelt gratitude and thanks to my supervisor, Prof. Richard Langley, for his support, patience, and encouragement throughout my PhD studies. His outstanding supervision and precious advice were essential to the achievements of this project. This work would not come through without his valuable information and suggestions.

I would also like to state my sincere appreciation to Dr. Lee Ford for his help with the material parameter measurements, to Dr. Jonathan Rigelsford, Prof. Barry Chambers and Mr. Steve Marsden, for their academic help and technical support during the process of my research. I would deeply thank Dr. Lester Low and Dr. Olanike Folayan who gave me much important advice to my work. Their friendship is very precious to me. Thanks also to all the staff of the communications and radar group.

I would also like to thank Luyi Liu for the contribution to this research from his MSc project. Furthermore, the friendship with Hui Zhang, Hyung-Joo Lee, and all the other PhD students in the research group, is the best memorable experience during these years. I am also grateful to Mrs. Denyse Menne, Miss Yiqing Liang and Dr. Benito Sanz at University of Kent for their wonderful friendship and support.

My thanks also go to Dr. Chinthana Panagamuwa at Loughborough University, who helped me with the SAR measurement; and people in the mechanical workshop here at the University of Sheffield for providing the technical assistance in my work.

Last, but not least, I would like to give my deepest gratitude to my parents and my husband Qiang Bai for their constant encouragement and love during the whole academic period. Their support means the most to me.

Publications:

1. **Folayan, O., Zhu, S. and Langley, R.J.,** "Compact EBG Antennas," *IEE Seminar on Metamaterials for Microwave & (Sub) Millimetre Wave Applications*, London, UK, Sep 2006.
2. **Zhu, S. and Langley, R.J.,** "Dual-band Wearable Antennas over EBG Substrate," *IET Electronics Letters*, Vol. 43: No. 3: pp141-143, Feb 2007.
3. **Liu, L., Zhu, S. and Langley, R.J.,** "Dual-band Triangular Patch Antenna with Modified Ground Plane," *IET Electronics Letters*, Vol. 43: pp140-141, Feb 2007.
4. **Zhu, S. and Langley, R.J.,** "Personal antennas for Mobile Networks," *IEEE International Workshop on Antenna Technology*, pp.45-48, Cambridge, Mar 2007.
5. **Zhu, S. Liu, L. and Langley, R.J.,** "Dual-band Body Worn Antenna," *Loughborough Antenna & Propagation Conference Proceedings*, Loughborough, UK, Apr 2007.
6. **Zhu, S. and Langley, R.J.,** "Body Worn Antennas," *The IET seminar on Antennas and Propagation for Body-centric Wireless Communications*, London, UK, Apr 2007.
7. **Zhu, S. and Langley, R.J.,** "Dual-band Antennas on an EBG Substrate," *First International Congress on Advanced Electromagnetic Materials in Microwaves and Optics*, Rome, Italy, Oct 2007.
8. **Zhu, S. and Langley, R.J.,** "Dual Band Body Worn Antenna," *2nd European Conference on Antenna & Propagation (EuCAP)*, Edinburgh, UK, Nov 2007.
9. **Zhu, S. and Langley, R.J.,** "Dual Band Wearable Textile Antennas on An EBG Substrate," Submitted to the *IEEE Transactions on Antennas and Propagation* review board, Dec 2007.
10. **Zhu, S. and Langley, R.J.,** "Dual Band Wearable Antennas," *Loughborough Antenna & Propagation Conference Proceedings*, Loughborough, UK, Apr 2008.

Table of Contents

List of Acronyms

2D	Two dimensional
3D	Three dimensional
AMC	Artificial Magnetic Conductor
AUT	Antenna under Test
B.W	Bandwidth
CPW	Coplanar Waveguide
CST MWS	Computer Simulation Technologies microwave studio
DCS	Digital Cellular Systems
EBG	Electromagnetic Bandgap Structures
EM	Electromagnetic field
FDTD	Finite Difference Time Domain
FFT	Fast Fourier transforms
FIT	Finite Integration Technique
FSS	Frequency Selective Surfaces
GSM	Global Systems for Mobile communications
HIS	High Impedance Surface
PBA	Perfect Boundary Approximation
PCB	Printed Circuit Board
PCS	Personal Communication Services
PEC	Perfect Electric Conductor
PMC	Perfect Magnetic Conductor
TST	Thin Sheet Technique
UC-PBG	Uniplanar Compact Photonic Bandgap structure
UMTS	Universal Mobile Telecommunication Systems
UWB	Ultra Wide band
WLAN	Wireless Local Area Networks

Chapter 1 Introduction

1.1 Overview

Body centric wireless communication is now concerned as an essential part of fourth generation mobile communication systems, and will be part of the forthcoming convergence and personalization across the various domains, like Personal Area Networks (PANs), and Body Area Networks (BANs) [1]. Applications of body-centric wireless communication include wearable computers, wearable entertainments, sports outfits, health monitoring and some specialized occupations, like military personnel and fire fighters. These potential applications have accelerated the research in this particular area. Relative studies include electromagnetic wave propagation through body channels [2], wearable antennas [3, 4] and smart clothing [5], human body modelling [6], body-sensor networks [7] and medical implant systems [8]. In this thesis, studies are concentrated on wearable antenna designs and antenna performance investigations in the body-centric environment.

As radio wave transmitting and receiving devices, antennas establish the interface between person and device or person and person. Therefore antennas will in the future play a central part for wireless wearable applications. Compared with conventional antennas which are used in electronic devices, such as cell phones, laptop antennas, wearable antennas encounter a more complicated near-body environment. From this particular environment has emerged the demand for antenna flexibility, which requires the antenna to have compact dimensions, light weight and a flexible structure.

Traditional antennas made of a combination of metal patches and insulators tend to be rigid and relatively non-flexible, therefore these antennas would be disadvantageous in some particular wearable applications, like sports or military. The idea of utilizing textile materials on antenna design was then encouraged. Smart clothes as a new wearable antenna concept were introduced in [5], and studies [9, 10] on the electromagnetic properties of materials have found that both dielectric and conducting textiles are existing to fulfil the requirement of integration with antenna systems. In

the future, the complete flexible body-worn antenna system may possibly be found in our everyday living environment.

1.2 Wearable Antennas Critical Design Issues

Unlike antennas embedded in portable devices, wearable antennas are aimed to work in the complicated body-centric environment. The factors under this environment that might cause significant influence on antenna performance can be summarized as following:

- Interactions between the antenna and the body. The human body can have a strong reaction to the wave propagating around because of the electromagnetic properties of its complicated tissues. This might cause a huge detuning of antenna resonance over a large frequency range. On the other hand, the radiation of the antenna towards the body can result in serious health problems for human beings.

- Uneven body surface and movement. These factors might deform the antenna structure if the antenna is made out of clothing materials.

- Weather conditions. Antennas have the risk of getting wet under bad weather conditions, like rain or snow. Also, strong wind might damage the antenna if it is not firm enough.

- Other electronic devices. Other electronic devices especially wireless elements can cause coupling problems to the antenna and result in a serious efficiency reduction.

- Limited space and limited carrying ability. These will restrict the requirements on antenna material and geometry.

According to the above problems, beside the general requirements for antenna design, there are several additional requirements for wearable antennas design that have to be fulfilled for body-centric applications, in terms of both physical size and radiation characteristics in the proximity of the human body. These include:

- Compact size and light weight in order to be comfortable to wear.
- Low cost.
- Considerable flexibility and stability. The antenna is desirable to have certain resistance to bending, stretching and creasing.
- Hidden or water proofing. To avoid unnecessary damage or bad weather conditions, the antenna needs to be hidden or made of water proofing materials.
- Capable of providing certain radiation shielding to the body. The international standard of Specific Absorption Ratio must be satisfied for the purpose of safe communication on body.

1.3 Project Specification

This project aims to study and design suitable antennas for off-body applications. A literature review has covered the most recent development in this area. From the earliest stage where conventional antennas, like monopoles, the loop, patch and patch arrays were tested in the on body environment [11] to the most recent watch-type chip antenna [12], the area has attracted more and more attention on both research and commercial applications.

According to body centric antenna applications, studies can be summarised into 10MHz body surface communications [13], FM radio reception and TV applications [14, 15], mobile communications [16-18], WLAN applications [19, 20] and Ultra Wide Band applications [21, 22].

In this study, we mainly characterize the wearable antenna system with respect to two conventional wireless communication systems as, cellular mobile systems (PCS, GSM and UMTS) and wireless local area networks (WLAN).

The studies that have been done on wearable antennas so far can also be categorised by antenna types. These include wearable dipole antennas [14], microstrip antennas

[23], planar PIFA antennas [24] and monopole button antennas [25]. Apart from the button antenna which has a multilayer and metal based structure, the rest of the antennas have a common factor in their planar geometry, and most of them can be integrated into textile materials. However, these antennas all have some drawbacks which can not meet the particular requirements we mentioned in the previous section. For example, microstrip antennas have the major disadvantages of low efficiency, narrow bandwidth, and are difficult to design for efficient multi-resonance operation. Some other types of antennas might not have a planar structure. Therefore, it is necessary and important to find a proper type of antenna to solve these problems.

In this research, we try to find a solution of antenna design which can satisfy as many of the requirements in section 1.2 as possible. First of all, textile and leather materials are preferred as they can be easily found in our daily clothing and accessories. Also these materials are flexible and comfortable in being worn. Once the electromagnetic properties of the materials are defined, there is great possibility of integrating these materials into antenna design and fabrication. Secondly, a planar structure is chosen in this study as it can be easily attached to a piece of clothing. Moreover, dual- and multi-band operation is one of the main design objectives in this study as these tend to be the trend of future antenna developments. New antenna designs will be proposed in this thesis. These antennas are made out of textile and leather materials. They are low profile, planar in geometry, and most importantly, they are capable of providing multi-band operation with wide bandwidth.

In order to reduce the interaction between the antenna and the human body, we present a new solution of placing an EBG array as a high impedance ground plane of the proposed antenna. The High Impedance Surface (HIS) can provide a perfect shielding layer for the body, and reduce the radiation toward the body. Furthermore, the HIS has been proved to be able to reduce the detuning of the antenna when placing it near the body without serious bandwidth reduction, and also to increase antenna gain and reduce mutual coupling from other devices.

In the end, unlike most previous studies which were only concentrated on antenna design and materials evaluation, this study carries out a series of experiments which can represent the body-centric environment. These include bending, washing,

wearing, coupling and SAR investigations. Antenna and HIS performance under a body worn environment is tested and discussed in this thesis.

The numerical design and analysis of the proposed antenna is performed using CST Microwave Studio, which utilises the Finite Integral Technique that applies the integral form of Maxwell's equation integrated over time. And most of the experiments are carried out in the University of Sheffield Antenna and Radar Communications Lab.

1.4 Thesis outline

As described previously, this thesis is about to give overviews of work in the research of wearable antennas for on body communications. In chapter 2, theoretical background on both antennas and EBGs are introduced based on the relative research background conceptions. Important parameters which are related to this study will be discussed, as well as the principles of the software and hardware methodology.

Because in this research, textile and leather are mainly concerned as the materials for antenna and EBG design. Thus it is important to find out the electromagnetic properties of the selected materials. Chapter 3 provides the basic knowledge of materials evaluation. Some basic parameters will be defined and the dielectric properties of a few textile and leather materials will be characterized. The conducting materials selection and the process of the material properties measurement will also be discussed.

Chapter 4 concentrates on the design of dual-band and multi-band wearable antennas for WLAN and GSM/UMTS applications. Fabric and leather materials are both used for WLAN antenna design, and the antenna performances are compared. Several novel designs will be introduced, as well as the design procedure and result analysis.

Chapter 5 presents the solution of introducing the EBG structure as a high impedance surface (HIS) ground plane for the antenna. It gives a brief idea of the EBG designing procedure, and the integration of the antenna with the EBG. The antenna performance

with the HIS is investigated in this chapter. And a conventional microstrip patch antenna is discussed in order to make a comparison with the HIS grounded antenna.

Chapter 6 deals with the body-centric environment experiments of the proposed antennas. Several situations which were tested in this research are presented. These include bending, washing, wearing, and coupling and SAR issues. Simulation and measurement results are discussed to give a brief idea for future on-body applications.

Chapter 7 summarizes this thesis briefly, and presents a few of challenges for the future study of this research area.

References:

[1] **Hall, P. S. and Hao, Y. (editors),** *Antennas and Propagation for Body Centric Communications Systems,* Artech House, Norwood, USA, 2006.

[2] **Hall, P.S., Ricci, M. and Hee, T.M.,** "Measurement of On-Body Propagation Channels," *IEEE Antennas & Propagation International Symposium*, pp.310-313, Jun 2002.

[3] **Lebaric, J. and Tan, A.T.,** "Ultra-Wideband Conformal Helmet Antenna," *IEEE Asia Pacific Microwave Conference*, pp.1477-1481, 2000.

[4] **Kohls, E.C., et al.,** "A Multi-Band Body-Worn Antenna Vest," *IEEE Antennas & Propagation International Symposium*, Vol.1, pp.447-450, 2004.

[5] **Rantanen, J., et al.,** "Smart clothing for the Arctic Environment," *IEEE 4th International Symposium on Wearable Computers*, pp.15-23, 2000.

[6] **Nagaoka, T.,** "Development of Realistic High-Resolution Whole-Body Voxel Models of Japanese Adult Males and Females of Average Height and Weight, and Application of Models to Radio-Frequency Electromagnetic-Field Dosimetry," *Physics in Medicine and Biology,* Vol.49, pp.1-15, 2004.

[7] **Mokwa, W. and Schnakenberg, U.,** "Micro-Transponder Systems for Medical Applications," *IEEE Transactions on Instrumentation and Measurements,* Vol.50, No.6, pp.1551-1555, Dec 2001.

[8] **Scanlon, W.G.,** "Analysis of Tissue-Coupled Antennas for UHF Intra-Body Communications," *IEEE International Conference on Antennas and Propagation,* pp.747-750, Apr 2003.

[9] **Salonen, P., Rahmat-Samii, Y., Schaffrath, M. and Kivikoski, M.,** "Effect of Textile Materials on Wearable Antenna Performance: A Case Study of GPS Antennas," *IEEE Antennas and Porpagation Society International Symposium,* Vol.1, pp.459-462, 2004.

[10] **Salonen, P., Rahmat-Samii, Y., Hurme, H. and Kivikoski, M.,** "Effect of Conductive Material on Wearable Antenna Performance: A Case Study of WLAN Antennas," *IEEE Antennas and Porpagation Society International Symposium,* Vol.1, pp.455-458, 2004.

[11] **Kamarudin, M.R., Nechayev, Y.I. and Hall, P.S.,** "Antennas for On-Body Communication Systems," IEEE *International Workshop on Antenna Technology, Small Antennas, Novel Metamaterials,* Singapore, pp.17-20, March 2005.

[12] **Wu, C., Wong, K., Lin, Y. and Su, S.,** "Conformal Bluetooth Antenna for the Watch-Type Wireless Communication Device Application," *IEEE Antennas & Propagation International Symposium,* pp.4156-4160, Hawaii, Jun 2007.

[13] **Fujii, K., Takahashi, M., Ito, K. and Inagaki, N.,** "Study on the Electric Field Distributions around whole Body Model with a Wearable Device using the Human Body as a Transmission Channel," *European Conference on Antennas and Propagation, EuCap06,* France, Nov 2006.

[14] **Kellomaki, T., Keikkinen, M. and Kivikoski, M.,** "Wearable Antennas for FM Reception," *European Conference on Antennas and Propagation, EuCap06,* France, Nov 2006.

[15] **Toosi, K. N.,** "VHF-LB Vest Antenna Design," *IEEE Int. Workshop on Antenna Technology, IWAT,* Cambridge, Mar 2007.

[16] **Salonen, P. and Rahmat-Samii, Y.,** "Textile Antennas: Effect of Antenna Bending on Input Matching and Impedance Bandwidth," *European Conference on Antennas and Propagation, EuCap06*, France, Nov 2006.

[17] **Klemm, M. and Troster, G.,** "Textile UWB Antennas for On-Body Communications," *European Conference on Antennas and Propagation, EuCap06*, France, Nov 2006.

[18] **Zhu, S., Liu, L. and Langley, R.J.,** "Dual Band Body Worn Antenna," *Loughborough Antennas and Propagation Conference*, Loughborough, UK, Apr 2007.

[19] **Zhu, S. and Langley, R. J.,** "Dual Band Wearable Antennas over EBG Substrate," *IET Electronics Letters*, Vol. 43: No. 3, pp141-143, Feb 2007.

[20] **Liu, L., Zhu, S. and Langley, R. J.,** "Dual Band Triangular Patch Antenna with Modified Ground Plane," *IET Electronics Letters*, Vol. 43, pp.140-141, Feb 2007.

[21] **Sanz, B., Batchelor, J. C. and Sohby, M.,** "Compact UWB wearable antenna," *Loughborough Antennas and Propagation Conference*, Loughborough, UK, Apr 2007.

[22] **Sanz, B., Young, P. R., Bai, Q. and Batchelor, J. C.,** "Compact UWB Monople for Multilayer Applications," *Electronics. Letters*, Vol. 42, No.1, pp 5-7, Jan 2006.

[23] **Tanaka, M. and Jang, J.H.,** "Wearable Microstrip Antenna," *IEEE Antennas & Propagation International Symposium*, Vol.2, pp.704-707, 2003.

[24] **Salonen, P., et al.,** "A small Planar Inverted_F Antenna for Wearable Applications," *Third International Symposium on Wearable Computers*, pp.95-100, 1999.

[25] **Sanz, B., Huang, F. and Batchelor, J. C.,** "Dual band Button Antennas for Wearable Applications," *IEEE Int. Workshop on Antenna Technology, IWAT*, New York, 2006.

Chapter 2 Theoretical background and Methodology

2.1 Introduction

Antennas have been developed so far can be classified into several types according to their materials or structures, like wire antennas, aperture antennas, microstrip antennas and array antennas, etc. The strip line structure is one of the most commonly used structures for antenna design. Its "planar" configuration makes the structure suitable as a circuit element in multiple electromagnetic applications. Especially for wearable application, planar strip line feed can simplify the antenna structure, and make the integration of antenna with clothing easier. Therefore, strip line feed antennas are chosen as the antenna design objective in this project. The basic theory of two typical strip line fed antennas, microstrip antenna and coplanar waveguide antenna will be introduced in this chapter.

The main antenna parameters, such as scattering parameters, input impedance, antenna gain, efficiency, and radiation patterns will then be introduced in this chapter. Examples and results will also be given to assist the analysis of the antenna performance.

Electromagnetic Band Gap (EBG) structures are generally defined in our research context as artificial dielectric structures that possess high impedance for electromagnetic waves at particular bands. The structure can be used as high impedance ground plane for low profile antennas as they have two important characteristics: in-phase reflection of an incident plane wave and surface EM wave suppression. These two properties of EBGs can solve some problems that occur in normal antennas and optimize antenna performance, therefore it leads to a wide range of applications in antenna design. According to this research, the EBG structure is investigated for the purpose of reducing the antenna backward radiation towards the human body, increasing antenna directivity and gain, and enhancing the antenna performance in the vicinity of the body. In this chapter, the conception of EBG will be

introduced as well as the design procedure. And the two main characteristics of EBGs with example descriptions will be discussed.

Following that, the sole commercial software tool used in this research, CST Microwave Studio, will be reviewed. The theory behind the software package so called finite integration technique will be briefly discussed.

Finally a full description of the measurement methods and techniques used to characterise antenna and EBG performance will be presented.

2.2 Strip Line Antennas

Planar antenna structures are favoured in this research since they can easily be integrated into clothing. Several transmission line structures can satisfy the requirement of being planar, like microstrip, slot line, coplanar waveguide and coplanar strips. Among these, the most commonly used structures in antenna applications are microstrip and coplanar waveguide antennas. Moreover, these two structures are both simple in design and fabrication. Therefore, the microstrip and coplanar waveguide structures are mostly concerned for antennas designed in this study.

2.2.1 Microstrip Antenna

The microstrip antenna is a typical low-profile antenna first introduced in 1950s by Deschamps [1]. The acceleration of its development started to take place since the 1970's since the availability of satisfactory substrates with ideal mechanical and electrical qualities as well as a reasonable loss tangent. It became then more and more popular in mobile radio and wireless communications. Microstrip antennas are normally simple and inexpensive to manufacture, and when the particular shape and mode are selected, they are very adaptable in terms of resonant frequency, polarization, pattern, and impedance. Major operational disadvantages of microstrip antennas are their low efficiency, low power, poor polarization purity and very narrow frequency bandwidth [2].

A transmission line model of microstrip antenna is shown in Figure 2.1. The structure is based on a metallic patch along with a strip line etching on one side of a suitable substrate, and a ground plane on the other side. Typical electric and magnetic field lines of this model are demonstrated in Figure 2.2.

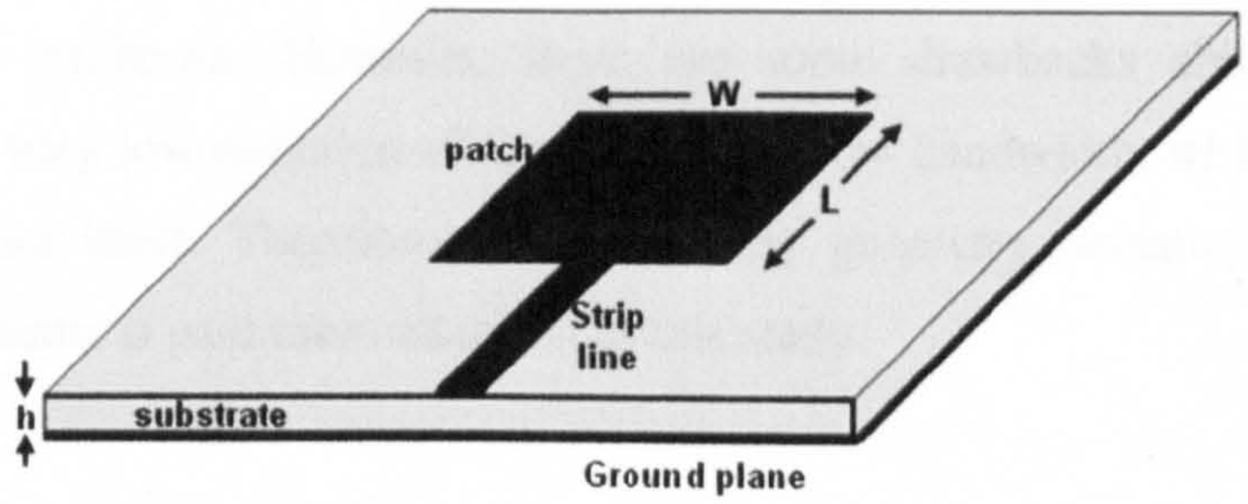

Figure 2.1 A rectangular microstrip antenna

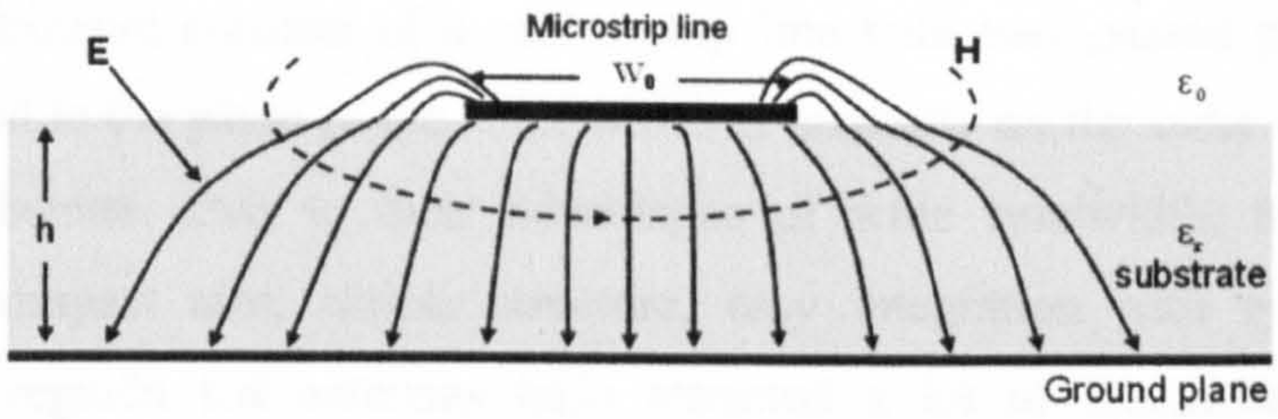

Figure 2.2 Electric and magnetic field lines at microstrip line edge

Most microstrip antennas can be treated as dielectric-loaded cavities with electric conducting walls on the top (patch) and bottom (ground). The dielectric height **h** is normally far far smaller than the cavity length and width (h<<W<<L). So that the fringing waves at the four edges of the patch will form the main radiation, and the pattern maximum is normal to the patch. With the dielectric substrate presence, the effective length and width of the patch needs to take into account of the dielectric constant of the substrate. By adjusting the size of the patch, the dominant mode of the cavity can be decided, and further more the antenna resonant frequency can be defined. The microstrip line width W_0, which is related to the height (h) and the permittivity (ε_r) of the substrate, is used to define the characteristic impedance of the

strip line, and it is very important in microstrip antenna design to determine the input impedance matching of the antenna.

Microstrip antenna has the advantages of being easy to design and analyze. It is preferred in wearable antenna design as the big ground plane provides good shielding between the antenna and the body. Therefore the interaction between these two can be reduced to a minimum. However, there are some drawbacks about microstrip antennas, like very low radiation efficiency and narrow bandwidth, which are caused by the structure itself. Therefore, another planar geometry antenna, the coplanar waveguide antenna is paid more attention in this study.

2.2.2 Coplanar Waveguide Antenna

Coplanar Waveguide (CPW) was proposed by Wen [3] in 1969. A typical coplanar waveguide structure consists of a centre strip line with two ground planes formed parallel to and in the plane of the strip, which is normally on the same surface of the dielectric substrate. Due to their advantages of wide bandwidth, high radiation efficiency, compact size, simple structure, easy integration with system circuit, coplanar waveguide fed antennas have attracted a lot of attentions in wireless communications.

A typical configuration of coplanar waveguide is shown in Figure 2.3. The approximation of the electric and magnetic field configurations of the structure are shown in Figure 2.4.

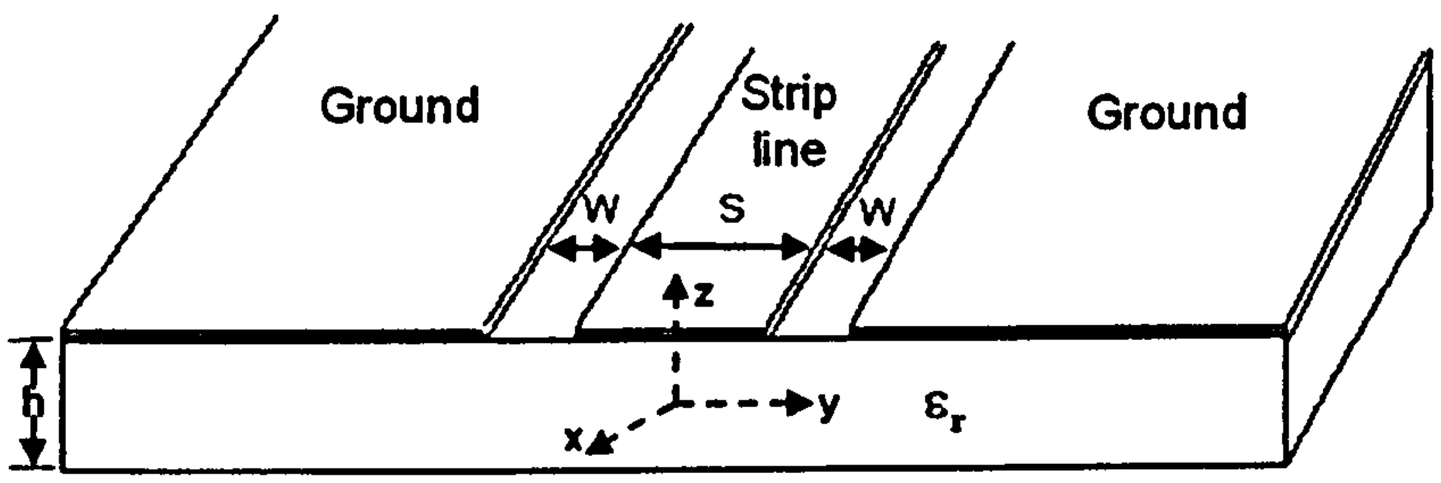

Figure 2.3 Coplanar Waveguide (CPW) geometry

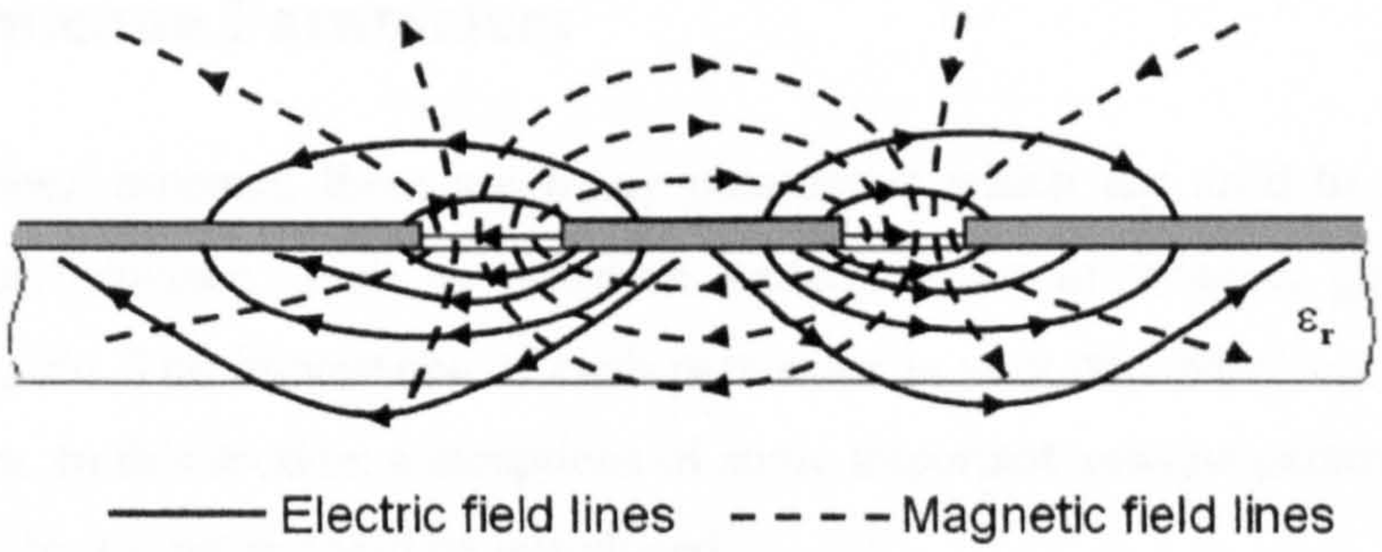

Figure 2.4 Electric and Magnetic field distributions in CPW

The CPW antenna has a structure similar to a microstrip antenna while the field distributions within it are more like those of a dipole antenna. As the centre strip carries the signal and both side planes are grounded, much less field goes into the substrate compared with microstrip structure. And unlike the microstrip antenna which has most radiations towards only one side of the antenna surface, the CPW antenna presents a dipole like radiation patterns which travel in the direction normal to the patch and along both side of the antenna. Gupta carried out the detailed analyses of coplanar lines in [4].

CPW antennas have achieved great success in a lot of applications, examples like double-layered coplanar patch antenna studied in [5], the compact size CPW-fed monopole antenna [6] designed for wireless application, and some CPW-fed UWB antennas presented in [7] and [8]. A simple example of CPW antenna geometry is shown in Figure 2.5.

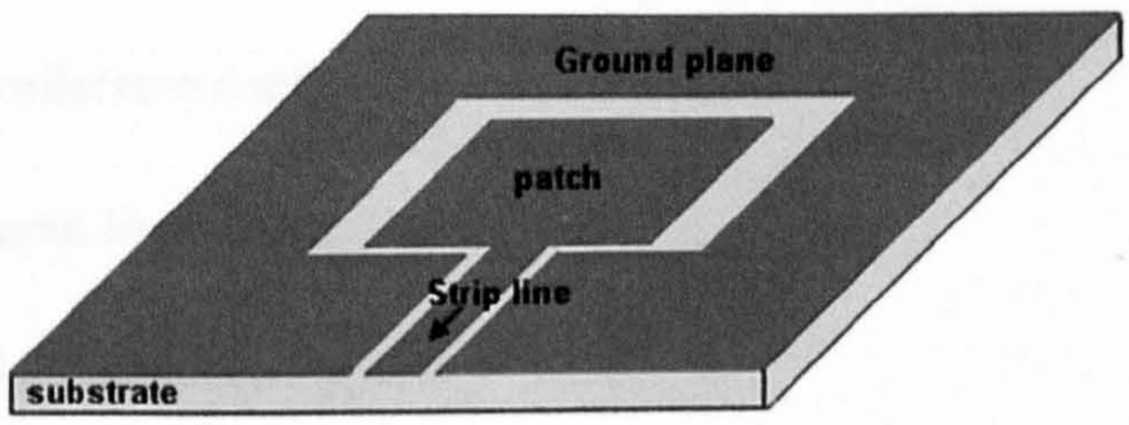

Figure 2.5 A CPW antenna example

2.3 Antenna Parameters

For a general antenna, there are many parameters which are used to analyse the antenna performance, such as radiation pattern, input impedance, gain, antenna efficiency, etc. The importance of each parameter is very dependant on the antenna application. In this section, conceptions of some important antenna parameters which are related to this project will be introduced.

2.3.1 S parameters

Scattering Parameters, or s-parameters, are the reflection and transmission coefficients between the incident and reflection waves. They are normally functions of frequency. They describe completely the behaviour of an antenna under linear conditions at microwave frequency range [9]. Each parameter is typically characterized by magnitude, decibel and phase. The expression in decibels is 20log ($S_{i,j}$) because s-parameters are voltage ratios of the waves.

In this project, the input reflection coefficient S_{11} is mostly concerned as being the return loss of the antenna. It is a measure of the amount of power reflected by the antenna toward the generator. A low reflected value suggests a good matching at a specific frequency. The return loss S_{11} of an antenna can be regarded as a measure of the ratio between the power reflected back from the antenna feeding point to that fed to the antenna at a particular frequency or band of frequencies.

$$S_{11} = \frac{V_{\text{reflected at port1}}}{V_{\text{towards port1}}} = \Gamma = \frac{Z_{input} - Z_0}{Z_{input} + Z_0} \tag{2-1}$$

Where Γ is the reflection coefficient

Z_{input}= antenna input impedance

Z_0= characteristic impedance (typically=50Ω).

The return loss in dB is calculated from:

$$\text{return loss (dB)} = -10\log\Gamma^2 = -20\log\Gamma \tag{2-2}$$

A typical return loss S_{11} in decibel for a CPW fed patch antenna obtained by using software CST Microwave Studio is shown in Figure 2.6. Theoretically, if the entire power is reflected back, S_{11} will be 0dB. While if the power is completely absorbed and radiated by the antenna, the value will be -∞dB. A low return loss value corresponds to a good matching at a particular frequency. Frequency bands where the S_{11} is lower than -10dB are considered as the useful band in this study, which indicates a 10% power reflection, and the minimum dB value point is defined as the centre resonant frequency.

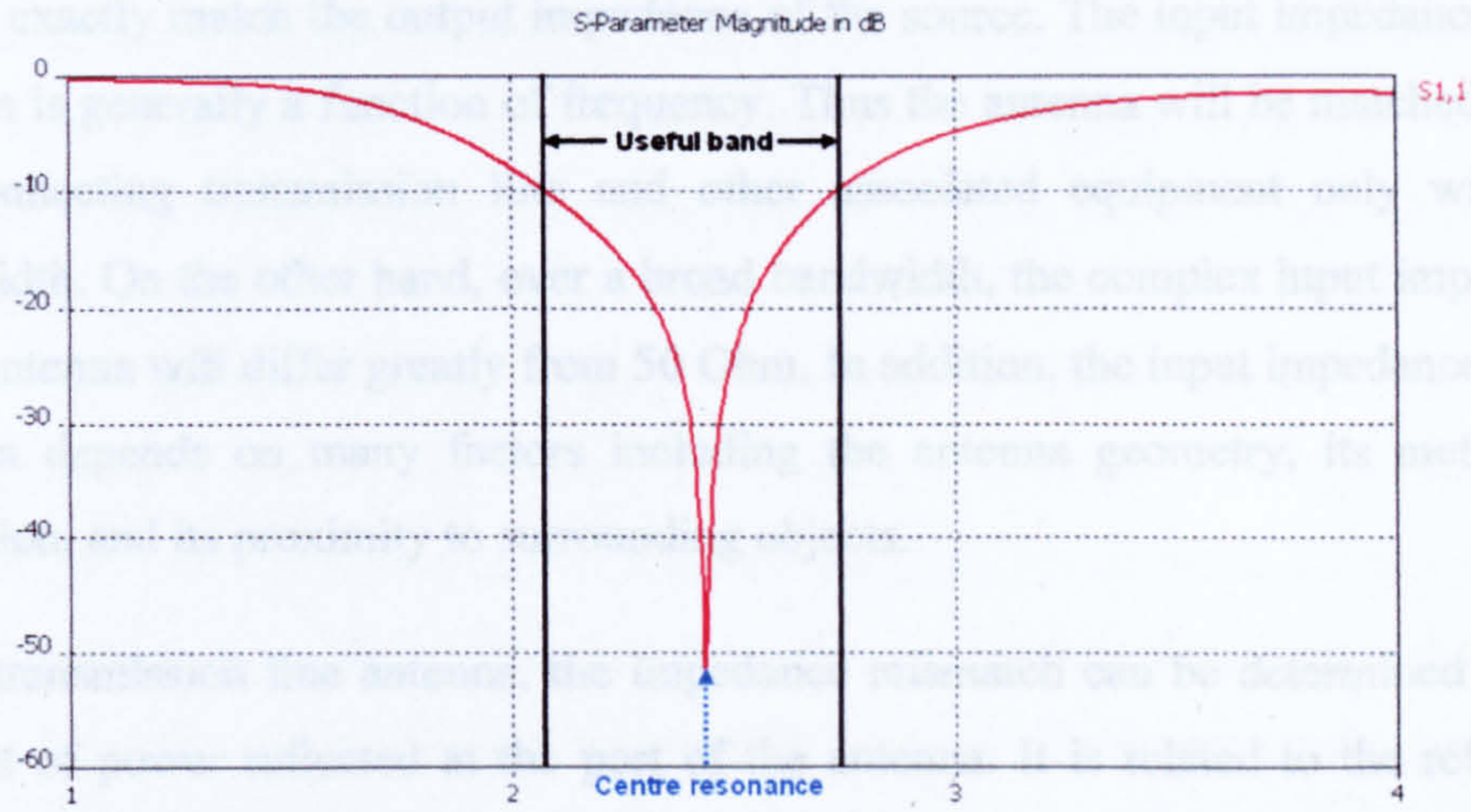

Figure 2.6 Return loss (S_{11}) for a 2.45GHz CPW fed patch antenna

For a two port device, the forward transmission coefficient S_{21} is the resulting signals on the output, from signals applied to port 1. It denotes the ratio of the output of port 2 to the incident wave at port 1. It is defined as the transmitted voltage divided by the incident voltage.

$$S_{21}(dB) = \frac{V_{\text{transmitted from port 2}}}{V_{\text{towards port 1}}} = 20 \log \tau \qquad (2\text{-}3)$$

Where τ =magnitude of the transmission coefficient

In this study, the forward transmission coefficient S_{21} is of interest in material dielectric constant measurement and EBG characteristics examination, which will be discussed later in chapter 3 and chapter 5 respectively.

2.3.2 Input Impedance

One of the important parameters to describe the performance of an antenna is based on impedances, which represents the antenna as a circuit or network. The input impedance, measured in ohms, is a complex number, and is the load impedance that the antenna presents to a connecting transmission line [10].

The ability of an antenna to accept power from a source is determined by the input impedance the antenna presents. For maximum power transfer, the input impedance should exactly match the output impedance of the source. The input impedance of an antenna is generally a function of frequency. Thus the antenna will be matched to the interconnecting transmission line and other associated equipment only within a bandwidth. On the other hand, over a broad bandwidth, the complex input impedance of an antenna will differ greatly from 50 Ohm. In addition, the input impedance of the antenna depends on many factors including the antenna geometry, its method of excitation, and its proximity to surrounding objects.

For a transmission line antenna, the impedance mismatch can be determined by the amount of power reflected at the port of the antenna. It is related to the reflection coefficient at the input of the antenna as

$$|\Gamma|^2 = \frac{P_{reflect}}{P_{incident}} = \frac{|Z_{input} - Z_c|^2}{|Z_{input} + Z_c|^2} \tag{2-4}$$

where Z_{input} is the antenna's complex input impedance and Z_c is the characteristic impedance of the transmission line [11].

2.3.3 Gain

Antenna gain is a measure of the directive property of the antenna, as well as how efficiently it transforms available input power into radiated power as compared to a theoretical antenna element [12]. It is usually measured in units of dBi (decibels as referenced to an isotropic antenna element) or dBd (decibels as referenced to a dipole antenna element, where 0 dBd = 2.1 dBi).

In most case, we deal with relative gain, which is the ratio of the power gain in a given direction to the power gain of a reference antenna in its referenced direction. The reference antenna is usually a dipole, horn, or any other antenna whose gain is known. In this study, the power gain is only taken in the direction of maximum radiation direction.

Antenna gain usually can be measured in free-space ranges. There are two basic methods: *absolute-gain* and *gain-comparison* measurements. The absolute-gain method requires particular measurement setup, therefore is not employed in this project. Gain-comparison methods [2] need to be used in combination with standard gain antennas to determine the absolute gain of the antenna under test. The two antennas that are most widely used and accepted as gain standards are the resonant half wavelength dipole (with a gain of about 2.1dB) and the pyramidal horn antenna (with a gain ranging from 12-25dBi). The simple procedure requires two sets of measurements. In one set, the antenna under test is used as the receiving antenna, the received power in the maximum radiation direction (P_T) is recorded. In the other set, the test antenna is replaced by the standard gain antenna and the maximum received power (P_S) into a matched load is recorded. In both sets, the geometrical arrangement is maintained intact, and the input power is maintained the same. For free-space ranges, the gain can be calculated with:

$$(G_T)_{dB} = (G_S)_{dB} + 10\log_{10}(\frac{P_T}{P_S}) \qquad (2\text{-}5)$$

The reference antenna which was used for the gain measurement in this project is the double-ridged waveguide horn antenna HF 906 with a gain ranging from 7dBi to 14dBi.

2.3.4 Antenna Efficiency

Antenna efficiency is a parameter which describes how efficient the power sending to an antenna is radiated. The total antenna efficiency is usually taken into account

losses at the input terminals and within the structure of the antenna. Such losses may be include

- reflection loss caused by the mismatch between the transmission line and the antenna
- conduction and dielectric losses

In general, the overall efficiency can be written as [2]

$$e = e_r e_{cd} = e_{cd}(1-|\Gamma|^2) \tag{2-6}$$

where e_r=reflection (mismatch) efficiency= $(1-|\Gamma|^2)$,

Γ = the reflection coefficient at the input terminal of the antenna,

$e_{cd}=e_c e_d$=antenna radiation efficiency (conduction efficiency and dielectric efficiency). The radiation efficiency is defined as the ratio of the total power radiated by the antenna to the total power accepted by the antenna at its input terminals during radiation. Impedance mismatch does not contribute to the radiation efficiency.

During the antenna efficiency measurement, the reflection efficiency can be directly calculated from the return loss (S_{11}) value at the particular frequency. The radiation efficiency is normally related to the gain and directivity of the antenna. It can be calculated, using the direction of maximum radiation as reference, as

$$Radiation\ efficiency = \frac{gain}{directivity} \tag{2-7}$$

2.3.5 Radiation Pattern

Radiation pattern is a mathematical function or a graphical representation of the radiation properties of the antenna as a function of space coordinates [2]. The space surrounding an antenna is usually subdivided into three regions: (a) reactive near-field, (b) radiating near-field and (c) far-field region. In most cases, the radiation

pattern is concerned in the far-field region where the angular field distribution of an antenna is essentially independent of the distance from the antenna. If the antenna has a maximum overall dimension D, the far-field region is commonly taken to exist at distances greater than $2D^2/\lambda$ from the antenna, λ being the wavelength.

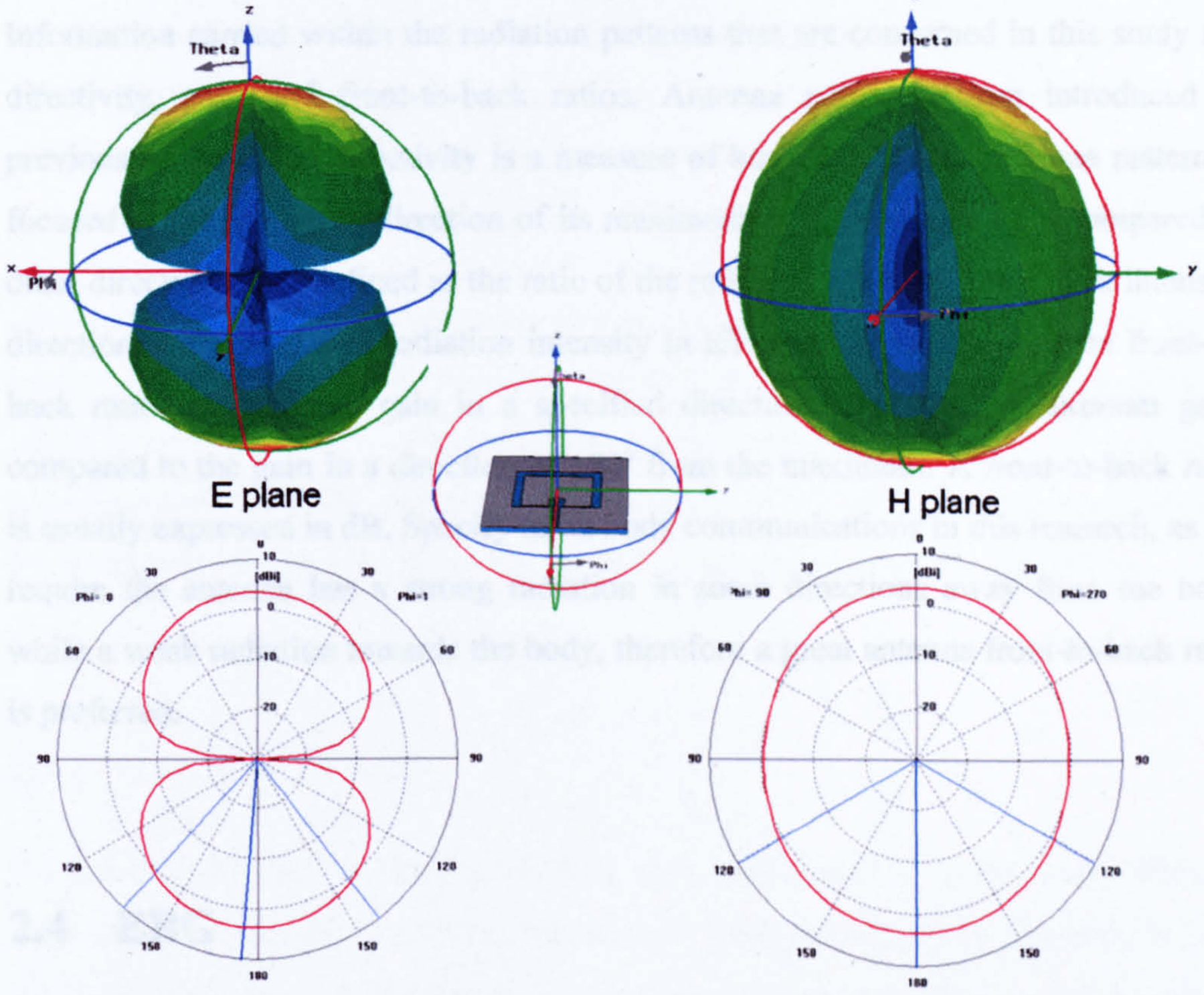

Figure 2.7 3D and 2D far-field plots for a CPW fed patch antenna

The radiation pattern is three-dimensional, but it is difficult to display the 3D radiation pattern in a meaningful manner. Therefore, antenna radiation patterns are usually taken at one frequency, one polarization, and one plane cut. Generally, for a linearly polarized antenna, the radiation pattern is often described in terms of its principal E- and H-plane patterns. The E-plane is defined as "the plane containing the electric-field vector and the direction of maximum radiation," and the H-plane as "the plane containing the magnetic-field vector and the direction of maximum radiation."

Figure 2.7 shows an example of the simulated three dimensional patterns and the 2D cuts of the E and H principle planes for a simple coplanar fed antenna (Figure 2.5). The coordinate system that the antenna orients is also shown as a reference. The in-between blue line in the 2D cuts represents the position of the maximum direction of the radiated power. And the neighbouring two lines give the half power (-3dB) beam position.

Information carried within the radiation patterns that are concerned in this study are directivity, gain and front-to-back ratios. Antenna gain has been introduced in previous section. The directivity is a measure of how strongly the antenna pattern is focused in the particular direction of its maximum reception sensitivity compared to other directions. It is defined as the ratio of the radiation intensity in the peak intensity direction to the averaged radiation intensity in all other directions [2]. The front-to-back ratio refers to the gain in a specified direction, usually the maximum gain, compared to the gain in a direction of 180° from the maximum. A front-to-back ratio is usually expressed in dB. Specify to on body communications in this research, as we require the antenna has a strong radiation in some directions away from the body while a weak radiation towards the body, therefore a great antenna front-to-back ratio is preferred.

2.4 EBG

Electromagnetic band gap (EBG) structures have attracted much attention recently as such materials can offer distinct properties in controlling the propagation of electromagnetic waves.

One of the particular applications is to use an EBG structure as a high impedance ground plane for a low-profile antenna to improve antenna radiating properties [13], and by aligning the resonant frequency of the antenna with the band gap of the EBG surface it is possible to improve antenna performance and reduce surface waves within the substrate. There are two major advantages of an EBG structure:

- In-phase reflection in a certain band of frequencies. This feature enables the EBG surfaces behave like a perfect magnetic conductors (PMC) [13]. On the contrast of a perfect electric conductor (PEC) which generates an 180° reflection phase for a normally incident plane wave, the perfect magnetic conductor (PMC) has a reflection phase of 0°. This in-phase reflection enables efficient radiation for antennas placed close to the EBG ground [14].

- Surface wave suppression. By forbidding the propagation of surface EM waves in certain frequency bands, EBGs can be used to block the propagation of waves and guide them in a desired direction [15]. This feature helps to improve antenna's performance such as increasing the antenna gain and reducing back radiation [16].

EBG structure also has the advantage of suppressing the higher-order harmonic waves when work with microstrip antennas. For the purpose of wearable communication which is related to this project, an EBG structure is desirable to reduce the radiating power towards the body, and also, with the guide of the EBG, wave propagation can be enhanced in the desired direction, as well as the antenna gain and directivity.

2.4.1 Overview of EBG

EBG structures are normally periodical cells composed of metallic or dielectric elements. A mushroom-like EBG structure was firstly introduced by Sievenpiper [13]. As shown in Figure 2.8, the structure is composed of ground plane, metallic patches, dielectric substrate and connecting vias.

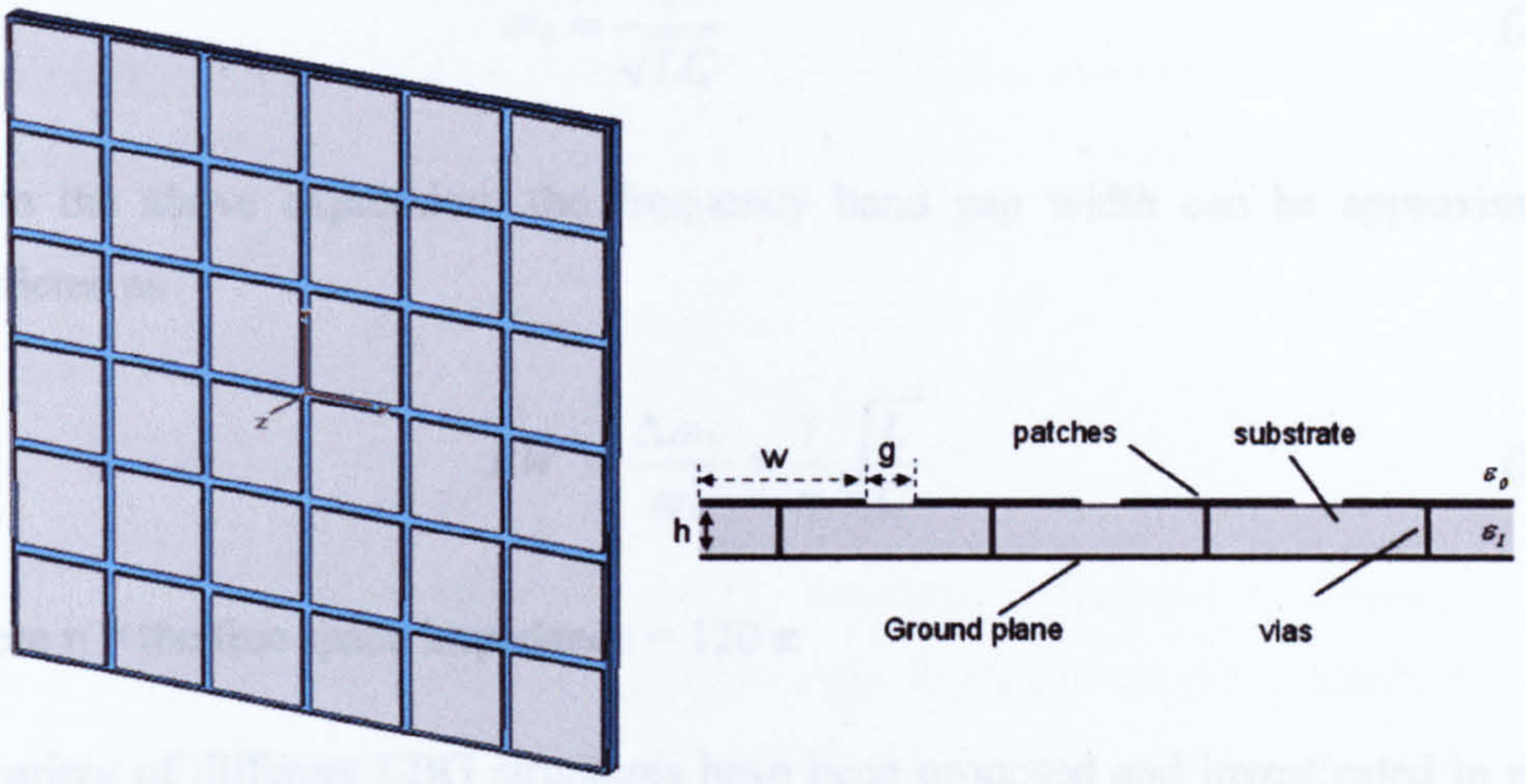

Figure 2.8 A mushroom-like EBG structure and side view

The operation mechanism of this EBG structure can be explained by an LC filter array or a parallel resonant circuit as shown in Figure 2.9: the inductor **L** results from the flowing current through adjacent cells, and the capacitor **C** comes from the fringing capacitance between neighboring co-planar metal plates.

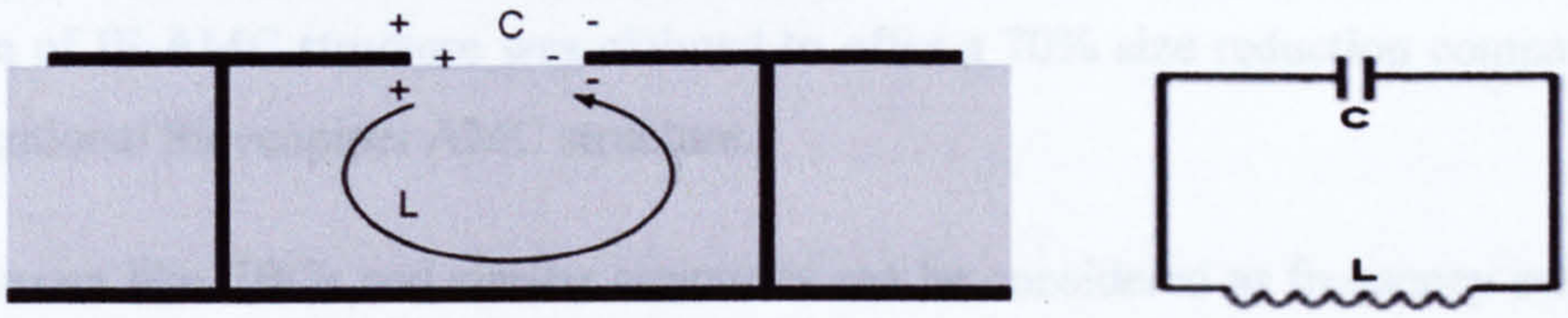

Figure 2.9 LC model of a mushroom-like EBG structure

For an EBG structure with patch width **W**, gap width **g**, substrate thickness **h** and dielectric constant ε_r, as shown in Figure 2.8, the values of the inductor and the capacitor are determined by the following formula [17]:

$$C = \frac{W(\varepsilon_0 + \varepsilon_r)}{\pi} \cosh^{-1}\left(\frac{2W+g}{g}\right) \tag{2-8}$$

$$L = \mu h \tag{2-9}$$

And the resonant frequency ω_0 expressed with following equation is obtained:

$$\omega_0 = \frac{1}{\sqrt{LC}} \tag{2-10}$$

From the above expression, the frequency band gap width can be approximately predicted as

$$BW = \frac{\Delta\omega_0}{\omega_0} = \frac{1}{\eta}\sqrt{\frac{L}{C}} \tag{2-11}$$

where η = the free space impedance = 120 π

A variety of different EBG structures have been proposed and investigated in recent years. In the earlier stages, the EBG structures proposed were fabricated through drilling holes with periodic patterns in the substrate [18] or adopting a square lattice of metallic patches shorted to the ground plane through vias, which is sometimes called a mushroom-like structure [13]. After the patch-via-ground plane structure, some up-to-date designs that are more effective and complicated, such as Uniplanar Compact EBG substrate (UC-EBGs) [19] have attracted notification. Later inter-embedded artificial magnetic conductor (IE-AMC) was presented in [20]. The novel design of IE-AMC structure was claimed to offer a 70% size reduction compared to conventional Sievenpiper AMC structure.

Mushroom like EBGs and similar structures can be considered as frequency selective surfaces (FSS) positioned on the interface of a thin layer of a metal backed dielectric slab with vias. In practice, grounding vias complicate the fabrication of AMC surfaces, particularly at upper microwave and millimetre-wave frequencies. In order to simplify the fabrication, several research groups have worked on implementing AMC surfaces without vias in a completely planar configuration. These structures are essentially periodic frequency selective surfaces (FSS) [21]. FSS can effectively suppress surface waves over a certain frequency range and it has the favourable reflection phase properties when it is grounded by a metal plane. Therefore this kind of structure could be used in many of the same applications as the EBGs, and it is commonly referred as high-impedance surface.

The design of an HIS is mainly based on the lattice resonance of the structure. For a simple square patch structure like Figure 2.8 but without vias presence, the resonance can be obtained by

$$\omega_0 \approx \frac{1}{\sqrt{\left(\varepsilon_0\varepsilon_r \frac{W^2}{h}\right)\cdot(\mu_0\mu_r h)}} = \frac{1}{\sqrt{LC}} \qquad (2\text{-}12)$$

In this project, a concentric square HIS structure is adopted to achieve a dual-resonance application. The design procedure will be described in Chapter 5. Although this kind of structure is not the best effective in bandwidth, but it has some advantages such as compactness, simplicity, easy fabrication and effective band gap for surface-wave propagation, which is useful to improve the radiating pattern of an antenna [14], [22]. In addition, its straightforward of arrangement in antenna substrate is also included in consideration.

2.4.2 Reflection Phase characteristic of EBG

In general, an EBG structure can be seen as a high impedance plane. Contrast to a smooth conducting sheet which has very low surface impedance, the periodical geometry surface of EBG can have high surface impedance in a particular frequency range, while low impedance at other frequencies. In the frequency range where the surface impedance is very high, the tangential magnetic field is small, even with a large electric field. Under ideal conditions, this high impedance plane can behave like a "perfect magnetic conductor". While in reality, such a structure is commonly used as an "Artificial Magnetic Conductor (AMC)".

Because of this unusual performance that the AMC can offer, the high impedance surface can perform as a new type of ground plane for low-profile antennas. It is known that when a radiating element is placed parallel and close to a conducting plane, it will suffer a dramatic reduction in radiation resistance due to cancellation from image currents [23]. Thus when an antenna is put close to a metal sheet, if the distance is smaller than a quarter wavelength, the phase of the impinging wave is reversed upon reflection, resulting in destructive interference with the wave propagated in the other direction, and in further lead to a very poor antenna radiation

efficiency. While for the high impedance ground plane, all of the power is reflected in-phase, rather than destructive interference, the direction of the image currents results in constructive, allowing the antenna to be directly adjacent to the surface and radiate efficiently.

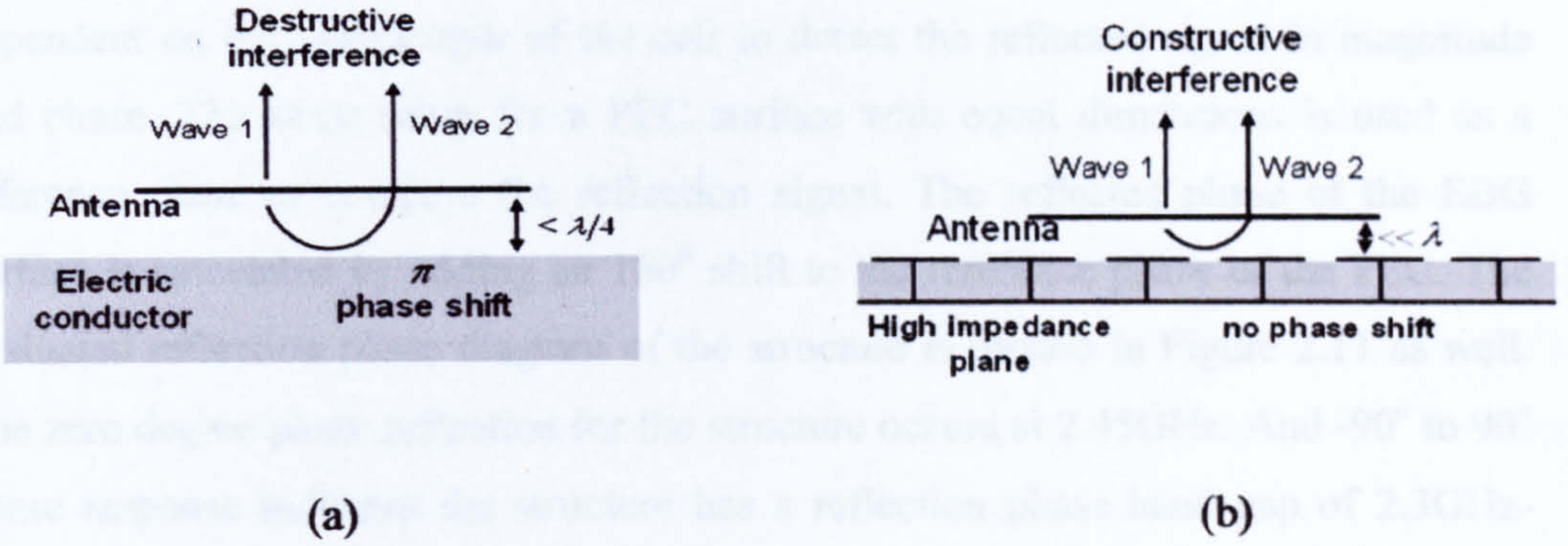

Figure 2.10 (a) An antenna on a metal ground plane (b) An antenna on a high impedance plane [17]

In practice, the reflection phase of an EBG surface varies continuously from +180° to -180° relative to the frequency. For one resonant mode, the reflection phase crosses zero at just on the desired frequency. The useful bandwidth of an EBG is generally defined as from +90° to -90° on either side of the central frequency, where at these frequencies, the magnitude of the surface impedance of the EBG will be greater than the impedance of free space.

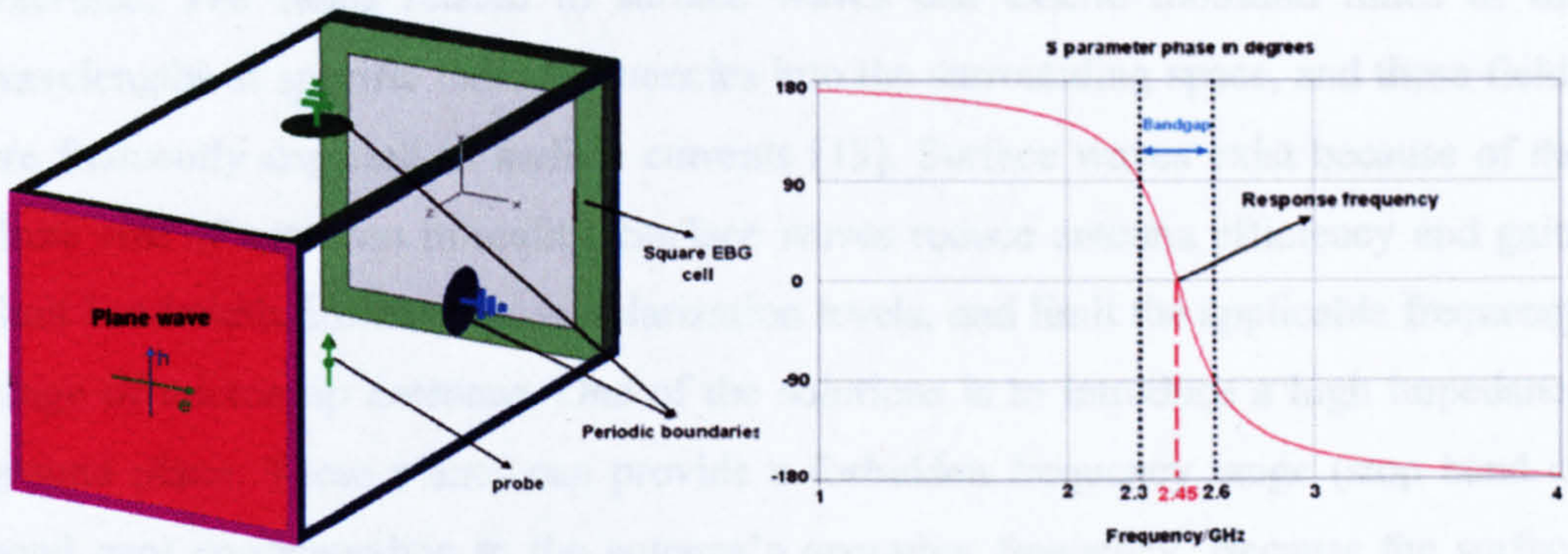

Figure 2.11 A 2.45GHz EBG unit cell model and reflection phase diagram

The reflection phase of an EBG plane can be modelled by using the phase difference between an incident wave illuminating the structure and the reflected wave at a

certain position above the surface. A unit cell model with periodic boundary conditions at the side walls of the cell is simulated to model an infinite structure [24]. A reflection phase model for a simple EBG unit cell set up in the software CST Microwave Studio environment is shown in Figure 2.11. A plane wave is launched in the direction normal to the surface and a field probe is located at a particular distance dependent on the wavelength of the cell to detect the reflected signal in magnitude and phase. The same setup for a PEC surface with equal dimensions is used as a reference plane to compare the reflection signal. The reflected phase of the EBG surface is calculated by adding an 180^0 shift to the reference phase of the PEC. The evaluated reflection phase diagram of the structure is plotted in Figure 2.11 as well. The zero degree phase reflection for the structure occurs at 2.45GHz. And -90° to 90° phase response indicates the structure has a reflection phase band gap of 2.3GHz-2.6GHz.

2.4.3 EM Wave Suppression

Another important feature of an EBG plane is that the structure can forbid the propagation of electromagnetic waves in certain frequency bands, and furthermore to guide them in a desired direction. Typical EM wave propagation that can cause a serious problem for microstrip antennas are surface waves. Surface waves occur on the interface between two different materials, such as air and metal. They are confined to the interface, and attenuate exponentially into the materials surrounding the interface. The fields related to surface waves can extend thousand times of the wavelengths at specific radio frequencies into the surrounding space, and these fields are frequently depicted as surface currents [13]. Surface waves exist because of the finite size of antennas in reality. Surface waves reduce antenna efficiency and gain, limit bandwidth, increase cross-polarization levels, and limit the applicable frequency range of microstrip antennas. One of the solutions is to introduce a high impedance ground plane. These planes can provide a forbidden frequency range (stop band or band gap) corresponding to the antenna's operating frequency. Because the surface wave cannot propagate along the high impedance surface, an increased amount of radiated power couples to the space wave. Antenna ground planes that use EBG surfaces have good radiation patterns without unwanted ripples based on suppressing the surface wave propagation within the band gap frequency range. Another

advantage of EBG surface on EM wave suppression is to reduce mutual coupling between two patch antennas. Study [25] has shown that by applying electromagnetic band-gap structure with appropriate size and position, the mutual coupling of patch antennas on thick and high dielectric constant substrate can be notably reduced.

EM wave suppression can be measured by several techniques. One of the commonly used methods is the transmission line method [24]. A suspended strip line with a port on either side is placed over the EBG ground plane. The S_{21} can be calculated by using one port as an exciting source and the other as a matched load. Theoretically, the EM wave transmission within the band gap of the EBG should be blocked. Thus the reduction of S_{21} at certain band of frequencies can indicate the EM wave suppression band gap of the EBG.

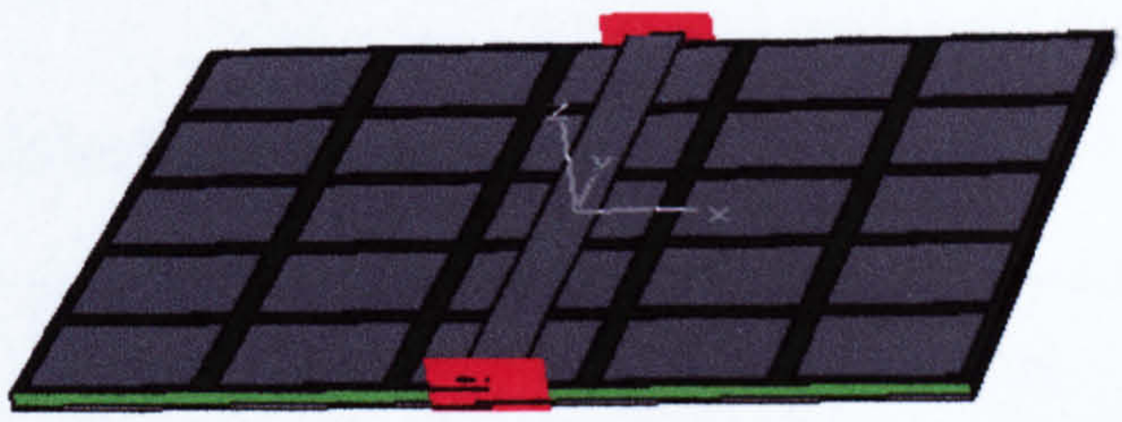

Figure 2.12 suspended strip line over EBG ground plane

2.5 Software Environment

In this project, simulation work plays an essential role regarding the evaluation at the design of antennas and EBGs. The computer software used for simulation is CST Microwave Studio®, which is the product of CST-Computer Simulation Technology.

CST Microwave Studio® is a general-purpose electromagnetic software package based on the Finite Integration Technique (FIT). This numerical method provides a universal spatial discretization scheme, applicable to various electromagnetic problems, ranging from static field calculations to high frequency applications in time or frequency domain. In the following section the main aspects of this procedure will be briefly explained and afterwards extended to a review of CST Microwave Studio.

2.5.1 Finite Integration Technique

Finite Integration Technique was first proposed by Weiland in 1977 [26]. Unlike most numerical methods, FIT discretizes the following *integral* form of Maxwell's equations, rather than the differential one:

$$\textit{Faraday's Law: } \oint_{\partial A} \vec{E} \cdot d\vec{s} = -\int_{A} \frac{\partial \vec{B}}{\partial t} \cdot d\vec{A}$$

$$\textit{Ampere's Law: } \oint_{\partial A} \vec{H} \cdot d\vec{s} = \int_{A} (\frac{\partial \vec{D}}{\partial t} + \vec{J}) \cdot d\vec{A}$$

$$\textit{Gauss's Law for electricity: } \oint_{\partial V} \vec{D} \cdot d\vec{A} = \int_{V} \rho \cdot dV$$

$$\textit{Gauss's Law for magnetism: } \oint_{\partial V} \vec{B} \cdot d\vec{A} = 0 \qquad \textbf{(2-13)}$$

E [V/m] =electric field vector; B [Wb/m^2] =magnetic flux density vector;

H [A/m] =magnetic field vector; D [C/m^2] =electric flux density vector;

J [A/m^2] = displacement current density; ρ[C/m^2] =volume charge density.

In order to solve these equations numerically, the first step of the FI-method consists in the restriction of the electromagnetic field problem, in which usually a finite calculation domain is defined, enclosing the considered space region of interest. The next step consists in the decomposition of the computational domain into a (locally) finite number of simplicial cells $\mathbf{A_n}$, such as tetra- or hexahedra under the premise that all cells have to fit exactly to each other. This decomposition yields the finite simplicial cells complex *G*, which serves as computational grid [27]. The whole decomposition procedure is shown in Figure 2.13. These grid cells are referred as mesh system in the software environment.

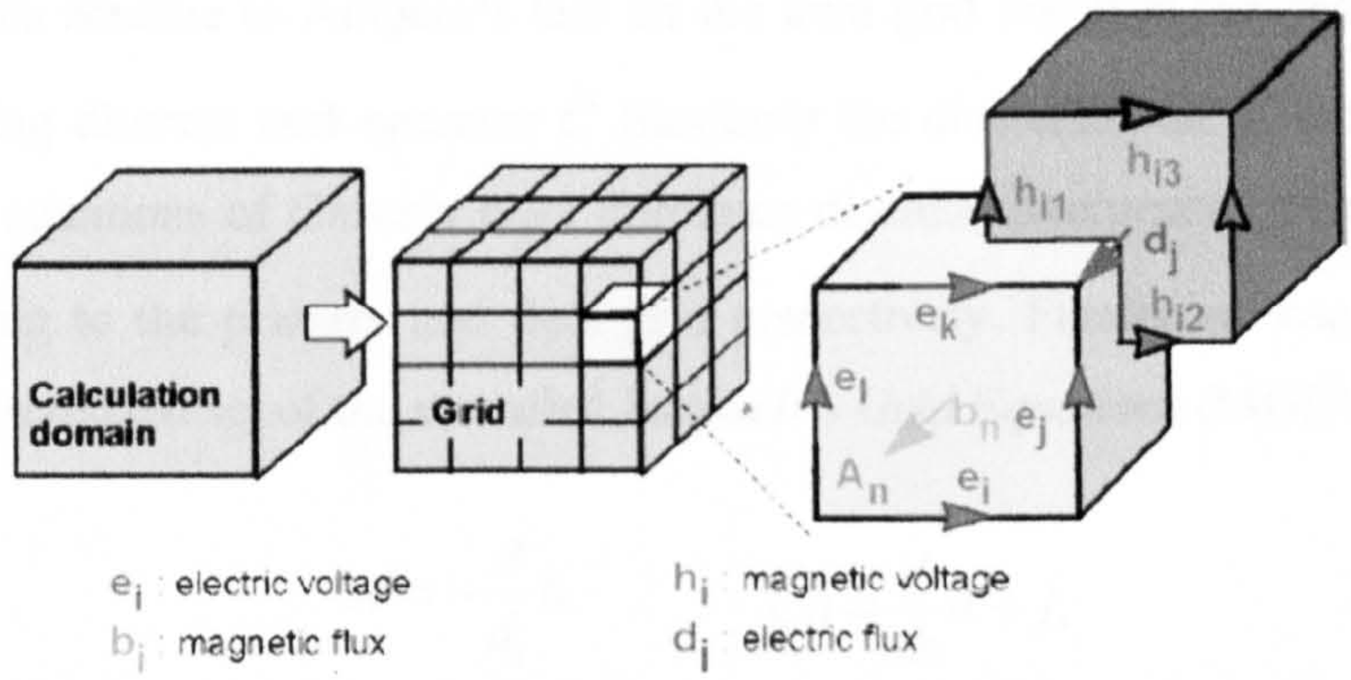

Figure 2.13 Decomposition of the computational domain in FIT [28]

The spatial discretization of Maxwell's equations is finally performed on these two orthogonal grid systems. Referring to the above picture, the electric grid voltages **e** and magnetic facet fluxes **b** are allocated on the primary grid G and the dielectric facet fluxes **d** as well as the magnetic grid voltages **h** on the dual grid $\tilde{G}$ [29].

Now Maxwell's equations are formulated for each of the cell facets separately. After the definition of the grid cell complex G, the further introduction of the FI-theory can be restricted to a single cell volume $\mathbf{A_n}$. Applying Faraday's law to the front facet in Figure 3.2, it can be rewritten as

$$e_i + e_j - e_k - e_l = -\frac{\partial}{\partial t} b_n \tag{2-14}$$

By repeating this procedure for all available cell facets, the calculation rule can be summarized in a matrix formulation, introducing the topological matrix $\boldsymbol{C}$ as the discrete equivalent of the analytical curl operator:

$$\underbrace{\begin{pmatrix} & \cdots & \cdots & \cdots & & \\ 1 & \cdots & 1 & \cdots & -1 & \cdots & -1 \\ & \cdots & \cdots & \cdots & & \end{pmatrix}}_{\boldsymbol{C}:=} \underbrace{\begin{pmatrix} \boldsymbol{e}_i \\ \vdots \\ \boldsymbol{e}_j \\ \vdots \\ \boldsymbol{e}_k \\ \vdots \\ \boldsymbol{e}_l \end{pmatrix}}_{\boldsymbol{e}} = -\frac{\partial}{\partial t} \underbrace{\begin{pmatrix} \vdots \\ \boldsymbol{b}_n \\ \vdots \end{pmatrix}}_{\boldsymbol{b}} \tag{2-15}$$

Applying this scheme to Ampere's law on the dual grid involves the definition of a corresponding discrete curl operator $\tilde{C}$ .Similarly the discretization of the remaining divergence equations of Gauss's laws introduce discrete divergence operators S and $\tilde{S}$, belonging to the primary and dual grid respectively. Finally we can obtain the complete discretized set of the so-called *Maxwell's Grid Equations* (MGE's) [27]:

$$Ce = -\frac{d}{d_t}b, \qquad \tilde{C}h = \frac{d}{dt}d + j, \qquad \tilde{S}d = q, \qquad Sb = 0. \tag{2-16}$$

Compared to the continuous form of Maxwell's equations, the similarity between both descriptions is obvious. Now all matrix equations are available to solve electromagnetic field problems on the discrete grid space. The process is repeated for all grid cells within the boundary until the desired accuracy is reached.

As demonstrated, the FIT formulation is a very general method and therefore can be applied to wide frequency ranges, as well as diversiform structures (from common topology to complex geometries). Compared to other numerical techniques, the major advantage of the FI-method is that the computational complexity increases linearly with problem size, while other method, like Method of Moment (MoM), forms a dense matrix increasing exponentially with problem size. Wideband results, useful for most wireless systems, can be obtained within only one simulation with FIT. Compare to the Finite Difference Time Domain (FDTD) method, which only operates time domain calculation, FIT is able to support a frequency domain solver and an Eigenmode solver which are based on Maxwell's equations in the harmonic case [30].

There are also a few weaknesses of the FIT method. First, the entire computational domain needs to be meshed, and the mesh grids must be small enough to assure the calculation accuracy. These will result in a large computational load for some situations. Second, it is very difficult to generate proper mesh properties for very long or very thin structures. Finally, for some curved structure or at the edge of the structure, the grid needs to be stair-cased, this will cause unstable or inaccurate results for some sensitive devices.

2.5.2 CST Microwave Studio

CST Microwave Studio® is a software tool for electromagnetic design and analysis in the frequency range of microwave engineering, and it has shown many advantages in high frequency electromagnetic design and modelling. It is distinctive on its windows-based operating interface and graphic feedback for the definition of device that is being developed.

The program also combines a user-friendly interface with unsurpassed simulation performance. A key feature of CST Microwave Studio is the approach of using the simulator or mesh type that is best suited to a particular problem. The software contains three different simulation techniques (transient solver, frequency domain solver, eigenmode solver) to best fit their particular applications.

The most flexible tool, transient solver, which is a time domain simulator, is also the mainly used solver in this research. It can obtain the entire broadband frequency behaviour of the simulated device from only one calculation run. It is remarkably efficient for the most kinds of high frequency applications.

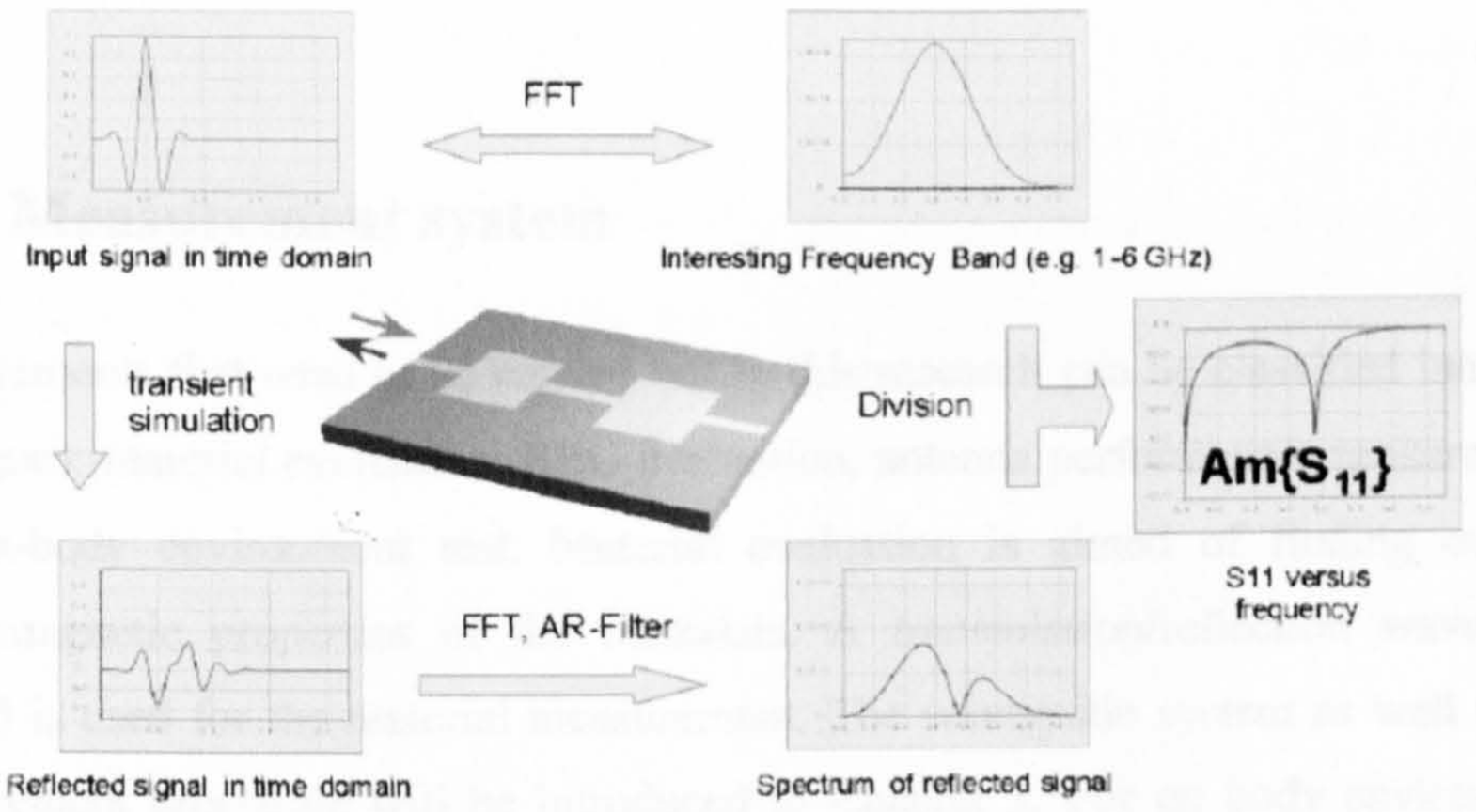

Fig 2.14 S-parameter calculation by transient solver [28]

The transient simulator permits a broadband calculation of S-parameters from one single calculation run by applying the Finite Integration Technique (FIT) method to time signals.The S-parameter calculation processed by the transient solver in CST is

shown in Figure 2.14. The calculation of the transient solver operates with time pulses, it can be easily transformed into the frequency domain by making use of a Fast Fourier Transformation (FFT) [28]. The S-parameters can then be derived from the resulting frequency domain spectra. This shows an obvious advantage of calculation in the time domain. CST Microwave Studio automatically calculates the appropriate excitation time pulse from the frequency range setting. The default Gaussian shaped pulse guarantees a smooth spectrum in the frequency domain, which allows a reliable calculation of the S-parameters [28].

According to the meshing weaknesses of the FIT, CST developed a few special meshing methods to enhance the calculating accuracy. They are the Perfect Boundary Approximation method (PBA), Thin Sheet Techniques (TST) and Multilevel Sub-gridding Scheme (MSS). These methods allow a better approximation of curved surfaces and finer field discretization within the mesh cells [30]. MSS is a useful function in this research when modelling human body in the simulation. By using the sub-gridding scheme, the body can be meshed into more refined grids than the surrounding free space. It has been found that the computational time can be much reduced by this method without affecting the entire accuracy.

2.6 Measurement system

Measurements that need to be carried out in this research can be classified into four catalogues: material evaluation, EBG evaluation, antenna performance measurement, and on-body environment test. Material evaluation is aimed of finding out the electromagnetic properties of the materials. A transmission/reflection waveguide method is used for the material measurement. The waveguide system as well as the measurement procedure will be introduced in Chapter 3. For on body environment testing, we mainly focus on the antenna performance with the presence of human body and the Specific Absorption Rate (SAR) values. These measurements need particular system setup, therefore the detailed description will be given in Chapter 6. In this section, the measurement setup for antenna performance evaluations will be introduced.

2.6.1 HP8720 Network Analyzer

The HP8720 is a high performance vector network analyzer for laboratory measurement of reflection and transmission parameters. It is used to measure both the return loss and the radiation patterns of the antenna. HP8720 has a working frequency range of 50MHz up to 18GHz, which is enough for the applications in this study. With a precise calibration in advance, the network analyzer can supply both graphical feedback and data results within the frequency range setup. In terms of input matching, it provides straightforward impedance and S_{11} values of the tested antenna as a function of frequency. The network analyzer can also provide the S_{21} measurement by using one of its ports as transmission and the other one as reflection. According to antenna radiation characteristic measurements, as a part of the system, the network analyzer is used as the source supplier for the testing antenna, as well as the data retrieve equipment for the radiating energy. The whole radiation measurement system including the anechoic chamber will be discussed in the following section.

2.6.2 Indoor Anechoic Chamber

Indoor anechoic chambers which have been developed as an alternative to outdoor testing are used to characterise antenna radiation performance. The enclosed measurement environment is accomplished to provide a controlled field environment, an all-weather capability, and security. By this method, the testing is performed inside a chamber having walls that are covered with RF absorber to minimize electromagnetic interference.

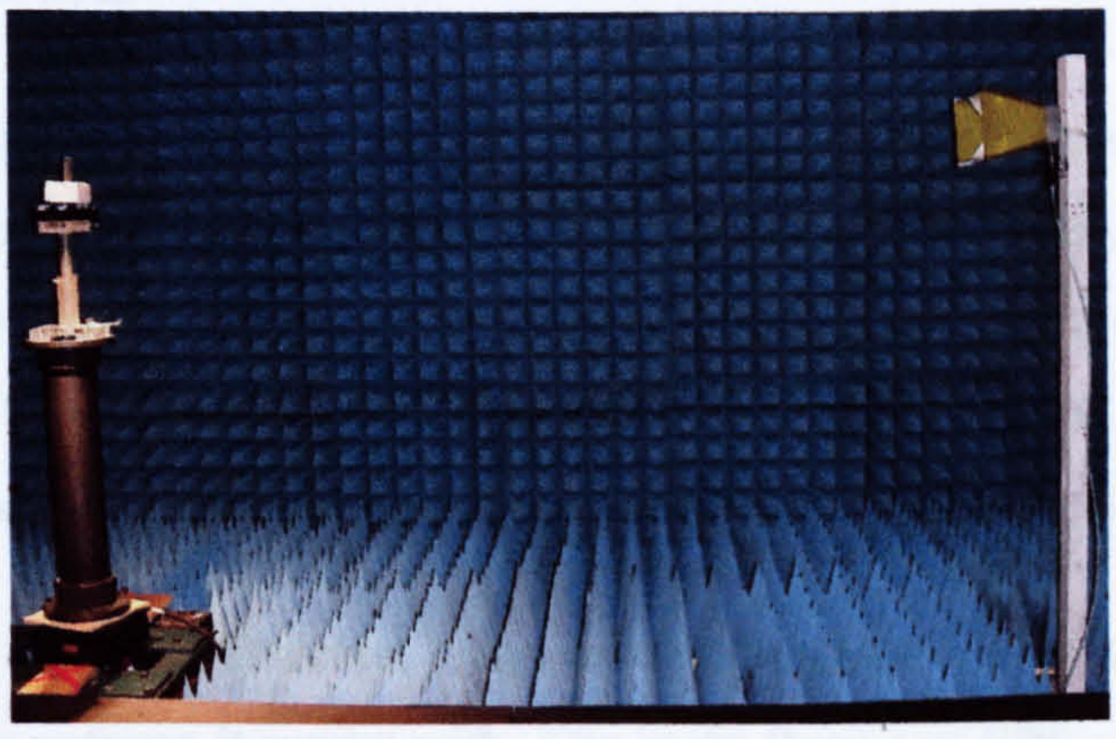

Figure 2.15 Indoor chamber setup for radiation pattern measurement

Radiation characteristics of all the antennas in this study were measured in an electromagnetically anechoic chamber with fully automatic measurement software so called NSI 800F-10 far-field antenna measurement system. The entire system is divided into two parts: control room which is outside the chamber, and inside chamber. The Outside control room has most of the control equipment for easy operation. It consists of a network analyzer, an antenna range controller, a standard beam controller and a computer. Inside the chamber provides a quite zone for the measurement. The setup which is shown in Figure 2.15 includes a transmitting antenna, an azimuth turn table and the antenna mounting case. A linearly polarized standard gain horn antenna (working frequency range: 900MHz-18GHz) was employed as the transmitting antenna. Antennas under test were mounted on the turn table in the far-field range distance from the transmitter. During the measurement, the turn table is automatically controlled by the software to rotate through a full 360° and the received power level is recorded as a function of the rotating phase. Importantly, the location of the measured antenna should be aligned to the centre of the turn table, thus the tested results can be symmetrical. The measured data is recorded by the network analyzer as a function of frequency and azimuth angle. The data is then transferred to the computer and plotted as a 2D radiation patterns. The 2D plots are taken for Theta (θ) and Phi (φ) cuts for vertical and horizontal polarisations in the azimuth plane in this study.

2.7 Conclusion

The two types of planar antennas which are mainly used for antenna design in this study have been introduced in this chapter. Their simple and planar geometries make them suitable for wearable applications. The basic antenna theory and parameters that are important to the foundation of the research were also reviewed. Examples were given to assist understanding and analyzing the antenna performances.

Electromagnetic Bandgap Structure plays an important role as it can bring a lot of advantages to the antenna it works with. The basic theory of EBGs was discussed in

this chapter, as well as its design procedure. The modelling and testing method to evaluate EBG performances were also introduced with examples.

A brief introduction on the commercial software used for this research was presented in this chapter. The theoretical background of the software package was also discussed. And finally, the description of the measurement system was documented to provide general information on how the antenna performances were tested in the lab.

This chapter generally gives the theoretical background and methodology on the subjects that are related to this research. The basic discussion will be helpful for understanding the further studies in the future chapters.

References:

[1] **Deschamps, G.A.,** "Microstrip Microwave Antennas," Presented at the Third USAF Symposium on Antennas, 1953.

[2] **Balanis, C. A.,** *Antenna Theory: Analysis and Design,* Third Edition, WILEY-INTERSCIENCE, 2005.

[3] **Wen, C. P.,** "Coplanar Waveguide: A Surface Strip Transmission Line Suitable for Non-Reciprocal Gyromagnetic Device Application," *IEEE Transactions on Antennas and Propagation, Vol. MTT-17,* pp. 1087-1090, 1969.

[4] **Gupta, K.C., Garg, R., Bahl, I. J.,** *Microstrip lines and slotlines,* chapter 7, Artech House, Inc, 1979.

[5] **Tong, K.F., Li, K., Matsui, T. and Izutst, M.,** "Broad-band double-layered coplanar Patch antennas with adjustable CPW feeding structure," *IEEE Transactions on Antennas and Propagation,* Vol. 52, No.11, Nov 2004.

[6] **Lee, T-I., Kim, S. and Wang, Y.E.,** "Compact polarisation and spatial multiplexing antenna for MIMO applications," *IET Electronics Letters,* Vol. 42, Issue. 15, pp. 839- 840, Jul 2006.

[7] **Klemm, M. and Troester, G.,** "Textile UWB antennas for wireless body area networks," *IEEE Transactions on Antennas and Propagation,* Vol. 54, No.11, Nov 2006.

[8] **Qiu, X. and Mohan, A.S.,** "The performance of a CPW-fed printed UWB antenna for wireless body-worn applications," *IEEE Antennas and Propagation Society International Symposium,* pp. 2109-2112, Jul 2006.

[9] **Sinnema, W.,** *Electronic Transmission Technology,* Prentice-Hall Inc, 1979.

[10] **Thiel, D.V. and Smith, S.,** "Wire Antenna Theory," Chapter 2 in *Switched Parasitic Antennas for Cellular Communications*, Norwood, MA: Artech House, 2002.

[11] **McLean, J., Sutton, R., and Hoffman, R., TDK RF Solutions,** "Interpreting Antenna Performance Parameters for EMC Applications," Part 1: *Radiation Efficiency and Input Impedance Match,* from *http://www.tdkrfsolutions.com/DataPDFs/antenna_paper_part1.pdf*

[12] **Website:** http://www.skycross.com/Technology/terminology.asp

[13] **Sievenpiper, D.F. et al,** "High-Impedance Electromagnetic Surfaces with a Forbidden Frequency Band," *IEEE Transactions on Microwave Theory and Techniques*, vol. 47, no. 11, pp. 2059-2074, November 1999.

[14] **Yang, F. and Rahmat-Samii, Y.,** "Reflection phase characterizations of the EBG ground plane for low profile wire antenna applications," *IEEE Transactions on antennas and propagation,* Vol.51, No.10, pp.2691-2703, Oct 2003.

[15] **Yang, F. and Rahmat-Samii, Y.,** "Mutual coupling reduction of microstrip antennas using electromagnetic band-gap structure," *IEEE Antennas and Propagation Society International Symposium,* Vol. 2, pp. 478–481, July 2001.

[16] **Sharma, S. and Shafai, L.,** "Enhanced performance of an aperture-coupled rectangular microstrip antenna on a simplified unipolar compact photonic bandgap (UCPBG) structure," *IEEE Antennas and Propagation Society International Symposium*, Vol. 2, pp. 498–501, July 2001.

[17] **Sievenpiper, D. F.,** "High-impedance Electromagnetic Surfaces," Ph.D. dissertation, UCLA, 1999.

[18] **Rahmat-Samii, Y. and Mosallaei, H.,** "Electromagnetic Band-gap Structures: Classification, Characterization and Applications," *the 11th International Conference on Antennas and Propagation*, No.480, pp.560-564, Apr 2001.

[19] **Yang, F. R., et al,** "PBG-Assisted Gain Enhancement of Patch Antennas on High-Dielectric Constant Substrate," *IEEE Antennas and Propagation Society International Symposium*, pp. 1920-1923, July 1999.

[20] **Yan, D., Gao, Q., Wang, C. and Yuan, N.,** "Novel compact inter-embedded AMC structure for suppressing surface wave," *Progress In Electromagnetic Research Symposium*, pp. 695-698, Aug 2005.

[21] **Vardaxoglou, J.C.,** *Frequency Selective Surfaces Analysis and Design*, New York, Wiley, 1997.

[22] **Yang, F. and Rahmat-Samii, Y.,** "Microstrip Antennas Integrated With Electromagnetic Band-Gap (EBG) Structures: A Low Mutual Coupling Design for Array Applications," *IEEE Transactions on Antennas and Propagation*, vol. 51, no. 10, pp. 2936-2946, Oct 2003.

[23] **Tse, S., Sanz, I.B., Batchelor, J.C. and Langley, L.J.,** "Reduced Sized Cells for Electromagnetic Bandgap Structures," *IEE Electronics Letters*, Vol.39, No.24, pp.1699-1701, Nov 2003.

[24] **Aminian, A., Yang, F. and Rahmat-Samii, Y.,** "In-phase Reflection and EM Wave Suppression Characteristics of Electromagnetic Band Gap Ground Planes," *IEEE Antennas and Propagation Society International Symposium*, pp. 430-433, 2003.

[25] **Yang. F. and Rahmat-Samii, Y.,** "Mutual Coupling Reduction of Microstrip Antennas using Electromagnetic Band-gap Structure," *IEEE Antennas and Propagation Society International Symposium*, Vol.2, pp.478-481, Jul 2001.

[26] **Weiland, T.,** "A discretization method for the solution of Maxwell's equations for six-component fields," *Electronics and Communications AEÜ*, Vol.31, No.3, pp.116-120, 1977.

[27] **Clemens, M. and Weiland, T.,** "Discrete Electromagnetism with The Finite Integration Technique," *Progress in Electromagnetics Research*, Vol.32, pp.65-87, 2001.

[28] **CST Microwave Studio menu,** "Advanced topics," Version 5, 2004.

[29] **Weiland, T.,** "Time Domain Electromagnetic Field Computation with Finite Difference Methods," *International Journal of Numerical Modelling*, Vol. 9, pp. 295-319, 1996.

[30] **Low, L.,** "Hidden Antennas for Automobiles," *PhD Thesis*, University of Kent, Sep 2005.

Chapter 3 Material Characterization

3.1 Introduction

Most existing wearable computers to date consist of bulky and rigid boxes and are portable rather than wearable. Some approaches have been made to integrate electronic components into clothing [1], but usually the textile itself just serves as a carrier of conventional electronics. Another approach is to use textiles for electrical functions such as transmission lines and sensors. Future wearable applications may require a full integration of the microwave circuits with our daily clothing. Thus to evaluate the electromagnetic properties of the textile materials and find out whether the textile materials can provide a smooth integration into RF circuits while preserving the typical properties of textiles is essential for textile antenna design and modelling.

The electromagnetic property of a microwave material can be defined by the responses of the material to electromagnetic fields. Specify to antenna technology, electric conductive materials which are generally good electric conductors are compulsory for being as the radiating or grounding elements of the antenna. Dielectric materials as poor electricity conductors are commonly used as substrate materials of the antenna. Recent studies on microwave materials have demonstrated that a lot of textile materials of our daily clothing can satisfy the dielectric property requirements of an antenna substrate [2]. And the new technology has developed high quality conductive textiles woven from metallic fibres. These conducting textiles have a great opportunity to replace metals in some particular applications [3]. Therefore, once the electromagnetic properties of the material can be defined, to design and develop an antenna or circuits with entire textile materials is not an unreachable target.

This chapter aims to provide basic knowledge of dielectric materials evaluation. Some basic parameters will be defined and the dielectric properties of a few textile and leather materials will be characterized. A waveguide method which was used for the dielectric material measurement will be explained in detail and followed by the results in terms of relative permittivity and loss tangent of the material.

Conductive materials as an important part will be introduced in the end of the chapter. A few high quality metal placed woven textile materials will be studied. Antennas made out of different conductive materials will be compared in terms of the return loss performance.

As all the materials employed in this research are not magnetic materials, therefore the magnetic properties of the materials are not considered in the study.

3.2 Dielectric Materials

The critical element that enabled the realization of microstrip patch antennas is the innovations of the materials of substrates. The substrate has to consist of some dielectric material [4]. This specific material may influence the electrical properties of the antenna, transmission line as well as circuits. Thus, a suitable substrate must satisfy the mechanical and electrical requirements at the same time.

A dielectric material is known as a poor electricity conductor, but a good medium of electrostatic current flow. When an electromagnetic wave travels through a dielectric, the velocity of the wave will be reduced and it will behave as if it had a shorter wavelength.

The measure of how a substance concentrates the electrostatic lines of flux is defined as dielectric permittivity ε [5]. ε can be obtained from their measured complex relative permittivity, expressed as

$$\varepsilon = \varepsilon' - j\varepsilon'' \tag{3-1}$$

where ε' is the relative permittivity of the material and ε'' the out-of-phase loss factor associated with it such that

$$\varepsilon'' = \sigma / \varepsilon_0 \omega \tag{3-2}$$

In this expression, σ is the total conductivity of the material, ε_0 is the permittivity of free space and ω the angular frequency of the field. The SI unit of conductivity is

siemens per meter (S/m) which presumes that in the above expression ε_0 is expressed in farads per meter (F/m) and ω in radians per second. The dielectric properties are determined as ε' and ε'' values, or relative permittivity and loss tangent which is relevant to both ε' and ε'', as a function of frequency.

3.2.1 Permittivity

Permittivity is the real part of the dielectric constant. The permittivity of a medium can be looked as the quality of a material that allows it to store electrical charge. For two flat plates those are filled with a dielectric material, the permittivity of the material can be written into:

$$\varepsilon = \varepsilon_r \varepsilon_0 = \frac{Q}{EA} \tag{3-3}$$

Where ε=permittivity of medium, Fm^{-1}

ε_r=relative permittivity of medium = $\varepsilon/\varepsilon_0$ (dimensionless)

Q=the charge that is uniformly distributed between the plates, C

E=electric field, Vm^{-1}

A=plate area, m^2

Therefore, a given mount of material with high permittivity can store more charges than a material with lower permittivity. A high permittivity tends to reduce any electric field present. The capacitance C between the plates is given by

$$C = \frac{\varepsilon A}{d} = \frac{\varepsilon_r \varepsilon_0 A}{d} \tag{3-4}$$

Where d=distance between two plates, m

Thus, the capacitance of a capacitor can be increased by increasing the permittivity of the dielectric material inside it.

Materials can be classified according to their permittivity. Those with a positive real part dielectric constant are dielectrics. Metals, those are good electrical conductors, have a negative permittivity at very high frequencies, in which no propagation of electromagnetic wave exists.

3.2.2 Loss Tangent

Loss tangent defines the lossiness of the medium. It is the negative ratio at any particular frequency between the imaginary and real parts of the dielectric constant of the material.

$$\text{Loss tangent: } tan(\delta(\omega)) = \frac{\varepsilon''(\omega)}{\varepsilon'(\omega)} = \frac{-\Im\{\varepsilon(\omega)\}}{\Re\{\varepsilon(\omega)\}} \tag{3-5}$$

A large loss tangent means the material has a lot of dielectric absorption, and a high loss of the power transmitted through the dielectric. Specify to antenna applications, as the radiation efficiency of an antenna is highly related to the loss factor of the material, a large loss tangent can lead to very low antenna efficiency.

3.3 Dielectric Material Measurement Procedure

3.3.1 Dielectric measurement overview

In order to design components and understand the interaction of electromagnetic fields with the dielectric materials we are working with, it is necessary to understand the dielectric properties of the materials and how to measure them at RF & Microwave frequencies.

So far electromagnetic property characterizations of dielectric materials are generally measured by two main methods: resonant methods and nonresonant methods. In resonant methods, like resonant perturbation methods [6-7], the sample under measurement is introduced to a resonator thus altering the electromagnetic boundaries of the resonator, and the electromagnetic properties of the sample are deduced from the change of the resonant properties of the resonator.

Non-resonant methods mainly include reflection methods and transmission/reflection methods. The reflection methods include open-circuit line methods [8] and short-circuit line methods [9]. The transmission/reflection methods have many varieties, including free-space, coaxial line, waveguide, and planar structures such as microstrip and stripline. In a transmission/reflection method, the sample under test is inserted into a segment of transmission line, and the permittivity of the sample is derived from the reflection and transmission characteristics of the sample-loaded unit. Owing to their relative simplicity, the transmission/reflection methods, are widely used in various fields of materials research and engineering. Also as nonresonant methods can cover certain frequency bands, they can be used for measurements of electromagnetic properties of materials for a multitude of applications.

3.3.2 Dielectric Fabric Materials Evaluation

In this section, the evaluation on the dielectric properties of some textile and leather materials through a transmission/reflection waveguide method will be introduced. The measurement setup is based on an HP 8720D network analyzer and a rectangular waveguide10 system (Two identical waveguide cavities with transition parts, a shorting board and a waveguide sample holder). The operating frequency range of the waveguide 10 system is at S band of 2.60-3.95GHz.

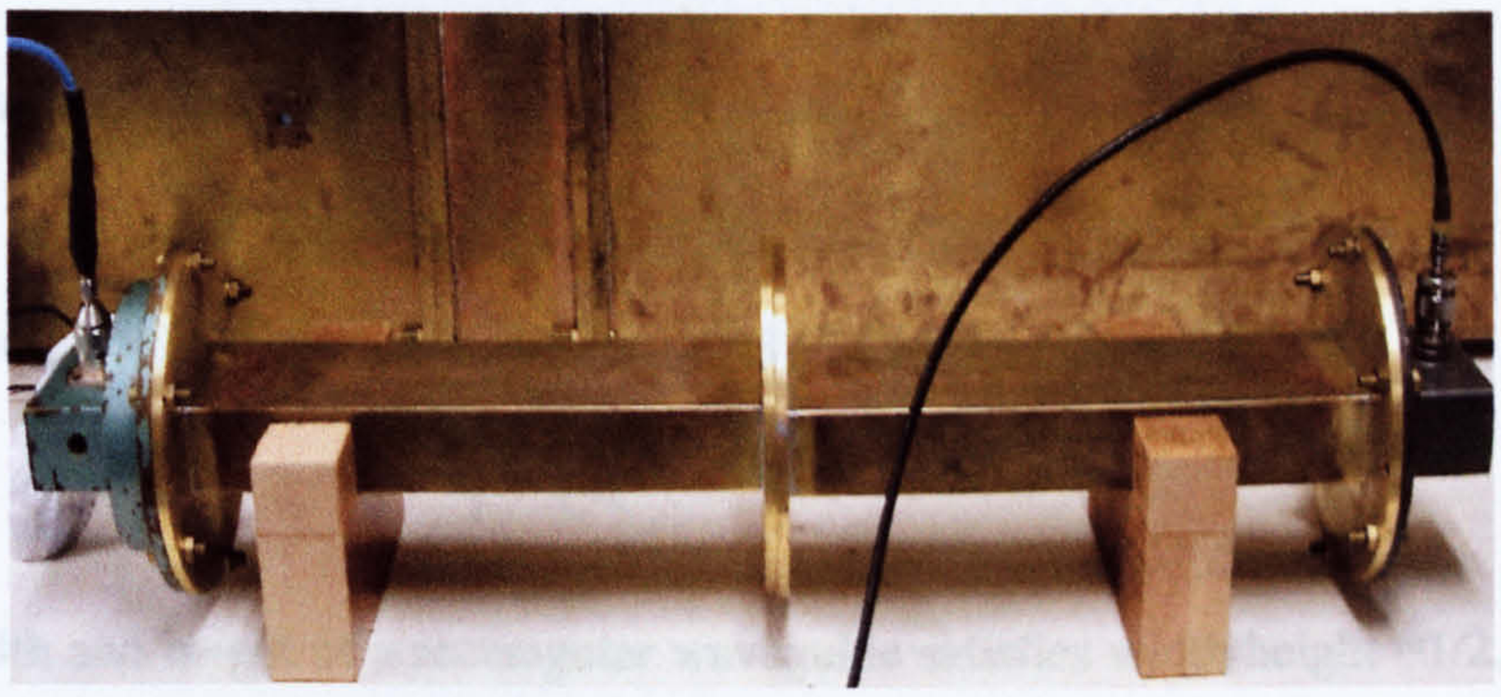

Figure 3.1 Waveguide10 system

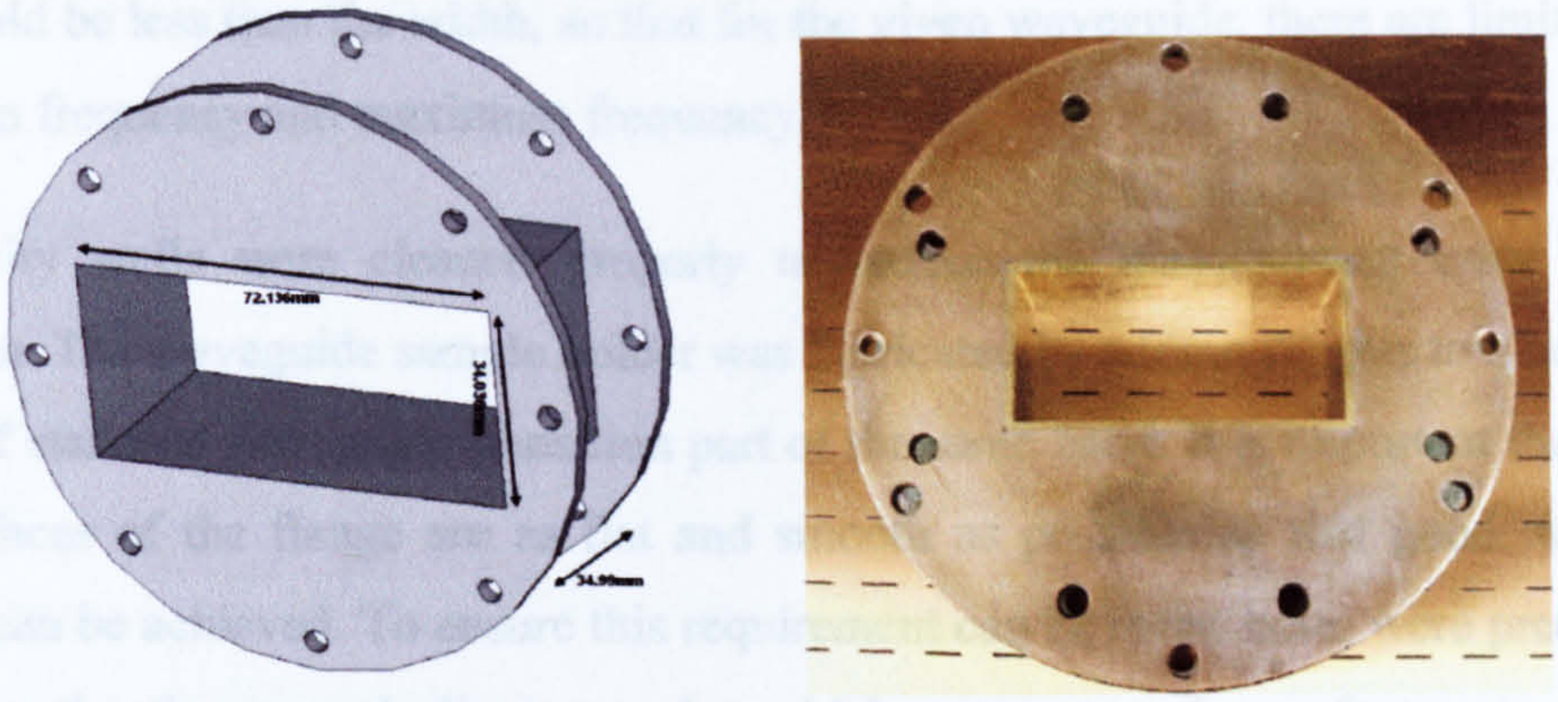

Figure 3.2 Waveguide sample holder

The waveguide 10 system and the sample holder are shown in Figure 3.1 and Figure 3.2 respectively. The important parameters of the waveguide system are listed as following:

Cavity inner width: 72.136mm, **Cavity inner height:** 34.036mm

Sample holder thickness: 34.99mm, **Frequency range:** 2.60-3.95GHz

Cut off frequency f_c : 2.08GHz

Centre frequency: $f_0 = \frac{f_L + f_U}{2} = \frac{2.60 + 3.95}{2} = 3.275GHz$

Cut off wavelength: $\lambda_c = \frac{c}{f_c} = 144.23mm$

Wavelength in free space: $\lambda_0 = \frac{c}{f_0} = 91.6mm$

Wavelength in guide: $\lambda_g = \frac{\lambda_0}{\sqrt{1 - \left(\frac{\lambda_0}{\lambda_c}\right)^2}} = 118.59mm$

The width and height of a rectangular waveguide satisfies width/height =1/2, and the waveguide usually works at TE_{10} mode. To ensure the single-mode requirement in materials property characterization, the wavelength should be larger than the height

and should be less than the width, so that for the given waveguide, there are limits for minimum frequency and maximum frequency.

The cavity walls were cleaned properly to reduce the measurement error to a minimum. The waveguide sample holder was fabricated by adding flanges to a certain length of standard waveguide transition part of the same band. It is important that the end surfaces of the flange are as flat and smooth as possible so that good mating contact can be achieved. To ensure this requirement can be meet, holes were properly drilled on the flange, and alignment pins which can ensure the perfect connection were manufactured by the Sheffield University workshop. Also, because the flanges are circular, two pieces of wooden holder were made to hold the whole system stable on the desk.

Six fabric samples and three reference solid samples (Rohacell, Perspex and PTFE), as shown in Figure 3.3, were measured with this system. All the fabrics are purchased from high street shops and they are very commonly used in our daily clothing. The solid samples were fabricated in the mechanical workshop. The description of the samples is shown in Table 3.1. All the samples were cut subtly into the waveguide inner size to fix the sample holder properly, as the air gap along the width or height may cause serious effect on the results [10].

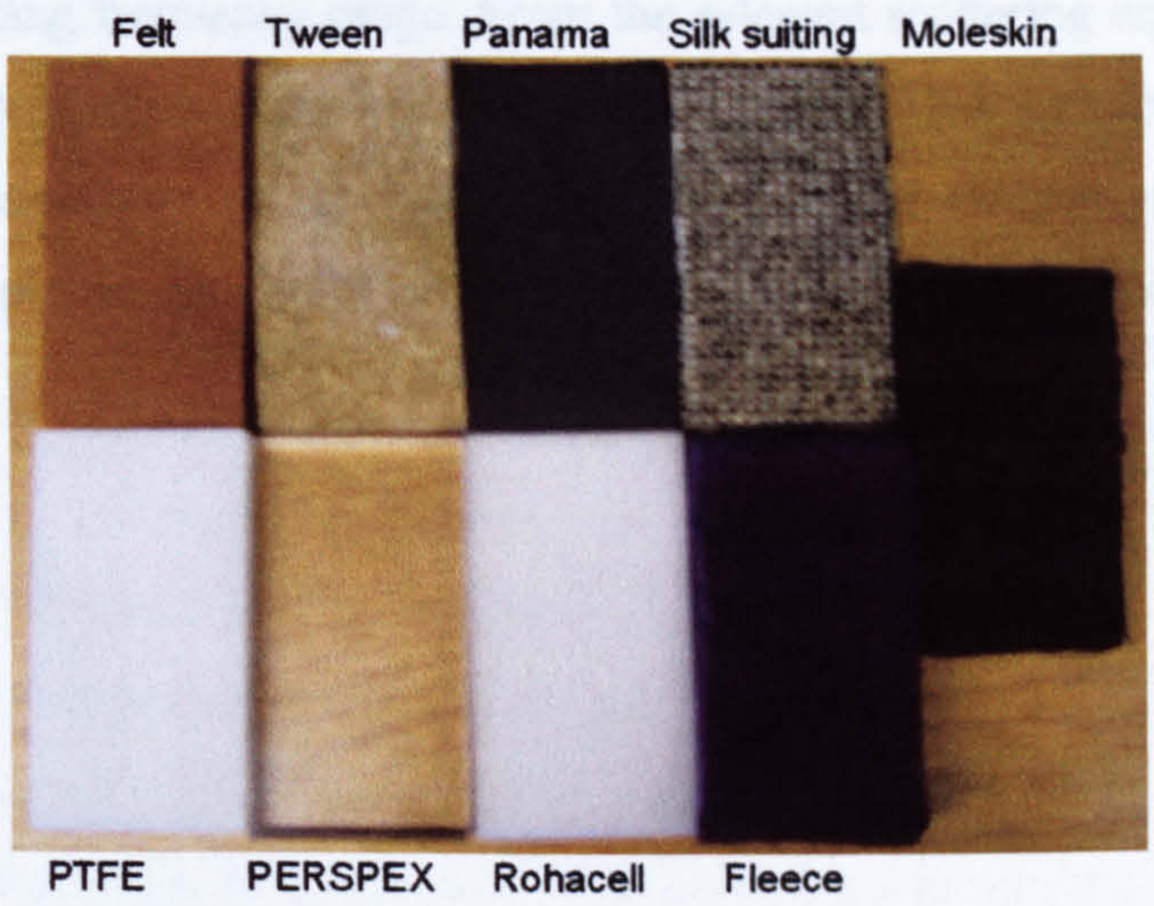

Figure 3.3 Samples under test

Table 3.1 Materials description

Name	Components	Thickness (mm)	Multilayer thickness (mm)
Silk suiting	100%silk	0.578	3.0275
Tween	49%Wool 29%Polyester	0.685	3.34
Panama	67%polyester 33%viscose	0.347	1.75
Moleskin	100%cotton	1.17	6.3575
Felt	70%viscose 30%wool	1.095	4.5325
Fleece	100%polyester	2.55	9.8725
Rohacell		1	3
PTFE		11.66	11.66
PERSPEX		11.67	11.67

During the measurement, the sample under test was inserted into the sample holder of the waveguide cavity. The waveguide sample holder has the advantage of rectangular shape that makes the sample easy to form. In the transmission/reflection method, all the four scattering parameters (S_{11}, S_{21}, S_{12} and S_{22}) can be measured over the waveguide working frequency range. From the relevant scattering equations relating the scattering parameters of the segment of waveguide filled with the sample under study to the permittivity of the sample, we can get the electric properties of the sample. The whole measurement procedure can be described as following in Figure 3.4.

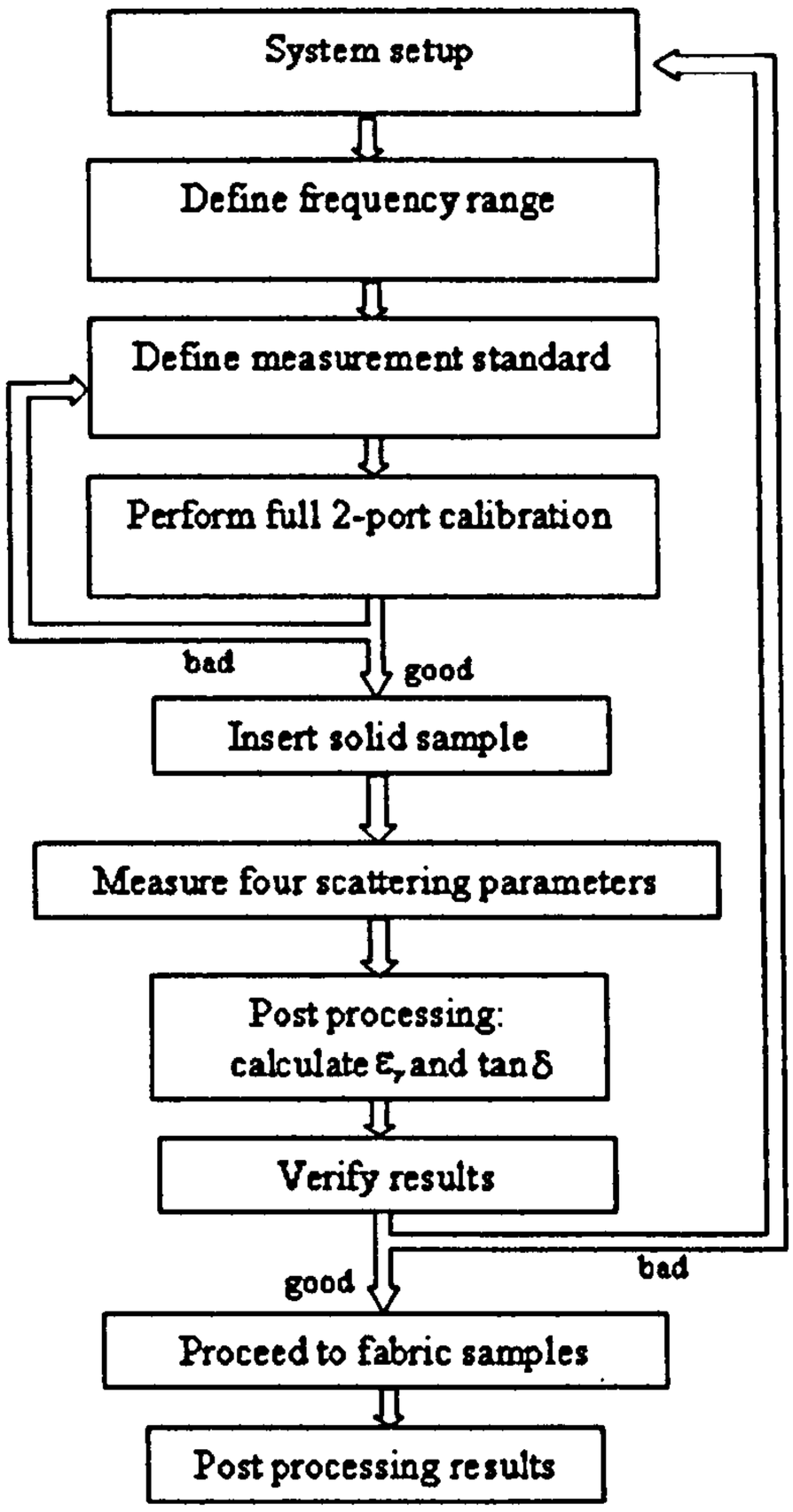

Figure 3.4 Measurement procedure of dielectric materials

In the process of measurement, a few sources of losses contribute to the total loss, like loss in the dielectric, loss in the metal walls, loss of power from the output and input coupling apertures and loss in the connecting cables. Therefore we must separate the dielectric loss from all of the others. Thus a high standard calibration is significant for the best accuracy and repeatability. For the measurement of S_{21} (ω), the full TRL (Through-Reflect-Line) 2-port calibration [11], which is convenient in that calibration standards can be fabricated for a specific measurement, is used. The detail of how TRL calibration works will be provided in appendix A. The advantage of TRL is that only three standards need to be characterized as opposed to 4 in the traditional open, short, load, and thru full 2-port calibrations. Further, the requirements for characterizing the T, R, and L standards are less stringent and these standards are more easily fabricated. The calibration standard can be evaluated by inserting the

empty sample holder, and checking the phase delay and the S_{21} magnitude along the frequency range. The phase delay at the centre frequency should be close to 90° because the length of the sample holder is about a quarter wavelength of the centre frequency, and the magnitude of the S_{21} should be close to zero. If the error of the empty cavity is serious, the calibration needs to be reprocessed until the standard can be met.

Solid samples were measured first to verify the accuracy of the system. As the dielectric properties of the material Perspex and PTFE are already well known, the measured results can be compared and the measurement system accuracy can be found. If the percentage error is big, the whole system setup needs to be checked again. Errors can be caused by imperfect cavity connection, bad quality cable, defective calibration, etc. Once the results of the solid materials are satisfied, the measurement can be proceeded to textile materials evaluation.

As we know that most of the fabrics have very low electric permittivity. To measure these kinds of materials within the waveguide, the transmission and reflection become very sensitive to noise and other effects. How to hold the sample in the sample holder as flat as possible is key to accurate the measurement. To resolve this, two samples of Rohacell foam layers (1mm each) which have a permittivity of 1.006 were used to hold the fabric samples into a sandwich shape. The Rohacell samples were measured with the system in advance, and the measured ε_r is equal to 1.0068, which has achieved a good agreement with the manufacture's specification. As the Rohacell sample is air like, the effect caused by those in the results can be ignored. Each fabric sample was also measured multi-layered by piling a few layers of samples together to check for systematic errors and make the measurement more accurate.

Conversion from S-parameter data measured by the HP8720D network analyzer to the dielectric properties was accomplished by reading trace data $S_{21}(\omega)$ into computer, performing the required calculations by integrating data into the conversion program (written by Dr. K.L. Ford) and then plotting the results into graphs. The permittivity derivation principle will be explained in Appendix B. The measured real and imaginary parts of the dielectric constant for each material are shown in Figure 3.5.

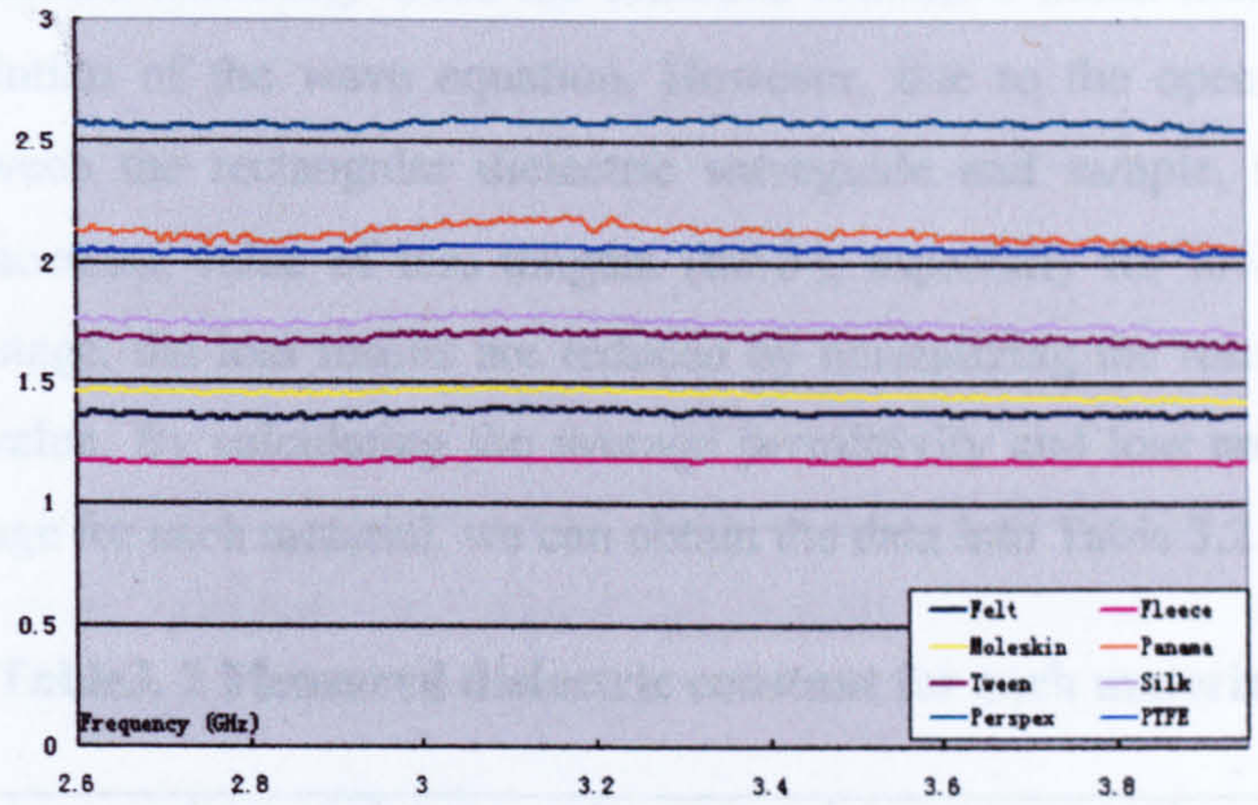

Real part

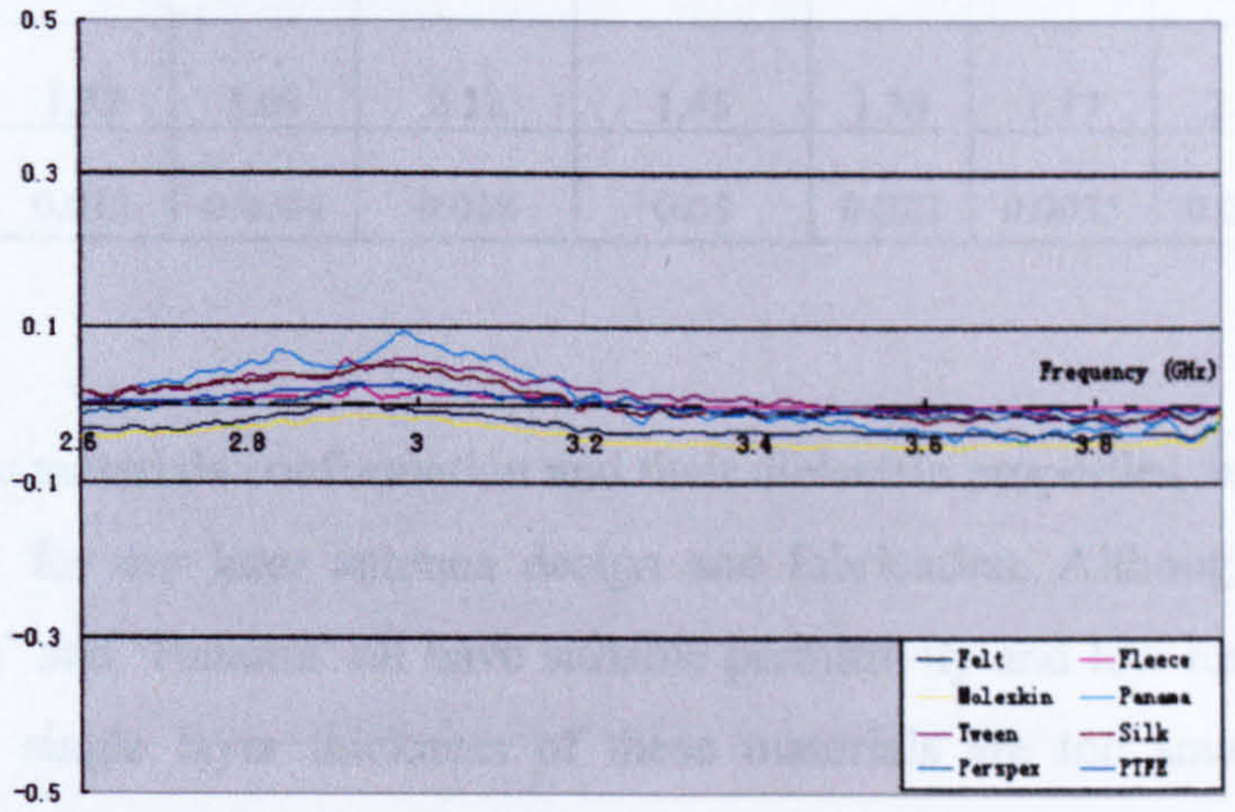

Imaginary part

Figure 3.5 Real & imaginary part of dielectric constant for textile & solid material

From the real part figures, we can clearly see most of the lines go stable and keep constant along the frequency range 2.6 to 3.95GHz. In order to prove the reliability of the measurement, we can take the Perspex and PTFE as samples. The measured permittivity for Perspex and PTFE are around 2.57 and 2.05 respectively, which are very close to the manufacture's specification (Perspex: 2.6, PTFE:2.08) around this band. For the imaginary part shown in Figure 3.5, noise has introduced some affects and finally formed the gain like prominence around 3GHz. Using this technique for the measurement of dielectric materials, the dielectric constant of the sample is

usually determined iteratively from the effective refractive index measurements by using the solution of the wave equation. However, due to the open discontinuity problem between the rectangular dielectric waveguide and sample, this technique cannot give accurate value of loss tangent ($\tan\delta$), especially for low-loss samples [10]. In this stage, the loss results are reduced by normalizing the results and taking the average value. By calculating the average permittivity and loss tangent over the frequency range for each material, we can obtain the data into Table 3.2.

Table3. 2 Measured dielectric constant for each material

Material	Silk	Tween	Panama	Moleskin	felt	fleece	PTFE	Perspex
Thickness(mm)	0.58	0.685	0.347	1.17	1.1	2.55	11.66	11.67
Permittivity	1.75	1.69	2.12	1.45	1.38	1.17	2.05	2.57
Loss tangent	0.012	0.0084	0.018	0.05	0.023	0.0035	0.0017	0.0008

Comparing the materials conformation and their dielectric properties, we have chosen material 'felt' for our later antenna design and fabrication. Although the material 'silk', 'Tween' and 'Panama' all have suitable permittivity and low loss for antennas substrate, the single layer thickness of these materials are too small for antenna fabrication. Furthermore, these materials are very soft, and softness is not preferable for on body application as it can cause a lot of problems like draping, being easily damaged and unsmooth integration with the conducting materials. The material 'fleece' is a common material for clothing, however the fleece tested in this project has a very loose structure. For wearable antennas, the substrate should have a smooth and firm surface and the conductive sheets can be fastened evenly and stoutly on the fabric. Therefore, fleece is not a good choice in this research. As for the material 'Moleskin', the component for this material is 100% cotton. However, for some reason, the loss factor for the material is relatively high, which is not preferable as well. Material 'felt' is another common material for our daily clothing. It is low cost and easy for fabricating. It has a firm, unelastic and smooth surface, and most importantly, the thickness and dielectric properties are all suitable for antenna applications.

3.3.3 Leather Materials

Leather is another material of interest as it is commonly used in our daily clothing, like coat, belt, bag, and shoes, etc. Leather materials generally have firm but flexible structures which are very suitable for wearable antennas application. Therefore, some leather materials as good potential antenna substrate were also studied in this project. Five leather samples are supplied by 'Andrew Muirhead & Son' Limited. The rectangular shape samples as shown in Figure 3.6 were tested with the Transmission/Reflection waveguide method.

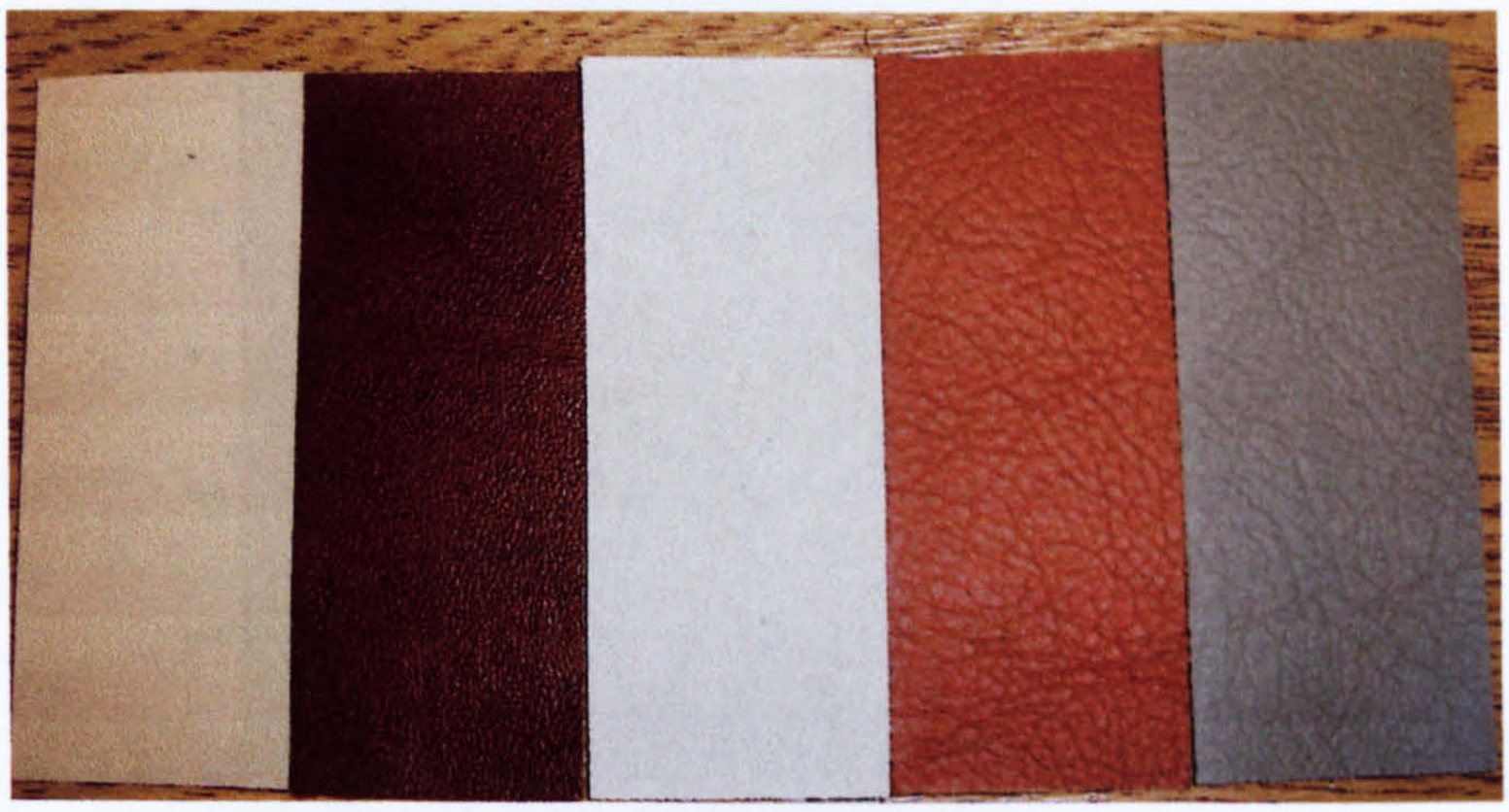

Figure 3.6 Leather samples under test

The measured relative permittivity and loss tangent of the five leather samples are plotted in Figure 3.7 coving the frequency band of 2.6 GHz to 3.95GHz. Compare to the textile materials, the leather materials tested have greater relative permittivity and much higher loss factor. The single layer thickness, as well as the predicted average dielectric constant of each sample is summarized in Table 3.3. Among these samples, leather 2 and leather 4 were selected for the later antenna's study, and the properties of these materials working as antenna substrate will be discussed in Chapter 4.

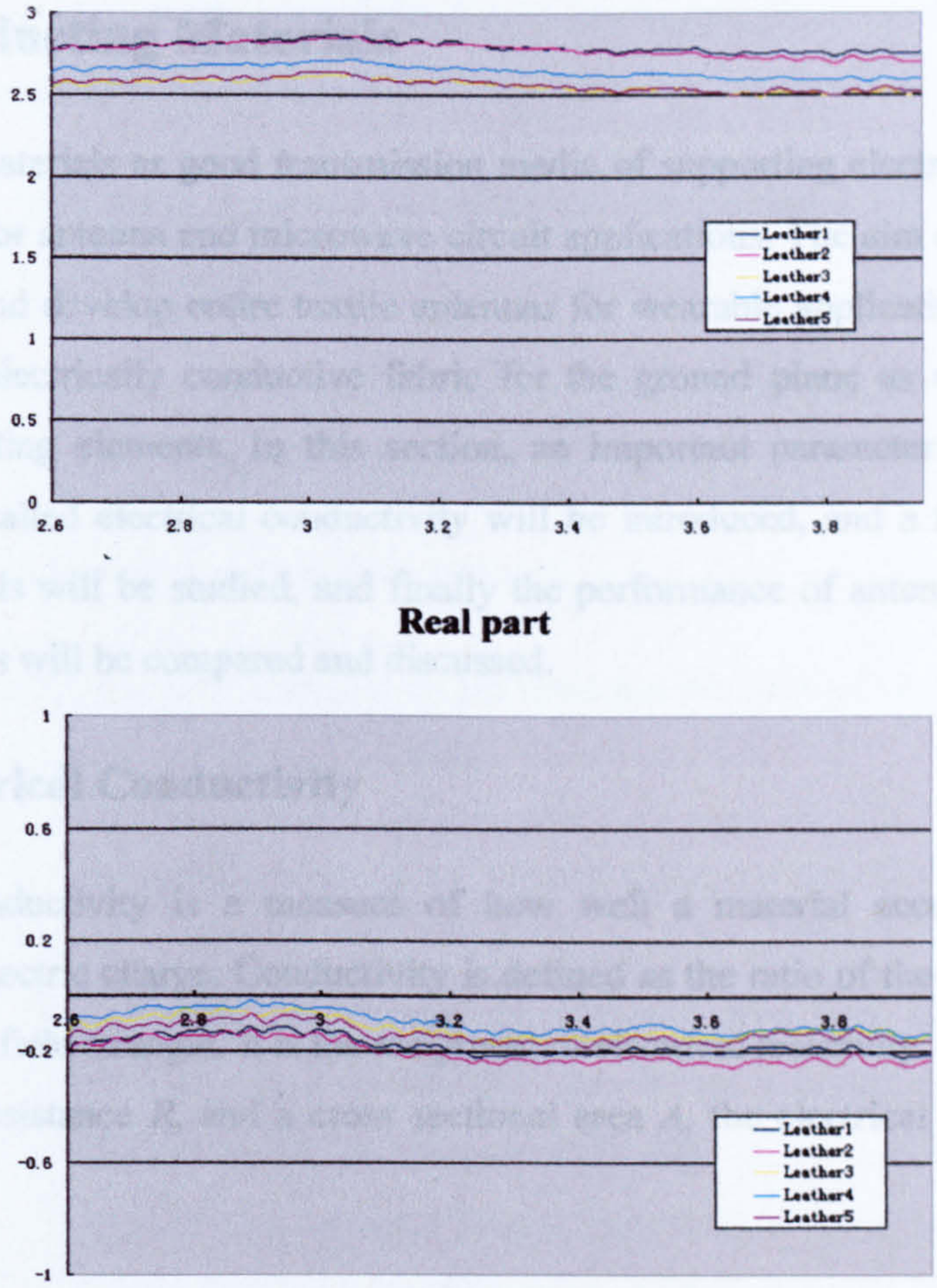

Real part

Imaginary part

Figure 3.7 Measured real & imaginary part for leather samples

Table3.3 Measured results for leather samples

	Leather1	Leather2	Leather3	Leather4	Leather5
Thickness (mm)	1.44	1.3867	1.30	1.39	1.43
Permittivity	2.79	2.78	2.56	2.65	2.57
Loss Tangent	0.063	0.073	0.045	0.035	0.051

3.4 Conducting Materials

Conducting materials as good transmission media of supporting electric current flow are essential for antenna and microwave circuit applications. The aim of this research is to design and develop entire textile antennas for wearable applications. Therefore, we need an electrically conductive fabric for the ground plane as well as for the antenna radiating elements. In this section, an important parameter of conducting materials so called electrical conductivity will be introduced, and a few conductive fabric materials will be studied, and finally the performance of antennas made from these materials will be compared and discussed.

3.4.1 Electrical Conductivity

Electrical conductivity is a measure of how well a material accommodates the transport of electric charge. Conductivity is defined as the ratio of the current density to the electric field strength. It is the reciprocal of electrical resistivity. For a specimen of length l, resistance R, and a cross sectional area A, the electrical conductivity is given by

$$\sigma = \frac{l}{RA} \tag{3-6}$$

The SI unit for conductivity is Siemens per meter (S/m). Most familiar conducting materials are metal based. For conducting materials, a higher conductivity indicates a better electric conductor. A perfect electric conductor (PEC) should have an infinite value of conductivity. However, PEC does not exist in the real life. A typical solid conductor, like copper, has a high conductivity of 5.9×10^7 S/m.

3.4.2 Conductive Fabrics Evaluation

Conducting textile materials have been widely used as a replacement of metal in many shielding applications. And opportunities have been found for high mechanical property conductive textiles to integrate within electromagnetic components such as antennas [12-13] and circuits.

For the purpose of a textile antenna design, a conductive fabric needs to satisfy the listed requirements below.

- A low and stable electrical resistance (≤1 ohm/square [13]) of the fabric is desired to minimize losses.

- The material must be homogeneous over the antenna area, and the variance of the resistance through the material should be small.

- The fabric should be flexible to be worn.

- The fabric should be inelastic, as the electrical property of elastic fabrics might change when stretching or bending.

To construct the conducting parts of an antenna using textiles, there is a variety of conducting fabric materials available. A few high quality conductive fabrics are tested in this research. These fabrics samples are obtained from Less EMF Inc. All the samples are metal based woven textiles but have different plated metallic materials. Most samples can satisfy the thickness, flexibility and most importantly low resistivity requirements of our antenna design. Therefore, three of the fabric samples and a metal material (laminated copper sheet) were fabricated with dielectric material 'felt' into antenna and the performance of these materials can be recognized. A return loss comparison of a dual-band CPW antenna using different materials with simulation (a conductivity of 5e+006S/m is defined for the conductors in simulation) is shown in Figure 3.8. For materials Shieldit and FlecTron-N, because of their relatively higher resistivity, large dispersion is generated over the desired frequency bands. In contrast to this, material Zelt shows a distinct high performance. The impedance is well matched at the desired resonant frequency. And the performance of the antenna made of Zelt is quite comparable to the antenna made of copper conductors.

Zelt has a high quality nylon based substrate and is plated with copper and tin. Its thickness is 0.06mm with a manufacturer's surface resistivity specification lower than 0.01ohm/square, which is excellent for creating efficient antennas and RF circuits at wireless communication frequencies. Also Zelt fabric is durable and tear resistant. From a manufacturing point of view, it can be cut using laser ablation into a precise

shape, also it can conform to any shape and be sewn like ordinary fabric to make highly effective clothing structures. Therefore, for all the antennas and structures used in this project, the woven conductive fabric, Zelt, is used.

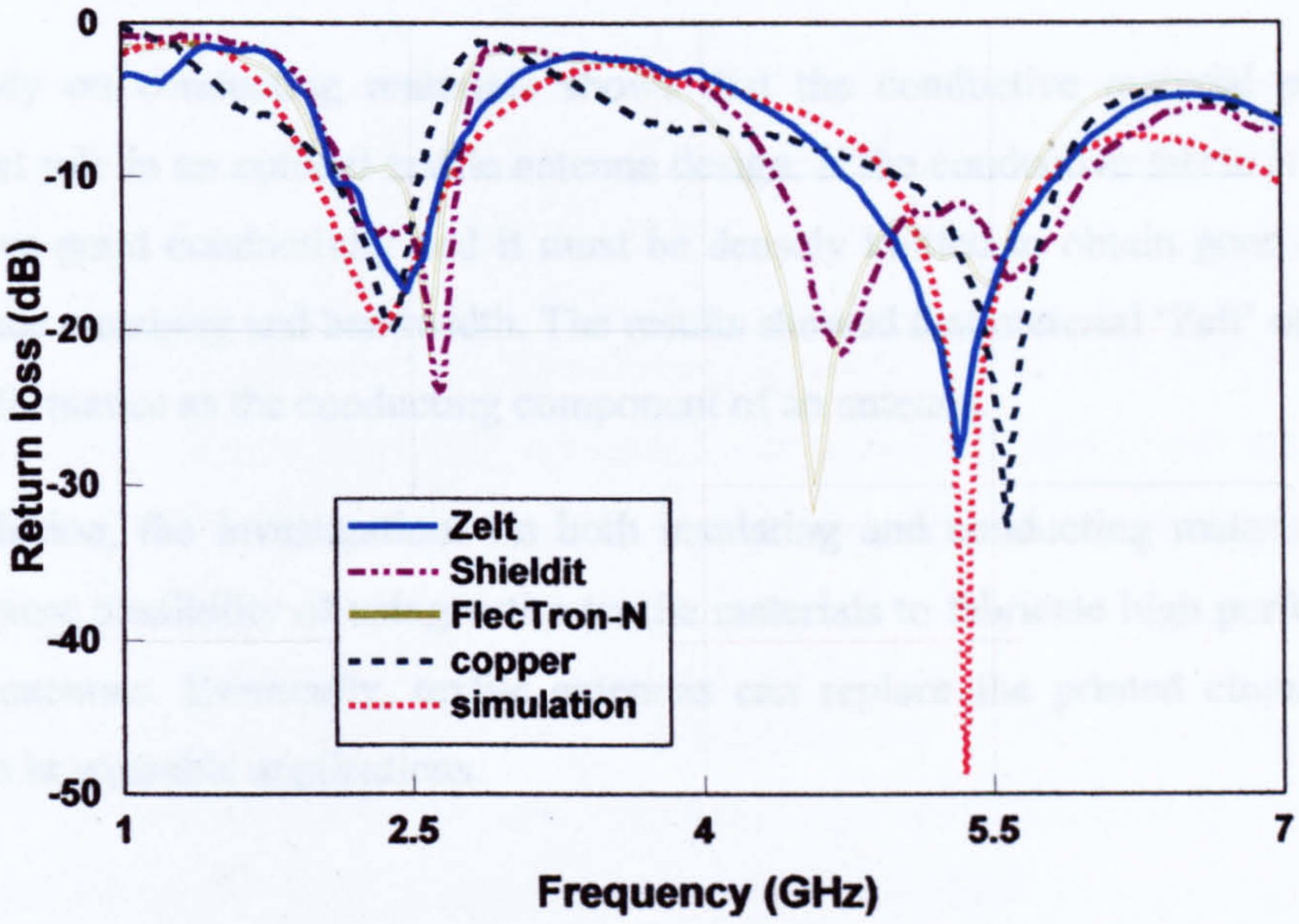

Figure 3.8 S_{11} results of antennas using different conductive materials

3.5 Conclusion

This chapter focused on characterizing the properties of a selection of textile and leather materials for the use of antenna substrates. A study was also carried out on the effects of different conductive materials on textile WLAN antenna performance.

The transmission/reflection waveguide method was mainly used for dielectric material characterization. Experiments have shown that this technique is superb for the measurement of the real part of the permittivity of solid materials, like fabric and leathers. However, it has shown some insufficiency of measuring the loss factor of the material. The measured results are fairly good and reliable. The errors are mainly caused by the noise generated by the system itself and also the imperfectly cut samples. But the overall results are acceptable for our future textile antennas design and fabrication.

It has been shown that a few dielectric materials in this study are suitable for antenna application. However, the physical properties of some materials might cause problems in order to maintain antenna's electrical performance parameters. Therefore, only the material 'felt' which has the optimum performance is chosen for our antenna design.

The study on conducting materials shows that the conductive material plays an important role in an optimal textile antenna design. If the conductive fabric is used, it must have good conductivity and it must be densely knitted to obtain good antenna impedance matching and bandwidth. The results showed that material 'Zelt' offers the best performance as the conducting component of an antenna.

In conclusion, the investigations on both insulating and conducting materials have shown great possibility of using entire textile materials to fabricate high performance textile antennas. Eventually, textile antennas can replace the printed circuit board antennas in wearable applications.

References:

[1] **Baber, C., et al.,** "A Wearable Computer for Paramedics: Studies in Model-Based, User-Centred and Industrial Design," *Interact'99*, pp.126-132, Sep 1999.

[2] **Salonen, P., Rahmat-Samii, Y., Schaffrath, M. and Kivikoski, M.,** "Effect of Textile Materials on Wearable Antenna Performance: A Case Study of GPS Antennas," *IEEE Antennas and Porpagation Society International Symposium,* Vol.1, pp.459-462, 2004.

[3] **Wong, T.C.P., Barnes, A., Chambers, B., Andenson, A.P. and Wright, P. V.,** "Microwave Characterization of Smart Materials Based on Conducting Polymer Composite Material," *IEE 10th International Conference on Antennas and Propagation (ICAP),* No.436, Vol. 1, pp.478-482. 1997.

[4] **Garg et al,** *Microstrip Antennas Design Handbook,* Artech House, Inc., 2001.

[5] **Inan, U.S. and Inan, A.S.,** *Electromagnetic Waves,* Prentice Hall, Inc., 2000.

[6] **Chen, L., Ong, C. K. and Tan, B. T. G.,** "Amendment of Cavity Perturbation Method for Permittivity Measurement of Extremely Low-loss Dielectrics," *IEEE Transactions on Instrumentation and Measurement,* Vol,48, No.6, pp.1031-1037, Dec 1999.

[7] **Kraszewski, A.W. and Nelson, S.O.,** "Observations on resonant cavity perturbation by dielectric objects," *IEEE Transactions on Microwave Theory Technology,* Vol.40, pp.151-155, Jan 1992.

[8] **Mosig, J. R., Besson, J-C. E., Gex-Fabry, M. and Gardiol, F.E.,** "Reflection of open-ended coaxial line and application to non-destructive measurement of materials," *IEEE Transactions on Instrumentation and Measurement,* Vol.IM-30, No.1, pp.46-51, 1981.

[9] **Baker-Jarvis, J., Janezic, M. D., Grovenor Jr, J. H. and Geyer, R.G.,** "Transmission/reflection and short-circuit line methods for measuring permittivity and permeability," NIST Technology, Note 1355, Dec 1993.

[10] **Chen, L.F., Ong, C.K, Neo, C.P. Varadan, V.V and Varadan V.K.,** *Microwave Electronics: Measurement and Materials Characterization,* Johan Wiley & Sons, Ltd, England, 2004.

[11] **HP8720 Network Analyzer menu.**

[12] **Salonen, P., Rahmat-Samii, Y, Hurme, H. and Kivikoski, M.,** "Effect of Conductive Material on Wearable Antenna Performance: A Case Study of WLAN Antennas," *IEEE Antennas and Porpagation Society International Symposium,* Vol.1, pp.455-458, 2004.

[13] **Locher, I., Klemm, M., Kirstein, T. and Troster, G.,** "Design and Characterization of Purely Textile Patch Antennas," *IEEE Transactions on Advanced Packaging,* Vol.29, No.4, pp.777-788, Nov 2006.

Chapter 4 Wearable Antennas Design

4.1 Introduction

Wearable antennas as an essential part of Body Area Networks have been studied in recent literature. Wu has presented a watch-type chip antenna [1] for Bluetooth devices. Sanz has promoted a wide range of button antennas for WLAN [2], [3] and UWB [4] applications. Wearable dipoles [5] and PIFAs [6] have also been studied. And most attractively, textile antennas together with the embedded body-worn system as a new concept of smart clothes have been popularly investigated. Comparing with all the other types of antennas, textile antennas can fulfil the special requests for wearable application, like light weight, low cost and can be integrated with our daily clothing.

Textile antennas have been presented in [7]-[10]. Effects of different conductive and dielectric textile materials have also been studied in [11] and [12]. Several papers have reported single frequency band wearable antennas [7] and [13]-[14] demonstrating acceptable performance at low cost. Later dual frequency band designs have emerged allowing network connection [15], [16].

This project aims to investigate the possibility of integrating low profile antennas with our daily clothing materials, like textile or leather, and study the performance of the antenna with the presence of the human body. Therefore, wearable antenna design is an essential part of this research. In this chapter, a few designs of wearable antennas for dual-band and multi-band applications will be presented. For the proposed antennas, only planar structures are chosen, as for wearable applications, using planar structures not only eases the antenna design but also simplifies the integration of the antennas with cloth. And using a strip line feed can guarantee a flat structure, and allow the assembly of electronic components directly on the fabric in antenna application.

A new design of dual-band coplanar waveguide fed antenna fabricated with the high quality conductive fabric 'Zelt' and the textile material 'Felt' will be presented in the

second part of this chapter, The antenna is modelled and compared with the same design of a printed circuit board antenna on FR4 material. Also, the same type of CPW antennas are designed and fabricated with selected leather materials. Antenna performance with different materials will be compared and discussed at the end of the section.

In the third section, a dual band triangle patch antenna with a parasitic element over a modified small ground plane will be presented. The antenna operates at WLAN bands with bandwidths exceeding 20% at the 2.45 GHz and 5 GHz network bands. The ground is modified by cutting a large rectangular slot in it that allows tuning of the frequency bands and adjustment of the band spacing ratio.

Finally, a multi-band hexagon ring fabric antenna will be introduced. The antenna also has a CPW feed structure. It is designed to cover the GSM (890-960MHz), DCS/PCS (1710-1990MHz), UMTS (1.88-2.20GHz) and WLAN (2.40-2.48GHz & 5.15-5.825GHz) bands. The geometry of the antenna is described together with the return loss and radiation patterns at the main operating bands.

4.2 Dual-band CPW-fed Antennas

4.2.1 Dual-band felt CPW Antenna at WLAN Bands

As explained above, the textile materials and the planar antenna shape provide a smooth integration into clothing and preserving the typical properties of textiles. In this project, we manage to design and study a novel dual band antenna [17] that can be worn within clothing covering 2.45GHz and 5.8GHz wireless networking bands. The antenna is a CPW fed rectangular shape patch. The substrate material used for this antenna is felt with a thickness of 1.1mm, whose dielectric properties have been measured by the method explained in chapter 3. The conducting components, coplanar feed line, patch antenna and ground plane, are manufactured from the woven conducting fabric 'Zelt', as we described before, it has a conductivity around 1e+006S/m. The antenna was constructed by cutting the conductive material accurately using laser ablation.

The antenna is a novel coplanar design consisting of an inner patch surrounded by a parasitic rectangular ring element with another outer rectangular ring connected as the ground, as shown in Figure 4.1a (top view) and b (side view). Main dimensions of the antenna are listed in Table 4-1. The antenna construction is based on a coplanar strip line feeding into a rectangular patch. The strip line width and the gap between the transmission line and the coplanar ground are adjusted to match the real coaxial cable impedance.

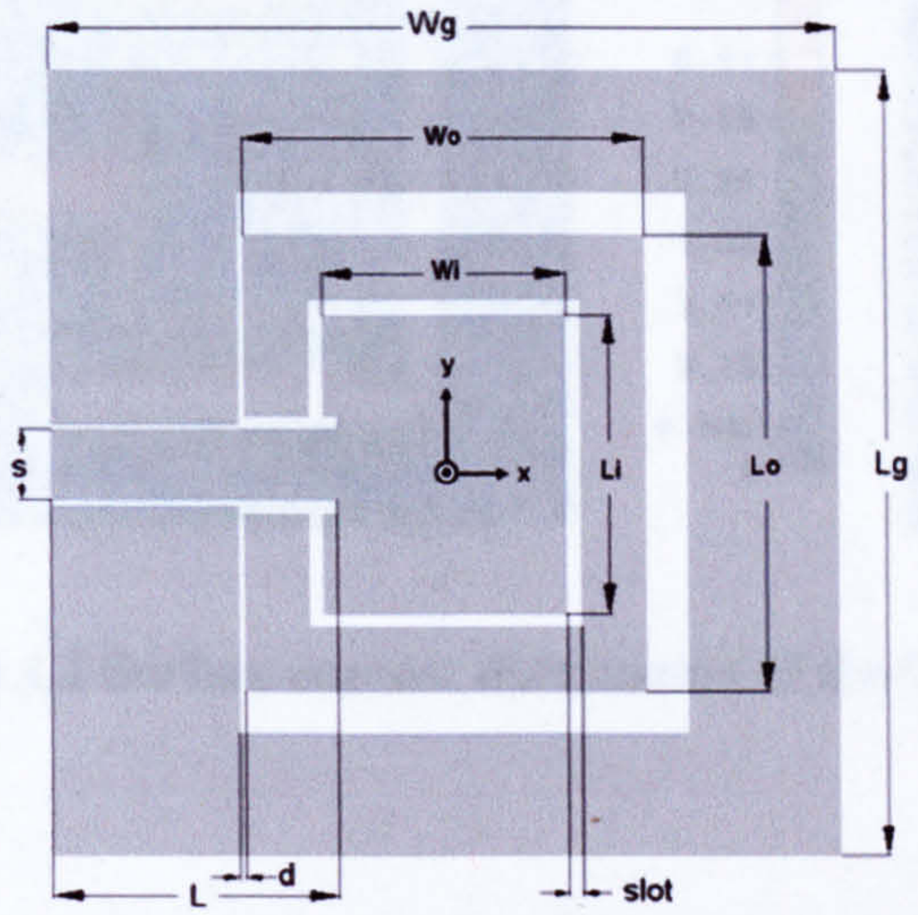

(a) Top view

Parameters	Value (mm)
Lg, Wg	55
Lo	32
Wo	28
Li	21
Wi	17
s	5

Table 4-1. Antenna dimensions

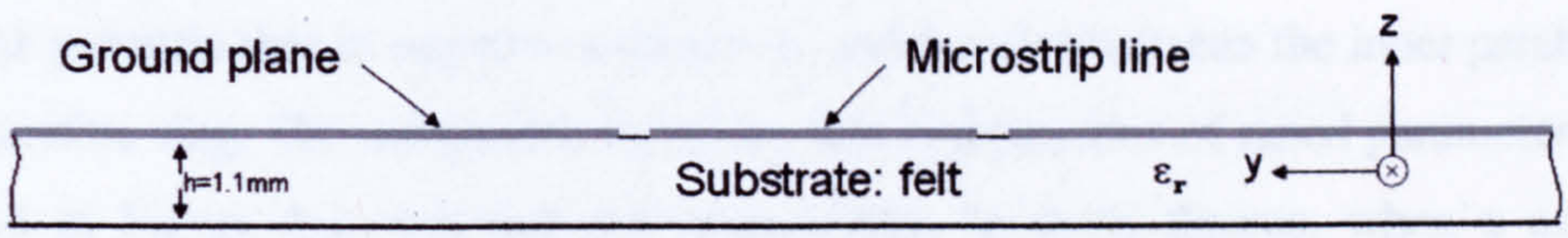

(b) Side view

Figure 4.1 Dual band CPW-fed fabric antenna geometry

The simulation was carried out by CST Microwave Studio. It is found that the upper and the lower band position are mainly controlled by the size of the patch itself and the size of the parasitic ring. The lower resonance at 2.45 GHz is largely due to the inner patch plus parasitic antenna ring while the patch alone provides the upper resonance. Figure 4.2 shows the computed surface current distribution of the antenna for both resonances. The maximum current is clamped at 10 Amperes per meter so that the distribution at both frequencies can be compared. It is evident that the current

concentrates at the strip line and the outer edges of the parasitic ring at the lower resonance 2.45GHz, while the current flows between the inner patch and the parasitic ring at 5.8GHz.

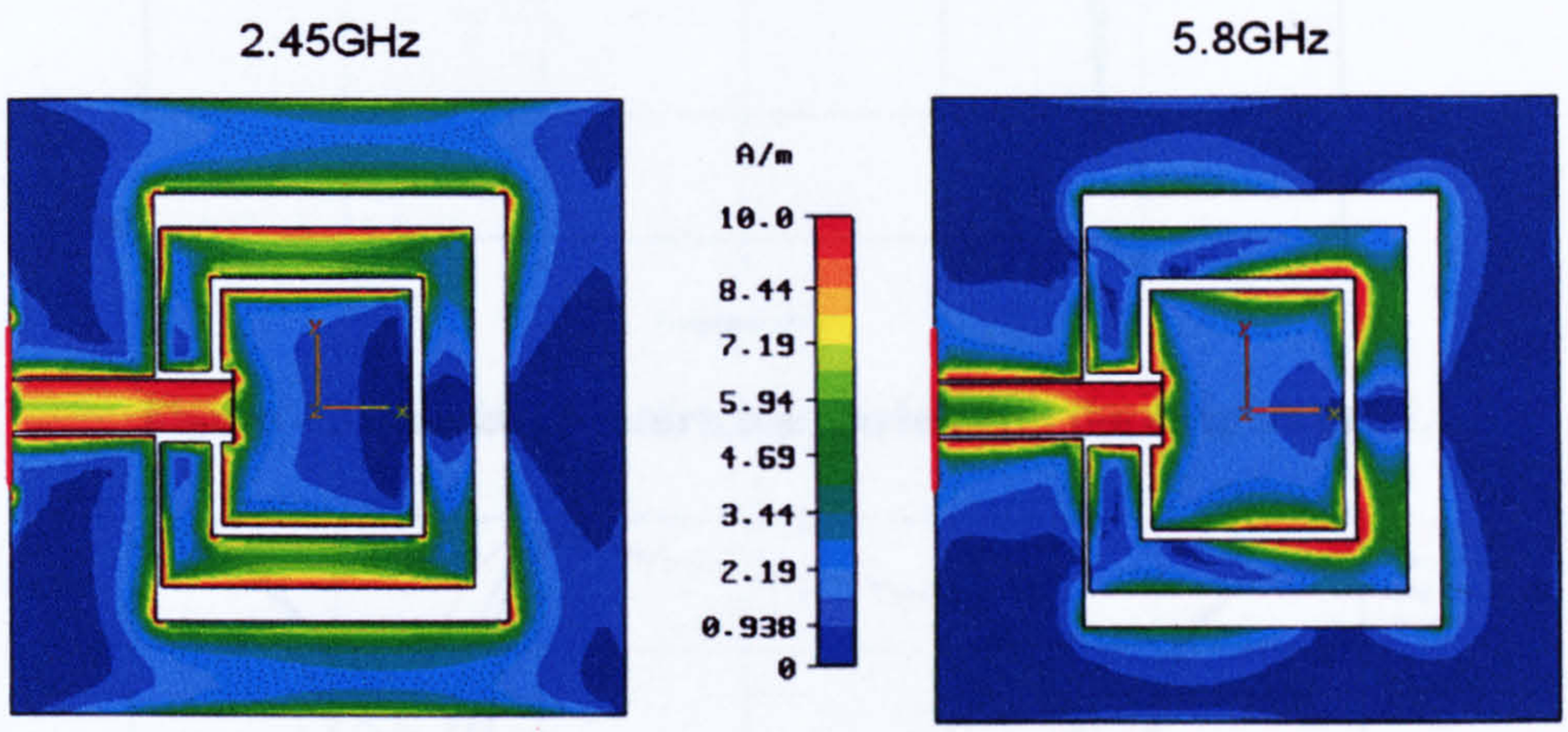

Figure 4.2 Surface current distribution of the CPW antenna at 2.45 & 5.8GHz

Other factors have been found that may change the antenna impedance matching performance significantly are the strip line length **L**, the gap **d** between the ground and the parasitic ring in negative x direction, and the **slot** between the inner patch and the parasitic ring. The computational return loss comparisons of tuned parameters are plotted in Figure 4.3, 4.4, and 4.5 respectively. In these figures, when a certain dimension parameter is varying, other parameters are fixed. Therefore we can see how much effect this dimension can cause on the antenna performance. Also study has found the shape of the coplanar ground plane has a significant influence on antenna performance as well. Three types of ground planes are studied and compared in Figure 4.6, in which block ground indicates two rectangular block grounds on each side of the strip line.

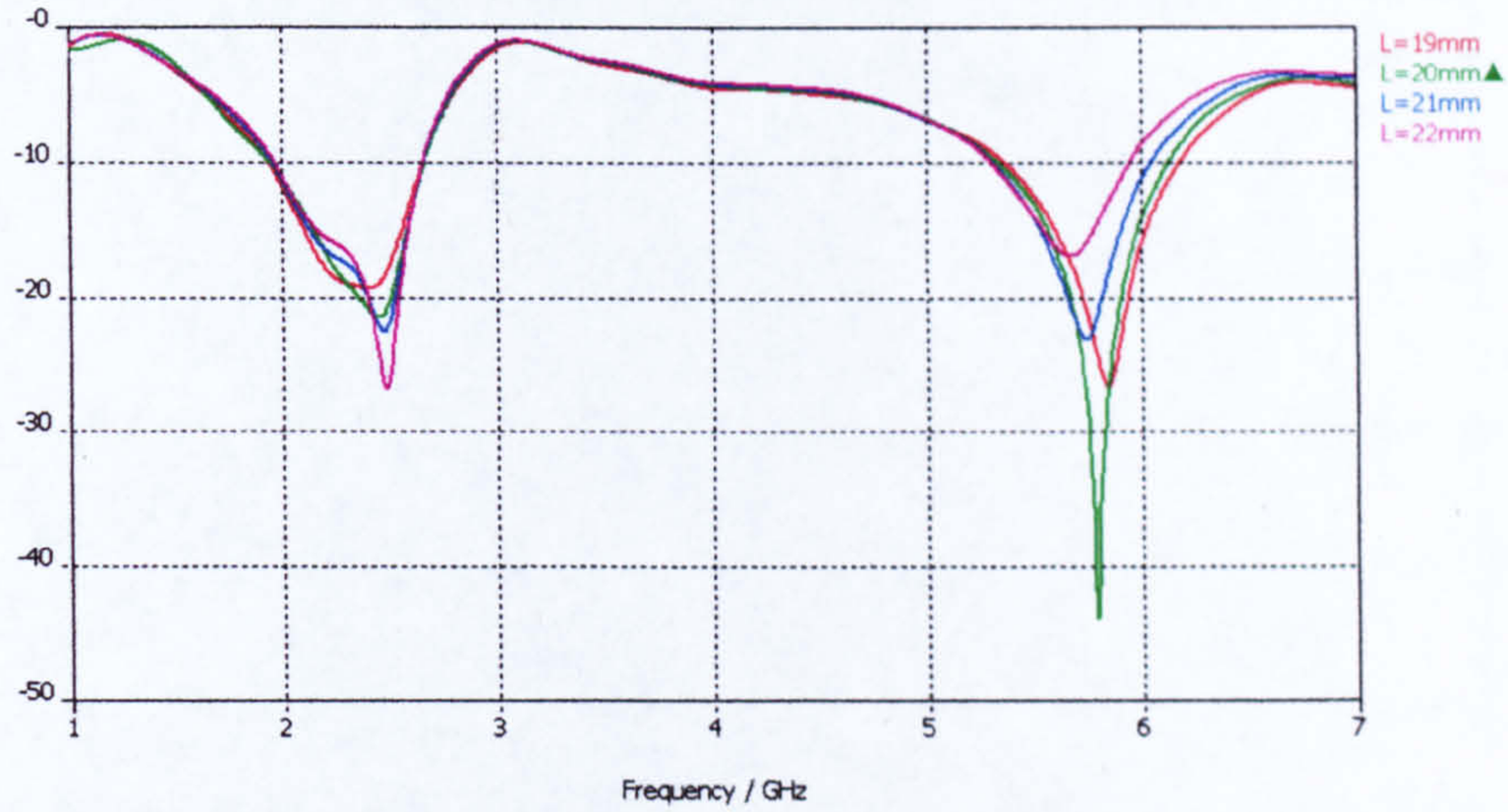

Figure 4.3 Simulated return loss varies with the strip length L

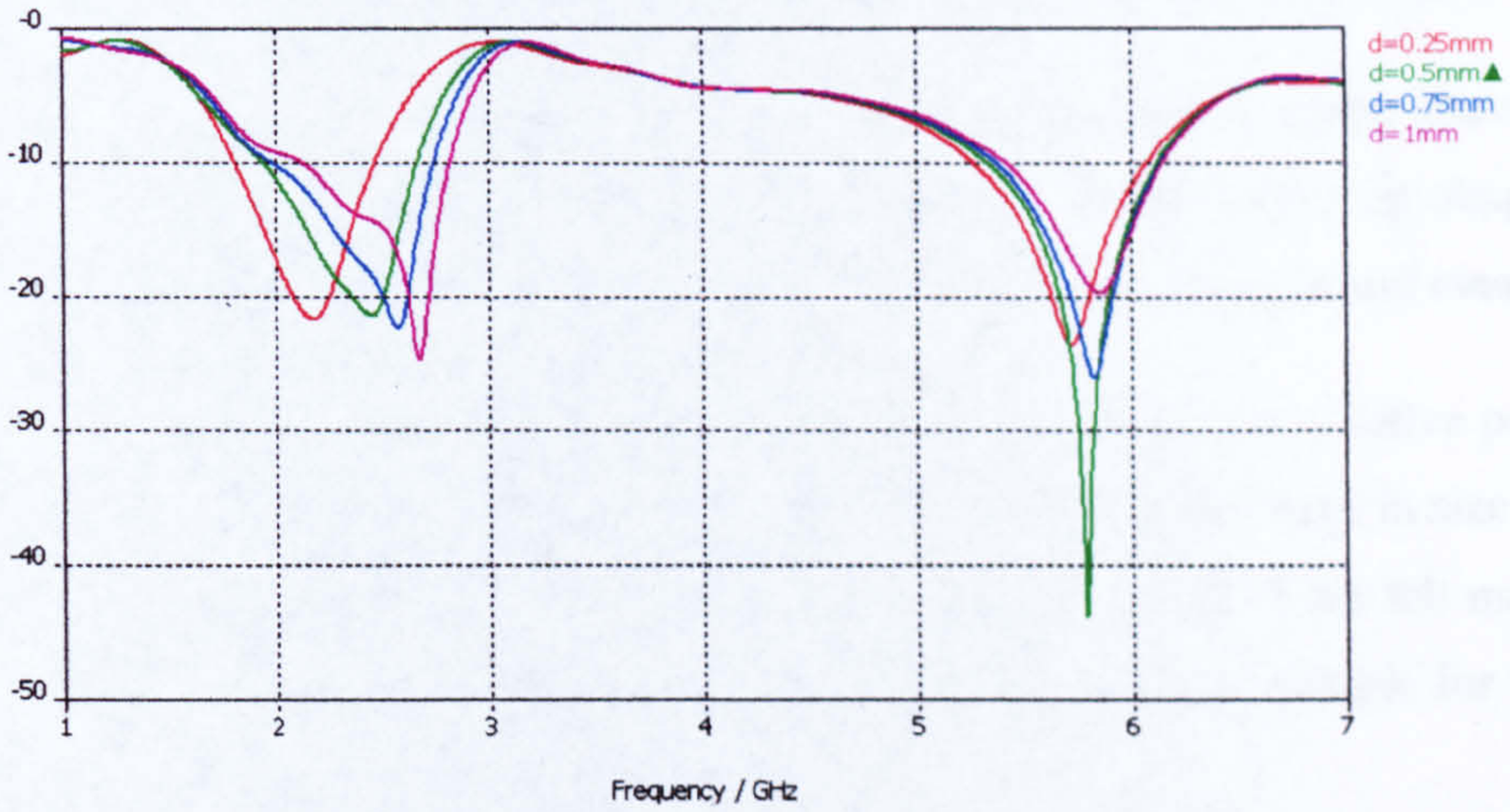

Figure 4.4 Simulated return loss varies with gap width d

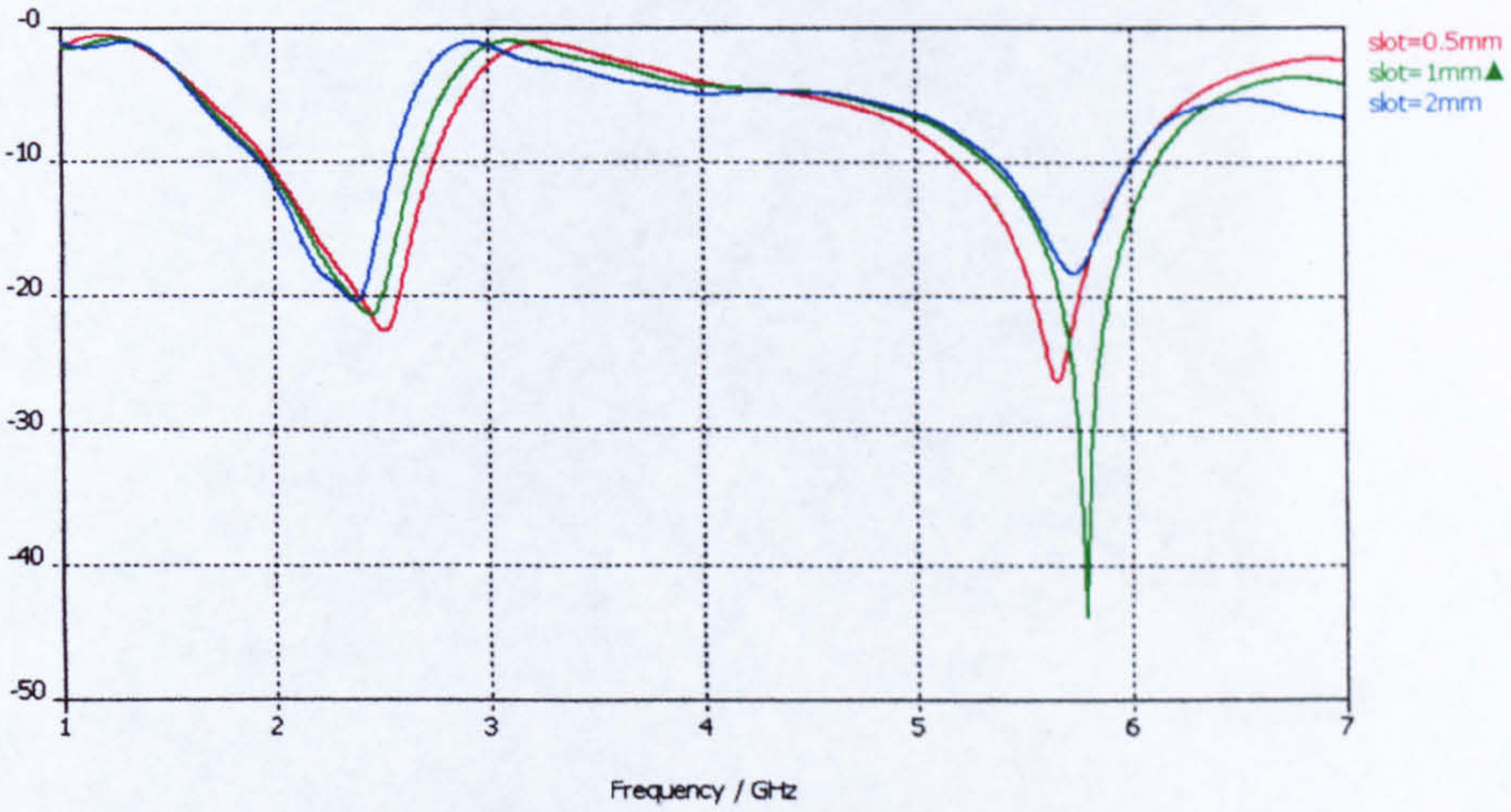

Figure 4.5 Simulated return loss varies with the slot between the patch and the parasitic ring

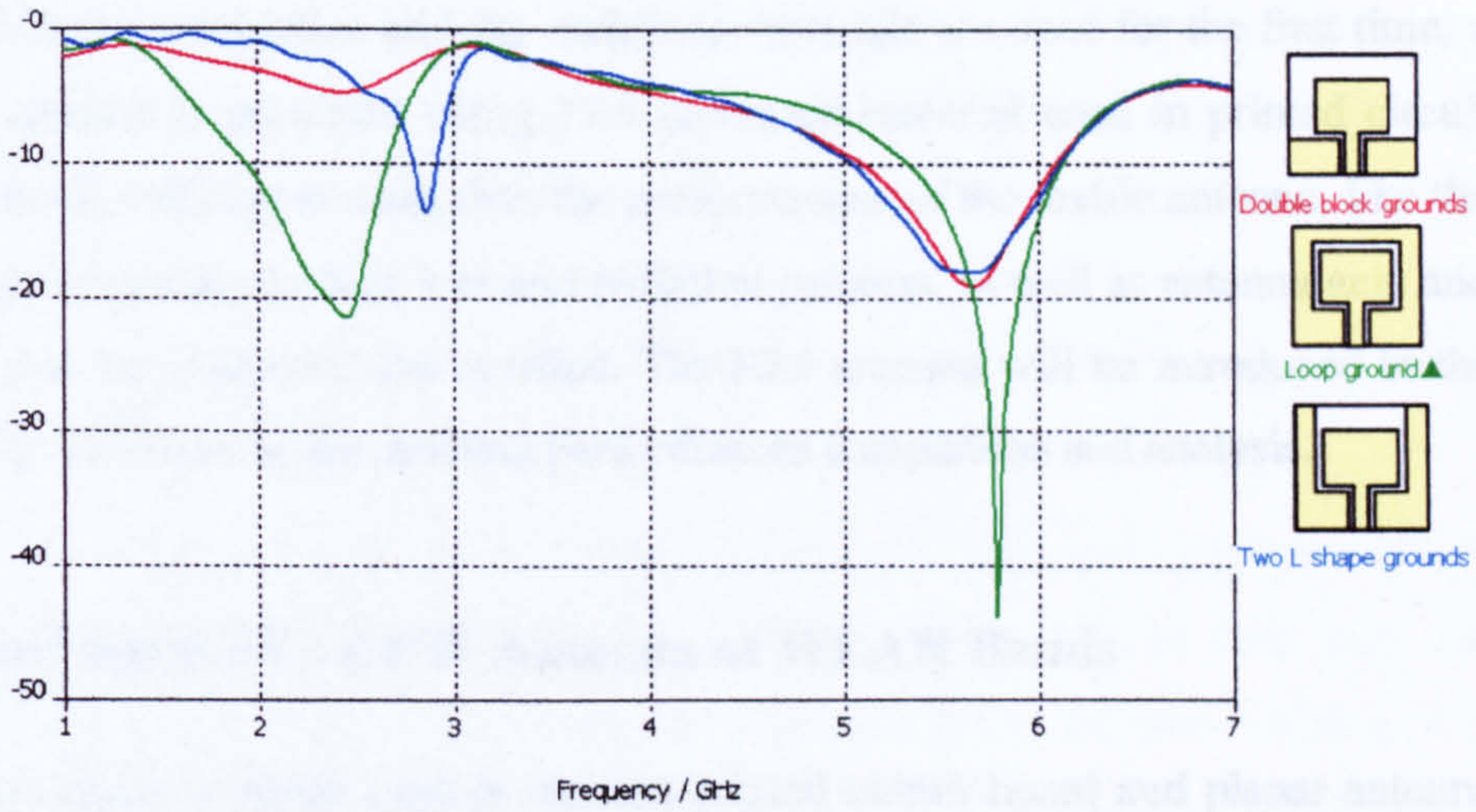

Figure 4.6 Simulated return loss varies with the shape of the ground

The optimum options for each parameter were marked in each figure above, and the values correspondingly are L=20mm, d=0.5mm, slot=1mm and loop shape ground plane, which are the parameters we used for the antenna fabrication and measurement.

A fabricated antenna is shown in Figure 4.7. Because of the low relative permittivity of textile materials, antennas made out of fabrics are generally large in size. However with the coplanar structure and the relatively small thickness of the felt material, the antenna has achieved a compact size of $55\times55mm^2$, which is suitable for wearing at most locations on human body.

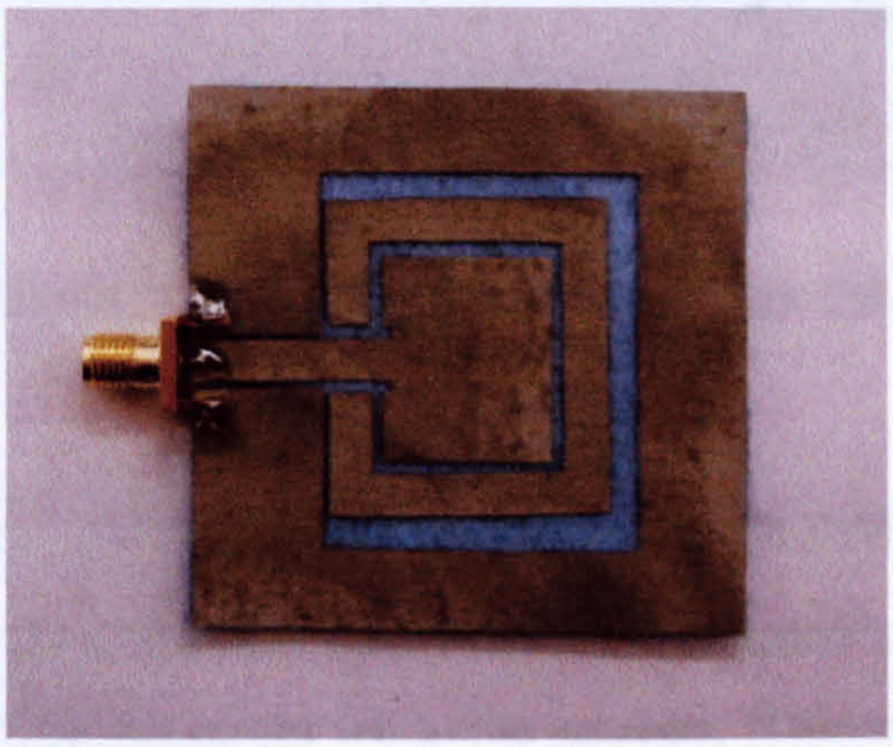

Figure 4.7 A dual-band coplanar textile antenna

Overall size: 55x55 mm^2

Substrate: 1.1mm felt, permittivity=1.38 Loss tangent=0.023

Because both the conductive and the dielectric materials are used for the first time, a reference antenna is produced using FR4 (common material used in printed circuit board) material and copper coat, thus the performances of the textile antenna, like the simulated and measured return loss and radiation patterns, as well as antenna gain and efficiency can be compared and verified. The FR4 antenna will be introduced in the next section, followed by the antenna performances comparison and analysis.

4.2.2 Dual-band FR4 CPW Antenna at WLAN Bands

FR4 is a common material used in modern printed circuit board and planar antenna fabrications. Therefore, a dual band FR4 CPW antenna working at WLAN bands was designed as a reference antenna to the fabric antenna. The FR4 material has an electric permittivity of 4.5 and thickness of 1.6mm. It is topped with a very thin layer of copper as the conductive elements. The design procedure followed that of the fabric antennas. Figure 4.8 shows the prototype of the FR4 antenna.

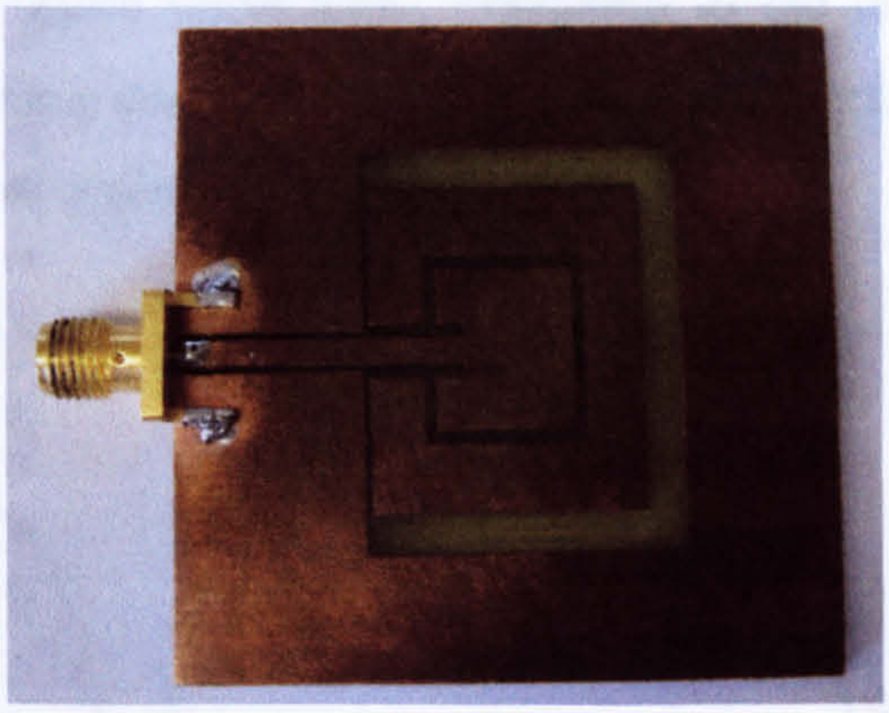

Figure 4.8 Geometry of dual-band coplanar FR4 antenna

Overall size 50x50 mm^2

Substrate: 1.6mm FR4, permittivity=4.5 Loss tangent=0.025

Return loss can be regarded as the ratio between the power reflected back from the antenna feeding point and the power fed to the antenna. If the entire power is reflected back, S_{11} will be 0dB. While if the power is completely absorbed and radiated by the antenna, the value will be -∞dB. A low return loss value corresponds to a good matching at a particular frequency. In this research, a -10dB S_{11} value is referred as a

standard for antenna design, which indicates a 10% power reflection. Frequency bands where the S_{11} is lower than -10dB are considered as the impedance matching band. The bandwidth is calculated by

$$BW = \frac{F_{upper} - F_{lower}}{F_{center}} \times 100\% \tag{4-1}$$

Simulated and measured return losses for both antennas are shown in Figure 4.9. It can be seen from the figure that the overall measurements agree well with the simulation results. However, at 2.45GHz, the measured fabric antenna differs a little from the simulation band. This is mainly because of the first resonance is dominated by the parasitic element. The imperfect manufacture may cause the element position to vary. Also the small percentage of error that might occur in the material measurement could cause the uncertainty of the material parameters. Table 4-2 summarizes the detailed results in terms of resonance frequency and input-match bandwidth for both antennas. Wide bandwidth has been achieved for both antennas at each frequency band. More importantly, compared to the reference FR4 material antenna, the fabric antenna demonstrates quite comparable performance, which shows good potential for future applications.

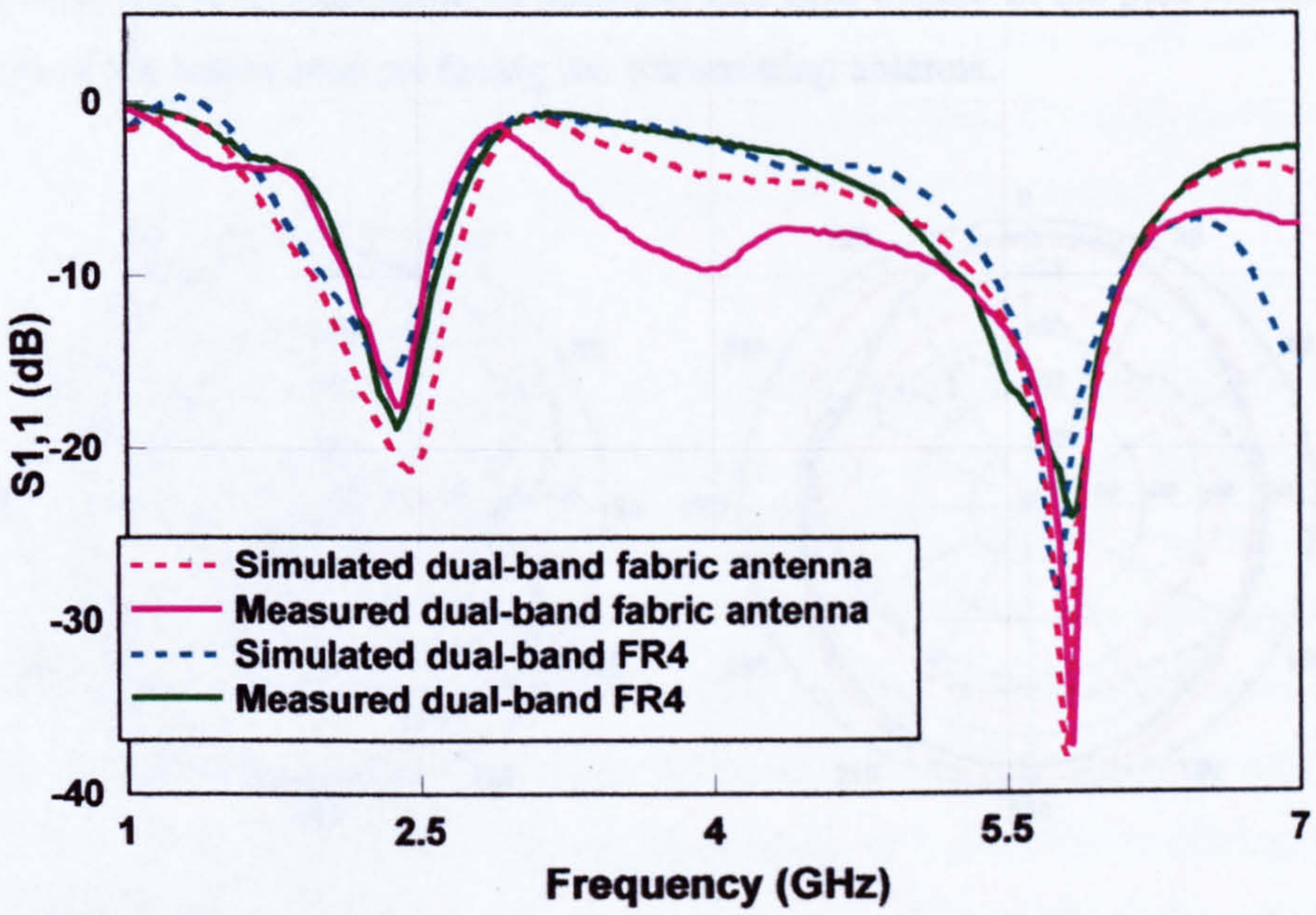

Figure 4.9 Simulated and measured return loss comparison

Table 4-2 Simulated and measured antenna resonant frequency and bandwidth

Antenna	Size	2.45GHz band & bandwidth		5GHz band & bandwidth	
		Simulation	Measurement	Simulation	Measurement
Fabric antenna	$55 \times 55 mm^2$	1.95-2.65GHz (28.6%)	2.12-2.54GHz (17%)	5.35-6.1GHz (13.6%)	5.15-6.1GHz (17.3%)
FR4 antenna	$50 \times 50 mm^2$	2.02-2.53GHz (20.8%)	2.14-2.59GHz (18.4%)	5.44-6.1GHz (12%)	5.26-6.13GHz (15.8%)

A radiation pattern shows the variation of the radiated far-field intensity of an antenna as an angular function at a specific frequency. Typically, they are shown as cuts along the XZ (principle E-plane) and YZ plane (principle H-plane) according to the coordinate system given in Figure 4.1. The measured radiation patterns of the fabric antenna and the FR4 antenna at 2.45GHz and 5.8GHz are shown in Figure 4.10, in which the solid lines refer to co-polarization and the dotted lines indicate the cross-polarization for each cutting plane. The measurement is carried out in the anechoic chamber. The location of the antenna at the centre of the turning table ensures that the pattern obtained is as symmetric as possible, and zero degree in the plot indicates the direction of the tested antenna facing the transmitting antenna.

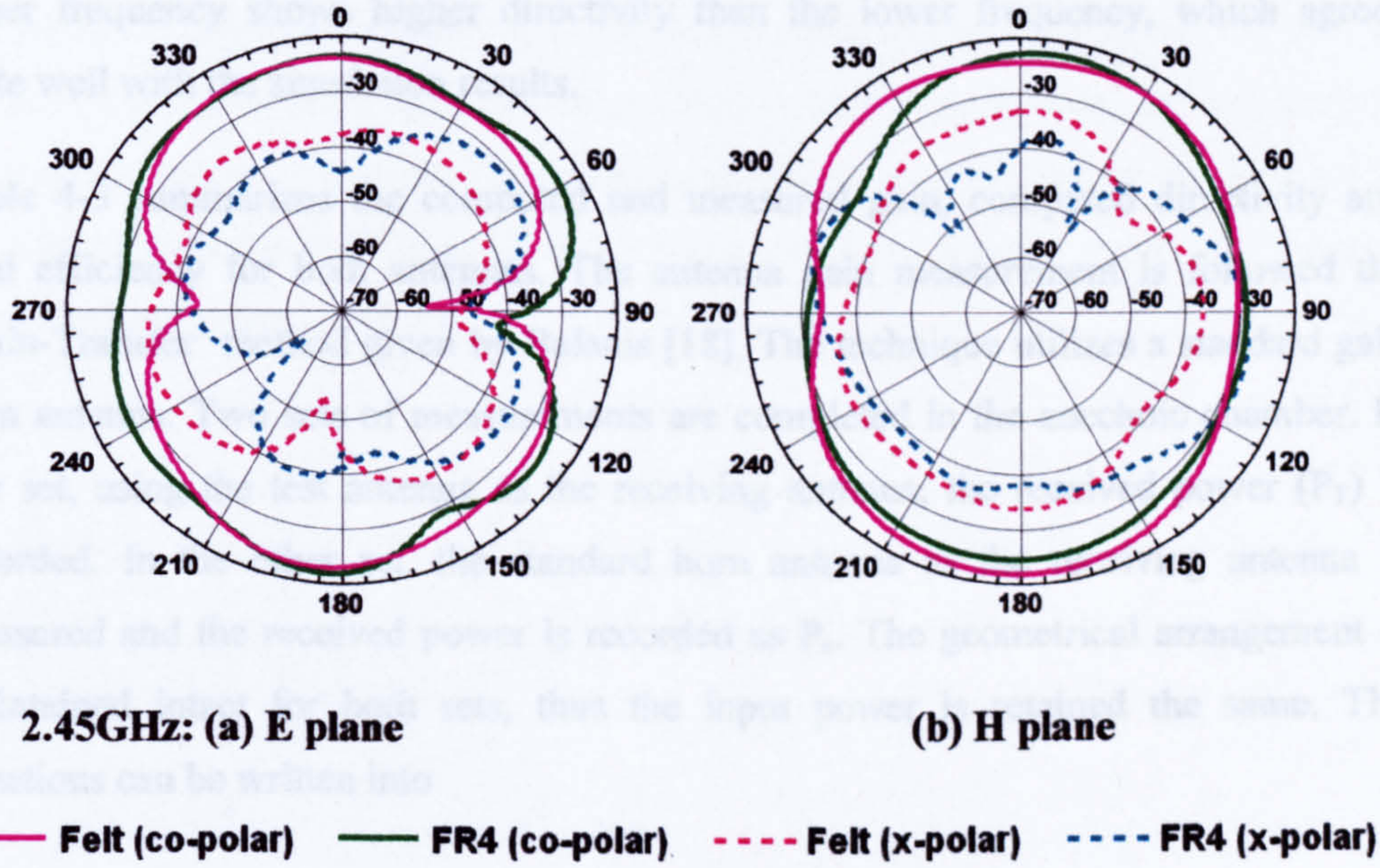

2.45GHz: (a) E plane **(b) H plane**

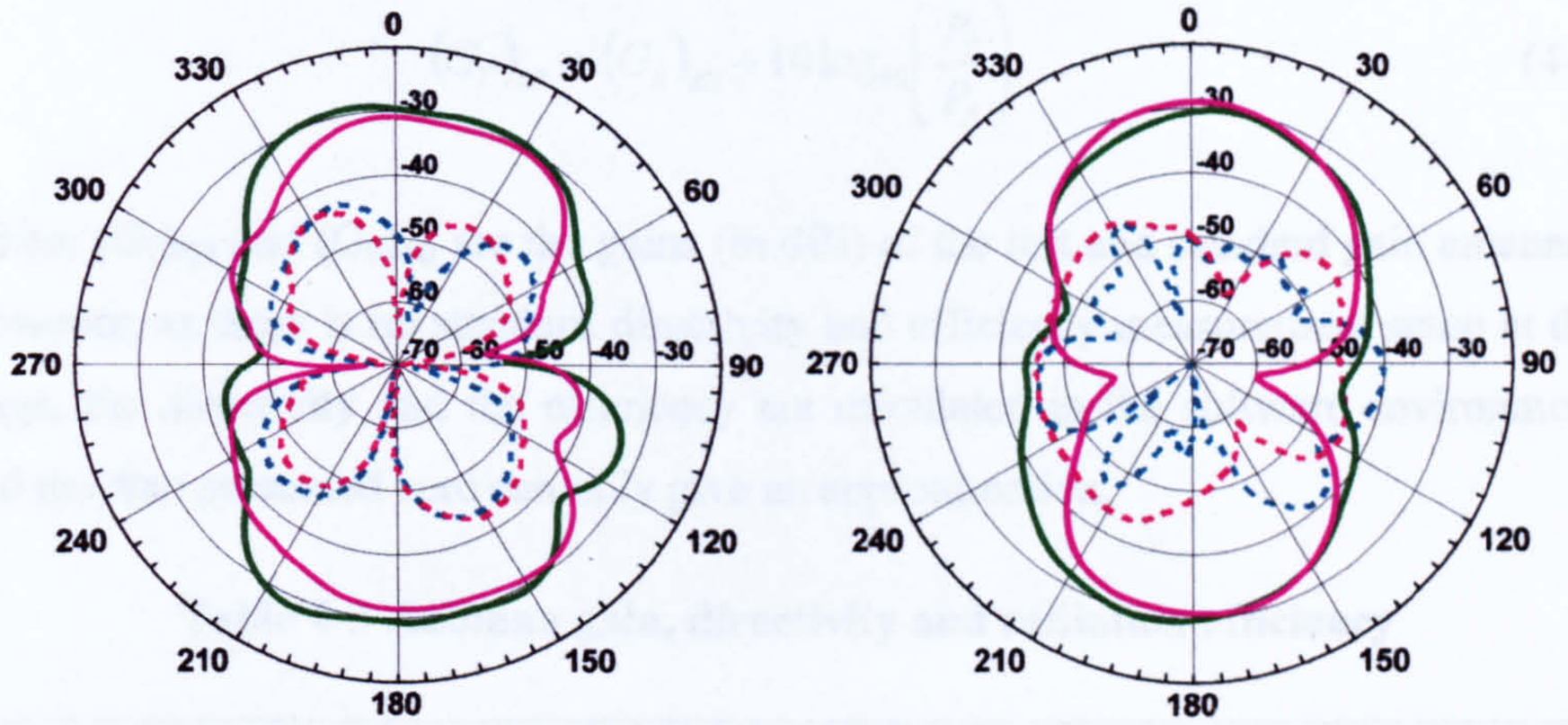

5.8GHz: (a) E plane **(b) H plane**

Figure 4.10 Measured radiation patterns for dual band fabric and FR4 antenna

From the figure we can see, the CPW antenna has a dipole like radiation characteristics. For both frequencies, the peak radiation intensity lies towards the front or back direction perpendicular to the patch surface. The slight asymmetry of the E-plane patterns is caused by the feed lines connected to one of the radiating edges of the antennas, also the effect of the connector and cable connection on one side of the antenna during the measurement. According to the patterns, the fabric antenna demonstrates a great similarity as comparing to the FR4 antenna, which indicates the high qualities of the conductive and the dielectric materials. For both antennas, the upper frequency shows higher directivity than the lower frequency, which agrees quite well with the simulation results.

Table 4-3 summarizes the computed and measured gain, computed directivity and total efficiency for both antennas. The antenna gain measurement is followed the 'Gain-Transfer' method given by Balanis [18]. The technique utilizes a standard gain horn antenna. Two sets of measurements are completed in the anechoic chamber. In one set, using the test antenna as the receiving antenna, the received power (P_T) is recorded. In the other set, the standard horn antenna as the receiving antenna is measured and the received power is recorded as P_s. The geometrical arrangement is maintained intact for both sets, thus the input power is retained the same. The equations can be written into

$$(G_T)_{dB} = (G_S)_{dB} + 10\log_{10}\left(\frac{P_T}{P_S}\right) \quad (4\text{-}2)$$

Where $(G_T)_{dB}$ and $(G_S)_{dB}$ are the gains (in dBi) of the test and standard gain antennas. However, as there is no standard directivity and efficiency measurement setup at this stage, the directivity and the efficiency are calculated in the software environment, and the data presented here can only give an approximation.

Table 4-3 Antenna gain, directivity and radiation efficiency

Antenna	Frequency (GHz)	Simulated Gain (dBi)	Measured Gain (dBi)	Directivity (dB)	Total efficiency
Standard Horn antenna	2.45		10.3		
	5.8		11.5		
Dual-band CPW felt antenna	2.45	3.77	3.87	4.018	93.8%
	5.8	5.87	5.177	6.398	88.6%
Dual-band FR4 antenna	2.45	3.40	3.889	3.91	86%
	5.8	4.66	5.026	5.73	78%

4.2.3 Dual-band Leather Antenna

Leather is another common used material for clothes, belts, shoes and bags. The idea of making an antenna with leather is that the antenna can be built within the belt, as human waist is one of the least movement parts over the whole body, the belt antenna can benefit from the very less distortion and interference. Also, due to the firmness of the leather material itself, the leather antenna can have a more stable performance compared to the fabric antenna.

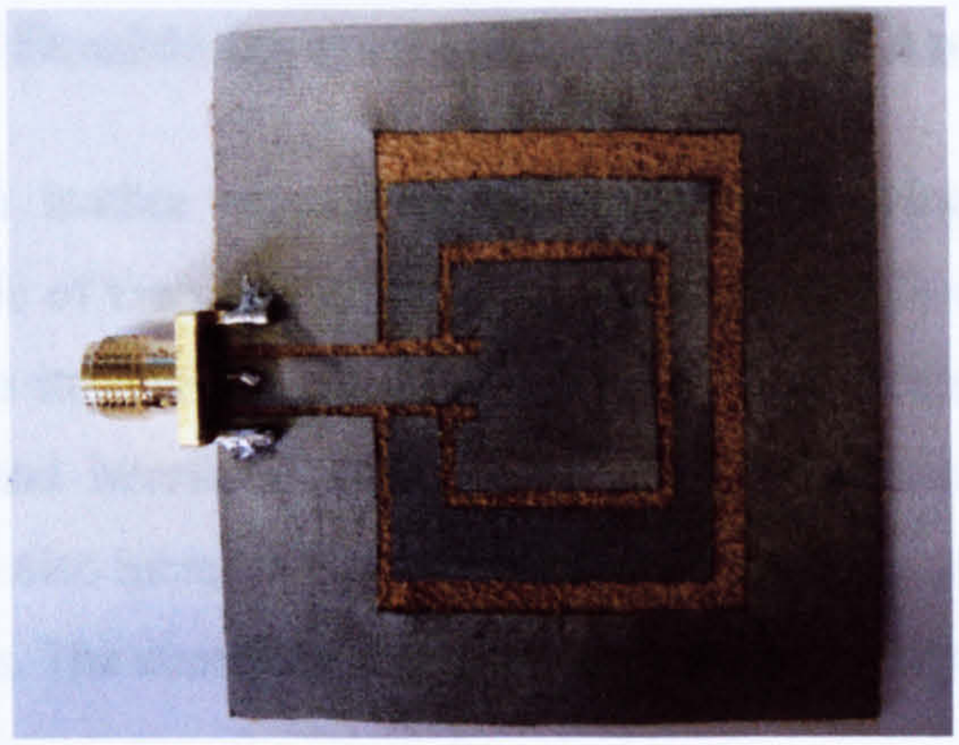

Figure 4.11 Geometry of dual-band coplanar leather antenna

Overall size: $50\times50\times1.38\ mm^3$, **parasitic ring size:** $24\times28mm^2$

Inner patch size: $15\times16mm^2$, **strip width:** 4mm

Substrate: Leather, Permittivity: 2.78, Loss tangent: 0.07

A dual-band coplanar leather antenna is designed. The antenna substrate is a leather sample from Andrew Muirhead & Son Limited, and the dielectric properties are tested by the transmission/reflection waveguide method explained in chapter 3. The measured relative permittivity of the substrate is 2.78, and the loss tangent is approximately 0.07. The conductive elements are still made out of the high performance shielding fabric 'Zelt', which has a conductivity of 1e+006S/m. The antenna development procedure is followed by that of the fabric antenna. It is composed of a rectangular inner patch, a parasitic ring and a loop ground plane. And the dual resonances are designed to be 2.45 and 5.8GHz WLAN applications.

Figure 4.11 shows the geometry of the simple dual-band coplanar leather antenna. The antenna has a very compact size of 50mm × 50mm, the outer patch size is 24mm×28mm, and the inner patch size is 15mm×16mm. 50Ω strip feed line width is 4mm and the gap between ground and strip line is 0.4mm. The antenna was measured in the anechoic chamber to test the return loss and the radiation characteristics. The S_{11} result is plotted in Figure 4.13, as a comparison will be made among antennas made out of different materials, and the discussion will be given in Section 4.2.5.

4.2.4 Dual-band Double-layered Hidden Leather Antenna

A dual-band hidden leather antenna is designed by covering a layer of leather substrate on each side of the patch and making the antenna into a sandwich structure. The advantage of this structure is that the conductive elements are hidden, and the risk of being damaged and interfered with can be reduced. The compact size and the hidden characteristic also increase the possibility of integrating antenna within the belt in future applications. The constructed prototype is shown in Figure 4.12.

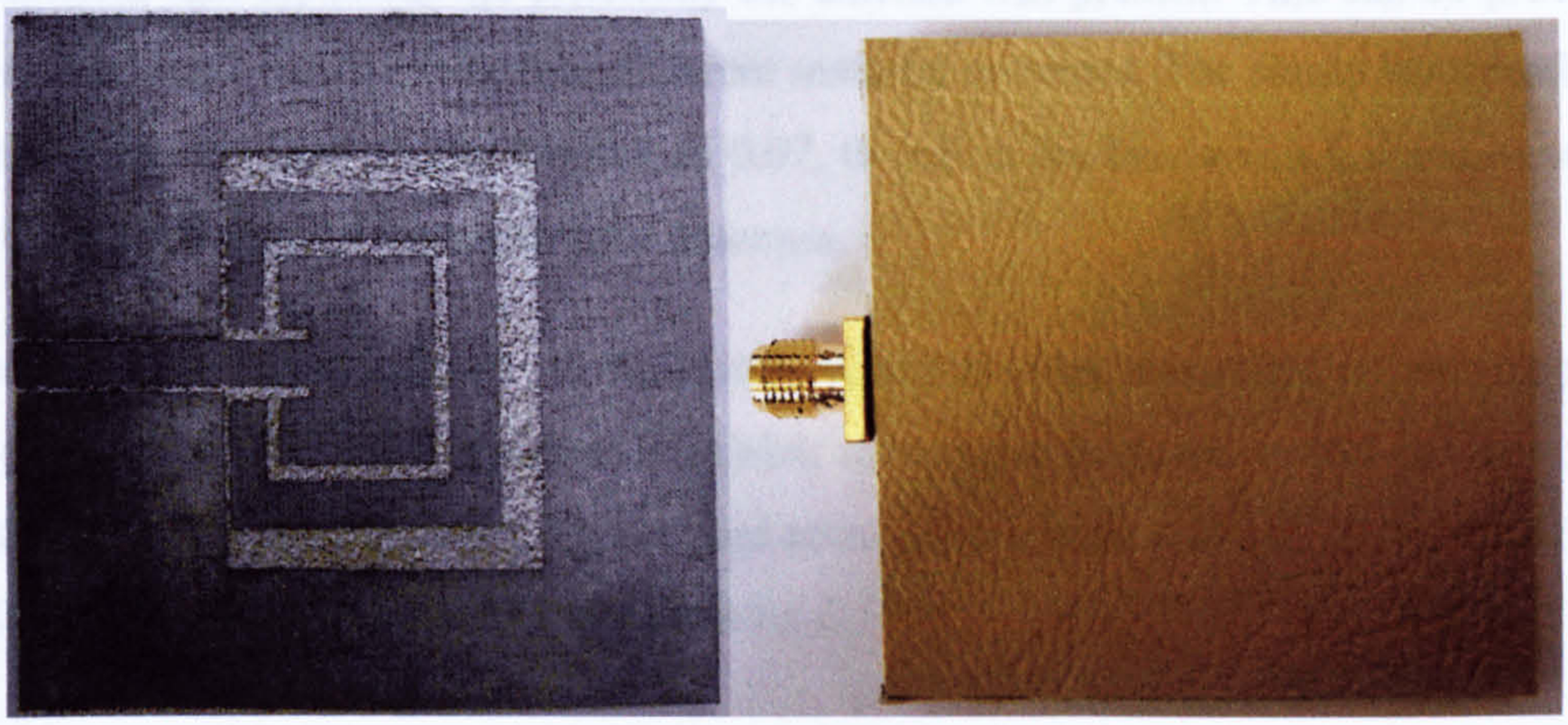

Figure 4.12 Dual-band hidden leather antenna

Overall size: $50\times50\times2.8\ mm^3$, **parasitic ring:** $24\times19mm^2$

Inner patch: $15\times11mm^2$, **strip line width:** 4.5mm

Substrate: Leather, permittivity: 2.65, Loss tangent: 0.035

A leather material which has a measured relative permittivity of 2.65 and loss tangent of 0.035 is chosen as the double layer substrate. The thickness of each substrate layer is 1.4mm. The material is provided by Andrew Muirhead & Son Limited. As the conductive textile material 'Zelt' has been proved to be a high quality electric conductor, it is used as the radiating elements in this antenna design as well. The width of the strip feed line and the gap between the ground plane and the microstrip were 4.5mm and 0.4mm respectively to match the 50Ω load.

4.2.5 Results Comparison

The comparison of the measured S_{11} of the four antennas discussed above is plotted in Figure 4.13. All of the four antennas display dual-band resonances as expected. As the antennas are designed differently, the resonant frequencies might differ from each other. But note that each measured return loss has achieved a good agreement with the computational result of the individual antenna. The resonant bandwidth is deeply related to the material loss factor. Generally, the more lossy the material is, the wider bandwidth and the lower the efficiency the antenna will present. This can be proved from the return losses of the four different material antennas. The single layer leather antenna has the highest loss tangent of 0.07, therefore the bandwidth it demonstrates is wider than those of the other three antennas.

The radiation characteristics of the leather antennas were measured as well in the anechoic chamber. All the antennas exhibit reasonable gain and useful patterns for each desired frequency band. The co and cross polarization patterns of the E and H principle planes will be plotted in Appendix C.

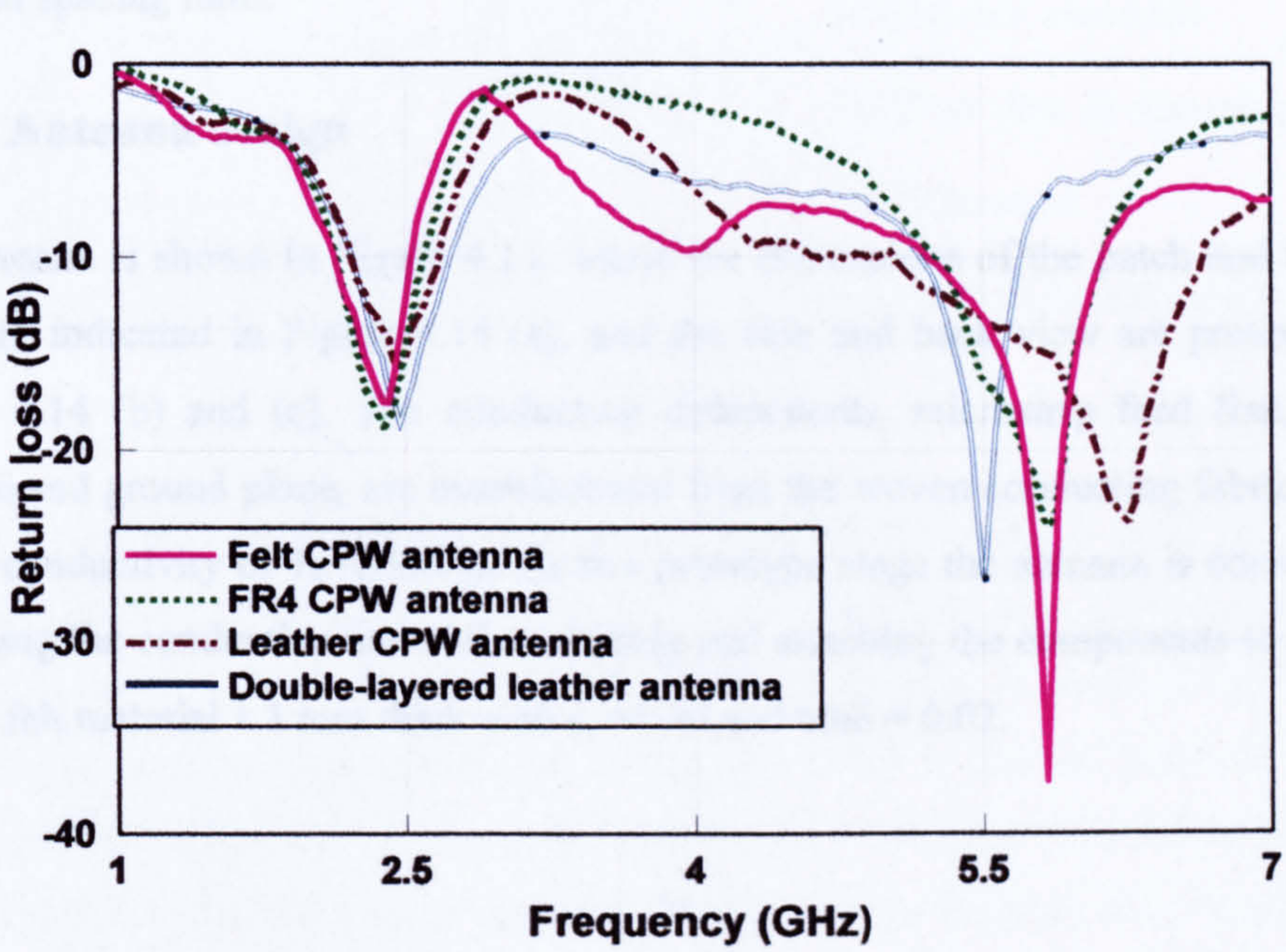

Figure 4.13 Dual-band fabric, FR4 and leather antenna return loss comparison

Experiments have shown the possibility of using fabric and leather materials for antenna design. All the proposed antennas demonstrate good performance in terms of return loss and radiation patterns. The coplanar parasitic ring structure has been proved to be able to provide dual frequency resonances. And the radiating elements can be etched in between two layers of substrates into a hidden structure. This presents a very useful method for future wearable application designs.

4.3 Dual-band Fabric Triangle Antenna

Triangular patches are found to provide radiation characteristics similar to those of rectangular patches, but with smaller size. In this section, a triangular antenna [19] with a parasitic element over a modified small ground plane will be presented. The antenna operates at two frequency bands with bandwidths exceeding 20% at the 2.45GHz and 5GHz wireless network bands. The ground is modified by cutting a large rectangular slot in it that allows tuning of the frequency bands and adjustment of the band spacing ratio.

4.3.1 Antenna design

The antenna is shown in Figure 4.14, where the dimensions of the patch and the top view are indicated in Figure 4.14 (a), and the side and back view are presented in Figure 4.14 (b) and (c). The conducting components, microstrip feed line, patch antenna and ground plane, are manufactured from the woven conducting fabric 'Zelt' with a conductivity of 1e+006S/m. At this prototype stage the antenna is constructed by cutting the conductive material accurately and attaching the components to a layer of thin felt material 1.1 mm thick with ε_r =1.38 and tanδ = 0.02.

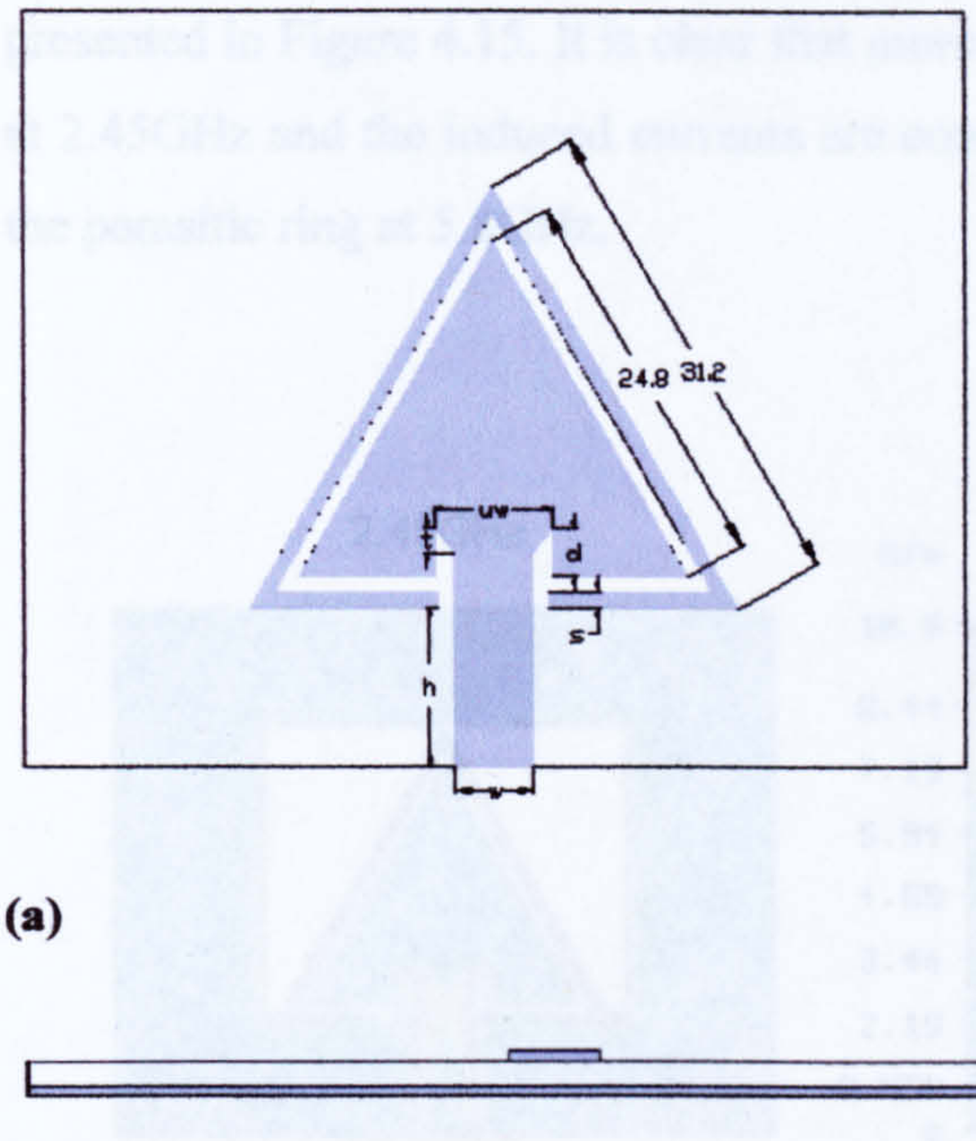

(a)

(b)

Parameter	Value(mm)
uw	7.4
d	3
t	1.5
s	1
h	10
w	4.5

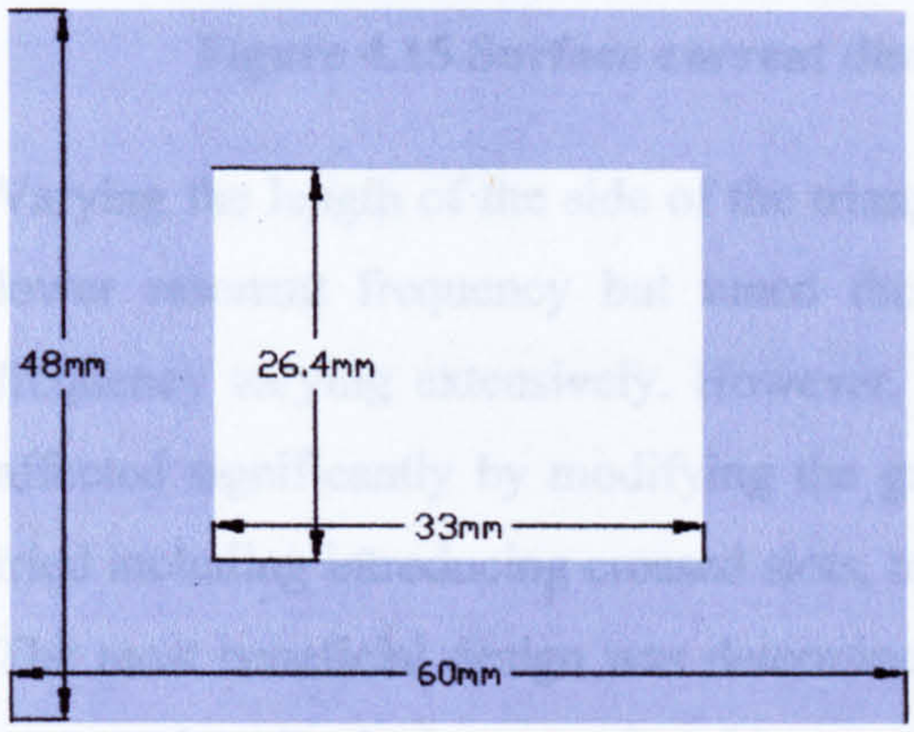

(c)

Figure 4.14

Configuration of the proposed triangular antenna:

(a) Top view & dimensions

(b) Side view

(c) Back Ground view

The structure of this antenna consists of an equilateral triangular base patch, side length of 24.8mm, with a triangular parasitic wire around the base patch excited by a microstrip line of 4.5mm wide. Slots are cut at the feed point to match the antenna to 50Ω. The parasitic triangular wire runs around the patch to provide resonance at the lower frequency band, this is 1 mm wide and spaced 1 mm from the patch in this case. The length of the parasitic wire was set at 31.2 mm in this instance for a resonance at 2.45 GHz. The antenna is backed by a ground plane as shown in Figure 4.14 (c) measuring 60 mm x 48 mm. Fundamentally, the length of the parasitic wire determines the low frequency resonance while the inner triangle patch primarily determines the upper band. The surface current distributions at both frequencies are

presented in Figure 4.15. It is clear that more currents are induced in the parasitic ring at 2.45GHz and the induced currents are concentrated in between the inner patch and the parasitic ring at 5.8GHz.

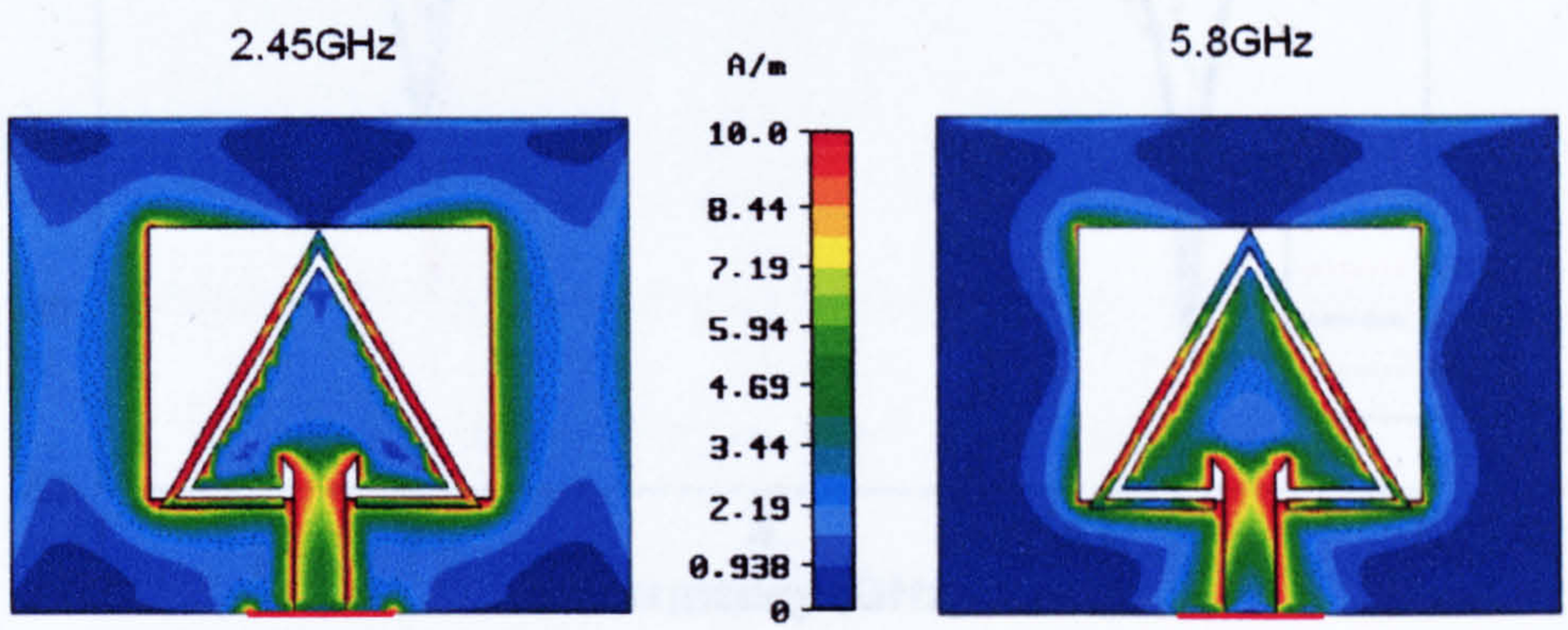

Figure 4.15 Surface current distribution of the triangle antenna

Varying the length of the side of the triangular patch has no significant affect on the lower resonant frequency but tuned the antenna at the higher band, the centre frequency varying extensively. However, the overall performance of the antenna is affected significantly by modifying the ground plane. A number of variations were tried including introducing crossed slots, triangles and a rectangular grid of slots [20]. The most beneficial design was determined to be modifying the ground by cutting a rectangular slot in it measuring 33 mm x 26.4 mm as shown inset in Figure 4.16, where the slot dimensions are M = 1.5K and N = 1.2K and K is a scaling factor. The size of the slot determines the impedance match and the band spacing as shown in the simulated return loss plotted in Figure 4.16, where the factor K was varied from 20 to 22.5. The centre frequency of each band varied, from 2.45GHz to 2.56GHz and 5.74GHz to 6.01GHz respectively, as did the frequency band ratio and the matching. For K set to 22 the lower frequency bandwidth was 30.6% (2.11-2.86 GHz) and the upper bandwidth 25.3% (5.02-6.49 GHz). The slot in the ground therefore provides a useful method of improving the impedance match at both bands and of tuning the frequency band ratio. The simulated performance was verified experimentally.

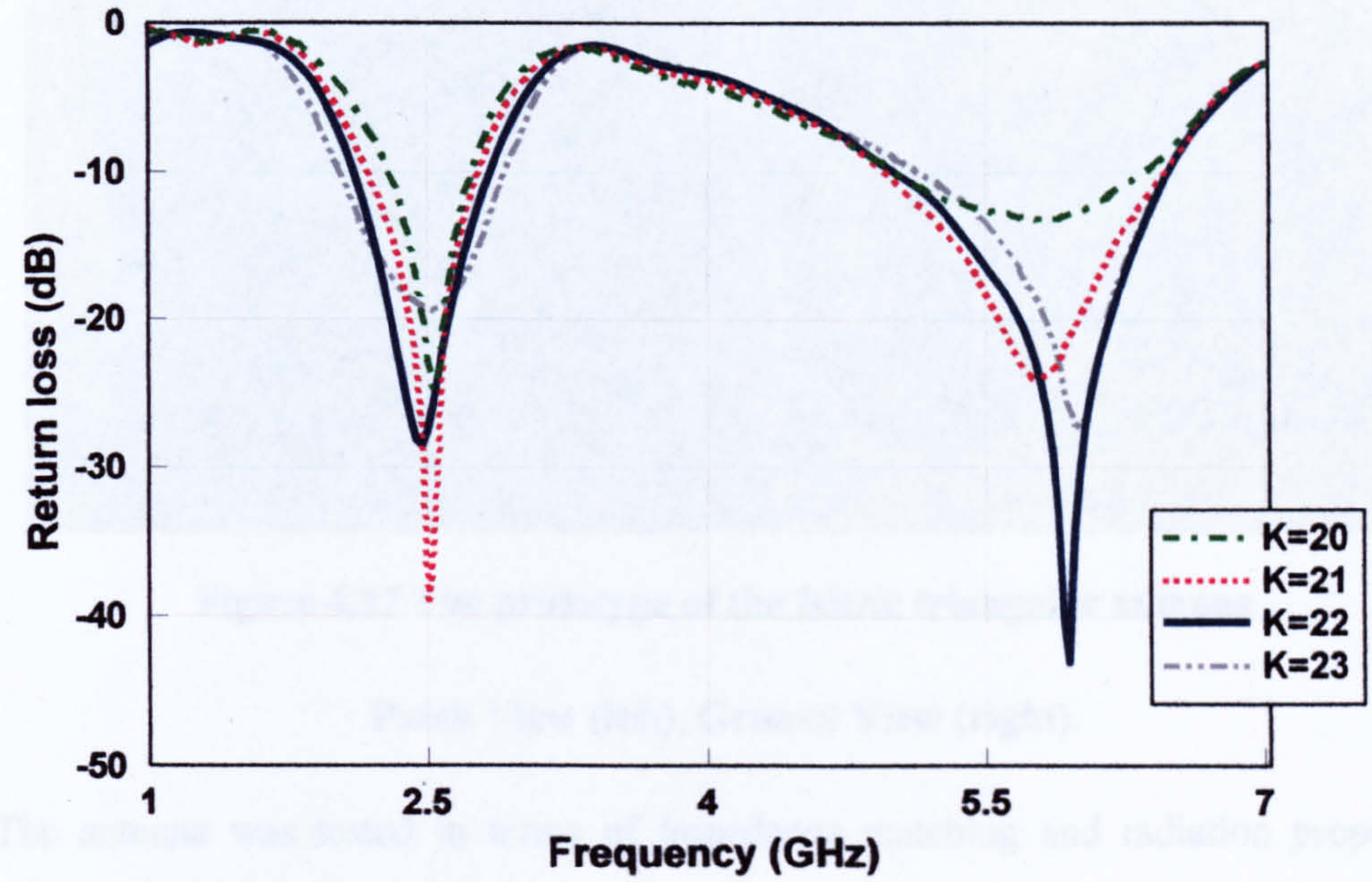

Figure 4.16 Simulated return loss for various slot dimension in ground plane

4.3.2 Results

The antenna was fabricated by cutting each element into the optimum simulated dimensions and sticking on the substrate carefully. The SMA connector was soldered onto the antenna at this stage, and this can be improved by using special designed connector in the future real application. The fabricated prototype of the antenna is shown in Figure 4.17 with the front and ground view respectively.

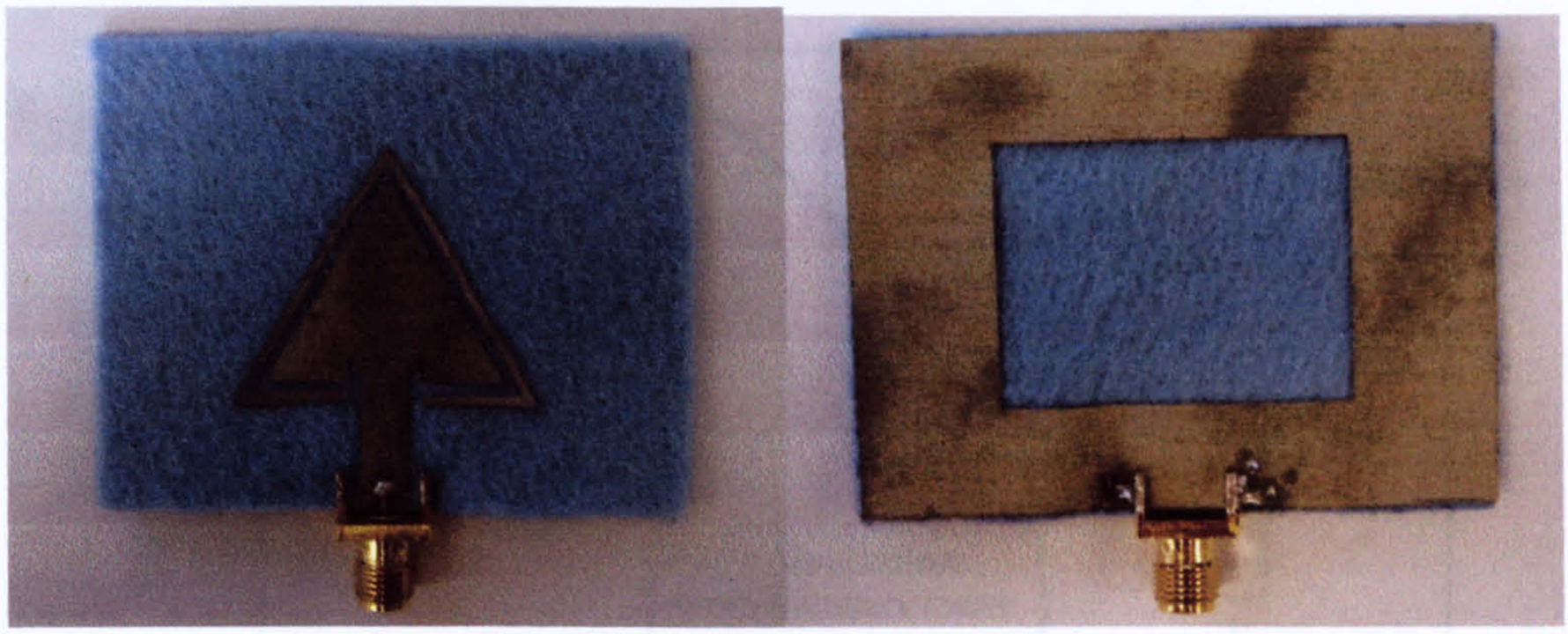

Figure 4.17 The prototype of the fabric triangular antenna

Patch View (left), Ground View (right).

The antenna was tested in terms of impedance matching and radiation properties correspondingly. The simulated and measured return losses of the proposed antenna are presented in Figure 4.18 in the frequency range of 1-7GHz. The frequency bands which are lower than -10dB in the figure represent the impedance matching bands of the antenna resonances. At the lower frequency band, the simulation and the measurement have a good agreement on the antenna centre frequency (2.47GHz in the simulation and 2.51 in the measurement) and the bandwidth (29.4% in the simulation and 24.5% in the measurement). However, for the upper frequency, although the centre frequency retains a high stability, the antenna produces a much wider bandwidth in the measurement (46%) than the simulation (25.3%). It covers an extra band around 4GHz (3.82-5.02GHz). This might be caused by the loose and lossy properties of the substrate material itself, and the use of liquid spray mount during the fabrication process might increase the loss factor of the material as well. The imperfect fabrication may cause a serious shape change of the parasitic ring, and this will change the capacitance between the inner patch and the parasitic ring. However, the measurement result proves that this scheme accomplishes the desired dual-band operation and fully covers the desired bands.

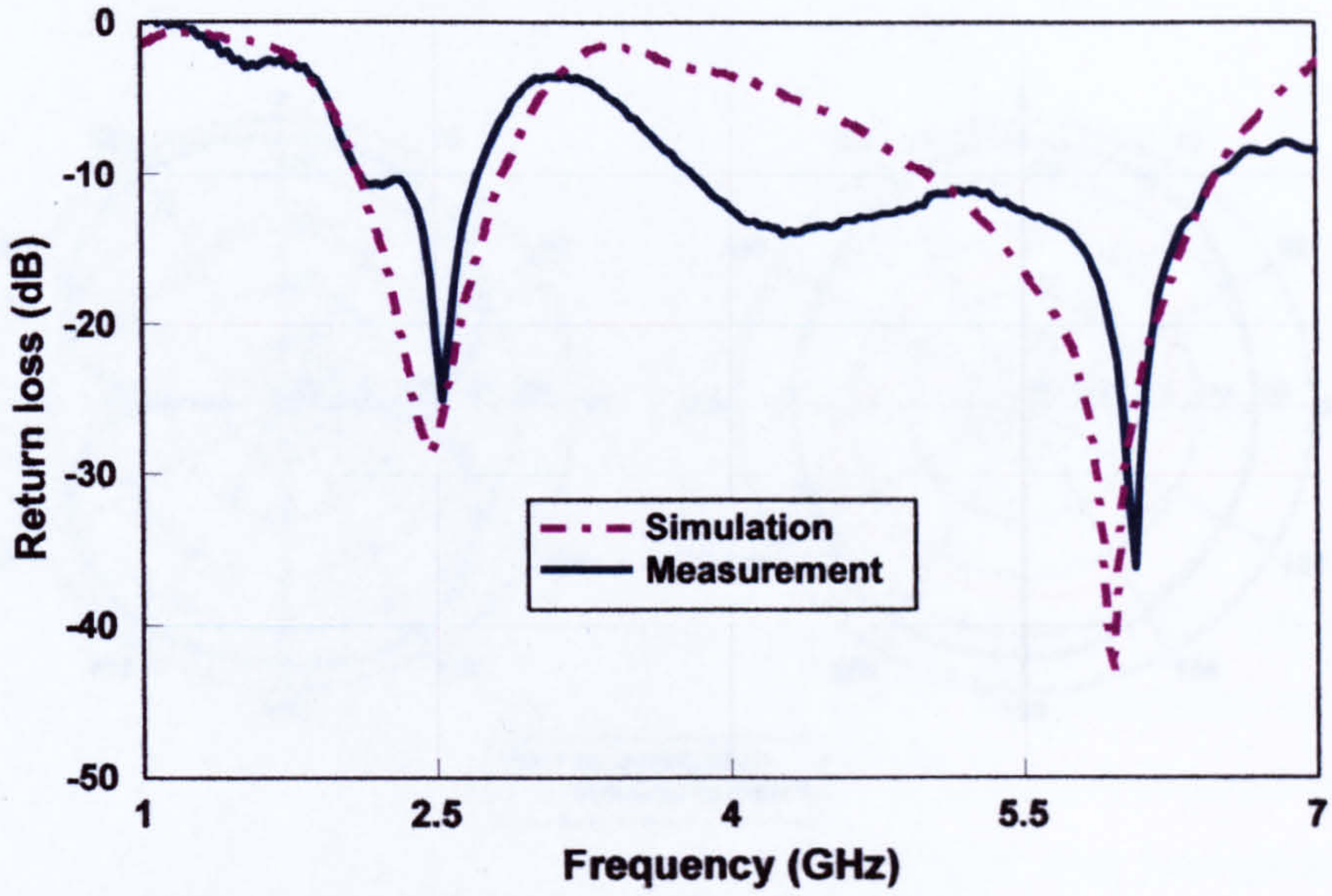

Figure 4.18 Simulated and measured return loss of the dual-band triangular antenna

Radiation patterns measured in the two principle planes are plotted in Figure 4.19 and Figure 4.20 at the centre of the lower frequency band 2.45 GHz and the upper frequency band 5.8GHz. The E-plane is the cut through the feed axis of the antenna. The blue solid line in the figure denotes the co-polarization pattern and the dotted red line indicates the cross polarization for the principle plane. The cross-polarization levels are less than -15dB in both planes. The antenna sits over a small ground plane and hence the back radiation is high. At the lower band the radiation patterns are very similar to a dipole antenna having a donut shape. At the upper band the pattern is more directional and there is an extra null in the patterns but they remain acceptable for these applications. The gains were measured at approximately 2.9 dBi at the lower frequency band and 3.5 dBi at the higher band.

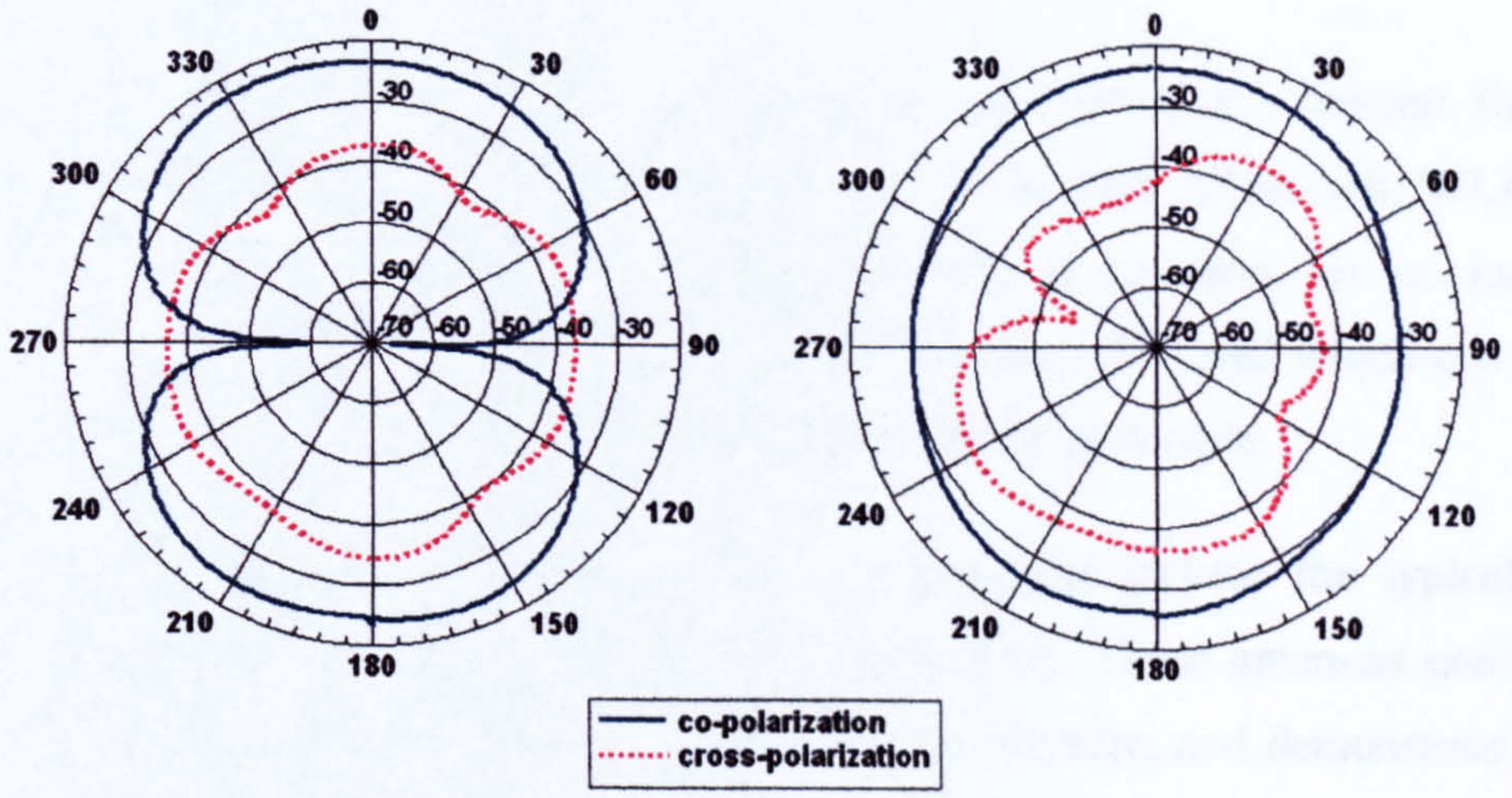

Figure 4.19 Measured radiation patterns of the triangular antenna at 2.45GHz

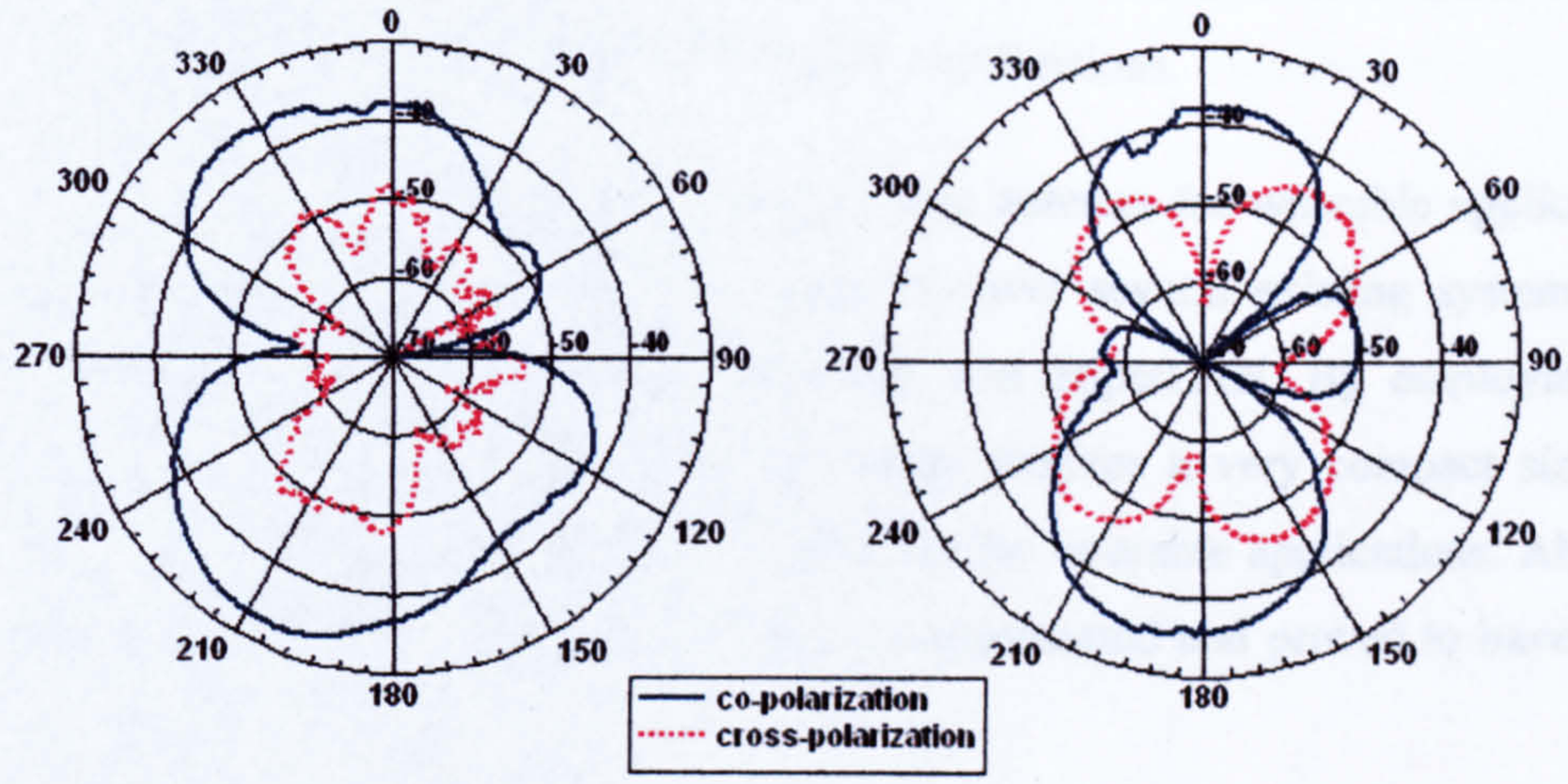

Figure 4.20 Measured radiation patterns of the triangular antenna at 5.8GHz

4.4 Multi-band Coplanar Fabric Antenna

The global success of wireless communication has provided a several frequency spectrum bands for different applications, like GSM, GPS, Bluetooth, WLAN, etc. This increases the demands of integrating multiple systems on an individual simultaneously. In stead of having numerous devices, a terminal which can provide multiband operations with a single antenna unit will be preferable.

Multi operational structures have been presented and include the typical fractal Sierpinski gasket [21-22] and Parany monopole [23]. These antennas consist of a series of scaled triangles forming a linear fractal structure, and demonstrate a quasi log periodic resonant property. Two multi-band multiple ring monopole antennas were developed by Song [24]. One consists of a set of self-similar circular rings, and the other one is realized by varying the circular structure to an elliptical one. Both antennas are capable of operating at multiple frequency bands, and optimum impedance bandwidth are obtained. However, these antennas have very complicated structures which largely increase the difficulties in the manufacture. Moreover, the non planar structure is not suitable for wearable applications.

In this section, a multi-band planar hexagon ring antenna for wearable applications will be presented. The antenna is designed to cover several existing systems like GSM, DCS, PCS, UMTS, WLAN, Bluetooth and HiperLAN. By employing the coplanar and hexagon ring structure, the design realizes a very compact size and simple planar geometry which are favourable for the wearable applications. Also the integration of antenna and fabric materials is implemented and proved to have good performance.

4.4.1 Antenna Design

Figure 4.21 shows the configuration of the proposed antenna design. The basis of the antenna structure is a radiating element, which includes two self-contained scaled hexagon rings and an inner hexagon patch, a feeding strip line, and two coplanar ground planes on each side of the strip line. The conductive elements are made out of

the 'Zelt' material which has a conductivity of 1e+006S/m. And the substrate material is a 1.1mm thick felt, which has been tested to have a relative permittivity of 1.38. The antenna has an overall compact size of 75mm × 90mm, which is about $0.22\lambda \times 0.27\lambda$ with respect to the lowest 900MHz GSM operating band. Compare with a conventional efficient rectangular patch antenna which needs a minimum practical dimension of 119.5mm×159.4mm (calculated by the equation 14-6 & 14-7 in [25]), the proposed antenna size has been reduced by 64.6%.

The dominant dimensions of the antenna geometry are computed in CST Microwave Studio environment, and the optimum values are listed in the right hand side table of Figure 4.21. Basically, the variety of the parameter L_1, L_2 and L_3 determine the position of the resonance excitation of each frequency band, while the tune of r_1 and r_2 which change the thickness of the hexagon rings show significant effects on the impedance bandwidth.

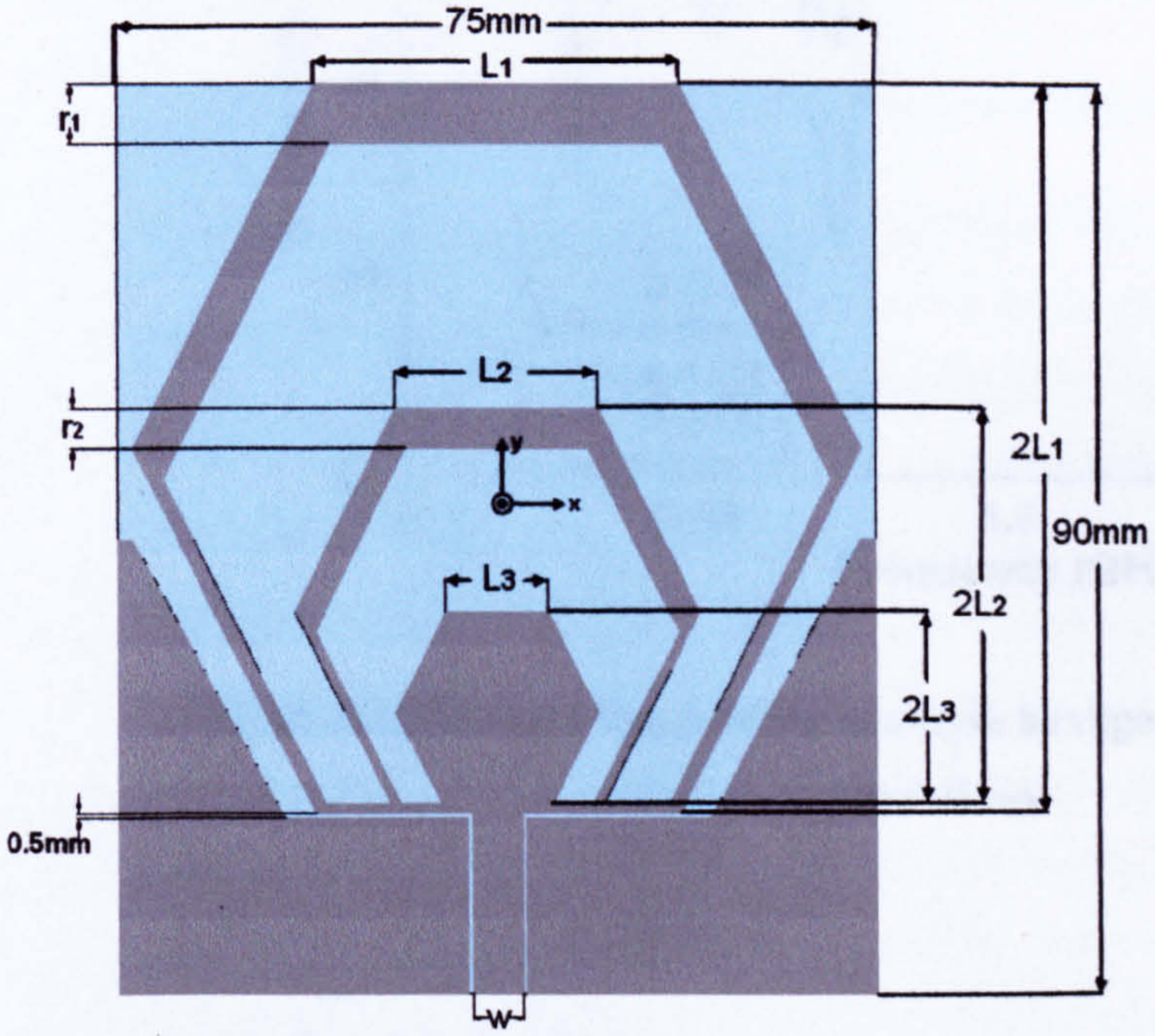

Parameter	Value(mm)
L_1	36
L_2	20
L_3	10
r_1	6
r_2	4
w	5

Figure 4.21 Structure of the multi-band fabric hexagon antenna and parameters

It has also been found from the simulations that with the number of hexagon rings increasing, more resonant frequency bands can be achieved correspondingly. The input reflection coefficient of the multiple hexagon ring structure was computed with two to five hexagon iterations, and the results are shown in Figure 4.22. It can be seen from the figure that the number of operation bands obtained is corresponding to the number of the multiple rings. And according to the computational result, the operation bands can be tuned by adjust the size and the thickness of each ring. Although at this stage, our desired bands can be well covered by 3 rings, the idea of this kind of structure design has very good potential for multi-band antenna design for other applications.

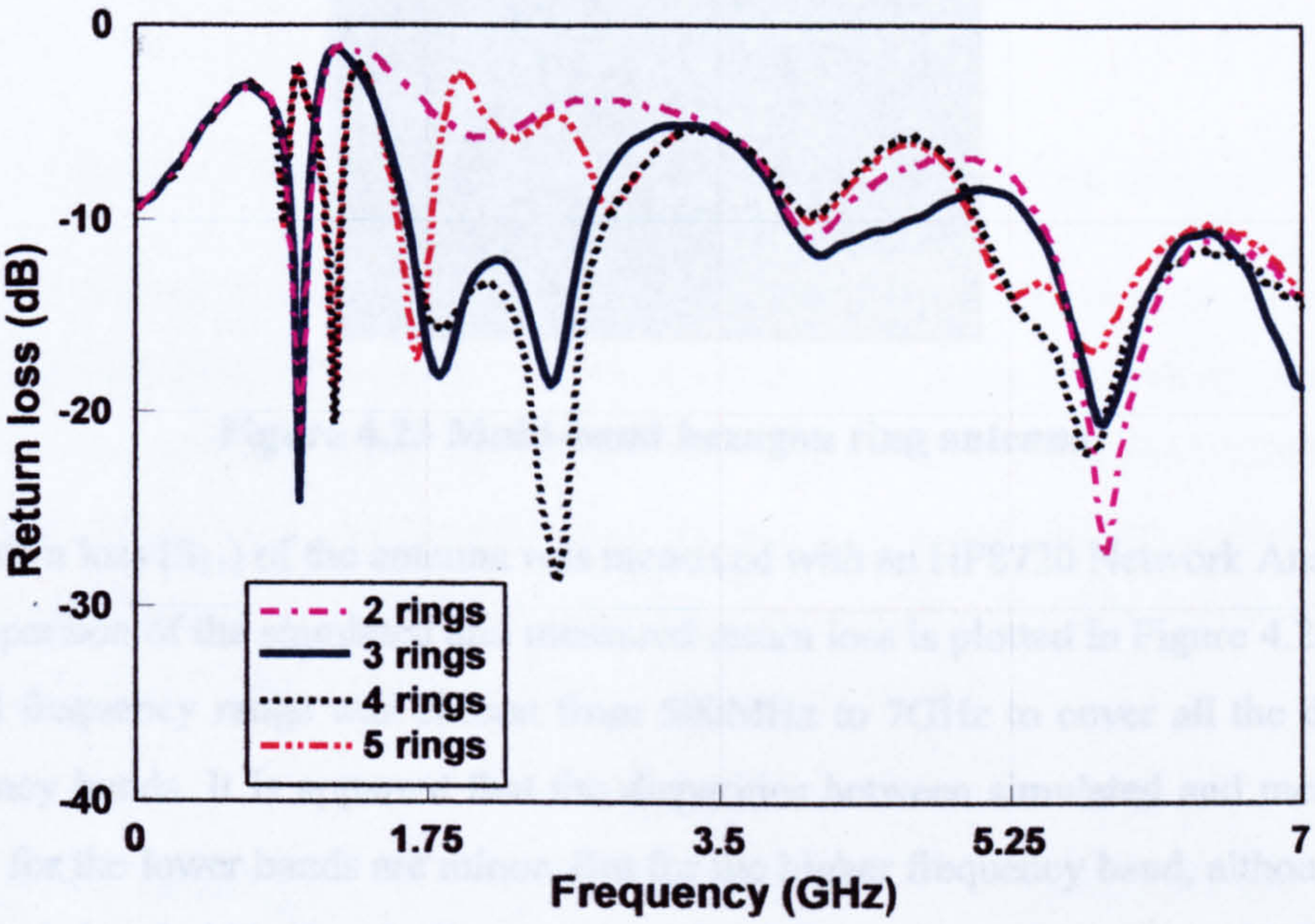

Figure 4.22 Return losses of the multiple hexagon ring antenna from 2 to 5 iterations

4.4.2 Results analysis

The prototype of the proposed multi-band CPW-fed hexagon antenna was constructed and shown in Figure 4.23. As the hexagon ring size is too big for laser ablation, this

antenna was hand cut. The elements were carefully stuck on the surface of the substrate, and the connector was soldered on the elements for experimental test.

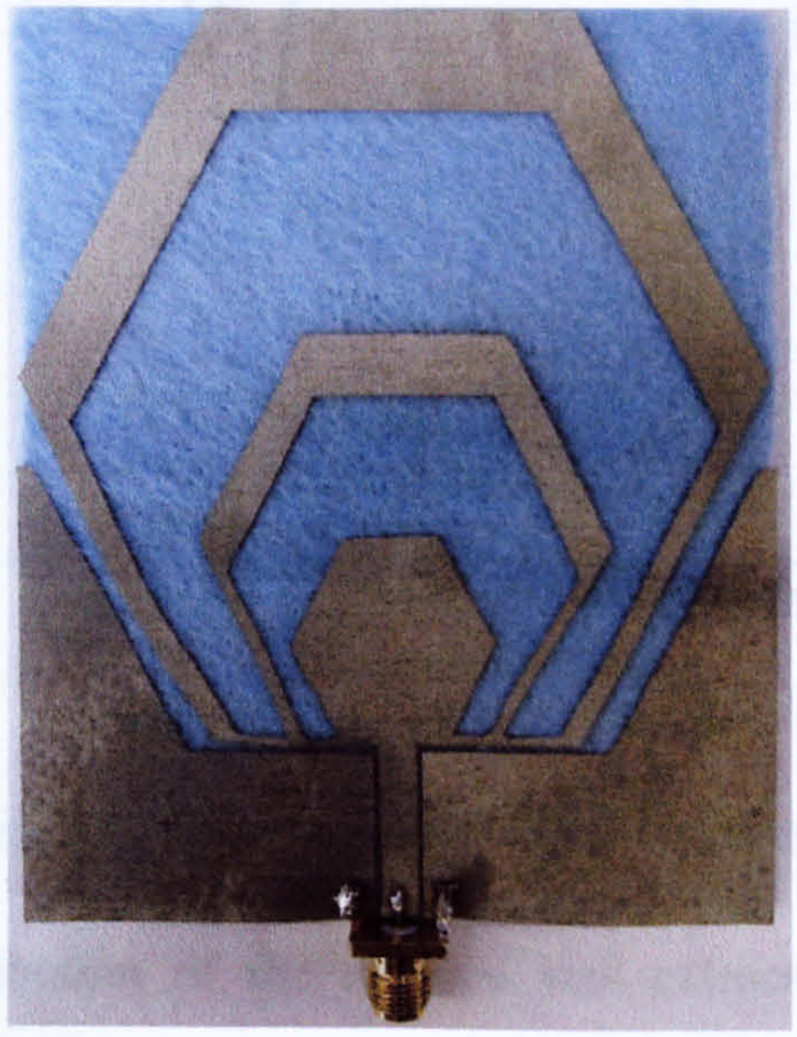

Figure 4.23 Multi-band hexagon ring antenna

The return loss (S_{11}) of the antenna was measured with an HP8720 Network Analyzer. A comparison of the simulated and measured return loss is plotted in Figure 4.24. The plotted frequency range was chosen from 500MHz to 7GHz to cover all the desired frequency bands. It is apparent that the disparities between simulated and measured results for the lower bands are minor. But for the higher frequency band, although the measured bandwidth is similar to the simulation, the agreement with center frequencies is not good. This could be due to the non accurate cutting dimensions of the elements, and also the imperfect fabrication might have some effects as well. In general these deviations are considered reasonable. The measured antenna has the useful bands of 825-1002MHz, 1.80-2.94GHz and 4.17-6.54GHz, which are capable to cover the GSM (890-960MHz), PCS (1850-1990MHz), UMTS (1.88-2.20GHz) and WLAN (2.40-2.48GHz & 5.15-5.825GHz) bands.

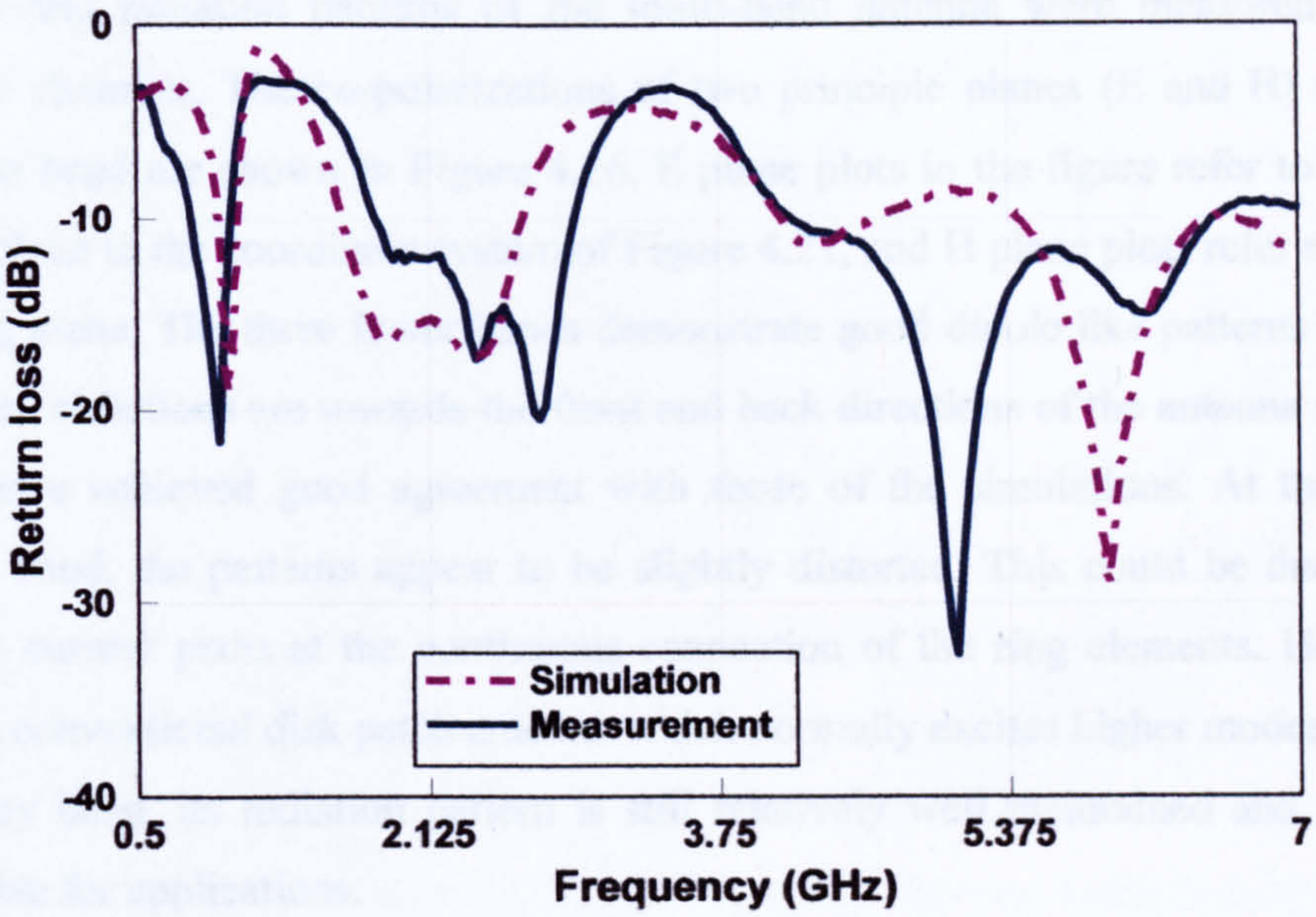

Figure 4.24 Return loss of the multi-band hexagon ring antenna

The total current distribution of the antenna was extracted from the simulation package at each band of operation, shown in Figure 4.25. It can bee seen from the plot that, the outer ring and the middle ring show high field intensity for 900MHz and 1800MHz respectively. As the operating frequency increase, the currents begin to move to the inner and the bottom of the rings. This confirms that the resonance of the antenna is primarily determined by its distinct resonating ring.

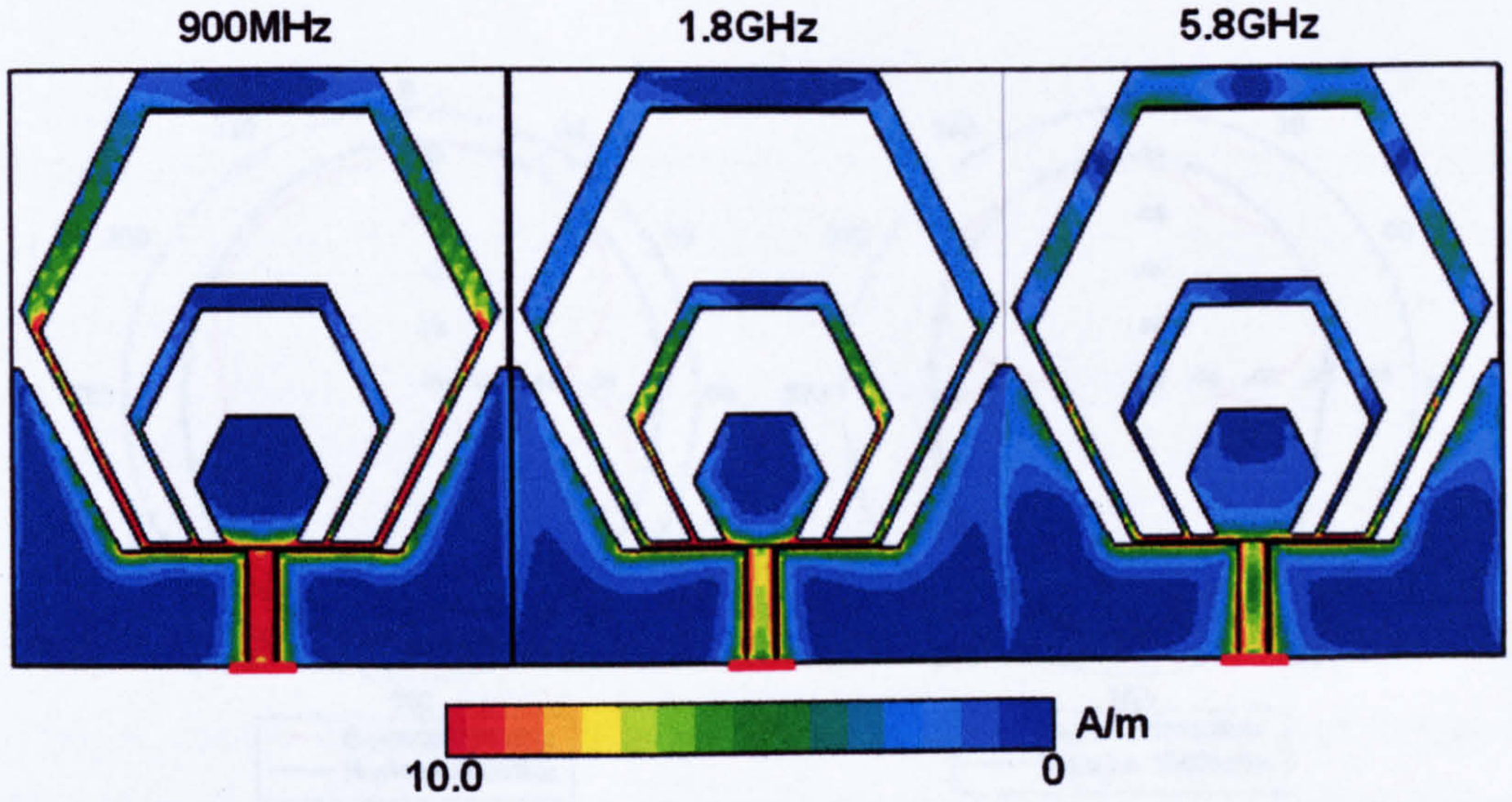

Figure 4.25 Simulated current distribution of the multiple hexagon ring antenna

The far-field radiation patterns of the multi-band antenna were measured in the anechoic chamber. The co-polarizations of two principle planes (E and H) of each operation band are shown in Figure 4.26. E plane plots in the figure refer to the y-z cutting plane in the coordinate system of Figure 4.21, and H plane plots refer to the x-z cutting plane. The three lower bands demonstrate good dipole like patterns and the maximum radiations are towards the front and back directions of the antenna surface. These have achieved good agreement with those of the simulations. At the upper 5.2GHz band, the patterns appear to be slightly distorted. This could be due to the multiple current paths at the continuous connection of the ring elements. However, unlike a conventional disk patch antenna which normally excites higher modes at high frequency band, its radiation pattern is still relatively well maintained and remains acceptable for applications.

More importantly, from the radiation characteristics, it is easy to see that this kind of structure has great radiation advantages over the Ultra-Wide Band disk antenna [26] which has a similar coplanar hexagonal structure. The UWB antenna generally has an extremely wide impedance bandwidth, but the antenna performance is restricted by its radiation patterns, which deteriorates as operating frequency increases. While with the multiple ring structure, numerous system bands can be covered independently and with useful, efficient radiation performance for each operation band.

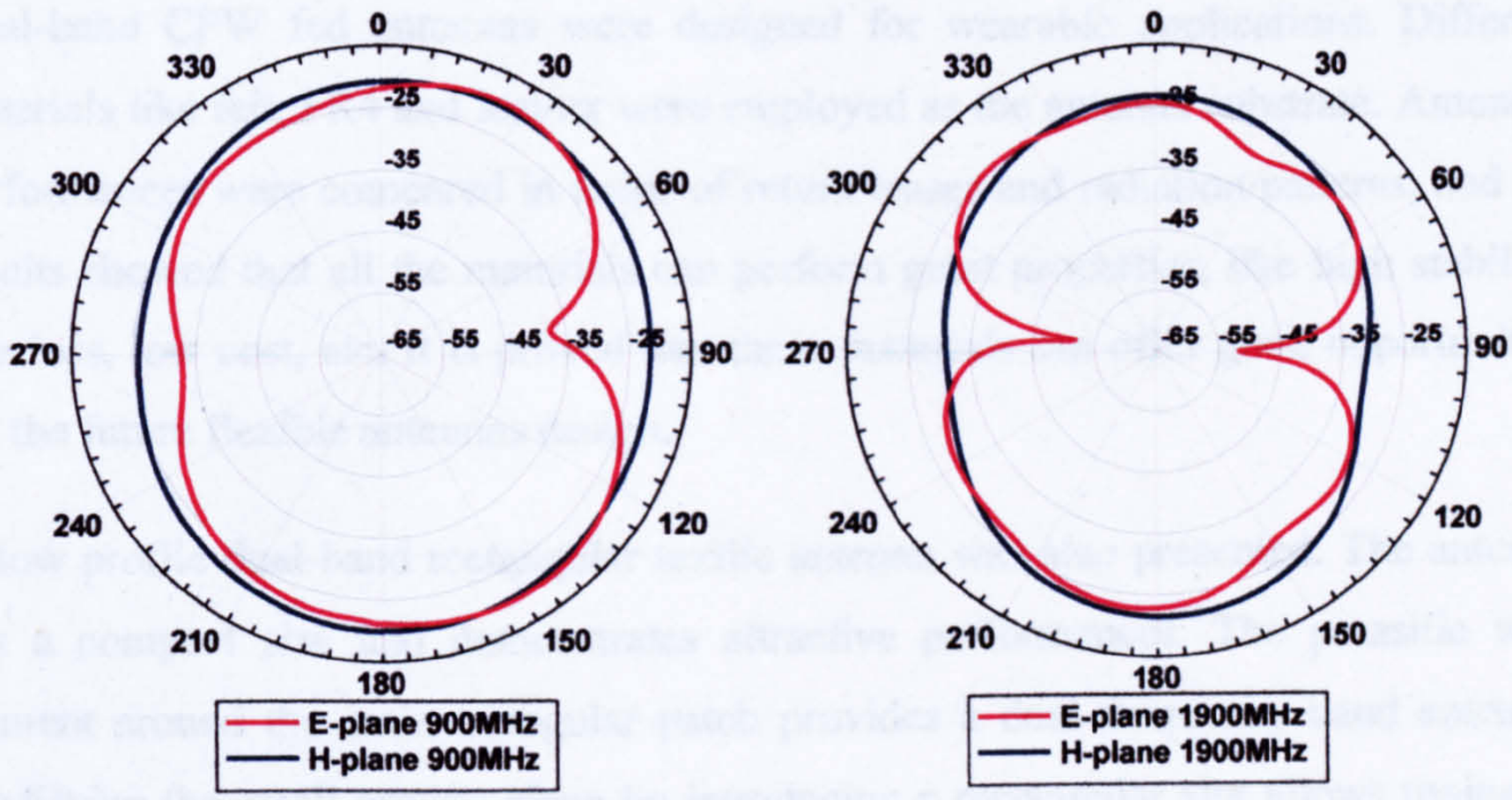

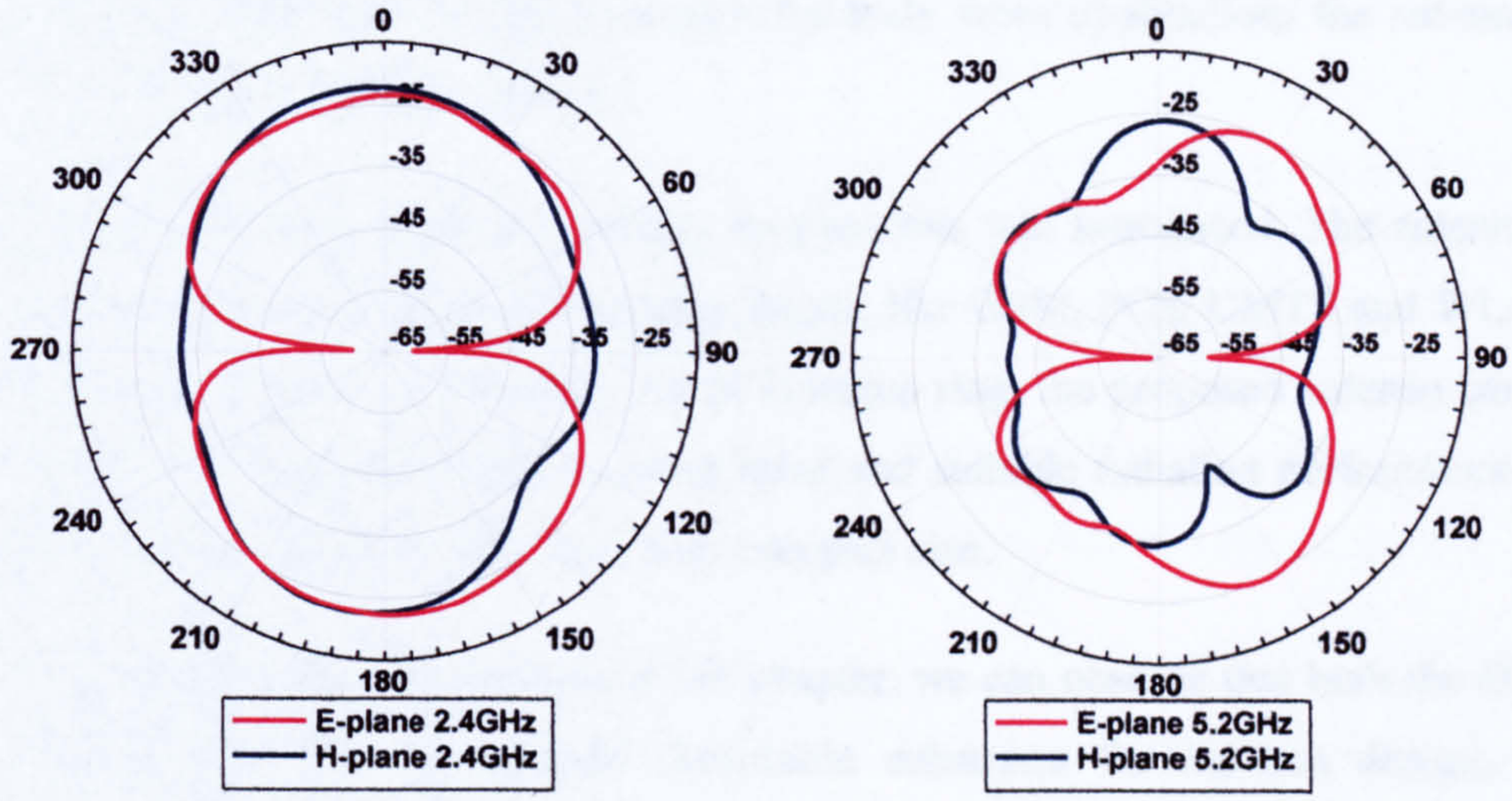

Figure 4.26 Measured far-field radiation patterns for the multi-band fabric antenna

4.5 Conclusion

This chapter has addressed the development of a few strip line fed textile and leather antennas. It has shown that the standard antenna design techniques perform well even for textile, leather substrate and conductive textiles. The antennas presented not only feature good properties, but also are easy to manufacture.

Dual-band CPW fed antennas were designed for wearable applications. Different materials like felt, FR4 and leather were employed as the antenna substrate. Antennas performances were compared in terms of return losses and radiation patterns, and the results showed that all the materials can perform great properties, like high stability, low loss, low cost, etc. It is proved that these materials can offer good opportunities for the future flexible antennas design.

A low profile dual-band rectangular textile antenna was also presented. The antenna has a compact size and demonstrates attractive performances. The parasitic wire element around the main triangular patch provides a dual frequency band antenna. Modifying the small ground plane by introducing a rectangular slot allows tuning of the frequency bands and the bandwidth. The antenna has bandwidths of 20% or more

at each band. Although initially designed for body worn applications the antenna is useful for many other applications.

Finally, a multi band coplanar hexagon ring antenna was introduced. The antenna is capable to cover the important frequency bands, like GSM, PCS, UMTS and WLAN. With the combination of different size of hexagon ring, the proposed antenna can be designed to have an adjustable resonant band and suitable radiation performance for individual band operation, but has a very compact size.

From the entire presented antenna in this chapter, we can observe that both the fabric and leather material can provide favourable substrates for antenna design, and different antenna structures combination can satisfy different frequency bands application. This offers large freedom in the future wearable antennas design and application.

All the antennas introduced in this chapter carry quasi- omni-directional patterns. However, antennas in wearable applications need directivity in order to avoid unnecessary radiation exposure to the human body and radiation losses. Therefore, to employ an EBG ground plane which can offer a lot of advantages to the antenna is an optimum solution. The EBG structure design and the performances working with the antenna will be introduced and discussed in next chapter.

References:

[1] **Wu, C., Wong, K., Lin, Y. and Su, S.,** "Conformal Bluetooth Antenna for the Watch-Type Wireless Communication Device Application," *IEEE Antennas & Propagation International Symposium*, pp.4156-4160, Hawaii, Jun 2007.

[2] **Sanz-Izquierdo, B., Huang, F. and Batchelor, J.C.,** "Convert Dual Band Wearable Button Antenna," *IET Electronics Letters*, Vol.42, No.12, pp.668-670, Jun 2006.

[3] **Sanz-Izquierdo, B., Huang, F. and Batchelor, J.C.,** "WLAN Jacket Mounted Antenna," *International Workshop on Antenna Technology* (IWAT), pp.57-60, Cambridge, Mar 2007.

[4] **Sanz-Izquierdo, B., Sobhy, M. I. and Batchelor, J.C.,** "UWB Wearable Button Antenna," *European Conference on Antennas and Propagation* (EuCAP), p.131, Nice, Nov 2006.

[5] **Kellomaki, T., Keikkinen, J. and Kivikoski, M.,** "Wearable Antennas for FM Reception," *European Conference on Antennas and Propagation (EuCAP)*, Nice, Nov 2006.

[6] **Sanz-Izquierdo, B., Sobhy, M.I. and Batchelor, J.C.,** "Dual-band Wearable PIFA," *Loughborough Antennas & Propagation Conference* (LAPC), pp.37-39, Loughborough, Apr 2006.

[7] **Massey, P.J.,** "Mobile Phone Antennas Integrated within Clothing," *IEE 11th International Conference on Antennas and Propagation* (ICAP 2001), Vol.1, No.480, Manchester, UK, pp.344-347, 2001.

[8] **Salonen, P. and Hurme, H.,** "Modeling of a Fabric GPS Antenna for Smart Clothing," *International Conference on Modelling and Simulation*, pp.18-23, 2003.

[9] **Salonen, P. and Hurme, H.,** "A Novel Fabric WLAN Antenna for Wearable Applications," *2003 IEEE Antennas and Propagation Society International Symposium*, Columbus, Vol.2, pp.700-703, 2003.

[10] **Rahman, A., Alomainy, A. and Hao. Y,** "Compact Body-Worn Coplanar Waveguide Fed Antenna for UWB Body-Centric Wireless Communications," *Second European Conference on Antenna and Propagation,* Nov 2007.

[11] **Salonen, P., et al.,** "Effect of Conductive Material on Wearable Antenna Performance: A Case Study of WLAN Antennas," *2004 IEEE Antennas and Propagation Society International Symposium,* Vol.1, Monterey, CA, pp.455-458, 2004.

[12] **Salonen, P., et al.,** "Effect of Textile Material on Wearable Antenna Performance: A Case Study of GPS Antennas," *2004 IEEE Antennas and Propagation Society International Symp.,* Vol.1, Monterey, CA, pp.459-462, 2004.

[13] **Salonen, P., Keskialammi, M. and Sydanheimo, L.,** "A low cost 2.45 GHz photonic band gap patch antenna for wearable systems," *IEE 11th International. Conerence on Antennas & Propagation* (ICAP2001), Manchester, UK, vol.2, pp. 719-723, 2001.

[14] **Tronquo, A., Rogier, H., Hertleer, C. and Van Langenhove, L.,** "Robust planar textile antenna for wireless body LANs operating in 2.45 GHz ISM band," *IEE Electronics Letters,* Vol. 42 (3), pp.142 – 143, 2006.

[15] **Salonen, P. O., Rahmat-Samii, Y., Hurme, H. and Kivikoski, M.,** "Dual-band Wearable Textile Antenna," *IEEE Antennas & Propagation International Symposium,* Vol.1, pp. 463-467, 2004.

[16] **Salonen, P. O., Kim, J. and Rahmat-Samii, Y.,** "Dual-Band E-Shaped Patch Wearable Textile Antenna," *IEEE Antennas & Propagation International Symposium,* Vol.1, pp. 459-463, 2005.

[17] **Zhu, S. and Langley, R. J.,** "Dual band wearable antennas over EBG substrate," *IET Electronics Letters,* Vol. 43: No. 3, pp141-143, Feb 2007.

[18] **Balanis, C. A.,** *Antenna Theory: Analysis and Design,* Third Edition, WILEY-INTERSCIENCE, pp.1033-1034. 2005.

[19] **Liu, L., Zhu, S. and Langley, R. J.,** "Dual band triangular patch antenna with modified ground plane," *IET Electronics Letters,* Vol. 43, pp.140-141, Feb 2007.

[20] **Liu, L.,** "A Wearable Microstrip Patch Antenna for Wireless LAN System," MSc Dissertation, University of Sheffield, UK, Sep 2006.

[21] **Puente, C., Romeu, J., Pous, R., Garcia, X. and Benitez, F.,** "Fractal multi-band antenna based on the Sierpinski gasket," *IEE Electronic Letters,* Vol.32, No.1, pp.1-2, Jan 1996.

[22] **Song, C. T. P., Hall, P. S. and Ghafouri-Shiraz, H.,** "Shorted Fractal Sierpinski Monopole antenna," *IEEE Transactions on Antennas and Propagation,* Vol.52, No.10, pp.2564-2570, Oct 2004.

[23] **Puente, C.,** "Fractal Antennas," PhD dissertation, Department of Signal Theory and Communications, Universitat Politecnica de Catalunya, Jun 1997.

[24] **Song, C. T. P., Hall, P. S. and Ghafouri-Shiraz, H.,** "Multiband Multiple Ring Monopole Antennas," *IEEE Transactions on Antennas and Propagation,* Vol.51, No.4, pp.722-729, Apr 2003.

[25] **Balanis, C. A.,** *Antenna Theory: Analysis and Design,* Third Edition, WILEY-INTERSCIENCE, Chapter 14, p.819, 2005.

[26] **Kwon, D.H. and Kim, Y.,** "CPW-Fed Planar Ultra-Wideband Antenna with Hexagonal Radiating Elements," *IEEE Antennas and Propagation Society International Symposium,* Vol.3, pp.2947-2950, Jun 2004.

Chapter 5 Electromagnetic Band Gap Structure

5.1 Introduction

An Electromagnetic Band Gap material in one form is a periodical structure in which high impedance exists for electromagnetic wave propagation within a certain frequency range. In antenna applications, the antenna can take advantage of the high impedance or surface wave band gap of an EBG within a particular frequency band. It has been found that antennas with EBG structures can offer remarkable improvements over conventional antennas and systems.

Wearable antennas are to be placed against the body and hence it is desirable to reduce the backward scattered radiation as much as possible. Review of recent publications [1, 2] shows that antennas with large ground planes can offer desire backward radiation reduction and maintain stable performance on body. Also planar structure is optimum to be integrated within clothes. Therefore, most antennas designed for wearable applications so far are textile patch antennas [3, 4]. However, general microstrip patch antennas possess narrow bandwidth, and with the surface wave existing, the antenna efficiency can be very low. Hence the incorporation of an electromagnetic band gap (EBG) material to act as a high impedance surface is desirable. EBG provides an effective method to suppress surface wave and higher order harmonics propagation, as well as a great backward scattered radiation reduction. Although for textile material, as the dielectric constant is relatively low, surface wave is not a serious problem, the other advantages of EBG structures, like high-order harmonics suppression, antenna radiation patterns improvement, antenna size reduction [5], etc, are still of interest for wearable antenna applications.

Two of the papers have incorporated single frequency electromagnetic band gap materials (EBGs) integrated into the wearable antenna designs [6], [7], and the EBG plane has shown a remarkable improvement on antenna performance over the conventional patch antenna. In this chapter, a simple dual band EBG structure will be introduced, as well as its reflection phase and EM wave suppression performances. The EBG structure is then integrated with the dual-band CPW fed fabric antenna as a high impedance ground plane, and the computational and experimental results will be

presented. And finally, the EBG antenna performance, with the comparison to a conventional slot patch antenna will be discussed.

5.2 Dual-band Fabric Concentric Square EBG

A very important feature of Electromagnetic Band-gap structures is the suppression of surface EM waves. Acting as a high impedance ground plane of the antenna, it helps to increase the antenna gain and reduce the back radiation. In this study, although surface wave rarely exists in our coplanar fabric antenna, the EBG plane can help reduce the interaction between the antenna and the body, enhance the antenna gain and directivity. Also for an antenna close to the body, the SAR values need to be controlled within the safe range. Therefore, to introduce an high impedance ground plane into our application is needed.

As described in Section 2.4, a lot of EBG structures have been developed to date for the purpose of increasing the band gap width and reducing the periodic size. For multi band application, multi band EBGs that have been developed include fractal EBGs [8], multi layered EBGs [9], interdigitated cells [10] and other multi resonant elements [11]. In this research, because of the restriction of the fabric materials, and also the difficulty in manufacturing, the simplest concentric square EBG structure becomes an optimum option. Although it was claimed [12] that mushroom like EBG can not provide good performance comparable with some complicated structures, its advantages like low cost, ease of fabrication, and reliability still gain the most attention. The high impedance dual frequency band-gap structure consists of concentric square elements previously found in FSS designs [13]. In this section, a dual-band entire fabric EBG structure will be presented and the results will be compared and discussed.

5.2.1 Dual-band Fabric EBG Structure

Ideally for dual band EBGs, two distinct modes should be generated for each frequency band. A simple approach to the design of a dual band EBG is to use a double resonant structure like the concentric square EBG. Double resonance can be achieved by a square patch nested in a bigger square loop and printed on the substrate surface. It is comprised of a simple square patch surrounded by a square loop backed by a grounded dielectric substrate. A unit cell model of the structure is shown in Figure 5.1. The fabric material 'felt' was chosen as the dielectric substrate in this design. Research [14] has shown that using a thicker substrate for an EBG plane can result in a smaller structure size and a wider bandwidth. However, massive elements are not convenient for on body applications. Therefore, two layers of felt which have a thickness of 2.2mm were employed, such that the thickness of the structure would not be too much for wearing, and it can offer a considerable bandwidth. Conductive parts, i.e. patch arrays and ground plane are made out of 'Zelt' fabric.

Note should be given that there is no via presence in this design. One reason is that for this entire fabric material structure, existence of vias will aggravate the difficulty of fabrication and reduce the worn flexibility. Secondly, studies [15, 16] have found that planar EBGs without vias can work as HIS on antennas, and they are shown to possess both surface wave and reflection phase bandgaps.

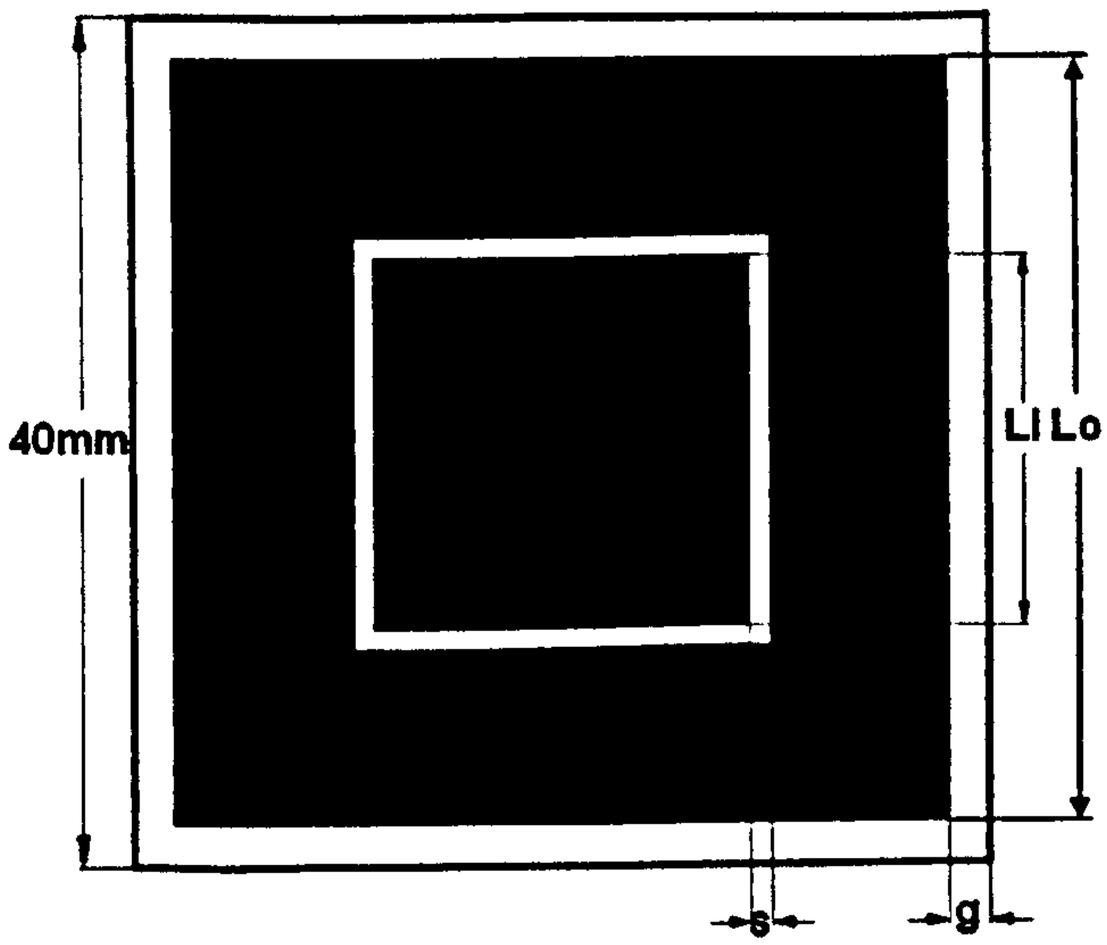

Parameter	Value (mm)
Lo	36
Li	17.5
s	1
g	2

Figure 5.1 Schematic diagram of front view of concentric square EBG

The resonances of this dual band EBG is mainly determined by the geometry. The transmission response creates two nulls at the reflection band corresponding to the inner square patch and outer loop [17]. The structure is designed so that the null points of the EBG reflection phase matches at 2.45GHz and 5.8GHz. The performance of the structure was computed using CST Microwave Studio, and the optimized dimensions for the concentric square EBG are depicted in Figure 5.1. Simulation has shown that increasing the gap **g** between each element raises the resonance at each band while increasing the elements length L_o, L_i lowers the resonant point at the corresponding band. The slot width s between the inner patch and the outer loop can be used to control the upper resonant band.

The surface current flows at both frequencies are distributed in Figure 5.2. It is clear that more currents are induced in the outer loop at 2.45GHz and the currents are concentrated in the inner patch at 5.8GHz.

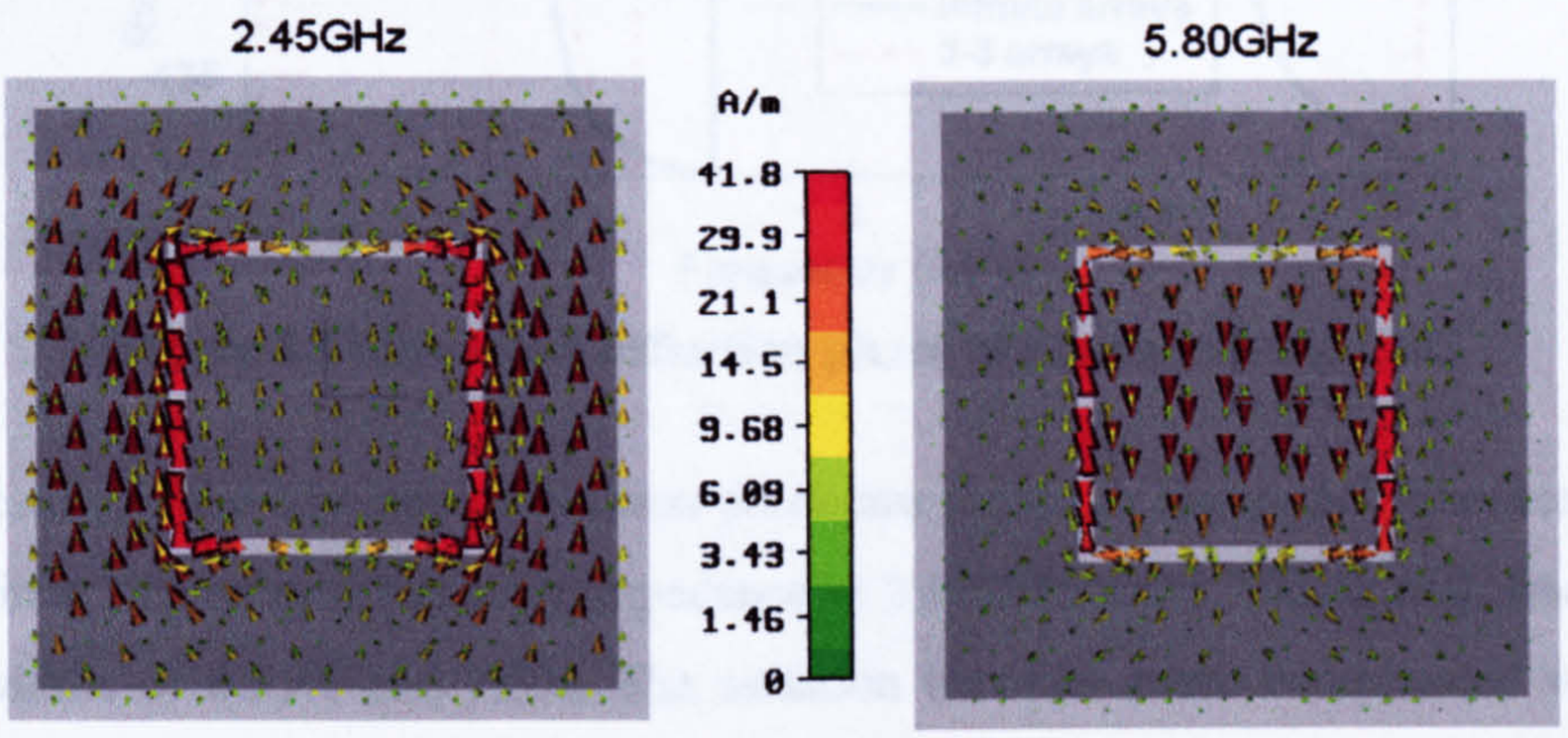

Figure 5.2 Surface current flows for a single cell at 2.45GHz & 5.8GHz

To investigate the high impedance bandgap of the EBG, a reflection phase model was established. A single cell of the EBG surface with periodic boundary conditions (PBC) on four sides is simulated to model an infinite size surface. A normal plane wave is launched to illuminate the structure and the EBG surface is chosen as the phase reference plane. This method has been explicitly explained in Chapter 2. The in-phase reflection feature of the EBG surface lies in a certain band of frequencies. The zero degree reflection phase defines the resonant point of the in-phase reflection.

And the useful band has been claimed to be from -90° to 90° on either side of the centre frequency [18]. Infinite size of the EBG surface is an ideal case, however in practice, the EBG is generally with limited number of cells. To observe the reflection phase difference from a finite size surface to the infinite size surface, a 3×3 array structure is modelled in the software as well. A plane wave normal to the surface is launched and the open boundary is used in stead of using a periodic boundary conditions.

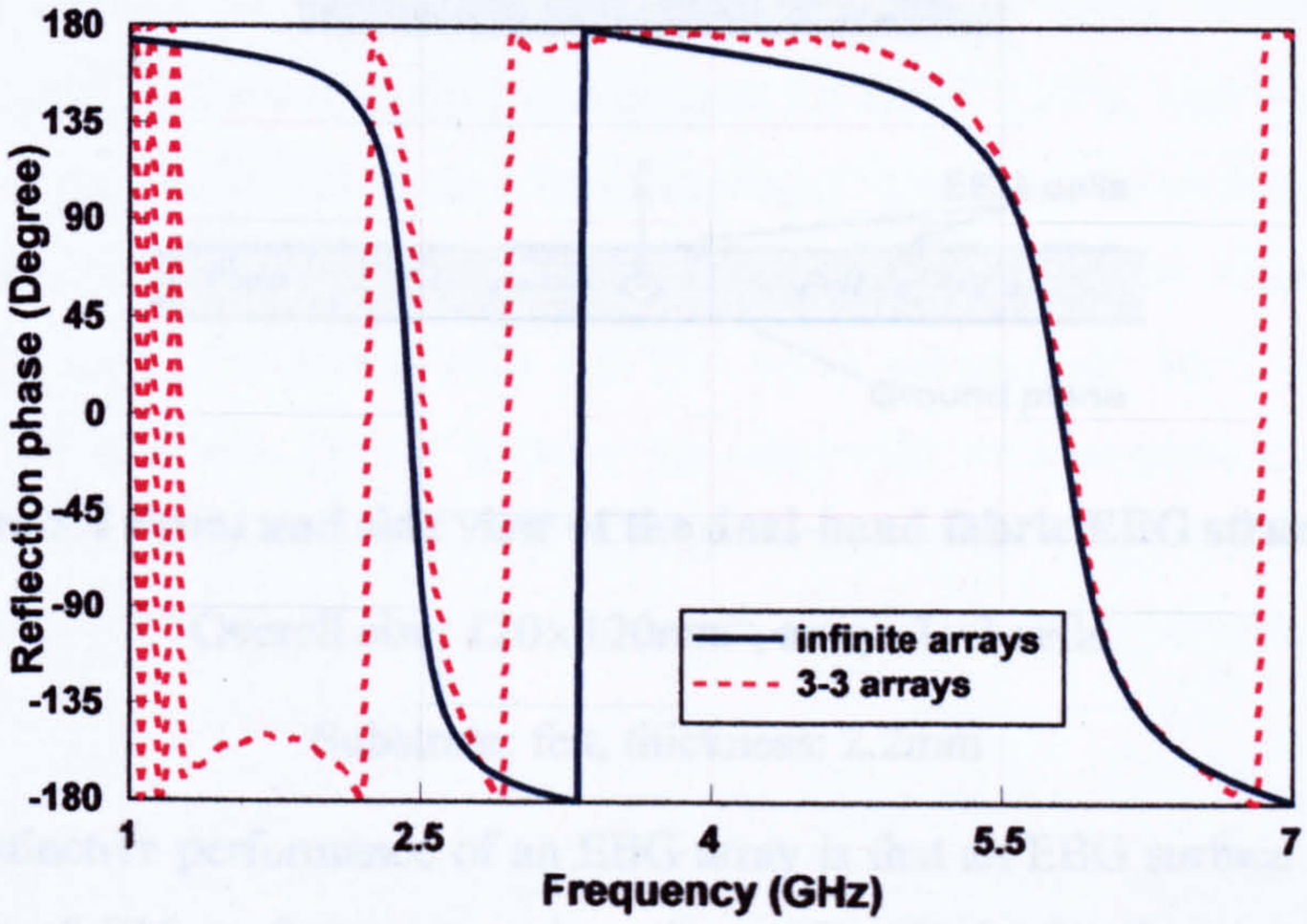

Figure 5.3 Simulated reflection phase of the concentric EBG

The results of the computed reflection phase are shown in Figure 5.3. The design of an infinite size array offers high impedance at 2.44GHz and 5.75GHz with fractional bandwidths of 6.55% and 7.5%. The situation becomes more complicated when a finite size surface is observed at low frequencies. However the reflection phase responses only differ very little to the infinite arrays at the two resonances. From both cases, it is obvious that a sufficient bandwidth for the lower band is achieved while at the higher band, this design offers an acceptable bandwidth response. Note the reflection phase in Figure 5.3 only gives the response reflected phase of a plane wave normal to the surface of the HIS. When an antenna is excited on the top of the HIS, the wave illuminating on the surface is not necessarily normal. Wave with different incident angles were also simulated in the software, and it was found that the phase reflection at the surface is not very sensitive to the angle of the incidence. Therefore we only plot the normal incident wave reflection phase to show the EBG performance.

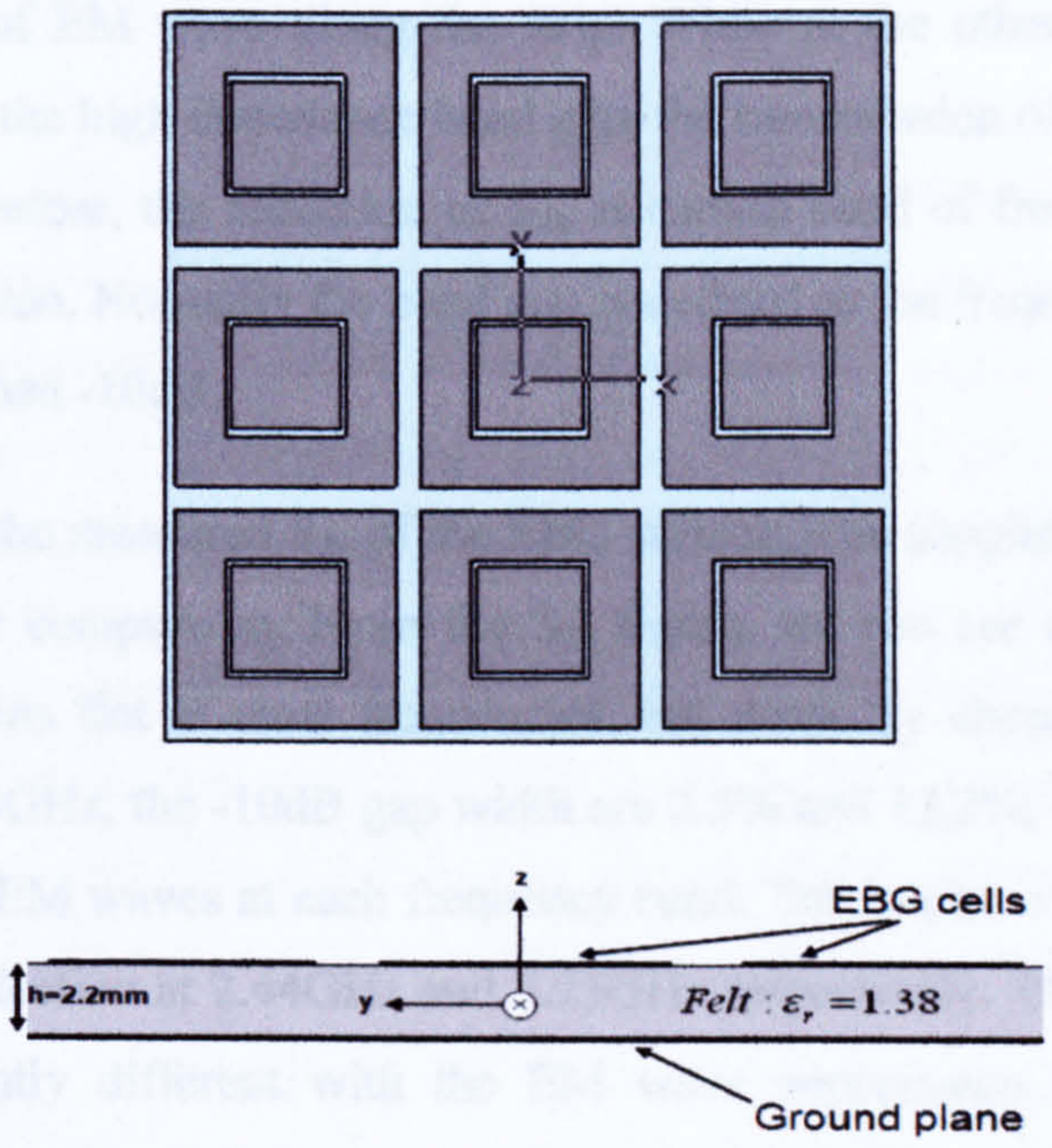

Figure 5.4 Front and side view of the dual-band fabric EBG structure

Overall size: $120 \times 120 mm^2$, array: 3×3 cells

Substrate: felt, thickness: 2.2mm

Another distinctive performance of an EBG array is that an EBG surface forbids the propagation of EM surface waves along its surface in its band gap region. It is important to determine the EM wave bandgap of an EBG so that they can be used to minimize the problem of surface waves in microstrip antennas. To experimentally verify the EM wave transmission behaviour of the concentric EBG, a 3×3 cells array was fabricated. The overall dual-band EBG structure measures $120 \times 120 mm^2$, consisting of just 9 elements with each cell measuring $40 \times 40 mm^2$ and consisting of an outer square loop $36 \times 36 mm^2$ and inner square $17.5 \times 17.5 mm^2$. The front and side views of the EBG arrays are shown in Figure 5.4.

A suspended strip line over and EBG ground plane is used to test the transmission response of the EM waves. The method [19] has been explained in detail in Chapter 2. The S_{21} was measured by connecting the strip line through the EBG array above the surface to the two coaxial ports: one as an exciting source and the other as a matched load. The strip line width was set to be 10mm to match at 50Ω above a 2mm air gap on a metal plane. It is expected that for frequencies within the band gap of the structure, the EBG ground plane will act as a high impedance plane which can block

the transmission of EM wave along the strip. While at the other frequency bands which are outside the high impedance band gap, the transmission of the power should be excellent. Therefore, the reduction of S_{21} at certain band of frequencies indicates the band gap position. Normally the band gap is defined as the frequency range within which S_{21} is less than -10dB.

Figure 5.5 shows the measured S_{21} of the EBG surface. The simulated phase response is also plotted for comparison. From the S_{21} figure, we can see that the EM wave propagation remains flat at most frequencies, but drops by about 20-50dB around 2.38GHz and 6.13GHz, the -10dB gap width are 2.5% and 13.2%, which indicate the stop bands of the EM waves at each frequency band. The in-phase reflection predicts the zero phase reflection at 2.44GHz and 5.75GHz respectively. The reflection phase band gap is slightly different with the EM wave suppression band gap for the designed EBG structure. This is because the suspended strip supports a quasi TEM mode with the dominant electric field component normal to the ground plane, while the normally incident plane wave is associated with the tangential component of the electric field [19].

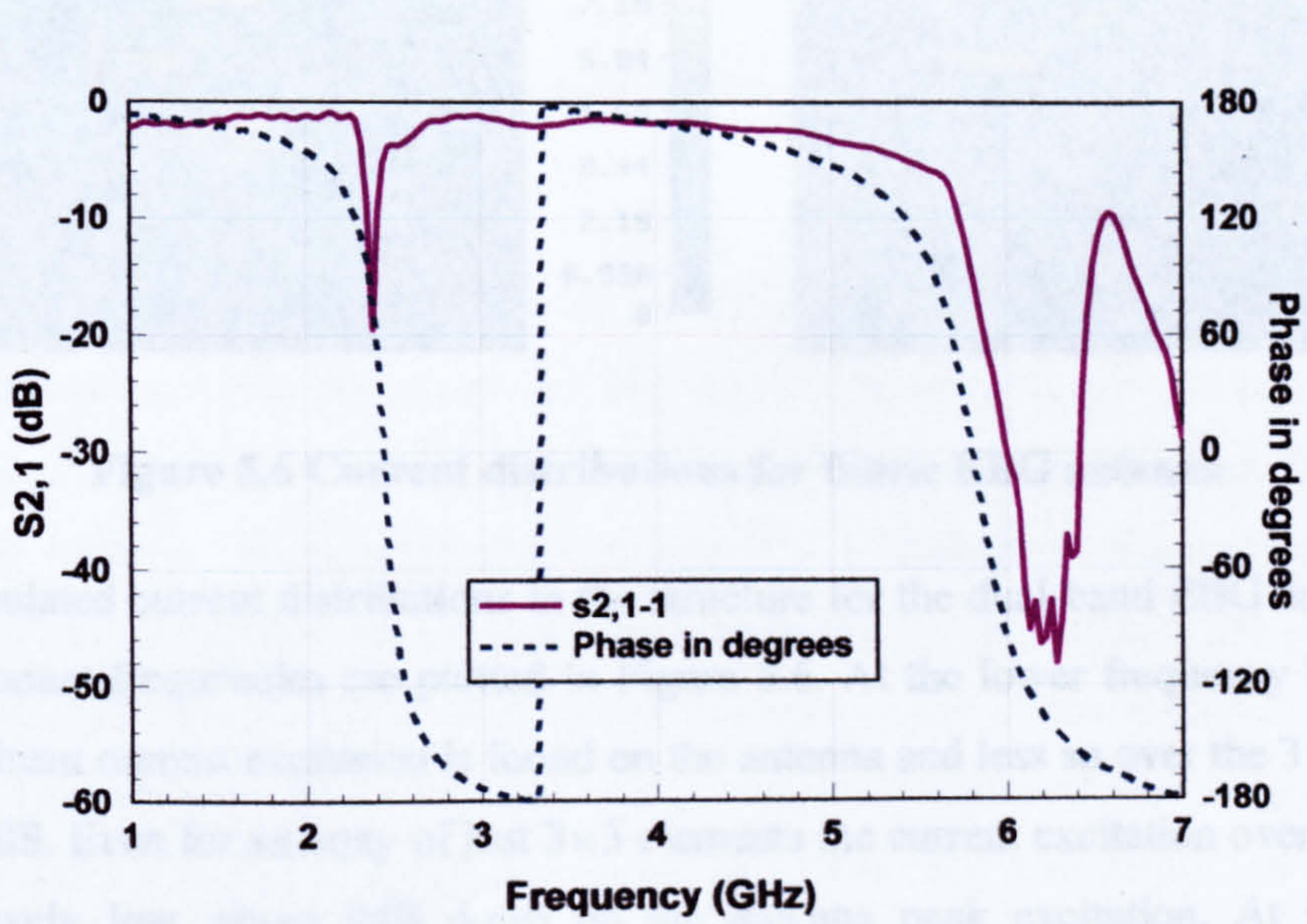

Figure 5.5 Comparison between simulated phase response and measured EM wave transmission bandgap for the concentric EBG array

5.2.2 Fabric Antenna on HIS Ground

The EBG array is designed to act as a high impedance plane for the low profile antenna. It is expected to control the plane wave reflection phase and suppress surface waves as a high impedance plane. Specified to body centric network, the HIS ground is desired to reduce the backward scattering wave towards the body and possibly minimize the coupling between an antenna and other nearby wearing elements.

This aspect of work combines the dual-band fabric CPW antenna with the 3×3 array fabric EBG. The antenna was mounted 1mm above the EBG plane to make sure that the antenna feeding connector is not contact with the EBG surface. CST Microwave Studio was used to simulate the entire model and measurements were carried out with band gaps near 2.45GHz and 5.8GHz resulted.

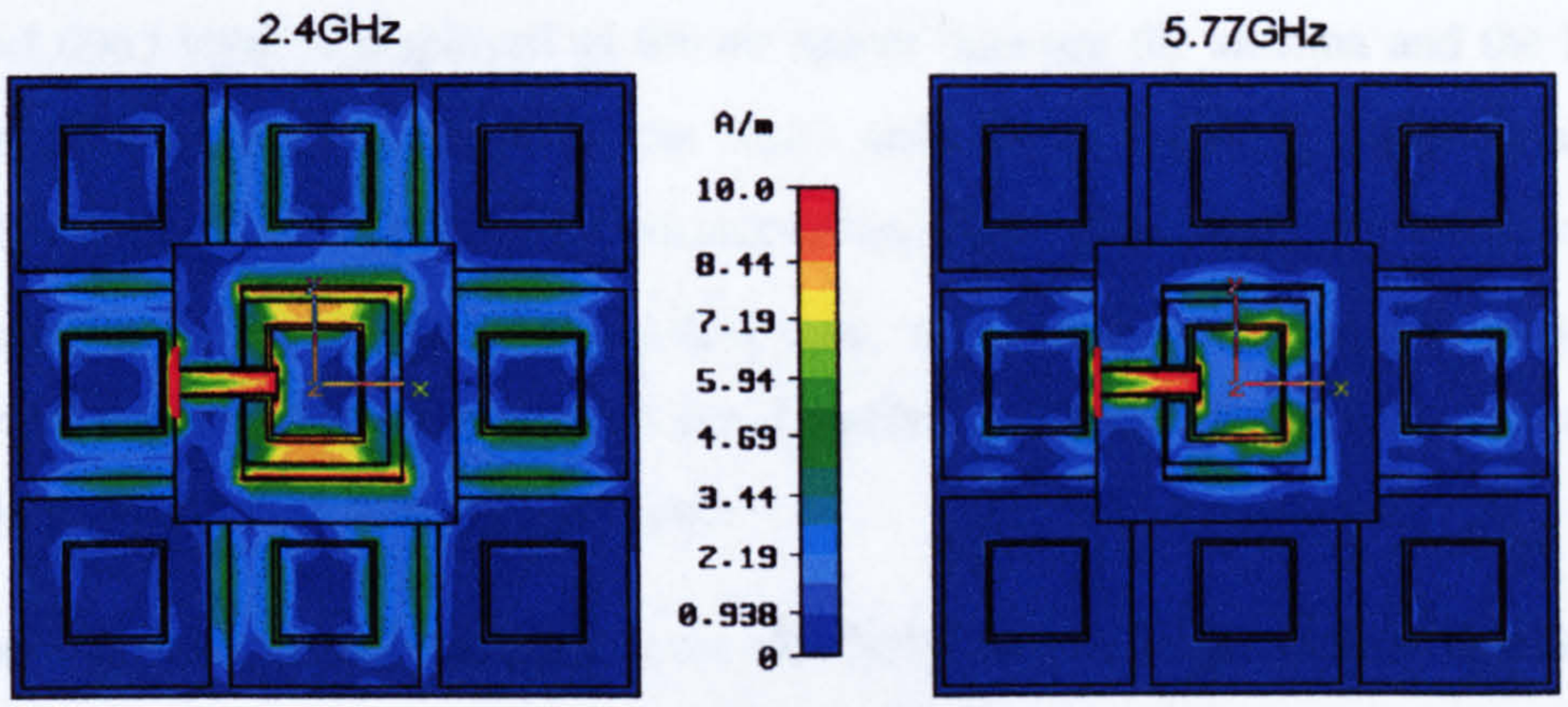

Figure 5.6 Current distributions for fabric EBG antenna

The simulated current distributions in the structure for the dual-band EBG antenna at two resonant frequencies are plotted in Figure 5.6. At the lower frequency band the predominant current excitation is found on the antenna and less so over the 3×3 array of the HIS. Even for an array of just 3×3 elements the current excitation over the HIS is relatively low, about 8dB down on the antenna peak excitation. At the high frequency band the current excitation is largely confined to the antenna and the 3 HIS elements along the feed plane with very low excitation of the remaining elements. This also shows the possibility of reducing the array size even further without affecting the wave shielding function of the EBG.

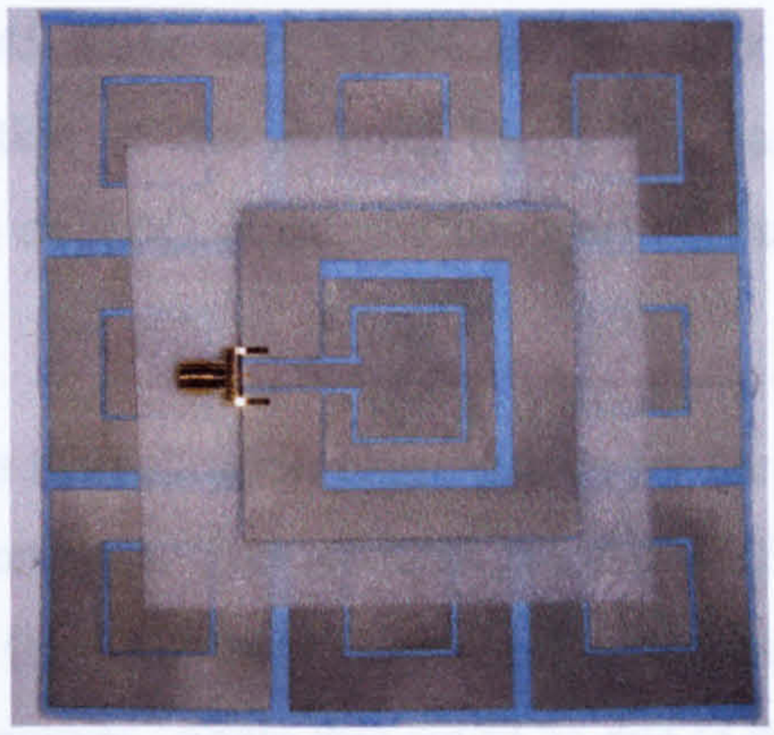

Figure 5.7 Fabricated dual-band fabric antenna on EBG plane

Overall thickness< 4.5mm

The fabricated EBG antenna model is shown in Figure 5.7. A 1mm rohacell ($\varepsilon_r = 1.006$) layer is employed as the air spacer between the antenna and the EBG plane. The overall thickness of the EBG antenna is 4.48mm, which is about 0.036λ for the 2.45GHz band. The measurements were completed in two terms to test the stability of the structure. In the first term, thin sellotape was used to stick the structure and then the structure was sewn together by thread. Results have shown a good agreement with two configurations.

When the antenna is combining with the HIS, there will be mutual impedance coupling between these two elements. The impedance coupling can cause resonance detuning. Thus in order to achieve the desired resonant bands, the antenna dimension is slightly modified when combining with the HIS. The simulation and measurement results of the return loss for the complete antenna/EBG combination are plotted in Figure 5.8. Both the simulation and the measurement show a bandwidth of 4% at the lower resonance band. The shift in the centre frequency is minor, and the percentage error is less than 3%. At the higher frequency band, the resonances are in broad agreement with the simulation and the measurement, while the bandwidth seems wider in the measurement result than that of the simulation. Compare the EBG antenna and the CPW antenna, the antenna alone resonates at the correct frequencies and the bandwidths were 17% at 2.45 GHz and 17.3% at 5.83 GHz at the -10 dB return loss points. On laying the antenna over the EBG material the bandwidths

reduced to 4.1% at 2.45 GHz and 11.9% at 5.8 GHz (5.41GHz – 6.13GHz) respectively. The reduction of the antenna bandwidth happens because when an antenna is working with an EBG plane, the bandgap of the EBG will dominant the wave propagation.

Figure 5.8 also compares the reflection phase results for the EBG and the return loss of the dual-band EBG antenna. The resonances of the EBG antenna (2.45GHz & 5.8GHz) slightly differ from the zero degree reflection phase points (2.44GHz & 5.75GHz) of the EBG structure. Again this could be due to the impedance coupling of the two structures. Also the incident wave with different angles launched to the EBG surface could be another reason. The EBG array manufactured in this study has a size around $0.5\,\lambda_{2.45GHz} \times 0.5\,\lambda_{2.45GHz}$, which is normally enough for antenna applications. And overall, the impedance matching bands of the antenna/EBG combination have achieved a broad agreement with the -90 to 90 degree reflection phase bandgap responses of the 3×3 EBG arrays.

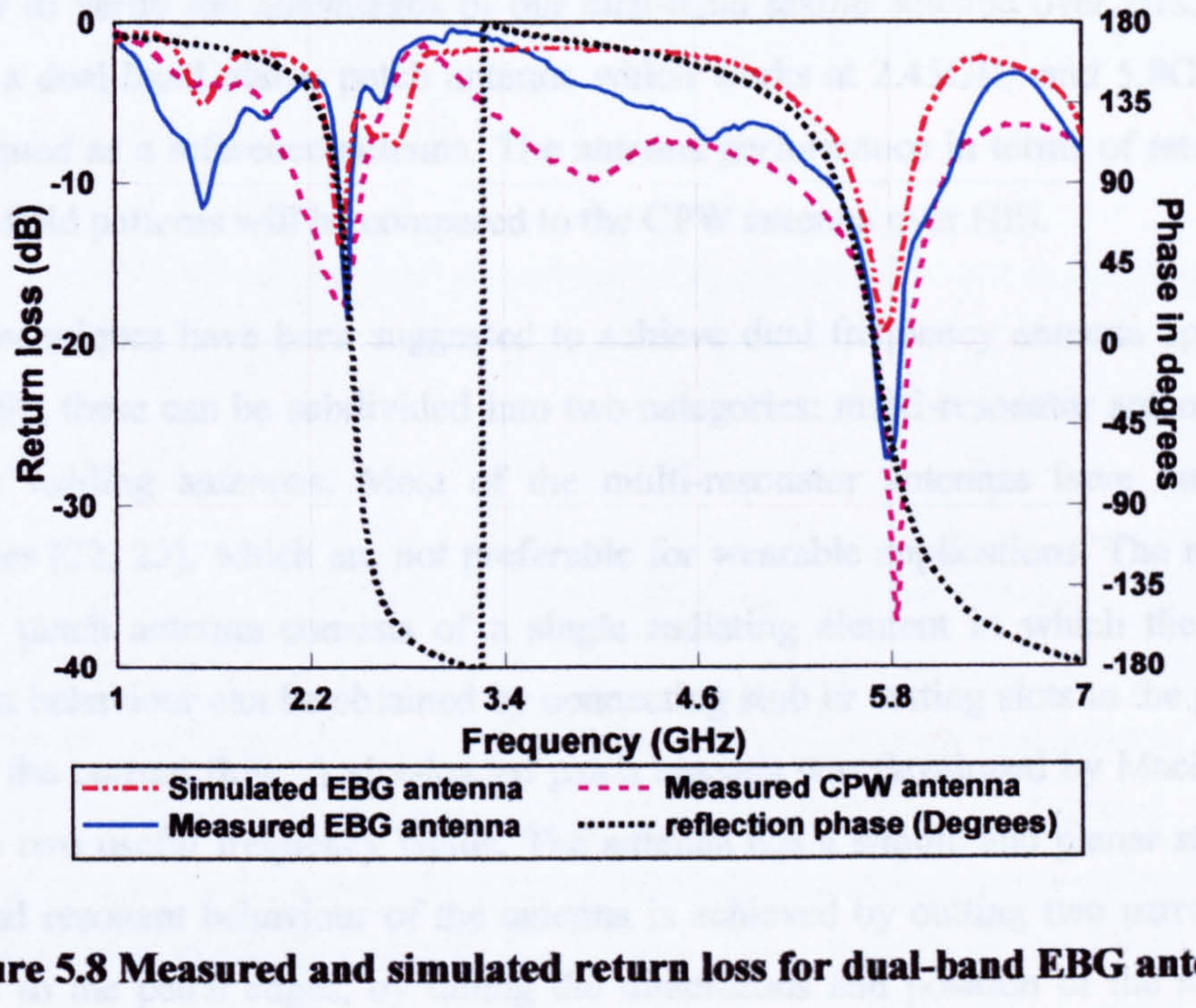

Figure 5.8 Measured and simulated return loss for dual-band EBG antenna

The radiation characteristics of the EBG antenna were also measured in the anechoic chamber. The results will be plotted in Figure 5.11 and Figure 5.12 with a comparison to a conventional microstrip antenna, and discuss will be given in section 5.2.4.

5.2.3 Dual-band Slots Patch Antenna

As we mentioned before, researchers have found that planar antennas with big ground planes can bring a lot of benefit to body-centric communications. Not only can the ground plane minimize the backward scattering wave towards the body, but also the detuning of this type of antenna in the vicinity of body is slight. Single [20] and dual [21] resonance textile patch antennas have been developed in recent studies. These antennas are proved to have relatively low backward radiation, and the body specific absorption rates (SAR) are calculated to be low. However, impedance matching bandwidths of these antennas are poor. The antenna in [20] barely offers useful bandwidth when put adjacent to human torso at 2.45GHz. The dual-band E-shape textile antenna in [21] only provides a 3% -10dB bandwidth at 2.2GHz and 3.6% -6dB bandwidth at 3GHz. Moreover, instead of having a central lobe, the radiation pattern of the dual E antenna at the upper frequency band has two lobes, which is not preferable for a patch antenna.

In order to verify the advantages of our dual-band textile antenna over HIS, in this section a dual-band planar patch antenna which works at 2.45GHz and 5.8GHz will be designed as a reference antenna. The antenna performance in terms of return loss and far-field patterns will be compared to the CPW antenna over HIS.

Many techniques have been suggested to achieve dual frequency antenna operation. Generally, these can be subdivided into two categories: multi-resonator antennas and reactive loading antennas. Most of the multi-resonator antennas have multilayer structures [22, 23], which are not preferable for wearable applications. The reactive-loading patch antenna consists of a single radiating element in which the double resonant behaviour can be obtained by connecting stub or cutting slots to the patch to change the current flow. A slot-loaded patch antenna was developed by Maci [24] to provide two useful frequency bands. The antenna has a simple and planar structure. The dual resonant behaviour of the antenna is achieved by cutting two narrow slots parallel to the patch edges, by tuning the dimensions and position of the slots, the higher mode (3^{rd}) current distribution can be modified to have a similar plot of the first mode. Therefore the two modes of operation show similar radiating properties.

The dual-band slot-loaded patch antenna in [24] was redesigned to work at WLAN bands (2.45GHz and 5.8GHz) in this project as a reference antenna. For consistency with the EBG array, the antenna was designed to have an overall size of 120 mm × 120 mm, and the fabric materials felt ($\varepsilon_r = 1.38$) and zelt ($\sigma = 1e10^6$S/m) are used as the dielectric substrate and conducting elements respectively. The geometry and prototype of the antenna are shown in Figure 5.9.

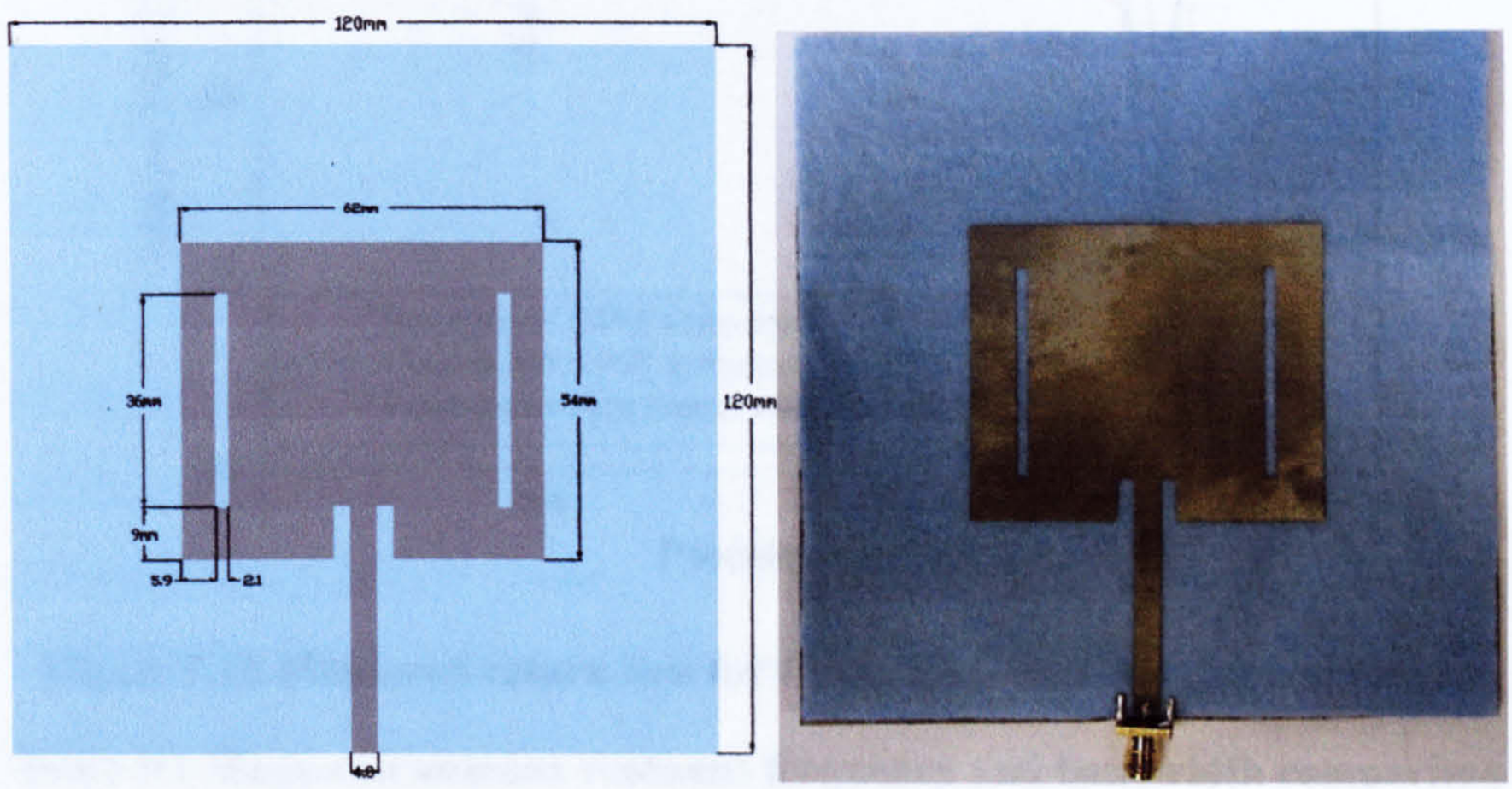

Figure 5.9 Geometry and prototype of dual-band slot patch antenna

5.2.4 Results Comparison

The measured return loss for the complete EBG/antenna combination is plotted in Figure 5.10 and compared with that for the CPW antenna alone. The return loss of the conventional dual frequency slot patch antenna is also shown for comparison. The slot patch antenna presents three fairly good matching resonances as expected. And the central of first and third resonant frequencies are corresponding to the desired WLAN bands at around 2.45GHz and 5.8GHz. However, the impedance bandwidths of the slot patch antenna are 2.5% and 4.6% at each band. Compare with the EBG antenna which has the bandwidths of 4.1% and 11.9%, the useful impedance matching bandwidths are reduced by 39% at 2.45GHz and 61% at 5.8GHz. The comparisons of

the central resonant frequencies and the bandwidths of the three antennas are listed in Table 5-1.

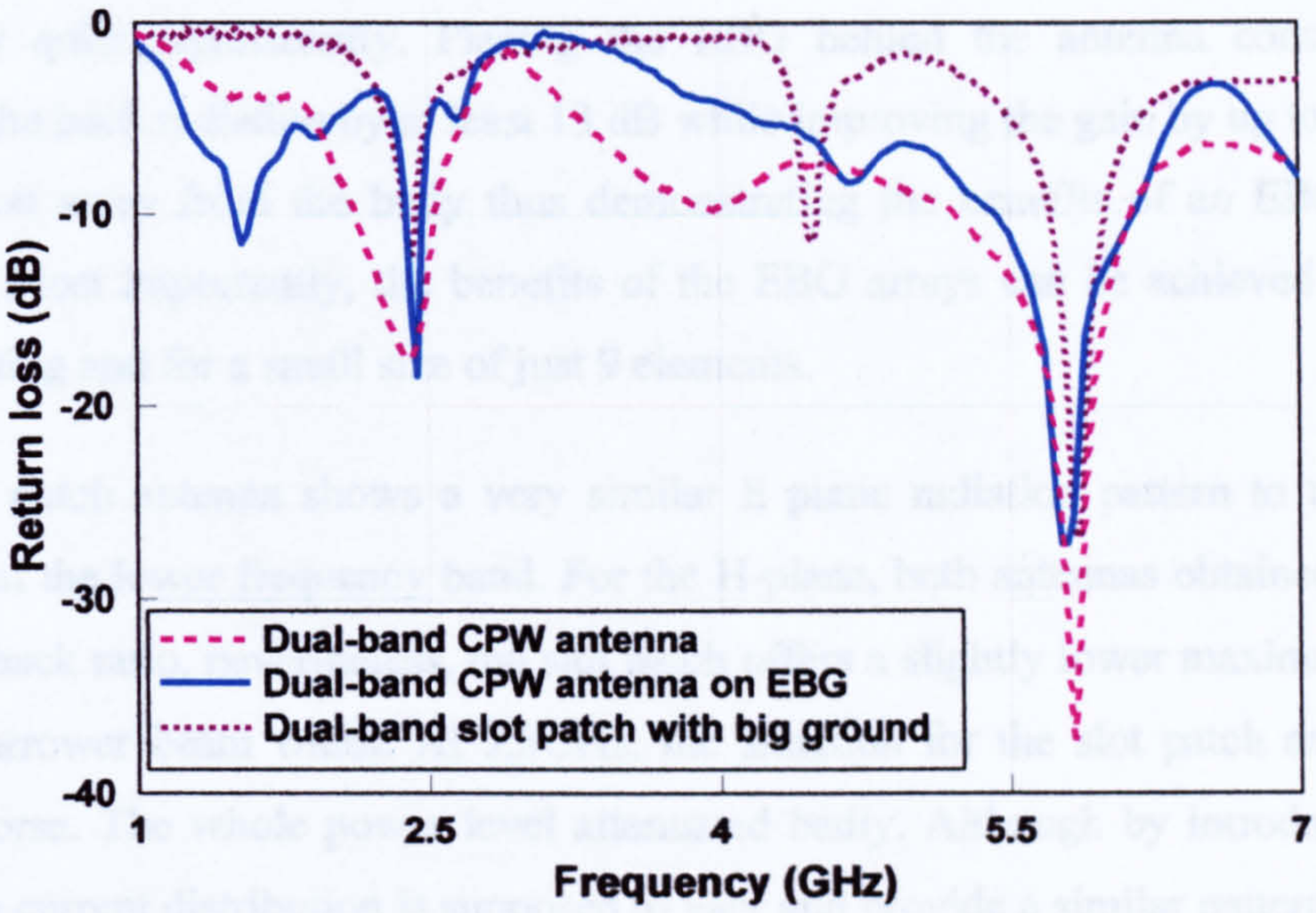

Figure 5.10 Measured return loss for CPW, EBG and slot patch antennas

Table 5-1 Measured antenna resonant frequency and bandwidth comparison

Antenna	Size (mm^2)	2.45GHz		5.8GHz	
		f_c	Bandwidth	f_c	Bandwidth
CPW	55×55	2.41GHz	17%	5.83GHz	17.3%
CPW/EBG	120×120	2.44GHz	4.1%	5.78GHz	11.9%
Slot patch	120×120	2.41GHz	2.5%	5.86GHz	4.6%

Finally the radiation patterns of the textile EBG antenna and the CPW antenna measured at 2.45GHz and 5.8GHz are shown in Figure 5.11 and 5.12 for both E-plane and H-plane patterns. The measurements were carried out in the anechoic chamber with the same set up. For the EBG antenna, the location of the antenna at the centre of the EBG also of the turning table ensures that the pattern obtained is as symmetric as possible. The patterns of the slot patch antenna are also plotted as a reference. It can be seen that the high impedance ground plane has caused obvious changes in antenna directivity. The EBG plane leads to a significant front to back ratio increasing and a higher maximum gain. And for wearable applications, the backward radiation towards

the body is desired to be reduced as much as possible. This has been well verified by our EBG antenna at both frequencies. For both E and H planes, the CPW antenna without the EBG backing has a dipole like radiation pattern and hence radiated into the body quite significantly. Placing the EBG behind the antenna considerably reduces the back radiation by at least 13 dB while improving the gain by up to 3 dB in a direction away from the body thus demonstrating the benefits of an EBG based antenna. Most importantly, the benefits of the EBG arrays can be achieved without vias existing and for a small size of just 9 elements.

The slot patch antenna shows a very similar E plane radiation pattern to the EBG antenna at the lower frequency band. For the H-plane, both antennas obtained a good front to back ratio, nevertheless, the slot patch offers a slightly lower maximum gain, and a narrower beam width. At 5.8GHz, the situation for the slot patch antenna is much worse. The whole power level attenuated badly. Although by introducing the slots, the current distribution is supposed to vary and provide a similar pattern like the lower frequency band, a measured three lobe pattern was shown along the E plane of the patch. For H plane, although there is no obvious side lobe, the received power level is too low to compare with that of the EBG antenna.

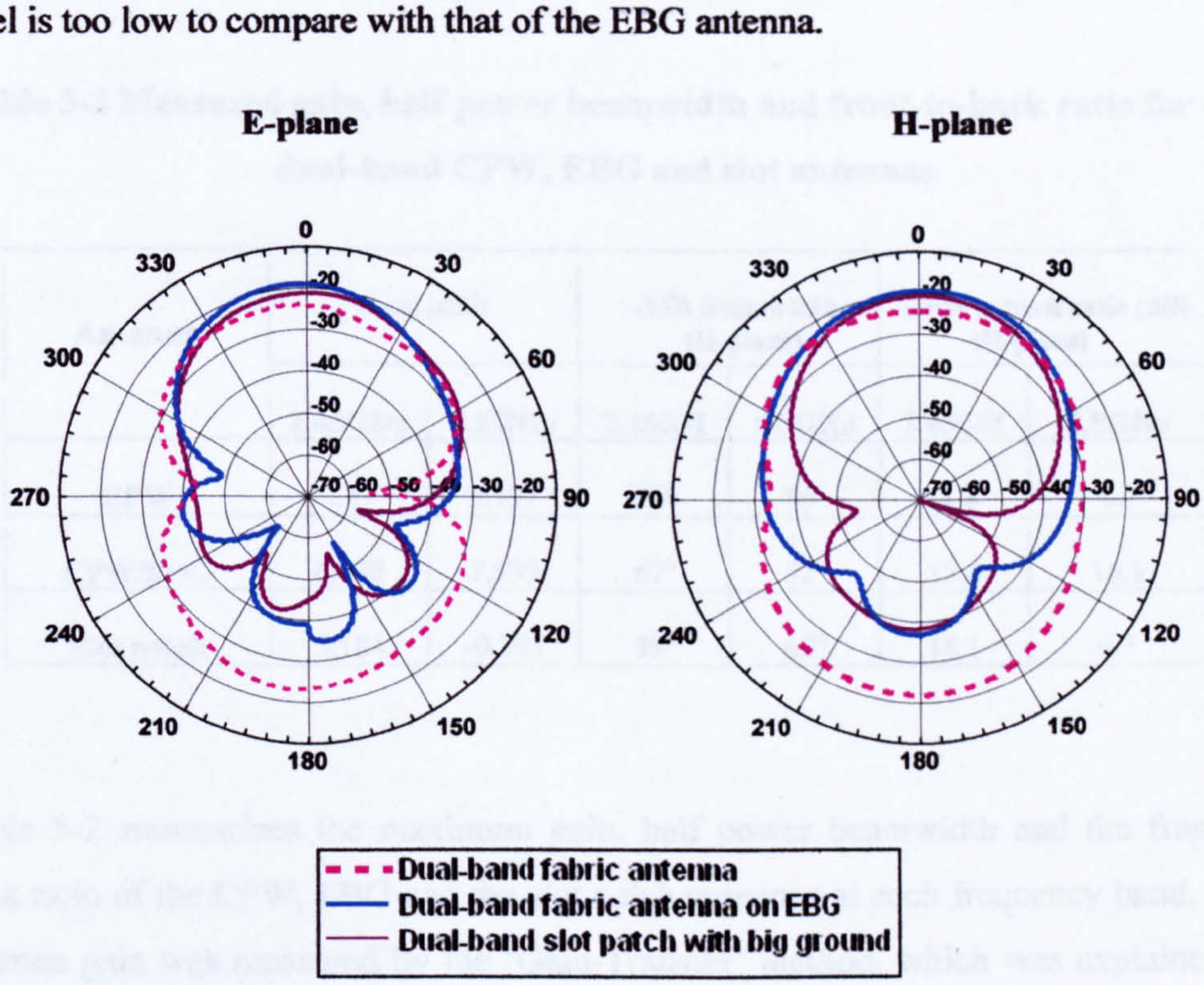

Figure 5.11 Measured radiation patterns at 2.45GHz

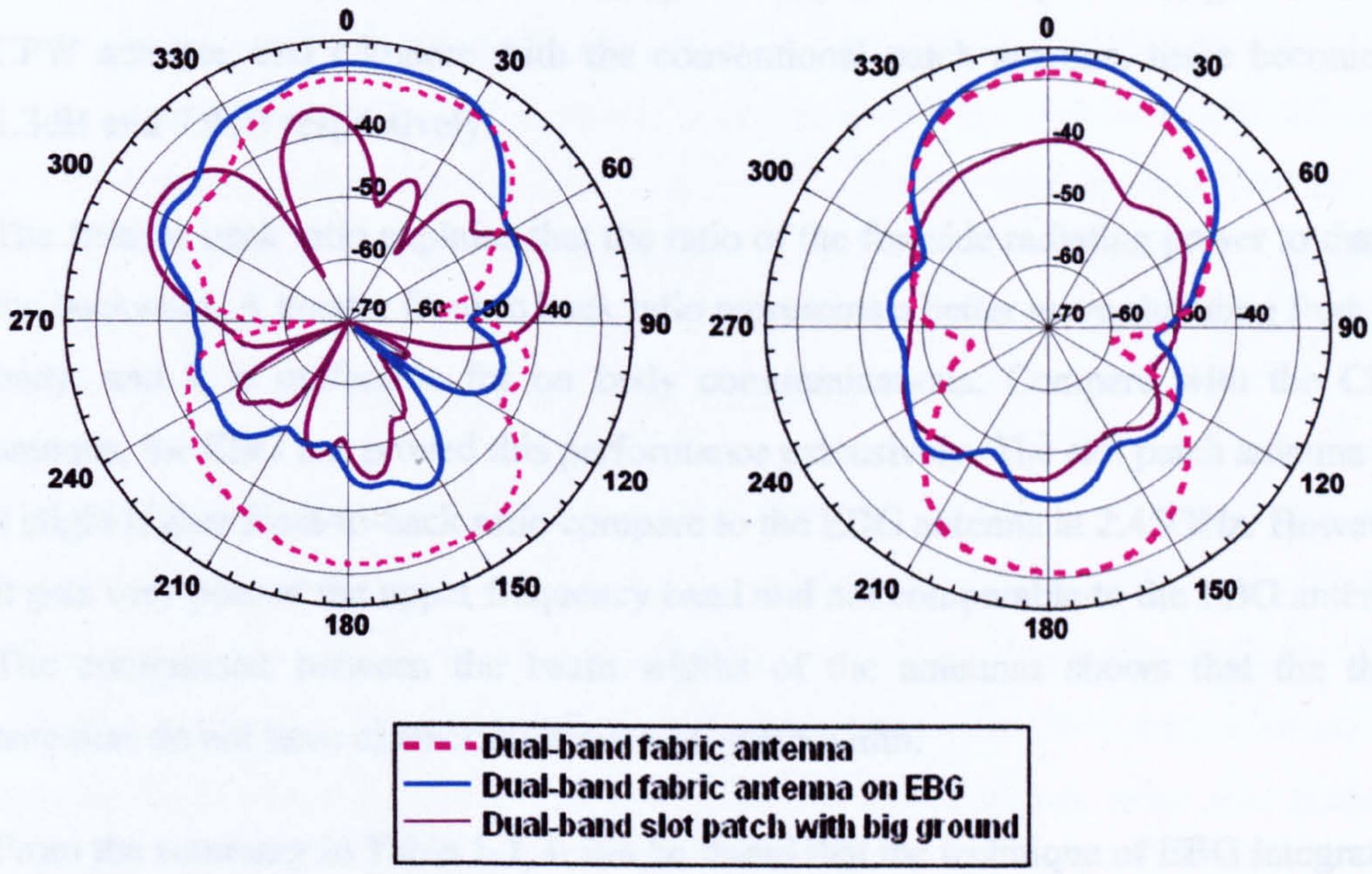

Figure 5.12 Measured radiation patterns at 5.8GHz

Table 5-2 Measured gain, half power beamwidth and front-to-back ratio for the dual-band CPW, EBG and slot antennas

Antenna	Gain (dBi)		-3dB Beamwidth (H-plane)		Front to back ratio (dB) (H-plane)	
	2.45GHz	5.8GHz	2.45GH	5.8GHz	2.45GH	5.8GHz
CPW	3.87	5.177	86°	56°	-1.8	1.7
CPW/EBG	6.438	7.599	67°	52°	17.4	16.1
Slot patch	5.184	-0.303	59°	62°	18.1	6.1

Table 5-2 summarizes the maximum gain, half power beamwidth and the front to back ratio of the CPW, EBG and the slot patch antennas at each frequency band. The antenna gain was measured by the 'Gain-Transfer' method, which was explained in detail in chapter 4.2. A standard gain horn antenna was employed as the gain

reference antenna. The EBG antenna appears to have the most directivity enhancement. It has achieved a 2.6dB (2.45GHz) and 2.4dB (5.8GHz) gain over the CPW antenna, and compare with the conventional patch antenna, these become to 1.3dB and 7.9dB respectively.

The front to back ratio explains that the ratio of the foreside radiating power to that of the backward. A greater front to back ratio represents a better wave shielding from the body, and it is preferable for on body communications. Compare with the CPW antenna, the EBG has proved this performance extensively. The slot patch antenna has a slight higher front-to-back ratio compare to the EBG antenna at 2.45GHz. However, it gets very poor at the upper frequency band and not comparable to the EBG antenna. The comparison between the beam widths of the antennas shows that the three antennas do not have distinct difference on beam width.

From the summary in Table 5-2, it can be found that the technique of EBG integration can enhance the gain, directivity of the antenna, decrease the beam width and maintain good front to back power ratio cross the frequency range. Also, improved radiation pattern control and bandwidth can been obtained for the dual band EBG antenna when compared to the conventional patch antenna.

5.3 Dual-band triangular antenna on EBG

The dual-band triangular antenna described in Chapter 4.3 was also tested on the concentric EBG plane, and the results in terms of return loss and radiation patterns are plotted in Appendix D.

Compared to the antenna alone, the presence of the EBG ground plane has reduced the bandwidths at both resonant bands but still adequate at 5% for 2.45GHz and more than 20% for 5GHz. The measured radiation patterns at 2.45GHz, 5.2GHz and 5.8GHz have also shown the benefits of an EBG based antenna. There is significant gain improvement in a direction away from the body and back radiation reduction at each measured frequency band.

5.4 Conclusion

For wearable applications, as the antenna is meant to operate in the vicinity of the body, it needs to provide with a ground plane to shield the body from the radiation. Electromagnetic Band Gap structure as a new concept has been proved to have a lot of advantages when working with antennas. For on body networks, the EBG array can act as a high impedance ground plane for wearable antennas to stop the radiation toward the body and improve antenna performances.

This chapter has presented a simple design structure for dual-band high impedance electromagnetic band gap materials. The simple structure reduces the difficulties of manufacturing the fabric material significantly, and it increases the accuracy of the cutting dimensions. The combination of the antenna and the EBG are conformal and manufactured from flexible materials that are readily hidden or sewn into items of clothing.

A detailed analysis of compact EBG antenna has been undertaken. The result has demonstrated a considerable good integration with a wearable coplanar antenna and an EBG surface that operates at two frequency bands of interest for wireless network communications. Although the EBG ground plane reduces the impedance bandwidth of the original coplanar antenna, the EBG antenna still offers 4.1% and 11.9% bandwidths for the WLAN bands, which are quite enough for the real application. In addition, the EBG plane introduces 2.6dB and 2.4dB gain over the CPW antenna in the front direction, and reduces the back radiation significantly.

A dual-band slot patch antenna as a reference antenna has been measured and compared to the EBG antenna. Results have demonstrated that the EBG antenna has advantages over the slot patch antenna on both the impedance matching and the radiation characteristics. The EBG antenna provides useful impedance bandwidths as nearly twice of the patch antenna, and most importantly, it is capable to maintain a rather good monopolar pattern at high frequency operating band.

References:

[1] **Alomainy, A., Hao, Y. and Davenport, D. M.,** "Parametric Study of Wearable Antennas with Varying Distances from the Body and Different On-Body Positions," *The IET Seminar on Antennas and Propagation for Body-centric Wireless Communications,* pp.84-89, Apr 2007.

[2]**Hurme, h., Salonen, P. and Rantanen, J.,** "On the Study of Antenna Placement in a Smart Clothing," *International Conference Modeling and Simulation proceedings*, pp.1-6, Feb 2003.

[3] **Hertleer, C., Rogier, H. and Van Langenhove, L.,** "A textile Antenna for Protective Clothing," *The IET Seminar on Antennas and Propagation for Body-centric Wireless Communications,* pp.44-46, Apr 2007.

[4] **Locher, I., Klemm, M., Kirstein, T. and Troster, G.,** "Design and Characterization of Purely Textile Patch Antennas," *IEEE Transactions on Advanced Packaging*, Vol.29, No.4, pp.777-788, Nov 2006.

[5] **Salonen, P. and Rahmat-Samii, Y.,** "Wearable Antennas: Advances in Design, Characterization, and Application," Chapter 6, *Antennas and Propagation for Body-Centric Wireless Communications,* Artech House, pp.151-188, 2006.

[6] **Salonen, P., Keskialammi, M. and Sydanheimo, L.,** "A low cost 2.45 GHz Photonic Band Gap Patch Antenna for Wearable Systems," *IEE 11th International Conference on Antennas & Propagation (ICAP2001),* vol.2, pp. 719-723 Manchester 2001.

[7] **Salonen, P. O., Yang, F., Rahmat-Samii, Y. and Kivikoski, M.,** "WEBGA – Wearable Electromagnetic Band-Gap Antenna," *IEEE Antennas and Propagation Society International Symposium*, Vol.1, pp. 455-459, 2004.

[8] **Bao, X. L. and Ammann, M. J.,** "Dual-Band GPS Patch Antenna based on Dualband Fractal EBG Technique," *LAPC Proceedings*, pp. 53-56, Apr 2006.

[9] **Monorchio, A., Manara, G. and Lanuzza, L.,** "Synthesis of Artificial Magnetic Conductors by using Multilayered Frequency Selective Surfaces," *IEEE Antennas Wireless Propagation Letters*, vol. 1, pp. 196-199, 2002.

[10] **Rogers, S., McKinzie, W. and Mendolia, G.,** "AMCs Comprised of Interdigital Capacitor FSS Layers Enable Lower Cost Applications," *IEEE Antennas and Propagation Society International Symposium*, vol. 2, pp. 411-414, 2003.

[11] **Feresidis, A. P., Chauraya, A., Goussetis, G., Vardaxoglou, J. C. and P'de Maagt,** "Multi-band artificial Magnetic Conductor Surfaces," *IEE Seminar on Metamaterials for Microwave and (Sub) mm wave Applications*, 2003.

[12] **Falayan, O.,** "Compact High Impedance Plane Antennas," *PhD Thesis, University of Sheffield,* Apr 2007.

[13] **Langley, R. J. and Parker, E. A.,** "Double Square Frequency Selective Surfaces and Their Equivalent Circuit," *IEE Electronics Letters,* Vol.19, pp. 675-677, 1983.

[14] **Yang. F. and Rahmat-Samii, Y.,** "Reflection Phase Characterizations of the EBG Ground Plane for Low Profile Wire Antenna Applications," *IEEE Transactions on Antennas & Propagation,* Vol.51, No.10, pp.2691-2703, Oct 2003.

[15] **Feresidis, A. P., Goussetis, G. and Vardaxoglou, J. C,** "Metallodielectirc Arrays without vias as Artificial Magnetic Conductors and Electromagnetic Bandgap Surfaces," *IEEE Antennas and Propagation Society International Symposium*, vol.2, pp.1159-1162, 2004.

[16] **Folayan, O. and Langley, L. J.,** "Compact Electromagnetic Bandgap Structures," *Loughborough Antennas & Propagation Conference Proceeding*, pp.293-296, Apr 2006.

[17] **Bray, M. G. and Werner, D. H.,** "A Novel Design Approach for an Independently Tunable Dual-band EBG AMC Surface," *IEEE Antennas and Propagation Society International Symposium*, vol.1, pp.289-292, 2004.

[18] **Sievenpiper, D., Zhang, L., Broas, R.F.J., Alexopolous, N.G. and Yablonovitch, E.,** "High-Impedance Electromagnetic Surfaces with a Forbidden Frequency Band," *IEEE Transactions on Microwave Theory Technology,* Vol.47, No.11, pp.2059-2074, 1999.

[19] **Aminian, A., Yang, F. and Rahmat-Samii, Y.,** "In-phase Reflection and EM Wave Suppression Characteristics of Electromagnetic Band Gap Ground Planes," *IEEE Antennas and Propagation Society International Symposium,* pp. 430-433, 2003.

[20] **Salonen, P., Rahmat-Samii, Y. and Kivikoski, M.,** "Wearable Antennas in the Vicinity of Human Body," *IEEE Antennas & Propagation International Symposium,* Vol.1, pp. 467-470, Jun 2004.

[21] **Salonen, P. O., Kim, J., Rahmat-Samii, Y.,** "Dual-Band E-Shaped Patch Wearable Textile Antenna," *IEEE Antennas & Propagation International Symposium,* Vol.1, pp. 459-463, 2005.

[22] **Lee, C-S., Nalbandian, V. and Schwering, F.,** "Multi-layer Dual-band Microstrip Antenna," *IEEE Antennas & Propagation Society International Symposium,* Vol.1, pp.472-475, Jun 1994.

[23] **Michail, G.C. and Uzunoglu, N. K.,** "Dual-frequency and Dual-polarization Multilayer Microstrip Antenna Element," *Microwave and Optical Technology Letters,* Vol.42, Issue 4, pp.311-315, Jun 2004.

[24] **Maci, S., Biffi Gentili, G., Piazzesi, P. and Salvador, C.,** "Dual-band Slot-Loaded Patch Antenna," *IEE Proceedings on Microwave& Antennas Propagations,* Vol.142, No.3, pp.225-232, Jun 1995.

Chapter 6

Antenna and EBG under On-body Environment

6.1 Introduction

The human body presents a very challenging environment for wearable antennas that need to communicate efficiently, not only because of the complexity and inhomogeneous nature of body, but also because of the dynamic conditions that the antennas might encounter. Apart from the serious interaction between the antenna and the body, other situations, like bending and moisturizing can also affect antenna performance. To demonstrate antenna performance in the dynamic body environment, the fabric CPW antenna as well as the EBG is tested under a few conditions: bending, washing, coupling and on body. Analysis will be focused on antenna impedance matching and radiation characteristics under these conditions and discussion will be given in this chapter.

When a textile antenna is integrated into a garment, the patch might bend. To evaluate how much bending might affect the antenna performance, several experiments have been undertaken in this project. The bending gauge models the real situation of antenna location on a human arm, leg or shoulder. Two different radii of curvature are employed, and the impedance matching and radiation characteristics are both tested.

The effect of the presence of human body lossy tissue on the antenna performance and the dependence of the antenna characteristics on distance and location on the body have been analysed and numerically investigated in [1]. Studies have found that antennas with backing ground plane generally provide the necessary components to achieve optimised performance, such as a monopole. In other antennas, like dipoles, the resonance is detuned when close to the body. Most of the data presented so far is computational; only a few measurements have been done on a real person. In this chapter, antenna performance is investigated on a real human body in terms of return losses and radiation patterns which are discussed and analysed.

For wearable applications, antennas have the possibility of being exposed under rain or snow. To make sure the antenna can work properly under wet conditions is a big challenge for designers. As for this project, fabric materials are preferentially chosen, to test the antenna and EBG performance under damp situations is necessary. Since it is difficult to model the damp condition in a software environment, groups of measurements are carried out to give a full analysis.

Furthermore, in the future personal communications, two or more antennas might be worn and activated on the body at the same time, thus coupling between elements can cause serious problems. The causes of coupling are complicated and the solutions are multiple. In this project, coupling between antenna pairs on the body are studied. Both simulation and measurements are completed, and it is found that the EBG ground plane can offer a great benefit of reducing the interference between antenna elements.

Finally the Specific Absorption Rate (SAR) which aids the quantitative study of power absorption issues, as an essential factor of near body communication, is studied. A liquid phantom which is filled with a liquid that has the same electrical characteristics as the tissues in the human body is employed in the measurement. The method uses direct measurement of the electric fields inside the phantom with a small probe, and provides a straightforward outcome of the test. Thus it is commonly used for SAR evaluations. A CPW antenna with and without an EBG ground plane are both measured and a comparison is made based on the results. Simulation is also carried out in CST Microwave Studio, which provides a comprehensive technique to calculate the electromagnetic field. To calculate the peak SAR values based on 1gram and 10gram tissues, two types of human torso models are constructed in the software. One model simulates the liquid phantom used in the measurements, and the other gives a stratified elliptical cylinder with different physical tissues of the human body trunk. Analysis is focused on the effect of the presence of the EBG ground plane, as well as the distance of the antenna from the human body.

6.2 Bending Gauge

Antenna's performance under bending conditions is one of the important factors for wearable applications. Under an on-body environment it is difficult to keep antenna in a flat condition especially for elements made of fabric materials. Therefore, it is necessary to model a bending set up to test the antenna performance. In order to evaluate the antenna and EBG functions on a bending set up that resembles a worn environment, two polystyrene cylinders (with relative permittivity close to air) are employed with diameter of 80mm and 140mm respectively, corresponding approximately to the typical size of a human arm and leg. Figure 6.1 shows the dual-band fabric antenna bending on a cylinder in the measurement. And the antenna and EBG are bent around the cylinder along two principal planes, E and H plane.

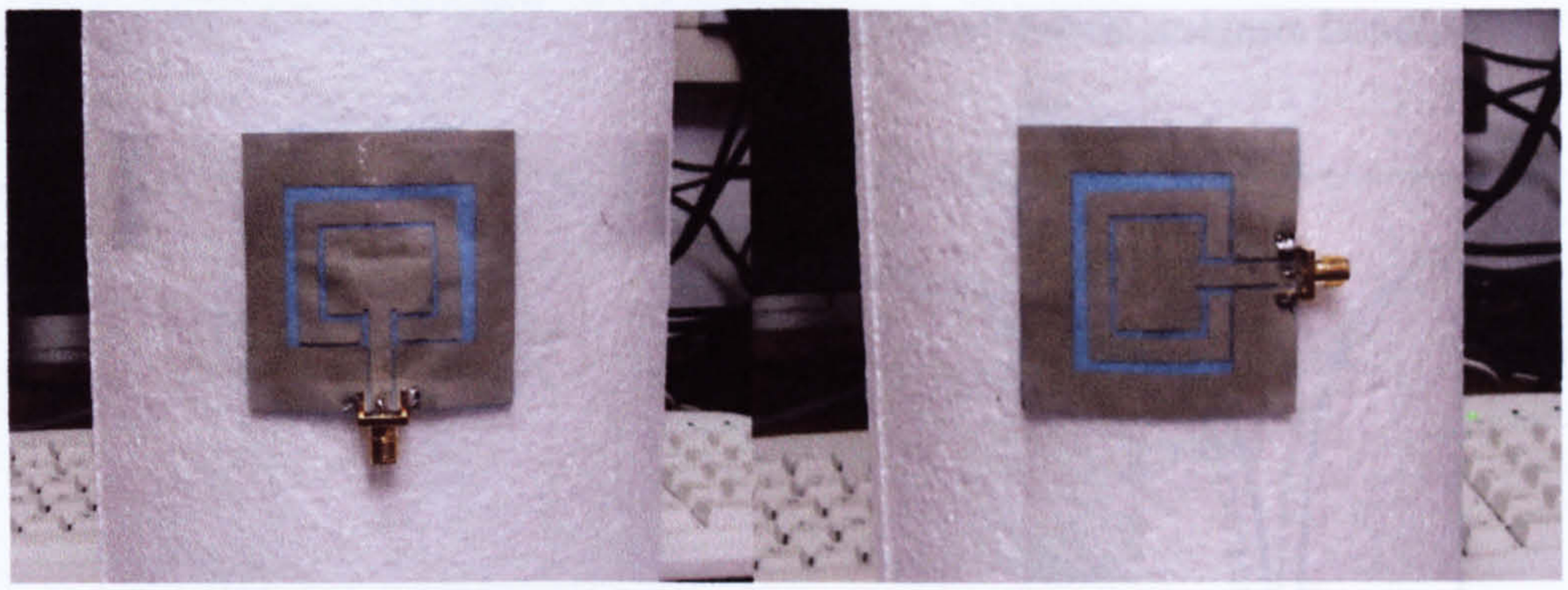

(a) Along H-plane (b) along E-plane

Figure 6.1 Antenna under bending gauge

The return losses were tested using a HP8720 network analyzer. In order to keep the setup stable, the antenna and EBG are fixed on the cylinder by using very thin sellotape at each corner. A very thin semi-rigid cable with SMA connectors is used for the connection. The measured return losses of the bent dual-band coplanar fabric antenna and EBG-antenna are plotted in Figure 6.2 and Fig 6.3 respectively. The values of the tested flat antenna/EBG in flat condition are also plotted for comparison.

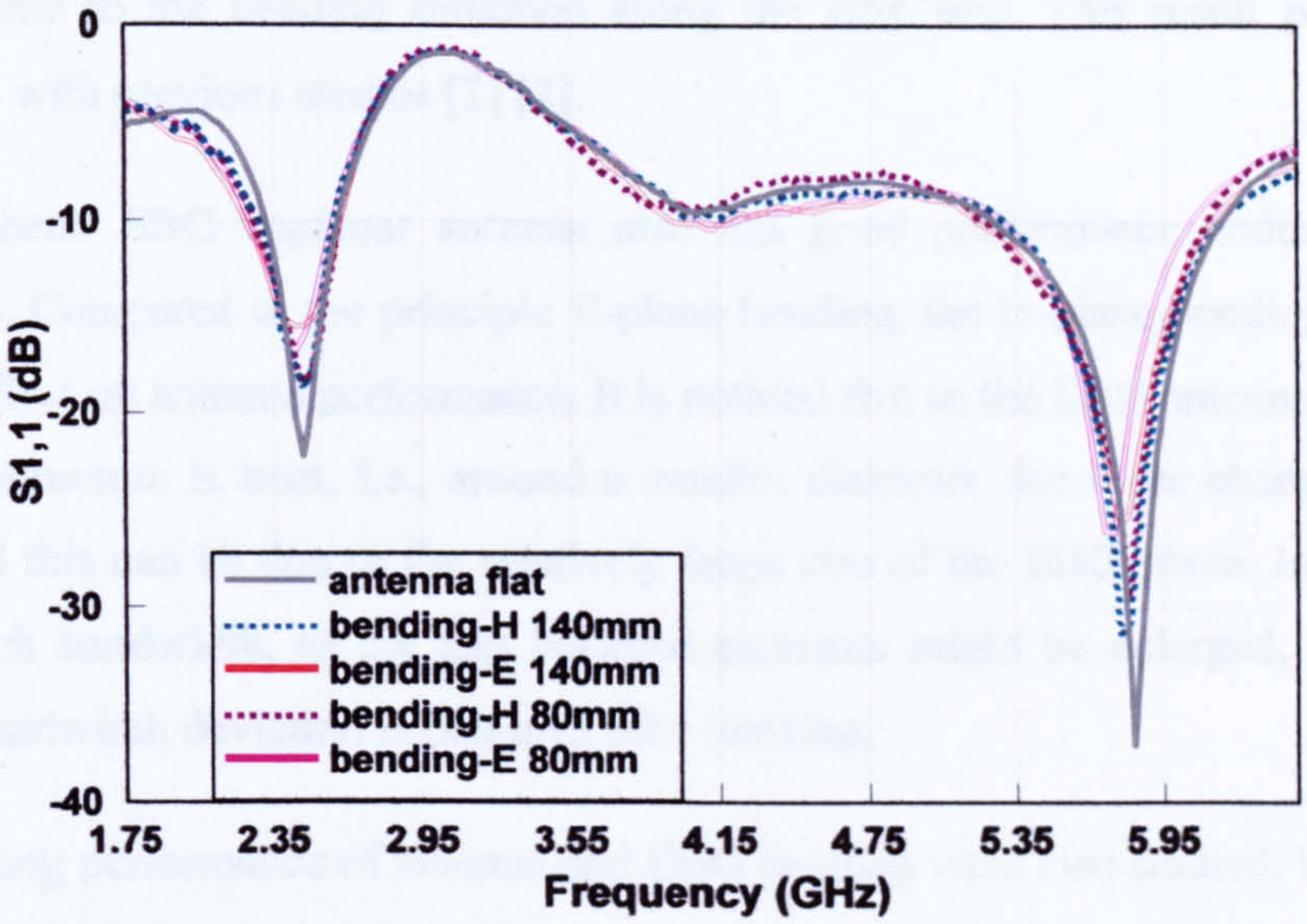

Figure6.2 Measured S_{11} results of dual-band fabric antenna bending

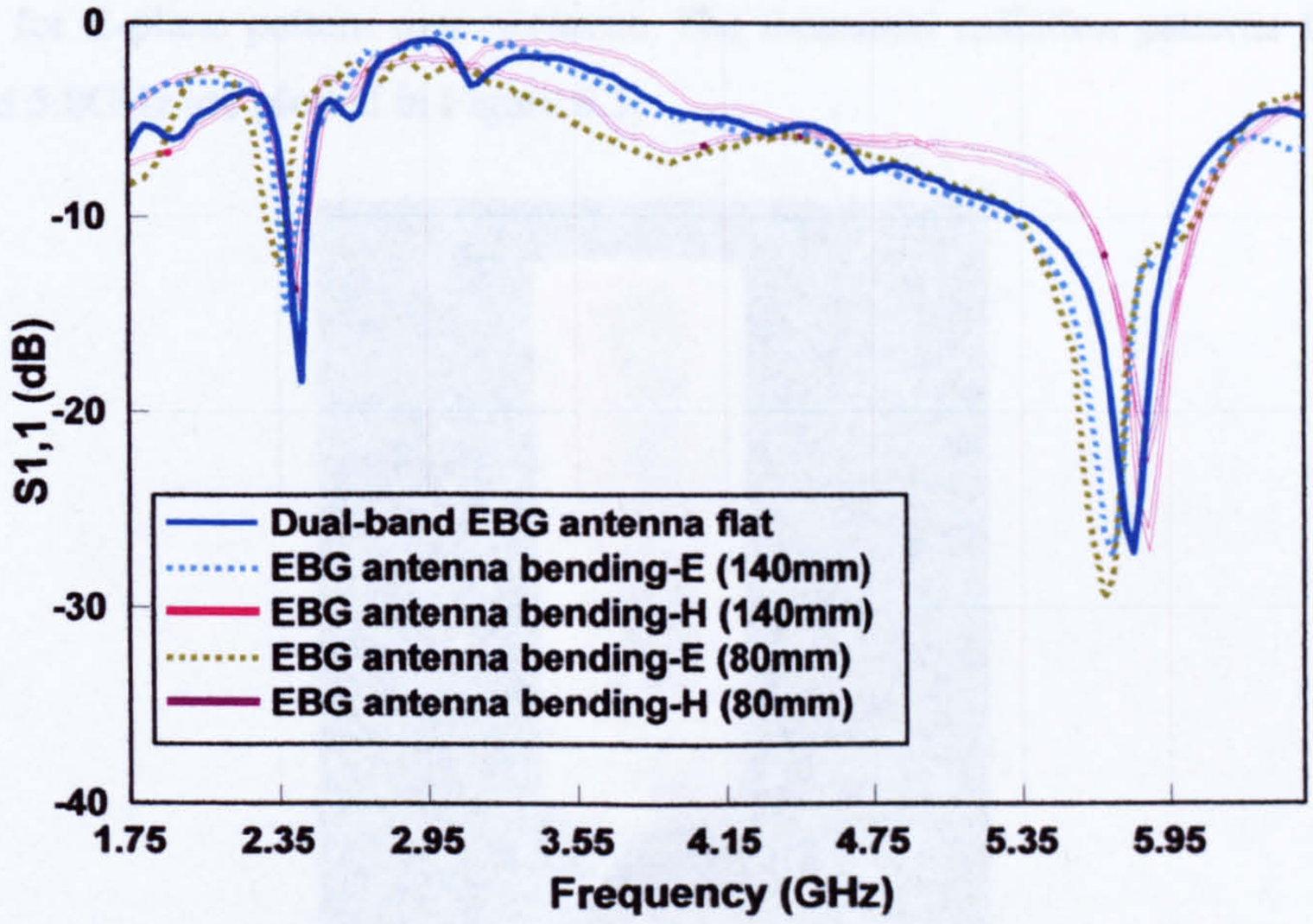

Figure 6.3 Measured S_{11} of dual-band EBG antenna bending

From the figures we can see that for the CPW antenna, which is compact in size compared to the cylinders, the resonance remains stable when bent. It also shows good bandwidth stability for both bands in Figure 6.2. It is observed that bending along the E-plane has a bit more effect on antenna performance compared to H-plane

which is due to the bending direction along the strip line. This result is in good agreement with previous studies [2] [3].

The dual-band EBG coplanar antenna also has good performance under bending conditions. Compared to the principle E-plane bending, the H-plane bending still has a minor effect on antenna performance. It is noticed that in the EBG antenna case, the more the structure is bent, i.e., around a smaller diameter, the more changes it can cause, and this can be due to the relatively large size of the EBG plane. In terms of input-match bandwidth, as the gap between elements might be enlarged, a slightly broader bandwidth deviation is obtained after bending.

The radiating performance of antenna and EBG bending were also studied. Figure 6.4 shows the bending measurement setup in the anechoic chamber. For the radiation measurement, only one bending direction is observed for each radiating plane, which is bending along the H plane for H-plane pattern measurement and bending along the E plane for E-plane pattern measurement. The measured radiation patterns for 2.45 GHz and 5.8GHz are plotted in Figure 6.5.

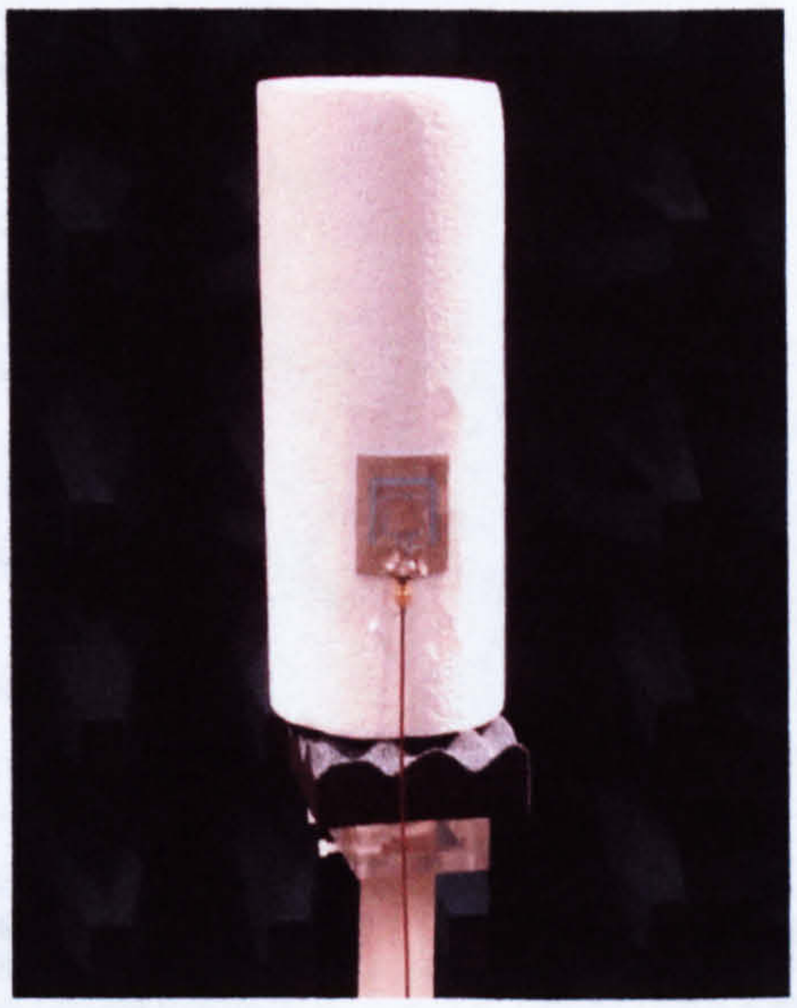

Figure6.4 Antenna-bending measurement setup in anechoic chamber

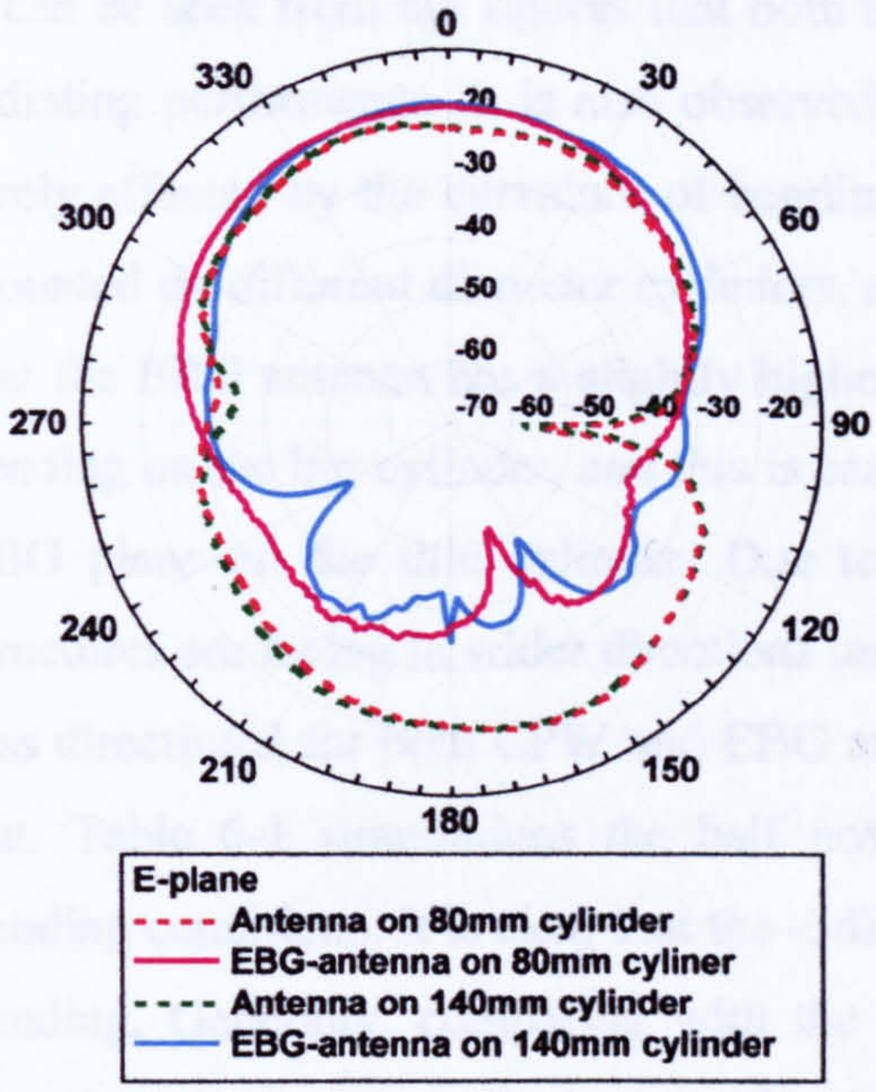

(a) E-plane 2.45G

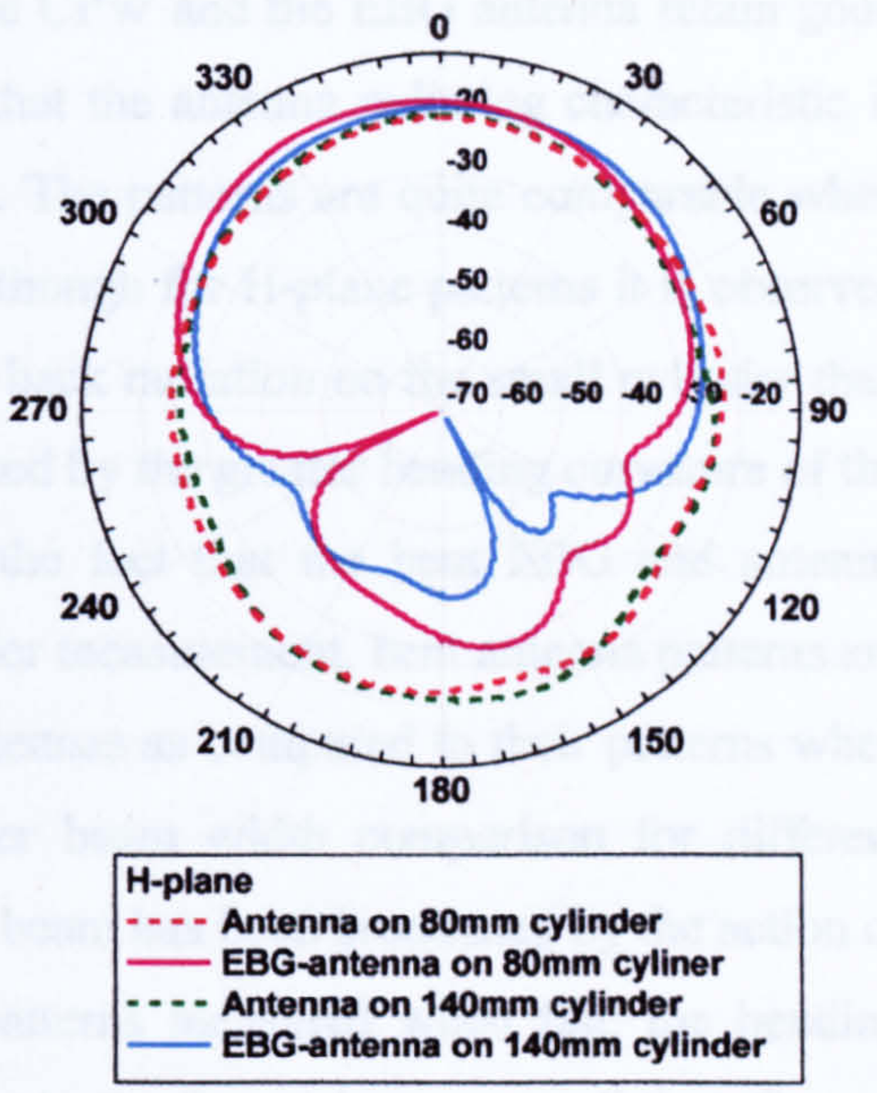

(b) H-plane 2.45G

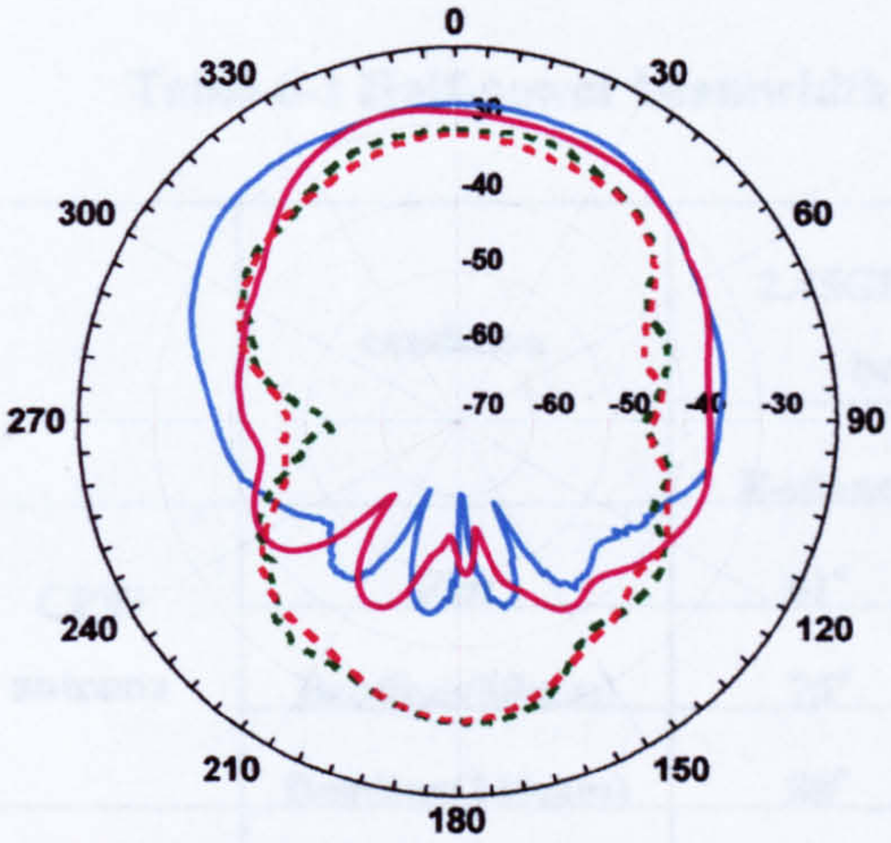

(c) E-plane 5.8G

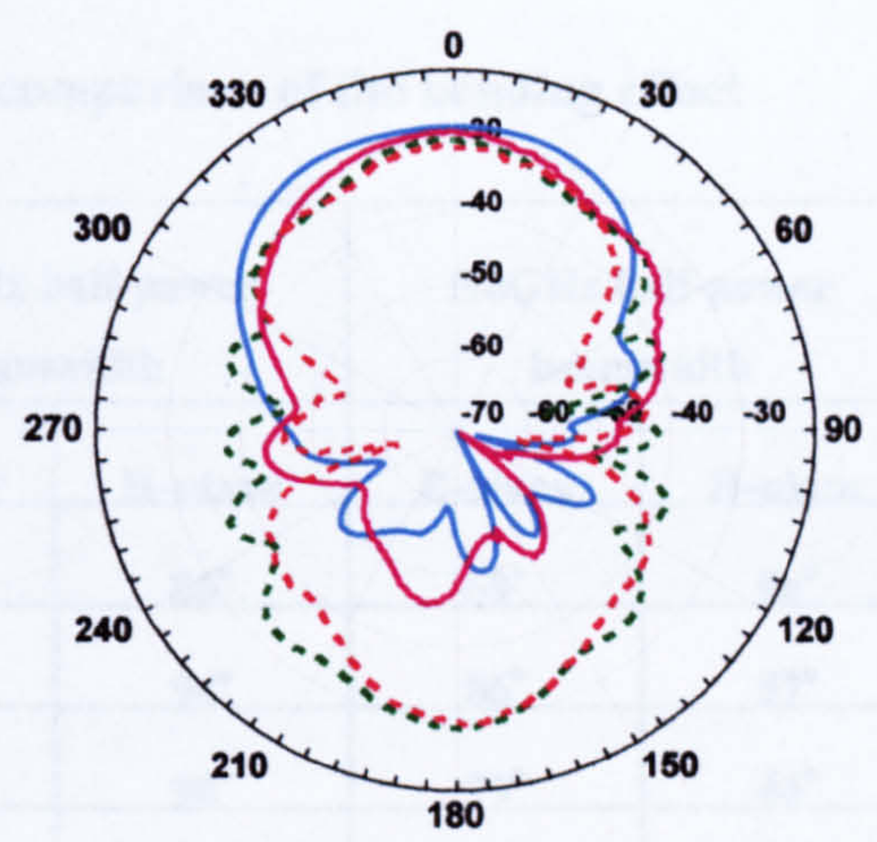

(d) H-plane 5.8G

Figure 6.5 (a)-(d) Measured radiation patterns of antenna/EBG bending

It can be seen from the figures that both the CPW and the EBG antenna retain good radiating performance. It is also observed that the antenna radiating characteristic is rarely affected by the curvature of bending. The patterns are quite comparable when mounted on different diameter cylinders, although for H-plane patterns it is observed that the EBG antenna has a slightly higher back radiation on the small cylinder than bending on the big cylinder, and this is caused by the greater bending curvature of the EBG plane on the thin cylinder. Due to the fact that the bent EBG and antenna structures are facing in wider directions under measurement, bent antenna patterns are less directional for both CPW and EBG antennas as compared to their patterns when flat. Table 6-1 summarizes the half power beam width comparison for different bending conditions. It is clear that the -3dB beam has been broadened by the action of bending. Generally, comparing with the patterns measured when flat, the bending directions (according to E-plane and H-plane in the figure) have a very little influence on antennas performance. The EBG antenna under bending conditions still generates a considerable gain in the front direction and reduces the back radiation significantly.

Table 6-1 Half-power beamwidth comparison of the bending effect

	condition	2.45GHz half-power beamwidth		5.8GHz half-power beamwidth	
		E-plane	H-plane	E-plane	H-plane
CPW antenna	Flat	61°	86°	69°	56°
	Bending(80mm)	75°	94°	86°	57°
	Bending(140mm)	80°	90°	79°	46°
EBG antenna	Flat	52°	66°	57°	49°
	Bending(80mm)	100°	104°	90°	66°
	Bending(140mm)	93°	90°	106°	83°

6.3 On body performances

The human body as a complex dielectric material has very serious interactions with antennas in proximity. As for mobile handsets, plenty of studies [4] have been devoted to the human head-antenna interactions. However, for future wearable antenna applications, the antennas will probably be integrated within cloth or be placed in the vicinity of the human torso. Therefore, some positions on body, like arm, shoulder should also be studied. In this section, the CPW and the EBG antennas are measured on selected locations on a real human body. The impedance match performance and the radiation characteristics in the vicinity of the human body will be discussed.

Three typical positions are selected for the measurement, thigh, arm and back. Figure 6.6 shows the set up of dual band EBG-coplanar antennas mounting on the cloth of thigh and back. The set up is also mounted around the arm directly on the skin.

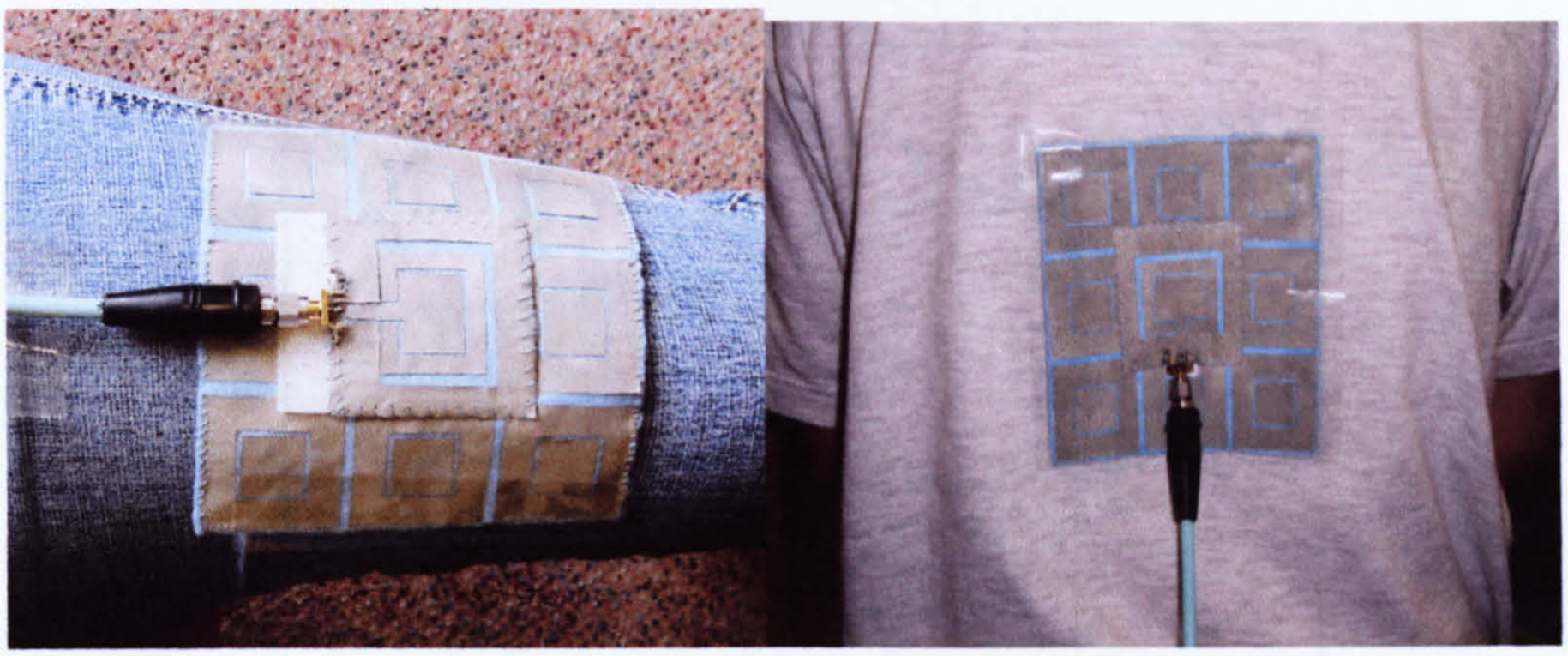

Figure 6.6 Dual-band EBG antenna mounting on the thigh and back

Figure 6.7 shows the measured impedance matching results for the dual-band CPW fabric antenna on different positions of body and in free space. Due to the coplanar structure of the antenna, the human body is acting as a new complex layer of substrate, therefore mounting the antenna directly on body causes a dramatically mismatch in the antennas performance. In this case, the interaction between the

antenna and the body is severe, and it is necessary to find a solution to reduce the body influence.

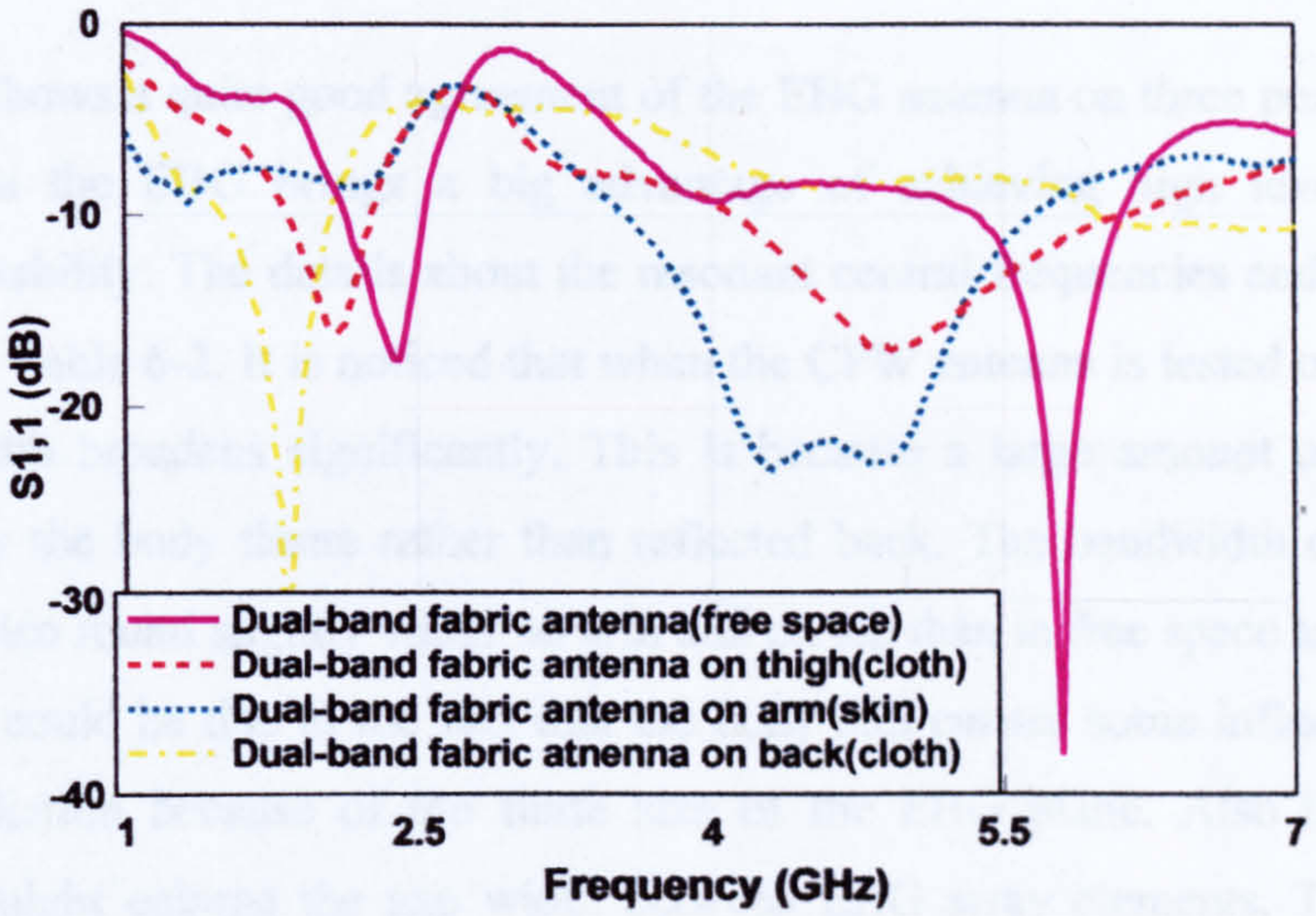

Figure 6.7 Measured S_{11} of CPW antenna in the presence of human body

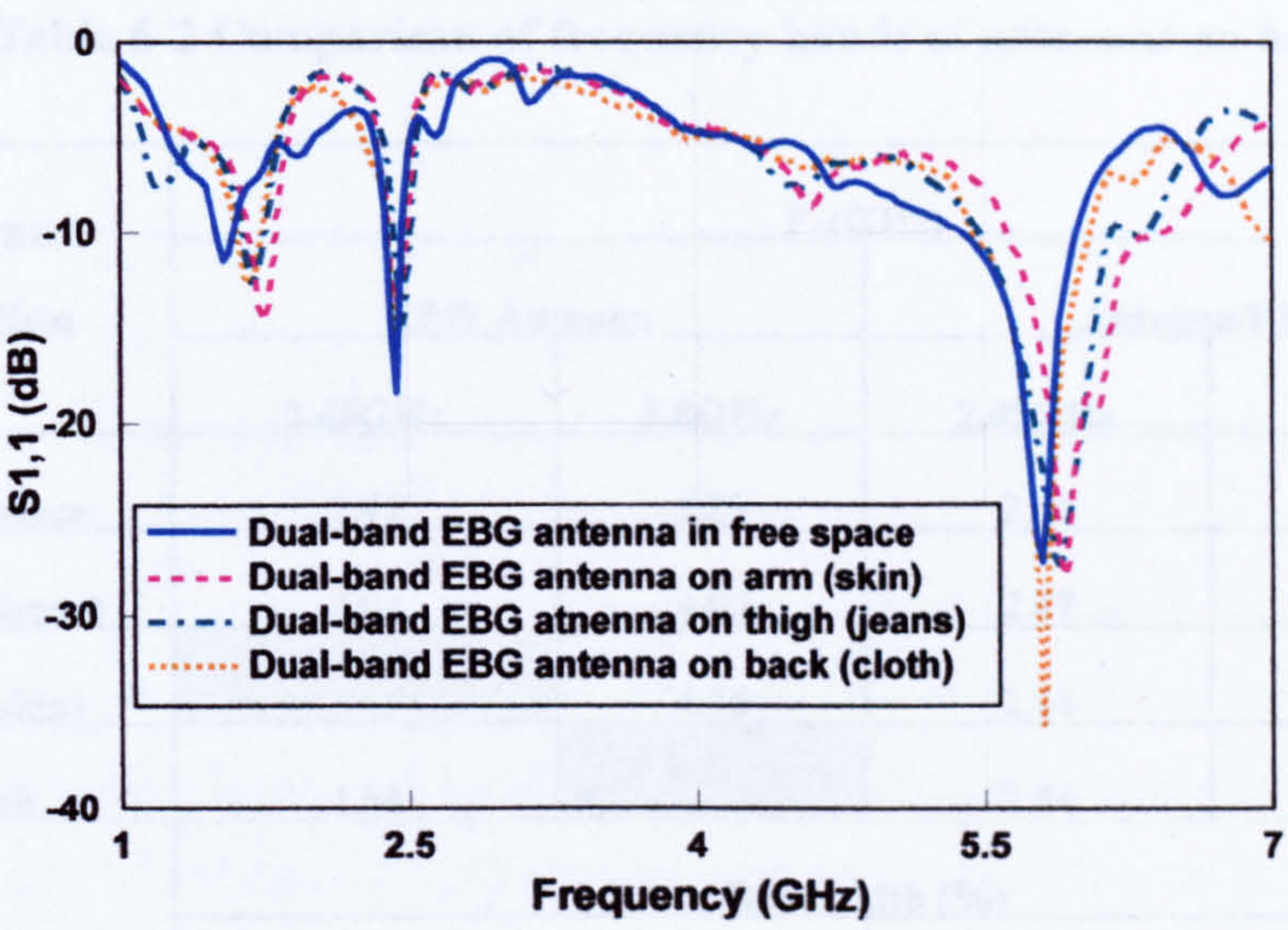

Figure 6.8 Measured S_{11} of EBG antenna in the presence of human body

To introduce an EBG ground plane is a good solution to solve the interaction between the antenna and the body. In contrast to the CPW antenna, the EBG antenna performs very well in all the cases on body as shown in Figure 6.8. Especially when the antenna is mounted on the back, the resonant frequencies hardly changes (<0.5% at 2.45GHz and <1% at 5.8GHz). This means the EBG plane has formed a good isolation layer between the antenna and the body. When the EBG antenna is placed on the thigh and

arm, there is a slight resonant shift at the upper frequency (90MHz on thigh, 120MHz on arm) which are 1.5% and 2% corresponding to the resonant frequency, and this is because of the bending behaviour caused by the curved structure of the arm and leg.

The figure shows a quite good agreement of the EBG antenna on three positions. It is obvious that the EBG brings a big advantage of achieving high level resonant frequency stability. The details about the resonant central frequencies and bandwidth are listed in Table 6-2. It is noticed that when the CPW antenna is tested on the body, the bandwidth broadens significantly. This is because a large amount of energy is absorbed by the body tissue rather than reflected back. The bandwidth of the EBG antenna is also found slightly wider on arm and on leg than in free space and on back. Again, this could be due to the fact that the body still causes some influence on the antenna radiation because of the finite size of the EBG plane. Also the bending behaviour might enlarge the gap width between EBG array elements. The reduced capacitance contributes to the wider bandwidth.

Table 6-2 Comparison of frequency bands of antennas on body

Antenna Position	F_C(GHz)			
	CPW Antenna		Antenna/EBG	
	2.45GHz	5.8GHz	2.45GHz	5.8GHz
Free space	2.41	5.83	2.44	5.8
Thigh(jeans)	2.08	4.90	2.47	5.89
Arm(skin)		4.36	2.44	5.92
Back	1.84		2.44	5.80
	Bandwidth (%)			
	CPW Antenna		Antenna/EBG	
	2.45GHz	5.8GHz	2.45GHz	5.8GHz
Free space	17%	17.3%	3%	10%
Thigh(jeans)	20.2%	39.2%	2.5%	11.9%
Arm(skin)		47.5%	3.7%	13.2%
Back	29.3%		3%	10.3%

The radiating characteristics of antenna in the vicinity of the human body are also measured in the wide range anechoic chamber at the Sheffield University Buxton site. The set up of the measurement is shown in Figure 6.9. In order to keep the antenna in a stable situation under test, the mounting position was chosen to be on the chest, and the cable can be hold by hand at a lower position. The person is standing in the centre of the turn table, facing the transmitting antenna as a reference to 0 degree in the patterns.

Figure 6.9 Measurement set up for antenna on body in anechoic chamber

Because of the limitations at the measurement site, only 2.45GHz far-field radiation patterns are tested. Moreover, the dual-band slot patch antenna described in Section 5.2.3 is also measured under the same setup to make a comparison. The radiation scan results are plotted in Figure 6.10. The slight asymmetry in the E plane is due to the effect of the cable and the arm rising on one side of the body during the measurement. For these three antennas, as the CPW antenna is placed on the body without a back ground plane, the power is absorbed by the body seriously especially the backward radiation. Therefore, the entire radiated power is very weak. This can be proved by the maximum power difference between the CPW and the EBG antenna. In free space, the EBG antenna has achieved a 3-4dB directive gain over the CPW antenna (chapter 5.2.4), while this gain has risen to 7-8dB in the vicinity of human body. Compare all the three antennas, the EBG antenna has the best power reception, as well as the greatest front to back ratio. The dual band slot patch antenna attains some gain over the CPW antenna as well, however, as the poor impedance match performance, more power is reflected back at the port, and the radiating performance on the body is not comparable to the antenna/EBG combination.

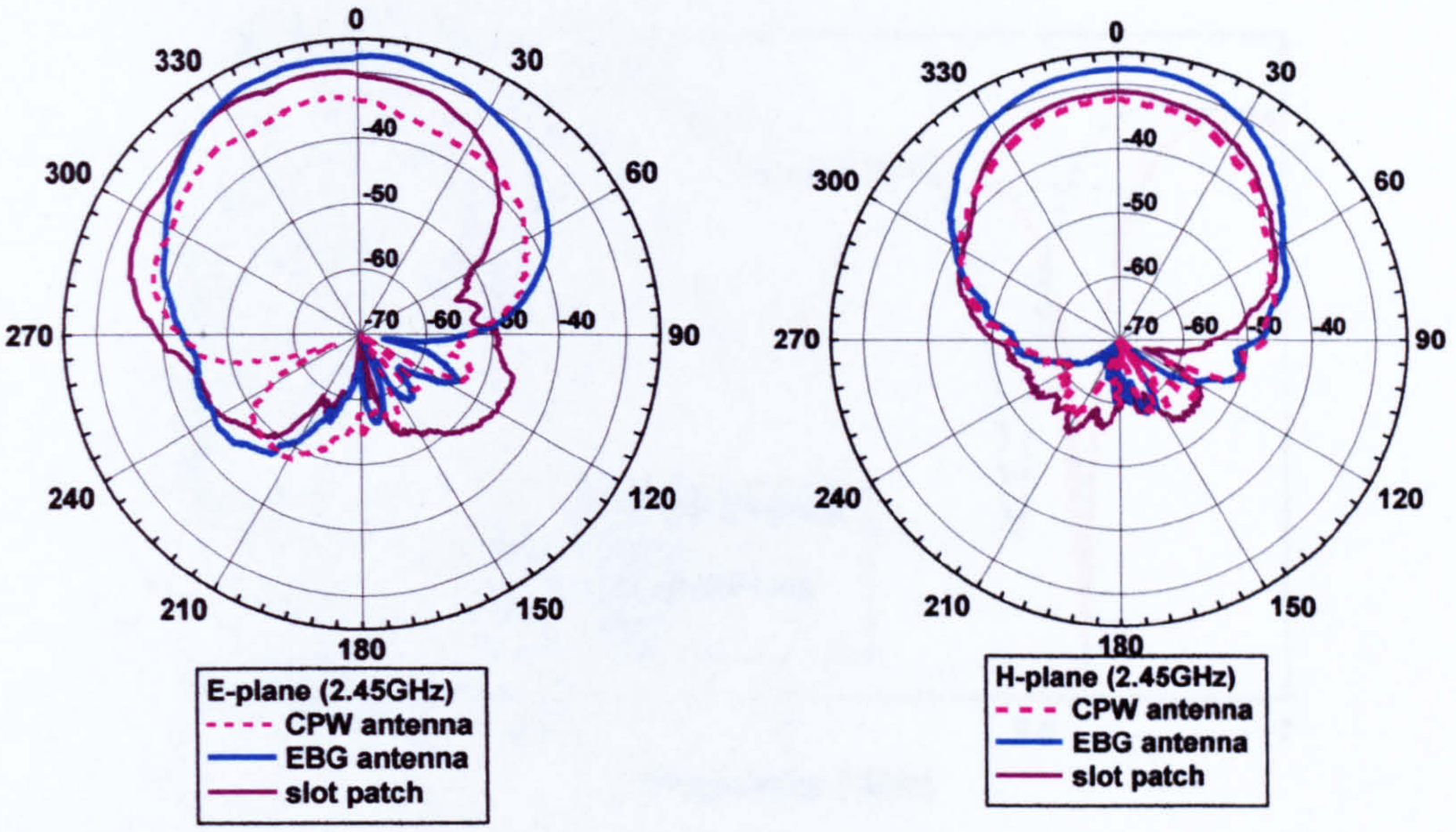

Figure 6.10 Measured far-field patterns of antennas on human body at 2.45GHz

6.4 Washing

Wearable fabric antennas are supposed to be integrated into our daily clothing for personal communication. Therefore there is the possibility of it getting wet in the rain or snow. As the materials we used for both antenna and EBG fabrication are not water proof, it is important and necessary to test the performance of the antenna after washing as well as the EBG structure. However it is probable that the antennas could be water proofed by covering them in a thin plastic coating.

When a fabric material gets wet, water penetrates into the material fibres. Still water has a very high relative permittivity of around 80, which indicates the wet material can have a much higher dielectric constant than in dry conditions. Plus any fabric can be expected to shrink about 1 to 3 percent after being dried. The shrinkage of the fabric is material dependant, normally manufactured fibres will shrink the least, and natural fibres the most. Therefore, even when the material is dried from damp, the original properties might change.

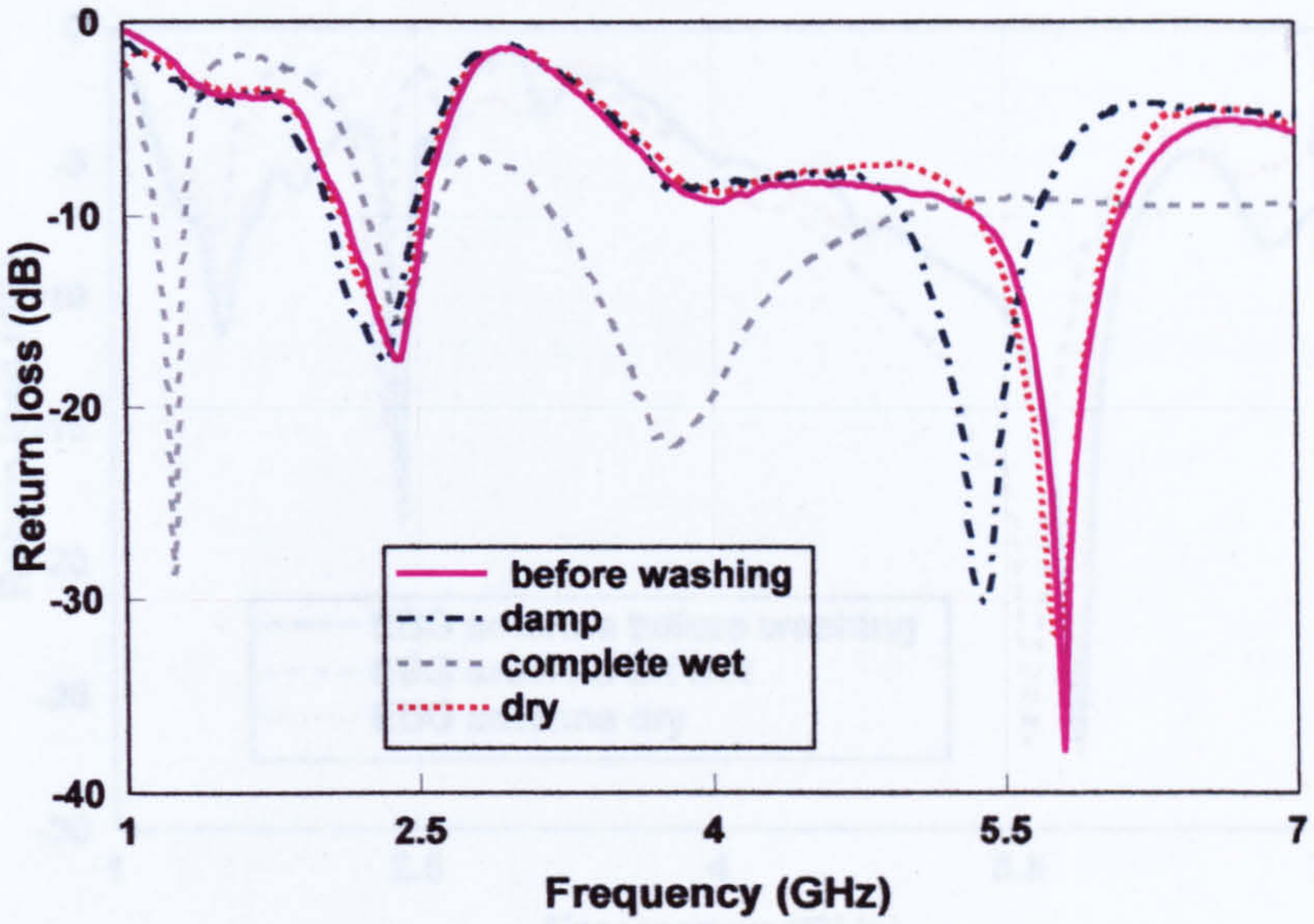

Figure 6.11 Measured return loss of CPW antenna wet

The measured return losses of the CPW antenna under wet conditions are presented in Figure 6.11. The antenna is subjected to hand washing twice before being dried. The structure is measured before washing, after washing and when very wet and damp, and finally when dry again. It can be seen from the figure that when wet the performance deteriorates dramatically as expected, the resonances changing with the degree of saturation when the antenna is fully wet. The higher dielectric constant of the water dominates antenna's performance by reducing resonant frequency. If fabric antennas are used near the skin, the aspect of wetness of the fabric becomes more important. When it is nearly dry, because there is still some moisture inside the material, the relative permittivity can be still higher than the original, therefore, both of the resonant bands move downward. It is also found that the property of the conductive material 'Zelt' does not change when it is dry again, while the substrate material 'felt' shrinks a very little (about 3.6%). Thus for the antennas performance, the bands have only a very slight shift after drying (about 30MHz at 5.8GHz while it is imperceptible at 2.45GHz). Although the antenna performance is not affected much after drying, the situation is still serious when it is wet. Therefore, in the future research, the antenna under wet conditions should be taken into account more seriously. Either water proof materials can be selected, or the antenna should be shielded from the rain.

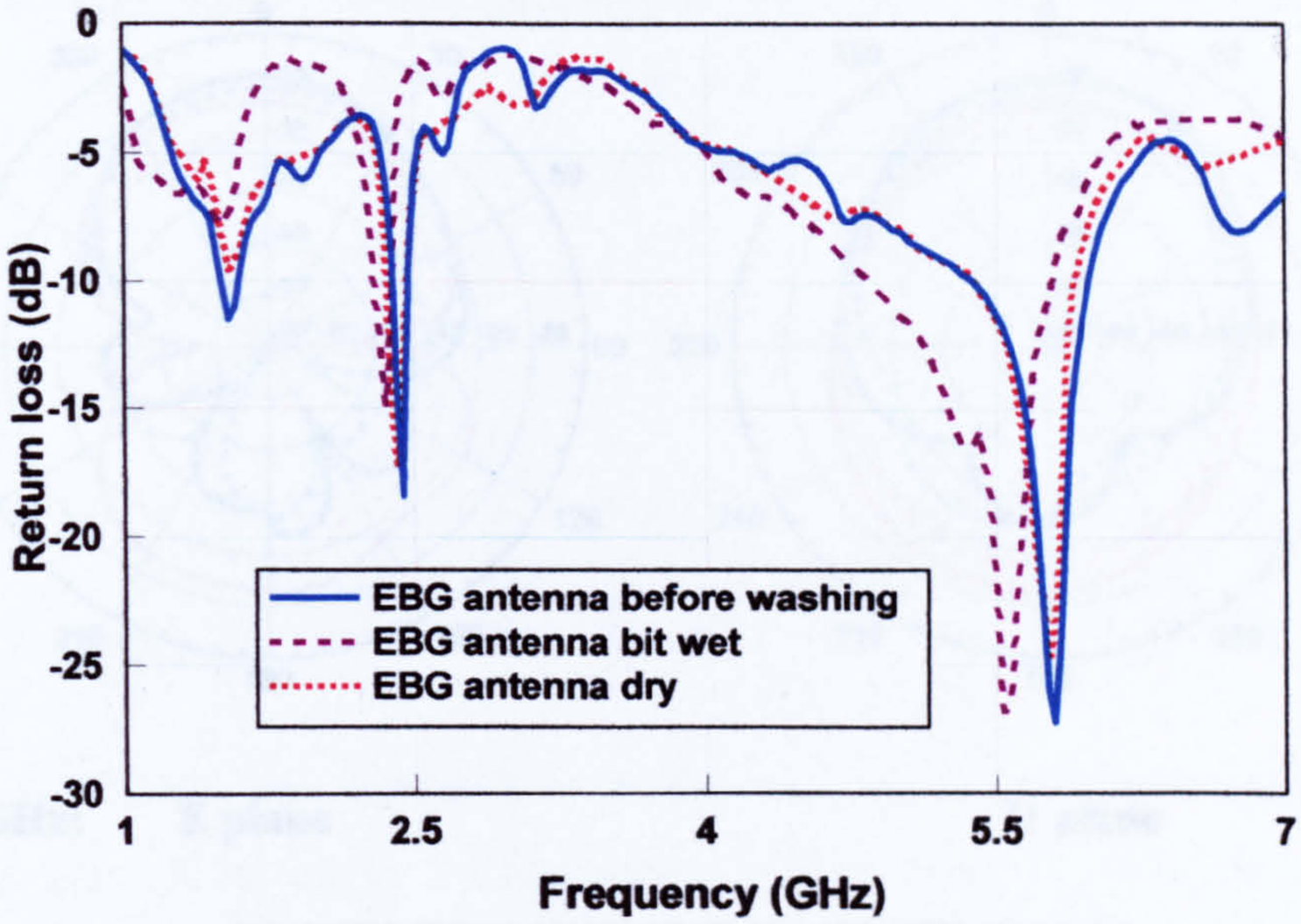

Figure 6.12 Measured return loss of EBG antenna wet

The CPW antenna with EBG ground plane under wet conditions was also measured. Similar outcomes have been obtained as shown in Figure 6.12. With a general EBG array, when the permittivity of the substrate is increasing, the response band position should move down and the bandwidth should be reduced [5]. However, from the brown dotted curve in the figure we can see that when the EBG antenna is damp, the centre frequencies for both the 2.45 and 5.8GHz bands are falling off, while the bandwidth is broadening. This is happening to the CPW antenna as well (Figure 6.12). This can be explained by the fact that the loss properties of the materials change when water exists. Unlike pure water is lossless, the water in our normal life or the rain is very lossy. Therefore, part of the power is absorbed by the material and leads to a lower power reflection. The bands shift back when the structure is dry again, however the bandwidth is decreased because of the EBG array gap width reduction caused by the substrate shrinking.

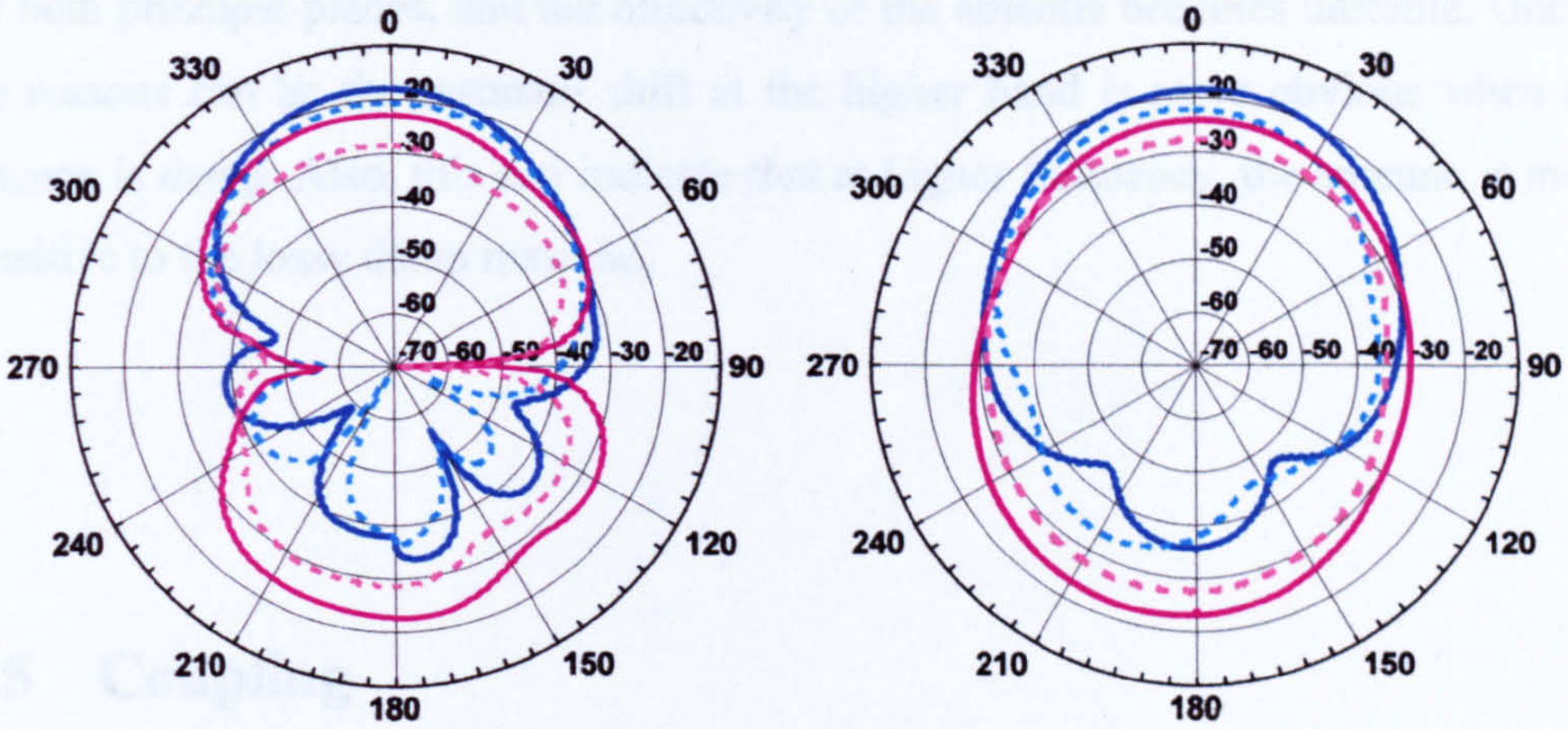

2.45GHz: E plane **H plane**

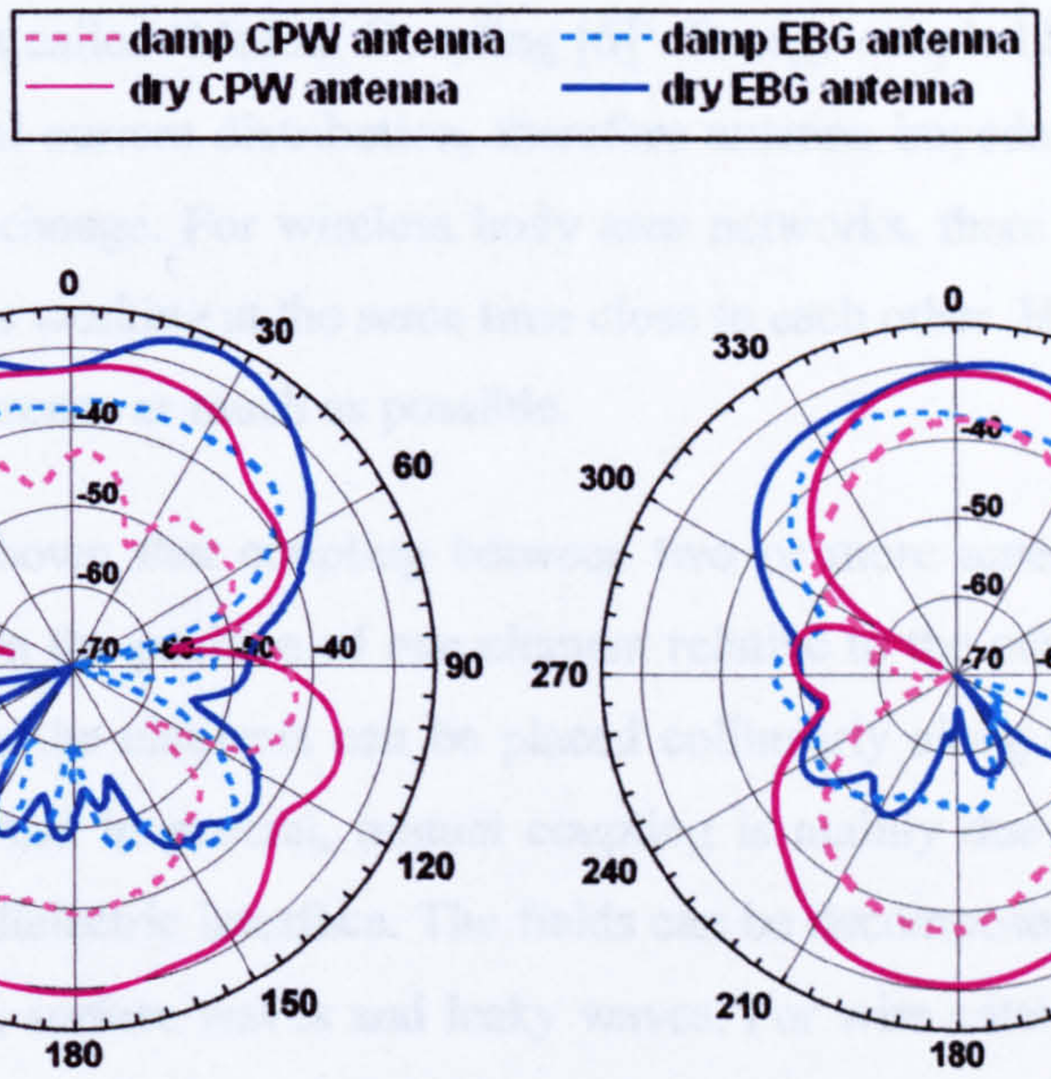

5.8GHz: E plane **H plane**

Figure 6.13 Radiation patterns comparison of dry and damp antennas

Finally the radiation patterns for the damp antenna were measured with and without the EBG where there was no apparent change in resonant frequency and these are plotted in Figure 6.13. At 2.45GHz, the damp combination has less gain (2 dB) but the overall radiation pattern remains acceptable and hence damp conditions may not significantly affect the overall performance of the antenna. However, it gets more serious for the higher frequency band. At 5.8GHz, the average gain drops about 7-8dB

for both principle planes, and the directivity of the antenna becomes unstable. One of the reasons can be the resonant shift at the higher band is more obvious when the antenna is damp. Also, this can indicate that at higher frequency, the antenna is more sensitive to the lossy damp material.

6.5 Coupling

When two antennas are near each other, whether one or both are transmitting or receiving, some of the energy for antenna one will probably couple to the other one. This phenomenon is called 'Mutual Coupling [6]'. Energy coupled between elements can alter the original current distribution, therefore antenna impedance and radiation characteristics will change. For wireless body area networks, there is the possibility that several antennas working at the same time close to each other. Hence, it is desired to reduce the interference as much as possible.

Research [7] has shown that coupling between two or more antenna elements are mainly dependant on the position of one element relative to the other. In the case of microstrip antennas, the elements can be placed collinearly along their principle E-plane or H-plane. And in general, mutual coupling is mainly due to the fields that exist along the air-dielectric interface. The fields can be decomposed to space waves, higher order waves, surface waves and leaky waves. For wire antennas, like dipoles, coupling can be analysed into side by side configuration and collinear configuration [8]. According to the CPW fabric antenna studied in this thesis, the coupling position can be aligned into face to face, as shown in Figure 6.14 (left) or side-by-side. For side-by-side elements, the position alignment can be considered in E-plane (Figure 6.14 (middle)) when the elements are positioned collinearly along the E-plane or H-plane (Figure 6.14 (right)) when the elements are positioned collinearly along the H-plane. ***S*** is the edge-to-edge separation.

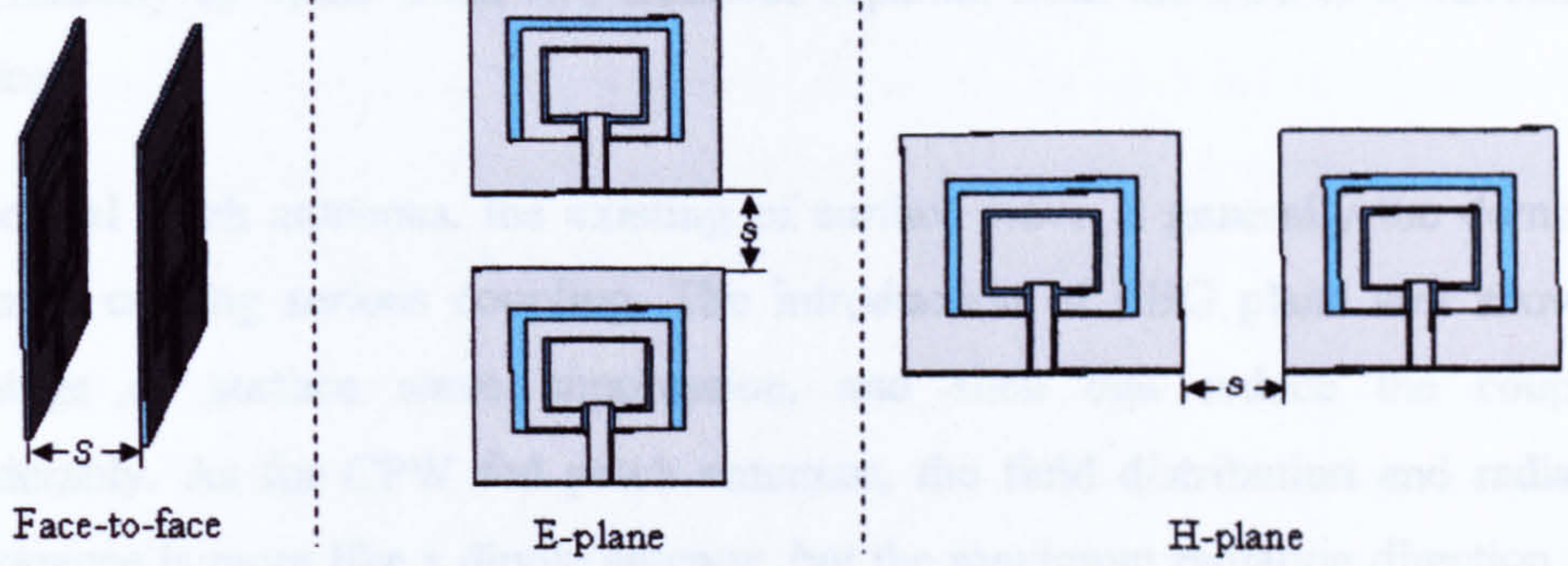

Figure 6.14 Position arrangements of patch antennas

In this section, computed and tested coupling between the dual-band CPW fabric antenna and the EBG will be presented. Measurements have been carried out both in free space and on body, and as H plane alignment is the most common practical situation, therefore the results for H-plane arrangement as an example will be discussed in detail.

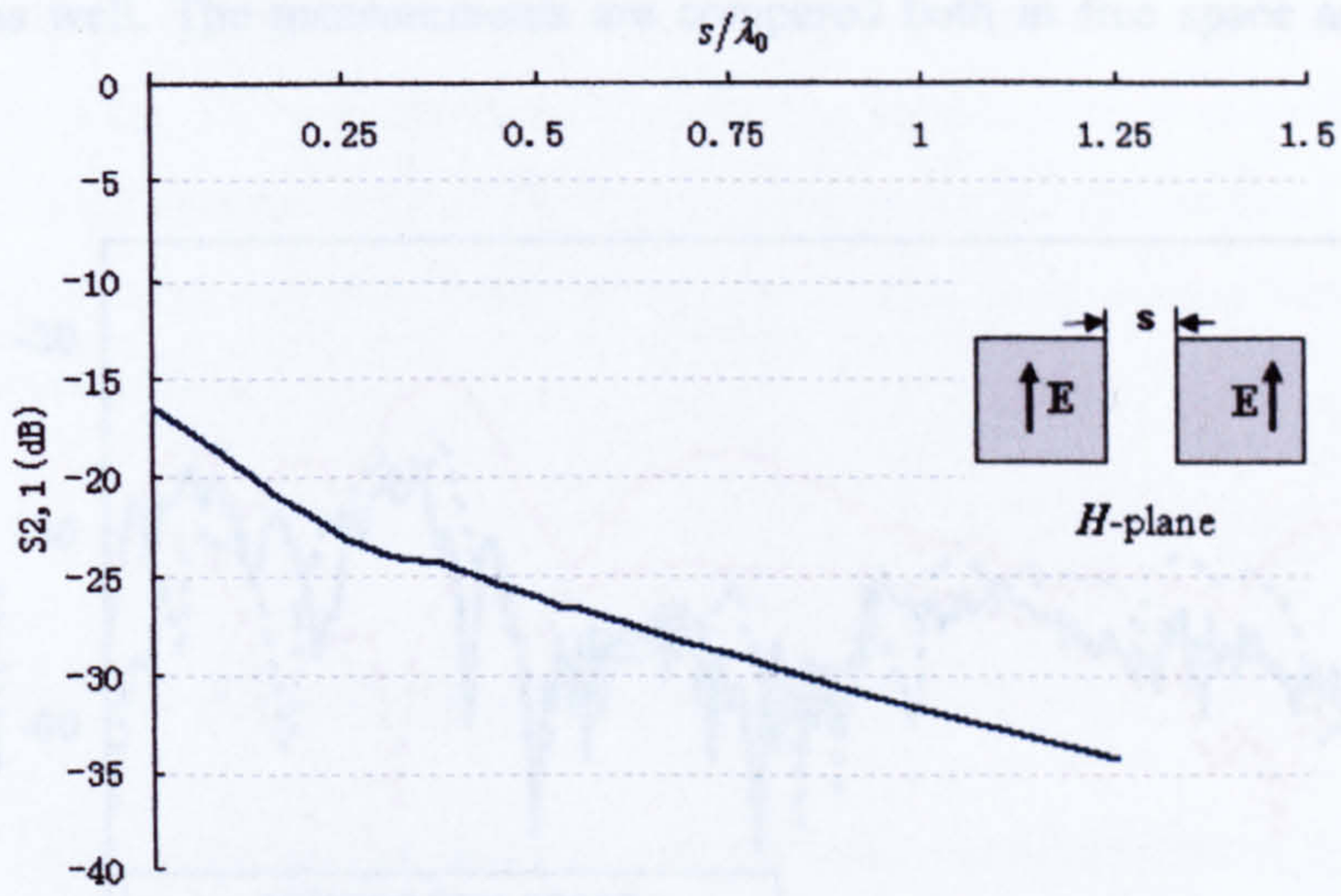

Figure 6.15 Calculated H-plane coupling between two antennas

Figure 6.15 shows the relationship between the mutual coupling and the spacing s/λ_0 for H-plane coupling. The result is calculated by CST microwave studio. Two identical dual-band CPW fabric antennas are both excited, and the first resonant frequency 2.45GHz is observed. From the figure we can see, the coupling level drops

gradually with the increase of elements separation. The S_{21} level dropped approximately by 15dB when two antennas separate from the zero to a wavelength distance.

For normal patch antennas, the existing of surface wave is generally the dominant reason of causing serious coupling. The introduction of EBG plane will show its advantage of surface wave suppression, and such that reduce the coupling considerably. As for CPW fed patch antennas, the field distribution and radiation performance is more like a dipole antenna, but the maximum radiating direction is in the plane normal to the antenna surface, therefore the coupling between two antennas sit side by side is not serious. However, as the EBG plane can enhance the antenna directivity, there is possibility of reducing mutual coupling between two antennas when they are placed side by side. The measured S_{21} of two excited CPW antennas collinearly positioned on their H-planes in free space is plotted in Figure 6.16. In order to evaluate the effect of EBG ground plane presence, the spacing *s* is fixed to a certain value of 65mm, such that the two 3×3 EBG cells are just next to each other. The measured couplings in H-plane between two antennas with EBGs are plotted in Fig 6.16 as well. The measurements are compared both in free space and on body trunk.

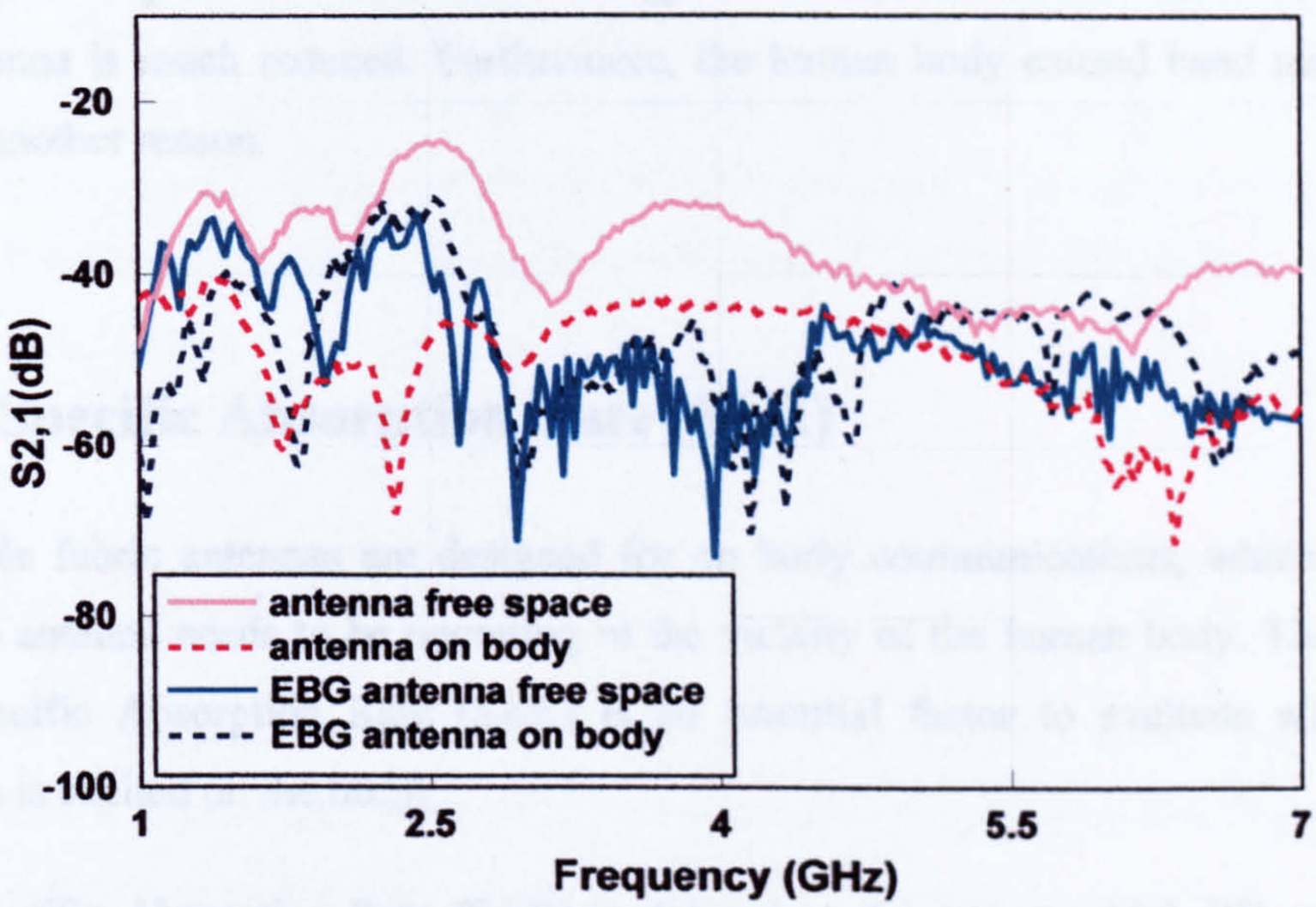

Figure 6.16 Measured H-plane coupling for proposed antennas and EBGs

The measured S_{21} values are plotted in Figure 6.16. Apart from the CPW antenna which is detuned on the body, other antennas have their strongest coupling at around 2.45GHz which refers to the first resonant frequency. As for 5.8GHz, because of the relative much smaller wavelength, and the antenna radiating characteristic has more directivity, the coupling is not as strong as that of the first resonance.

It is obvious that the coupling between antennas in free space is higher than all the other cases. At the first resonant frequency of 2.45GHz, the coupling reaches the highest level of S_{21} close to -24dB. The presence of the EBG plane has reduced this level by about 8dB. This is because of the fact that the EBG plane has introduced more directivity to the antenna, and it also suppressed the wave travelling along the surface. Through the measured frequency range, the S_{21} level reduces about 10dB on average for the EBG antennas as compared to the CPW antennas in free space. Moreover, there is a good agreement between the results of antenna with EBG in free space and antenna with EBG on body, which means that the EBG provides a considerable shielding function between the antenna and the body, and the interaction between the antenna and the human body has been reduced to minimum. The red dotted curve in the figure represents the coupling between two identical CPW antennas on body. The noticeable drop in the S_{21} level is mainly caused by the fact that human body absorbs some of the energy, thus the power radiated and received by the antenna is much reduced. Furthermore, the human body caused band mismatch can be another reason.

6.6 Specific Absorption Rate (SAR)

Wearable fabric antennas are designed for on body communications, which means that the antenna needs to be operating in the vicinity of the human body. Therefore, the Specific Absorption Rate (SAR) is an essential factor to evaluate when the antenna is excited on the body.

The Specific Absorption Rate (SAR) is defined as the rate at which RF energy is imparted to a unit of mass of a biological body. The SAR value is normally described in units of watts per kilogram (W/Kg) and it can be expressed as

$$SAR = E_{tot}^2 \cdot \frac{\sigma}{\rho} \tag{6-1}$$

where SAR = local specific absorption rate in W/kg

E_{tot} = total field strength in V/m

σ = conductivity in S/m

ρ = equivalent tissue density in kg/m^3

Research has been done including the whole body averaged SAR [9], the interaction between mobile handset and the human head [4], dipole, patch and CPW UWB antennas on different positions of the body [10]-[11]. The Federal Communications Commission (FCC) has adopted limits for safe exposure to RF energy produced by mobile devices and requires that mobile phone antennas in the U.S. have a SAR level at or below 1.6 watts per kilogram (W/kg) taken over a volume of 1 gram of tissue. In the EU the corresponding limit is 2 W/kg taken over a volume of 10 grams [12].

In this section, the SAR measurement and simulation based on fabric antennas and EBGs will be discussed. The measurement part was carried out at Loughborough University. As the system was only calibrated at GSM bands (900MHz and 1800MHz), the antenna and EBG which work at WLAN bands are not capable to be measured directly. Therefore, a single band CPW fabric antenna which works at 1800MHz was designed to complete the measurement as well as a 3×3 cells EBG array. The model was then built and the computational results and the measured data are compared. Based on the results at 1800MHz, the model was used to calculate the SAR values for the WLAN antenna and EBG in CST, and conclusions will be made in end of this section.

6.6.1 SAR Measurement

The SAR measurements were processed by the Dosimetric Assessment System (DASY4) at Loughborough University. The system structure is shown in Figure 6.17.

Fig 6.17 DASY4 system structure [13]

DASY4 [13] is a professional system supplied by Schmidt & Partner Engineering (SPEGA) of Zurich, Switzerland. It can provide precise SAR measurements by evaluating all real-time field data and surface detection inside the standard tissue simulating liquids. The system is based on a high precision 6-axis robot (with a working range greater that 1.1m), which positions the SAR measurement probes with a positional repeatability of better than ±0.02 mm. The probe is specially designed and calibrated for use in liquids with high permittivity.

The SAM twin phantom is used to model the human body in the measurement. It has a 2mm thick fiberglass shell building into three measurement areas: left hand and right hand parts simulating the head and the centre flat phantom modeling the body. During the measurement, the shell is filled with a glycol-water based liquid which represents the average material properties of the body. The glycol-water based liquids use organic solvents to decrease the water permittivity. With water, glycol and salt almost any parameters are possible. The liquid properties at 1800MHz are listed in Table 6-3 [13].

Table 6-3 The glycol-water based liquid parameters

Liquid type: HSL 1800-F					
Ingredient	**weight [g]**	**weight [%]**	**Frequency [MHz]**	**Relative Permittivity**	**Conductivity [S/m]**
Water	552.42	55.24	**1800**	**40**	**1.4**
DGBE	444.52	44.45			
Salt	3.06	0.31			

The antenna/EBG is fixed to the centre of flat section shell of the SAM-twin phantom. Figure 6.18 (a) and (b) show the bottom and top view of the setup. The CPW antenna and the EBG antenna are measured separately to make a comparison. Note that when measuring the CPW antenna, a space of 4.5mm (Rohacell layer $\varepsilon_r = 1.006$) is inserted between the antenna and the shell in order to make it comparable to the situation of the EBG grounded.

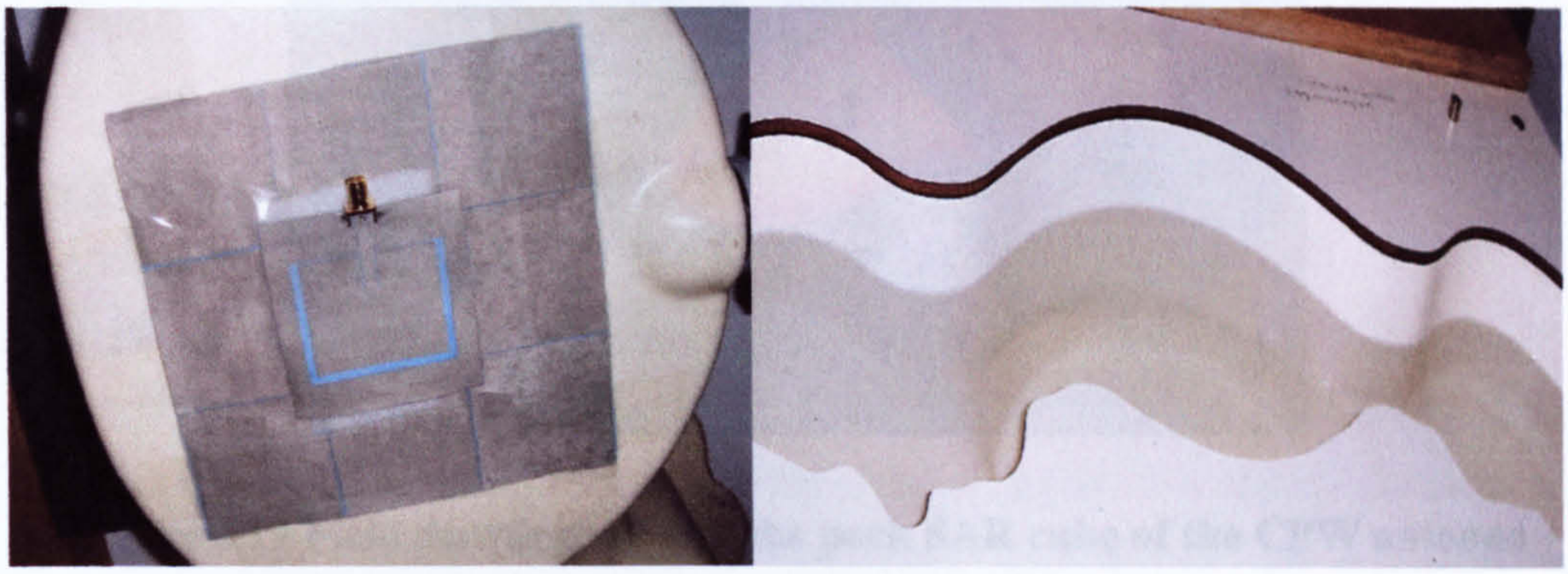

Figure 6.18 (a) Bottom view of the SAR measurement setup

(b) Top view of the SAR measurement setup

The procedure for spatial peak SAR evaluation has been implemented according to the IEEE1529 standard. It can be conducted for 1 g and 10 g, as well as for user-specific masses. Two main steps are executed to accomplish the evaluation:

- A fast area scan in two dimensions to find the area of high field values. This will locate the approximate location of the local peak SAR values.
- A further 3-D scan is performed in a cube with the volume of 30mm^3(7x7x7 points). The cube is built based on the maximum selected area at the first step. The measured volume must include the 1 g and 10 g cubes with the highest averaged SAR values. For this purpose, the center of the measured volume is aligned to the interpolated peak SAR value of a previously performed area scan. In this step, the entire 3-D field values are measured within the high resolution grid.

The spatial-peak SAR within masses of 1g and 10g can therefore be calculated from Equation (6-1). Field distributions and the peak SAR cubes of the antenna/with EBG are shown in Figure 6.19 and 6.20, in which the two red frame boxes are corresponding to peak 1g and 10g tissues. From the field distributions we can see that

the peak field of the CPW antenna is concentrated around the centre of the phantom, which is also the centre of the antenna, while the highest values shift to the edge of the EBG when the antenna is ground by the EBG arrays. And this can be verified by the calculated field distributions presented in next section.

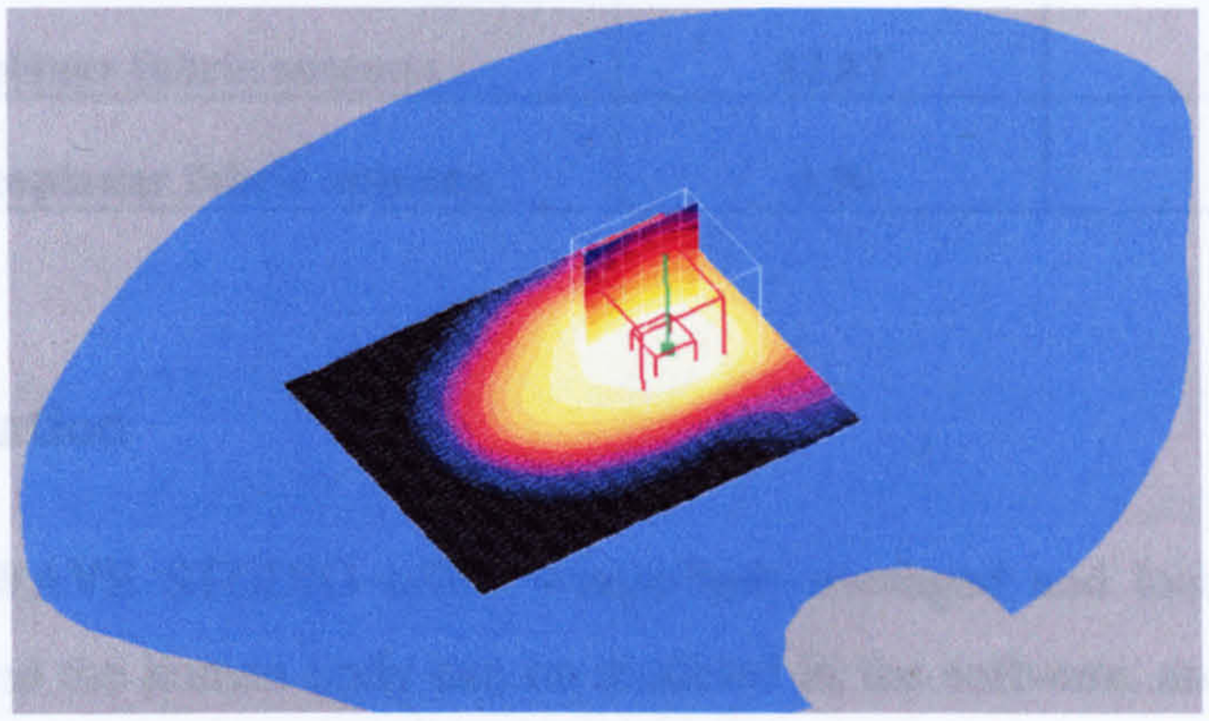

Figure 6.19 Field distribution and the peak SAR cube of the CPW antenna

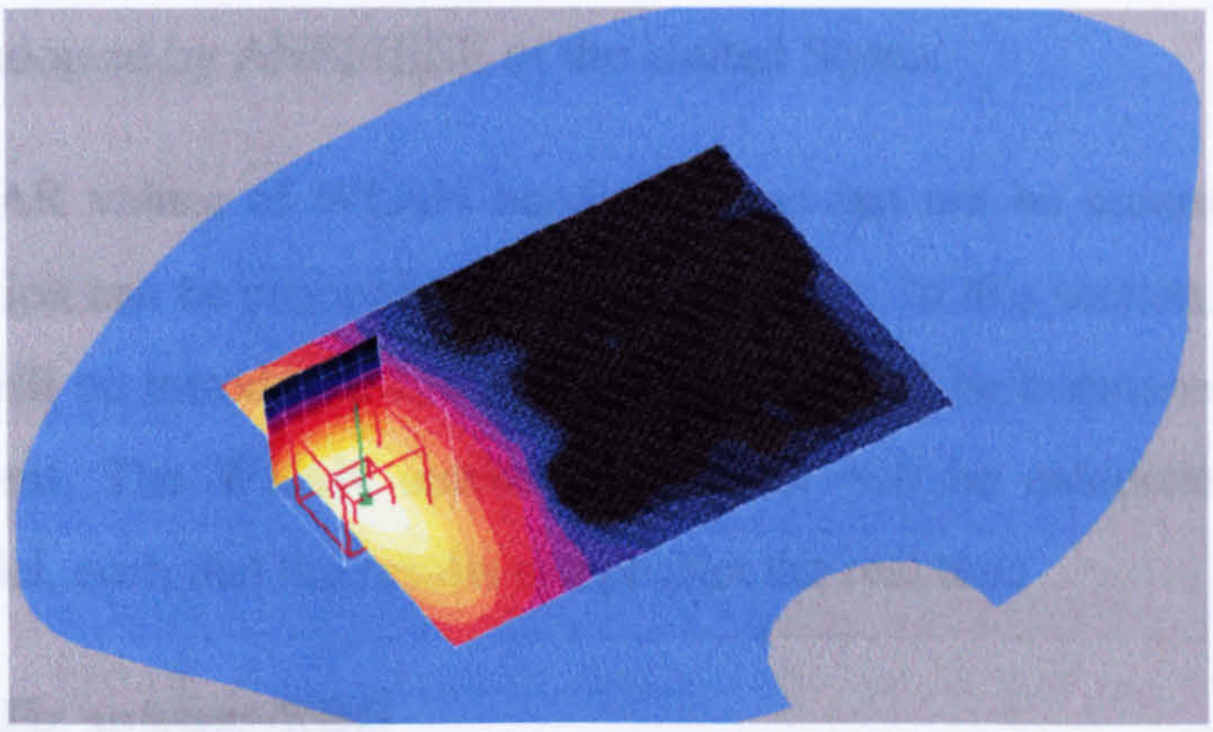

Figure 6.20 Field distribution and the peak SAR cube of the EBG antenna

The measured SAR values for fabric antenna with/out EBG are listed in Table 6-4. The results are normalized to the standard 1watt power input. As it is expected, the antenna itself generates huge radiation towards the body. While by adding the EBG ground, the SAR values are reduced by 93% and 95% respectively, and the IEEE SAR standards for both 1g and 10g tissues can then be satisfied.

Table 6-4 Measured SAR values at 1800MHz

Peak SAR values at 1800MHz (normalized to 1W input power)—W/Kg		
	1 gram tissue	10 gram tissue
Coplanar fabric antenna	12.87	7.96
EBG coplanar fabric antenna	0.90	0.42

6.6.2 Simulation

CST MICROWAVE STUDIO offers whole-body-averaged and local SAR values. The antenna and the human body can be modeled in the software, and the particular parameters can be specified to each individual material. By setting up a proper meshing property, CST can calculate the entire field within the computational boundary. Thus typical local SAR values can be obtained in tissue masses of around 10g specified by the Telecommunication Technology Council Agenda, whereas the value of 1g is adopted by ANSI/IEEE of the United States.

Because the SAR values of WLAN band antennas can not be measured, a relevant precise simulation can be proceed to predict the results. In this section, the simulation at 1800MHz will be introduced first, and the results will be compared with those of the measurement. The WLAN antenna and EBG will be calculated base on the 1800MHz model, such that the results can predict the real test.

6.6.2.1 1800MHz antenna/EBG

A two layer rectangular model is built in the software to represent the human body, as shown in Figure 6.21. The size of the model is $50\times 30\times 15cm^3$, which is approximate to the entire size of the SAM phantom in measurement. The top layer is 2mm thick to model the phantom shell, and the relative parameters are set to: $\varepsilon_r = 3.5$ loss $tan\,\delta = 0.02$, density $\rho = 1000\,kg/m^3$. The bottom layer is to stand for the liquid, which has the dielectric parameters listed in Table 6-3 at 1800MHz. The structure under test is located in the centre of the body shell surface. The antenna has a 4.5mm space from the body and the EBG is directly on the body surface.

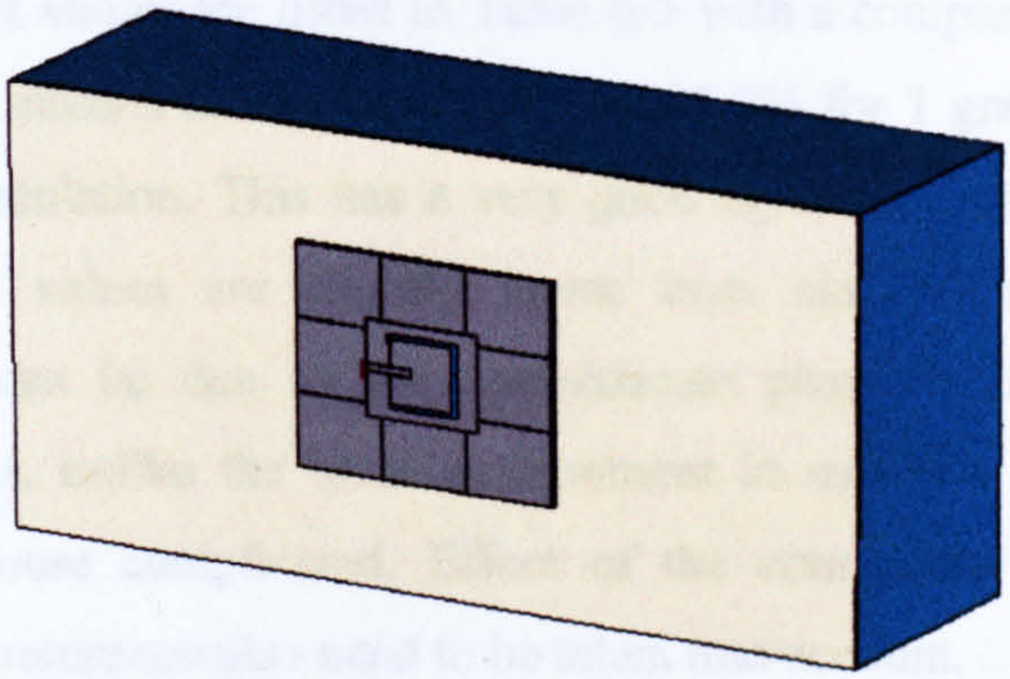

Figure 6.21 Human man model and EBG antenna in simulation

The simulated field distribution for both the CPW and EBG antenna are shown in Figure 6.22. Red colour in the plot indicates the highest field strength. It can be seen that the strongest field for the CPW antenna locates in the centre of the antenna, which is well agreed with the measured result in Figure 6.19. For the EBG antenna, the peak values are at the two EBG edges which are different to that of the measurement. This is due to the connector and cable effect in the measurement. There might be some power leaking from the connector and the cable, therefore the highest field shows at the edge which is close to the feed point of the antenna.

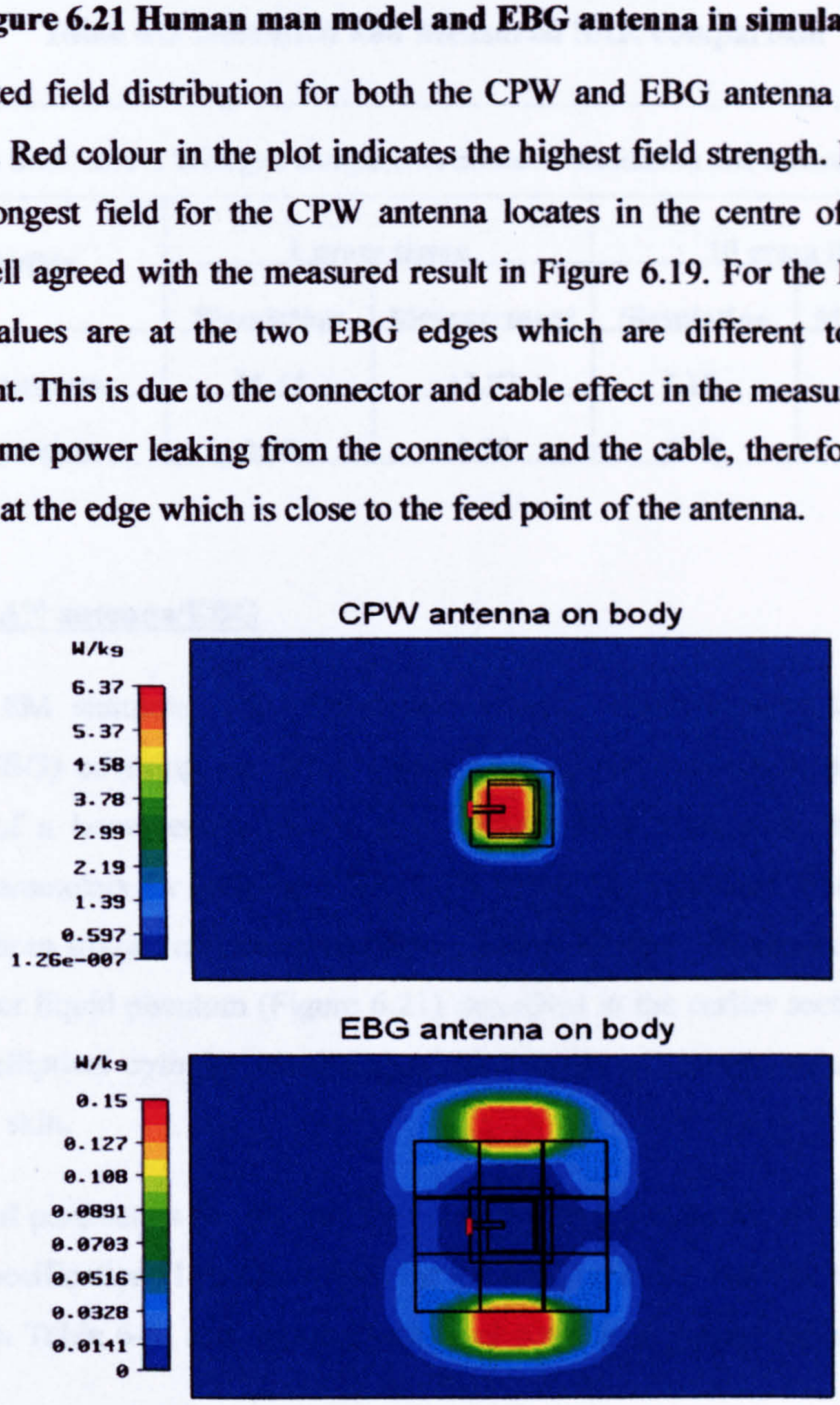

Figure 6.22 Field strength for CPW and EBG antenna in simulation

The simulated SAR values are listed in Table 6-5 with a comparison of the measured results. The EBG antenna has reduced SAR by 95.9% for 1 gram and 95.7% for 10 gram tissues in simulation. This has a very good agreement with the measurement. The overall SAR values are slightly lower from simulation than those of the measurement. It can be due to the approximate phantom size modelled in the simulation, besides, unlike the ideal environment in software, the condition under measurement is more complicated. Effect of the connectors, cables, surrounding devices and temperature are also need to be taken into account.

Table 6-5 Simulated and Measured SAR comparison

Peak SAR values W/Kg: a comparison between simulation and measurement				
1800MHz	**1 gram tissue**		**10 gram tissue**	
	Simulation	**Measurement**	**Simulation**	**Measurement**
CPW antenna	**11.47**	**12.87**	**7.18**	**7.96**
EBG antenna	**0.48**	**0.90**	**0.31**	**0.42**

6.6.2.2 WLAN antenna/EBG

Using the EM simulator CST Microwave Studio, simulations of fabric antenna (with/out EBG) covering the WLAN bands for wireless communications in close proximity of a homogenous human body model were done with the appropriate dielectric parameters for each band. The SAR values of the antenna with and without EBG have been studied on two human body models. One has the same construction as the two layer liquid phantom (Figure 6.21) described in the earlier section. The other one is an elliptical cylinder consisting of four layers of tissues: spine, body fluid, muscle and skin.

The physical parameters for the rectangular liquid body model are achieved the SAM phantom specification [13]. The values for the liquid and the shell for each frequency are listed in Table 6-6, and the computational peak SAR results are summarized in Table 6-7.

Table 6-6 Tissue parameters set up in the simulation

	shell			liquid		
	ε_r	Loss tangent	Densityρ [kg/m3]	ε_r	conductivity σ [S/m]	Densityρ [kg/m3]
2.45GHz	3.3	0.03	1000	39.2	1.8	1000
5.8GHz	3	0.035	1000	35.114	3.717	1000

Table 6.7 Simulated SAR of WLAN antennas on the rectangular liquid body

Peak SAR values W/Kg-dual band WLAN antennas				
	2.45GHz		5.8GHz	
	1g tissue	10g tissue	1g tissue	10g tissue
CPW antenna	13.85	7.819	20.29	11.808
EBG antenna	0.131	0.086	0.117	0.070

The results clearly demonstrate that the EBG has brought the power absorption down significantly. The advantage of the EBG ground is even distinctive at the higher frequency, as generally the human tissue has a much larger conductivity at higher frequency, the SAR value is normally greater than that of the lower frequency. However, the presence of the large EBG plane has reduced the field strength significantly, and a lower SAR value is observed for 5.8GHz than that of the 2.45GHz in the EBG antenna case. Although the real measurement can not be carried out, the simulation shows a prediction of the real data.

The multi layer elliptical cylinder body model is shown in Figure 6.23. The torso consists of four main layers of body tissues: bone, fluid, muscle and skin. This model is used to study the antenna performance when the antenna is located on upper portion of human body. The electrical parameters corresponding to each tissue around the operating is obtained from [14] and listed in Table 6-8.

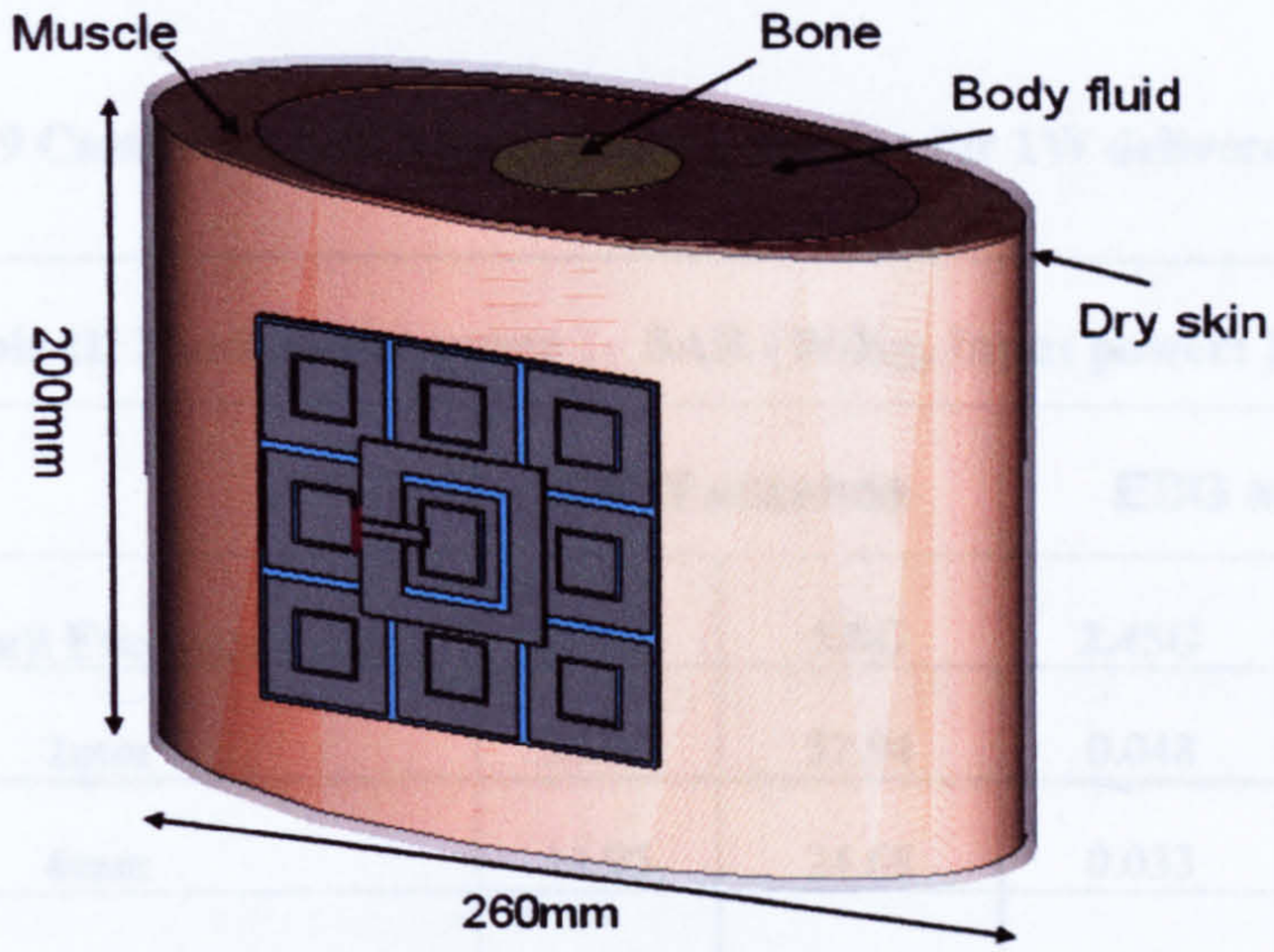

Figure 6.23 Multi layered body contrasted in CST

Table 6-8 Parameters of the layered human model

	2.45GHz			5.8GHz			
	Conductivity [S/m]	ε_r	Loss tangent	Conductivity [S/m]	ε_r	Loss tangent	Density ρ [kg/m3]
Bone cortical	0.40411	11.352	0.25597	1.0821	9.8085	0.36058	1810
Body Fluid	2.4392	68.24	0.26771	6.1833	65.179	0.31005	1019-1063
Muscle	1.773	52.668	0.24205	4.609	48.883	0.30815	1040
Skin Dry	1.4876	37.952	0.28184	3.4631	35.363	0.32006	1010

Two factors were investigated for this model: the distance between the antenna and the body, and the antenna with/out the EBG ground plane. The distances are set to be 2mm, 6mm and 10mm from the antenna bottom to the body. The calculated SAR values over the volume of 1g and 10g for each distance are shown in Table 6-9 and 6-10.

Table 6.9 Computed SAR values over 1g volume for 1W delivered power

Table II: Maximum average 1g SAR (W/Kg, Input power: 1W)				
	CPW antenna		EBG antenna	
Distance(mm)\ Frequency(GHz)	2.45G	5.8G	2.45G	5.8G
2mm	25.99	57.94	0.048	0.037
6mm	14.95	24.68	0.033	0.025
10mm	9.86	11.93	0.022	0.017

Table 6.10 Computed SAR values over 10g volume for 1W delivered power

Table III: Maximum average 10g SAR (W/Kg, Input power: 1W)				
	CPW antenna		EBG antenna	
Distance(mm)\ Frequency(GHz)	2.45G	5.8G	2.45G	5.8G
2mm	15.68	22.13	0.0352	0.0105
6mm	9.35	12.57	0.0204	0.0093
10mm	6.71	7.12	0.0176	0.0084

Results have shown similar SAR outcome as compare to the rectangular liquid model. The EBG plane guarantees a safe communication for the near body wireless network. And it is found that the SAR value is much related to the antenna and human body separation. When the antenna moves further away from the body, the power absorbed by the body decreases significantly.

6.7 Conclusion

This chapter has focused on studying the effects of the vicinity of a human body on textile WLAN antenna and EBG performances. Studies have been carried out including bending, washing, on body, coupling and SAR evaluation. Each part can be concluded as follows:

- Bending has a minor effect on both CPW and EBG antennas. For a linear polarized patch antenna, bending direction and bending curvature can affect the antennas performances. And overall bending will bring a wider beam width.

- Human body has a strong interaction with the CPW antenna. The antenna works poorly in the vicinity of the body. With the introduction of the EBG ground plane, the antenna detuning can be reduced to a minimum, and the antenna is capable of keeping a stable performance.

- Moisture can influence the antenna characteristics seriously. Water brings to the substrate a much higher permittivity, as well as a large loss factor. Although the antenna performances are not affected much when it is dry again, better solutions should be considered in the future research.

- When two antenna elements are working together on body, it is desired to have a small coupling between them. The coupling level is dependant on the antenna position alignment and the separation of the elements. Generally, if two antennas are located very close, the coupling between them can be a serious problem. With the EBG ground plane, the coupling between elements is reduced significantly and it is thus possible to locate two elements very close to each other.

- Simulation and measurement are both done to evaluate antenna SAR on body. For the coplanar fabric antenna, there is no shielding behind, plenty of power radiates towards the body, and the absorption rate is high. In contrast to this, the EBG can form a good shielding layer between the antenna and the body. Both the simulated and measured SAR values for the EBG antenna can satisfy the international communication standard.

To sum up, the EBG structure can bring a lot of advantages into on body communications. Although it suffers under wet conditions which can be solved by choosing water proof materials, the EBG arrays provide an overall greater performance for on body applications.

References:

[1] **Alomainy, A., Hao, Y. and Davenport, M.,** "Parametric Study of Wearable Antennas with Varying Distances from the Body and Different On-Body Positions," *The IET seminar on Antennas and Propagation for Body Centric Wireless Communications*, pp. 84-89, Apr 2007.

[2] **Tanake, M. and Jang, J-H.,** "Wearable microstrip antenna," *IEEE Antennas and Propagation Society International Symposium*, Vol.2, pp.704-707, June 2003.

[3] **Locher, I., Klemm, M., Kirstein, T. and Troster, G.,** "Design and Characterization of Purely Textile Patch Antennas," *IEEE Transactions on Advanced Packaging*, Vol.29, No.4, pp.777-788, Nov 2006.

[4] **Jensen, M. A. and Rahmat-Samii, Y.,** "EM Interaction of Handset Antennas and a Human in Personal Communications," *Proceedings of the IEEE*, Vol.83, pp.7-17, 1995.

[5] **Yang. F. and Rahmat-Samii, Y.,** "Reflection Phase Characterizations of the EBG Ground Plane for Low Profile Wire Antenna Applications," *IEEE Transactions on Antenna and Propagation*, Vol.51, No.10, pp.2691-2703, Oct 2003.

[6] **Allen, J.L. and Diamond, B. L.,** "Mutual Coupling in Array Antennas," Technical Report EDS-66-443, Lincoln Lab., MIT, Oct 1966.

[7] **Pozar, D. M.,** "Input Impedance and Mutual Coupling of Rectangular Microstrip Antennas," *IEEE Transactions on Antennas and Propagation*, Vol. AP-30, No.6, Nov 1982.

[8] **Balanis, C. A.,** *Antenna Theory: Analysis and Design*, Third Edition, WILEY-INTERSCIENCE, 2005.

[9] **Dimbylow, P. J.,** "FDTD calculations of the whole-body averaged SAR in an anatomically realistic voxel model of the human body from 1MHz to 1GHz," Physics in Medicine and Biology, vol.42, pp.479-490, 1997.

[10] **Salonen, P. and Rahmat-Samii, Y.,** "Wearable Antennas: Advances in Design, Characterization, and Application," *Antennas and Propagation for Body-centric Wireless Communications*, Artech House, pp.151-188, 2006.

[11] **Qiu, X. and Mohan, A. S.,** "The performance of a CPW-fed printed UWB Antenna for Wireless Body-Worn Application," *IEEE Antennas and propagation Society International Symposium*, pp.2109-2112, 2006.

[12] **FCC Webpage:** http://www.fcc.gov/cgb/sar.

[13] **DASY4 System Handbook**, Schmid & Partner Engineering AG, DASY4 Manual V4.5, Mar 2005.

[14] **Webpage:**http://niremf.ifac.cnr.it/tissprop/htmlclie/htmlclie.htm.

Chapter 7 Conclusion and Future work

7.1 Over Project Summary

This study investigated wearable antennas for on-body wireless communication systems. Critical design parameters of wearable antennas for various personal wireless communication systems were discussed. Emphasis was put on wireless local area network (WLAN) applications. A variety of antenna design approaches were given in order to fulfil the particular requirements for on-body applications. And antenna performance in the dynamic body environment was demonstrated. This chapter will evaluate this research, discuss the significance of the research and draw conclusions based on the results obtained. The achievements of this study will also be highlighted.

Chapter 3 focused on characterizing the properties of a selection of textile and leather materials for the use of antenna substrates. Study was also carried out on the effects of different conducting materials on textile antenna performance. The investigations have shown great possibility of using entire textile materials to fabricate high performance antennas. Insulating material 'Felt' and conducting fabric 'Zelt' were mainly chosen for the later antenna designs.

The development of a few strip line fed textile and leather antennas were addressed in Chapter 4. Dual-band CPW fed antennas were designed for wearable applications. The results showed that this type of antenna has compact size, low cost, low loss and high stability. Both the impedance matching performance and the radiation characteristics are promising for WLAN band applications. A low profile dual-band rectangular textile antenna was also presented. The antenna has a compact size and demonstrates attractive performances. The parasitic wire element around the main triangular patch provides a dual frequency band antenna. Modifying the small ground plane by introducing a rectangular slot allows tuning of the frequency bands and the band width. The antenna has achieved a wide bandwidth at each band. In addition, it is an excellent shape for compact antenna design due to its geometrical structure.

Finally, a multi-band coplanar hexagon ring antenna was introduced. The antenna is capable to cover most of the personal mobile networks, like GSM, DCS, UMTS and WLAN. With the combination of different sizes of hexagon ring, the proposed antenna can be designed to have an adjustable resonant band and suitable radiation performance for individual band operation, but has a very compact size. In most of the designs, simulations have been compared to measurements and shown in broad agreement. These antennas have been proved to have good performance, although they were initially designed for body worn applications the designs are useful for many other applications, for example they can be used for automotive antenna investigations.

Antennas in wearable applications need directivity in order to avoid unnecessary radiation exposure to the human body and radiation losses. Therefore, a solution was proposed by introducing an EBG array to the antenna as a high impedance ground plane. A simple design structure of dual-band electromagnetic band gap materials was presented in chapter 5. The simple concentric square loop structure was employed to reduce the difficulties of manufacturing the fabric material and increase the accuracy of the cutting dimensions. Also the design was developed without vias to ease the fabrication process. The array has only 3×3 cells and a thickness of 2.2mm which make the combination of the antenna and the EBG is readily hidden or sewn into items of clothing. The measured EBG antenna showed 4.1% and 11.9% bandwidths for the lower and upper WLAN bands, which are quite enough for the real application. In addition, the EBG plane added 2.6dB and 2.4dB gain over the CPW antenna in the desired direction, and reduced the towards body radiation significantly. A comparison between the EBG antenna and a conventional dual-band slot patch antenna which has the same size was also addressed in chapter 5. The EBG antenna has shown to provide useful impedance bandwidths a nearly twice that of the patch antenna, and most importantly, it has shown to be capable to maintain a rather good radiation pattern at the higher frequency operating band.

Chapter 6 has focused on studying the effects of the vicinity of a human body on textile WLAN antenna and EBG performances. Studies have been carried out including bending, washing, wearing and coupling effect on antenna performances. SAR evaluation in both simulation and human body phantom measurement were also

processed. The EBG ground plane showed obvious advantages in most of the body-centric situations. It minimized the antenna detuning problem on the body, reduced mutual coupling from other elements, and shielded the scattering radiations towards the body. The EBG antenna has shown a great promising application for the future on-body communications.

To summarise, this research has provided useful information for improving wearable antenna designs and added value to the further on-body system development for real life applications. The study and experiments in this research have proved that there is a great possibility of using wearable textile antennas to replace conventional rigid antennas in various applications. In the future, the complete flexible body-worn antenna system is possibly to be found in our everyday living.

7.2 Future Work Expectations

There is still an enormous amount of research and development that needs to be performed in this area in order to reach an optimal performance level. First of all, the connectors used for the antenna measurements in this study were the common metallic SMA connectors. These connectors were soldered on the antennas at this stage. Therefore the fabric-to-metal connection tends to break easily. Different types of connectors would be suggested in the future study. Smaller size, light weight connectors would be preferred. And better mounting method can be investigated to enhance the connection.

Secondly, the need of developing more compact structures to meet the requirements of modern on-body systems can not be ignored. If the manufacturing accuracy can be assured, more complex geometries can be investigated to enhance the EBG band gap width, and to reduce the array size.

Attention needs to be paid on the materials selection as well. Firmness of the textile materials should be considered to avoid unnecessary damage and breakage. Moreover, the antennas proposed in this study have shown to suffer under wet conditions. Thus water proof materials can be considered in the future research, and a hidden structure design is strongly recommended for further studies.

Finally, a more efficient human body phantom should be developed for both simulation and measurement in the future. The most of current physical or numerical phantom are still not controllable. In the future, the phantom should be able to present the electromagnetic properties of a live human body as much as possible.

Appendix A

TRL: Thru-reflect-line method

- Why use TRL calibration?

This method is convenient in that calibration standards can be fabricated for a specific measurement environment, such as a transistor test fixture or microstrip. A calibration at the coaxial ports of the network analyzer removes the effects of the network analyzer and any cables or adapters before the fixture; however, the effects of the fixture itself are not accounted for. In microstrip, a short circuit is inductive, an open circuit radiates energy, and a high-quality purely resistive load is difficult to produce over a broad frequency range. The Thru-Reflect-Line (TRL) 2-port calibration is an alternative to the traditional SOLT Full 2-port calibration technique that utilizes simpler, more convenient standards for device measurements in the microstrip environment.

The advantage of TRL is that only three standards need to be characterized as opposed to 4 in the traditional open, short, load, and thru full 2-port calibrations. Further, the requirements for characterizing the T, R, and L standards are less stringent and these standards are more easily fabricated.

- TRL calibration procedure:

1. Define user Cal kit for TRL

    a. Modify the standard definition. To define the Short, Thru/Line and Line/Match standard, and to label these standards.

    b. Assign the standards to the various TRL classes.

    c. Label the calibration kit.

2. TRL calibration

a. Set average factor and error-correction method.

b. Measure Through. For this step, the test ports are connected together directly and transmission frequency response and port match are measured in both directions by measuring all four S-parameters.

c. Measure reflection. For the reflect step, identical high reflection coefficient standards are connected to each test port and measured (S11 and S22).

d. Measure line/match. For the line step, a short length of transmission line is inserted between port 1 and port 2 and again the frequency response and port match are measured in both directions by measuring all four S-parameters.

In total, all the measurements are resulting in independent equations, then all the error factors can be calculated and used for the accuracy enhancement.

3. Check response and save calibration

Read the phase response for both the S_{12} and S_{21}, the phase at the centre frequency should be 90°, or very close to 90°. The magnitude for S_{12} and S_{21} should be the same, and the lines should be very flat.

Appendix B

Dielectric property derivation from transmission/reflection method

A diagram of the waveguide sample holder with filled material is shown in Figure B.1. The whole calculation method is based on Mason's non-touching loop rule. The loop can be described in a simple two port transmission line, as shown in Figure B.1 right.

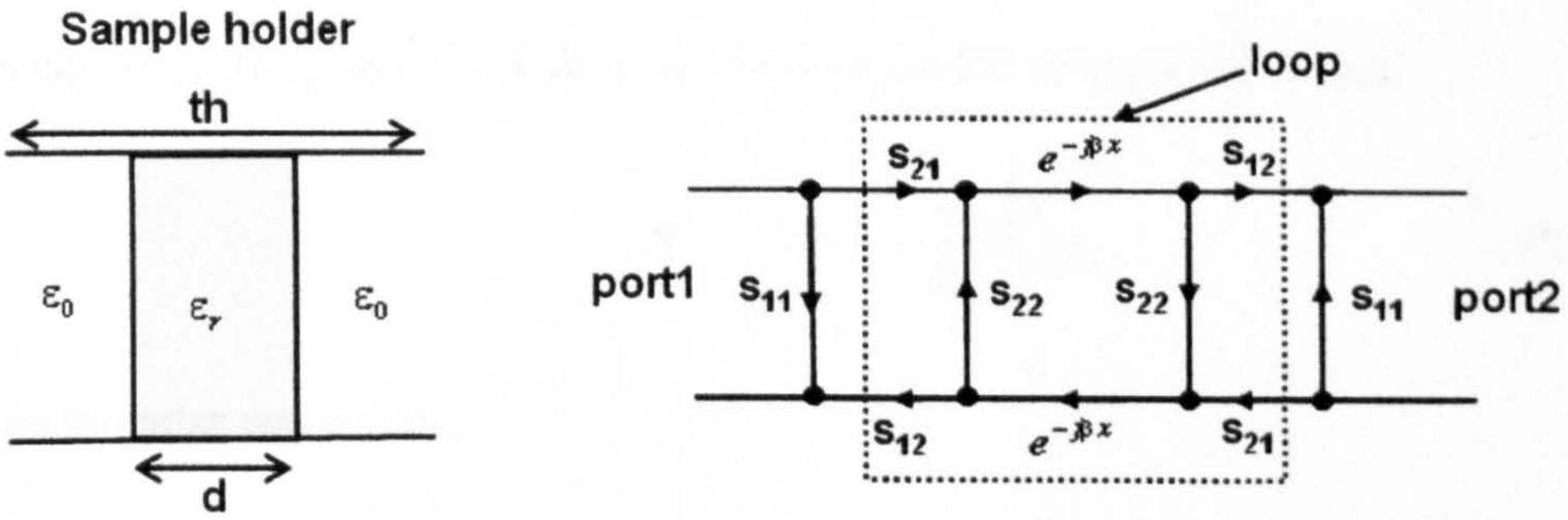

Figure B.1 (left) Waveguide cavity with filled material

(right) Mason's non touching loop

For multi-loop, the transmission can be calculated by:

$$T = \frac{P_1\left(1 - \sum L_1^{\langle 1\rangle} + \sum L_2^{\langle 1\rangle} - \cdots\right) + P_2(\cdots)}{1 - \sum L_1 + \sum L_2 - \cdots} \tag{B-1}$$

Where for a single loop case like the diagram in Figure B.1, it can be written into

$$T = \frac{P_1\left(1 - \sum L_1^{\langle 1\rangle}\right)}{1 - \sum L_1} \tag{B-2}$$

And in this case, $P_1 = S_{21}S_{12}e^{-j\beta x}$, $\sum L_1^{\langle 1\rangle} = 0$ and $\sum L_1 = S_{22}^2 e^{-2j\beta x}$

where $\beta = \frac{2\pi}{\lambda_g}$, and λ_g is the guiding wavelength.

Also in waveguide,

$$S_{22} = \frac{Z_g - Z_l}{Z_g + Z_l} \tag{B-3}$$

and $$S_{12} = 1 + S_{22},\ S_{21} = 1 + S_{11},\ S_{11} = -S_{22} \tag{B-4}$$

Therefore, $$S_{12}S_{21} = (1 + S_{22})(1 - S_{22}) = 1 - S_{22}^2 \tag{B-5}$$

From equation (B-2) and (B-5), the transmission coefficient can be written:

$$S_{21} = T = \frac{(1 - S_{22}^2)e^{-j\beta x}}{1 - S_{22}^2 e^{-2j\beta x}} \tag{B-6}$$

In a rectangular waveguide,

$$\lambda_g = \frac{\lambda_0}{\sqrt{1 - \left(\frac{\lambda_0}{\lambda_c}\right)^2}} \tag{B-7}$$

Where λ_0 is free space wavelength, and λ_c is the cut off wavelength in the waveguide. Therefore,

$$Z_g = Z_0\lambda_g = \frac{Z_0\lambda_0}{\sqrt{1 - \left(\frac{\lambda_0}{\lambda_c}\right)^2}} \tag{B-8}$$

and $$Z_l = \frac{Z_g}{\sqrt{\varepsilon_r}} = \frac{Z_0\lambda_0}{\sqrt{\varepsilon_r - \left(\frac{\lambda_0}{\lambda_c}\right)^2}} \tag{B-9}$$

From (B-3), (B-8) and (B-9), we can get

$$S_{22} = \frac{Z_g - Z_l}{Z_g + Z_l} = \frac{\sqrt{\varepsilon_r - \left(\frac{\lambda_0}{\lambda_c}\right)^2} - \sqrt{1 - \left(\frac{\lambda_0}{\lambda_c}\right)^2}}{\sqrt{\varepsilon_r - \left(\frac{\lambda_0}{\lambda_c}\right)^2} + \sqrt{1 - \left(\frac{\lambda_0}{\lambda_c}\right)^2}} \qquad \text{(B-10)}$$

Combine equation (B-6) and (B-10), the relationship between $S_{21}$and the permittivity of the material can be written as follow:

$$S_{21} = \frac{\left[1 - \left[\frac{\sqrt{\varepsilon_r - \left(\frac{\lambda_0}{\lambda_c}\right)^2} - \sqrt{1 - \left(\frac{\lambda_0}{\lambda_c}\right)^2}}{\sqrt{\varepsilon_r - \left(\frac{\lambda_0}{\lambda_c}\right)^2} + \sqrt{1 - \left(\frac{\lambda_0}{\lambda_c}\right)^2}}\right]^2\right] \cdot e^{-j\frac{2\pi}{\lambda_0}\sqrt{\varepsilon_r - \left(\frac{\lambda_0}{\lambda_c}\right)^2} \cdot d} \cdot e^{-j\frac{2\pi}{\lambda_0}\sqrt{1 - \left(\frac{\lambda_0}{\lambda_c}\right)^2} \cdot (th - d)}}{1 - \left[\frac{\sqrt{\varepsilon_r - \left(\frac{\lambda_0}{\lambda_c}\right)^2} - \sqrt{1 - \left(\frac{\lambda_0}{\lambda_c}\right)^2}}{\sqrt{\varepsilon_r - \left(\frac{\lambda_0}{\lambda_c}\right)^2} + \sqrt{1 - \left(\frac{\lambda_0}{\lambda_c}\right)^2}}\right]^2 \cdot e^{-j\frac{4\pi}{\lambda_0}\sqrt{\varepsilon_r - \left(\frac{\lambda_0}{\lambda_c}\right)^2} \cdot d}} \qquad \text{(B-11)}$$

The real and imaginary part of the calculated ε_r will give the permittivity and the loss factor of the measured material.

Appendix C

Radiation characteristics of the CPW fed leather antennas

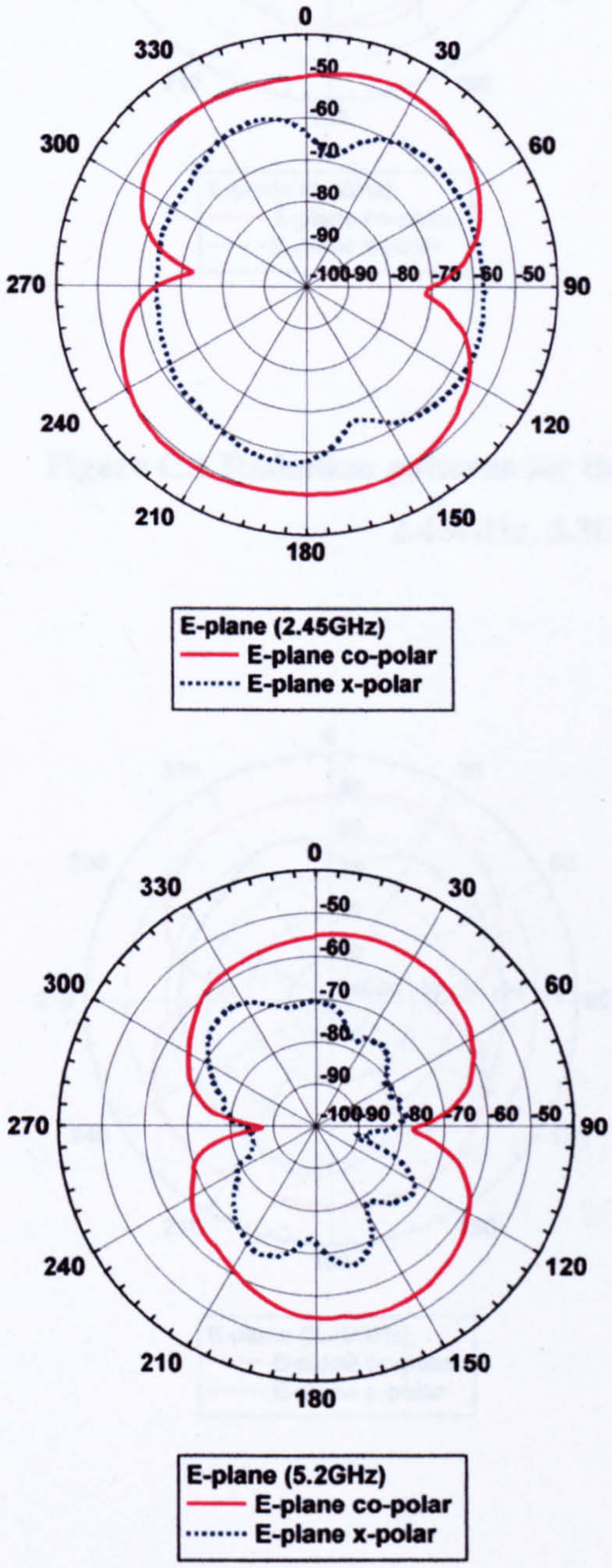

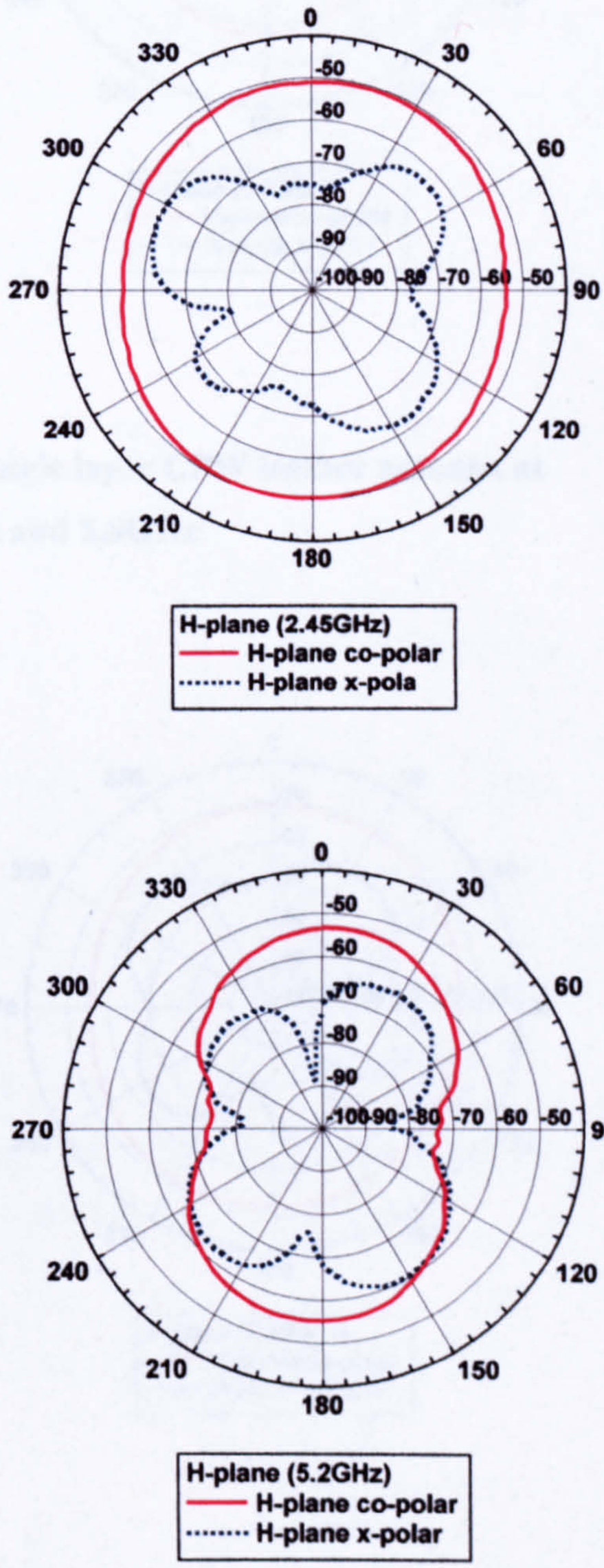

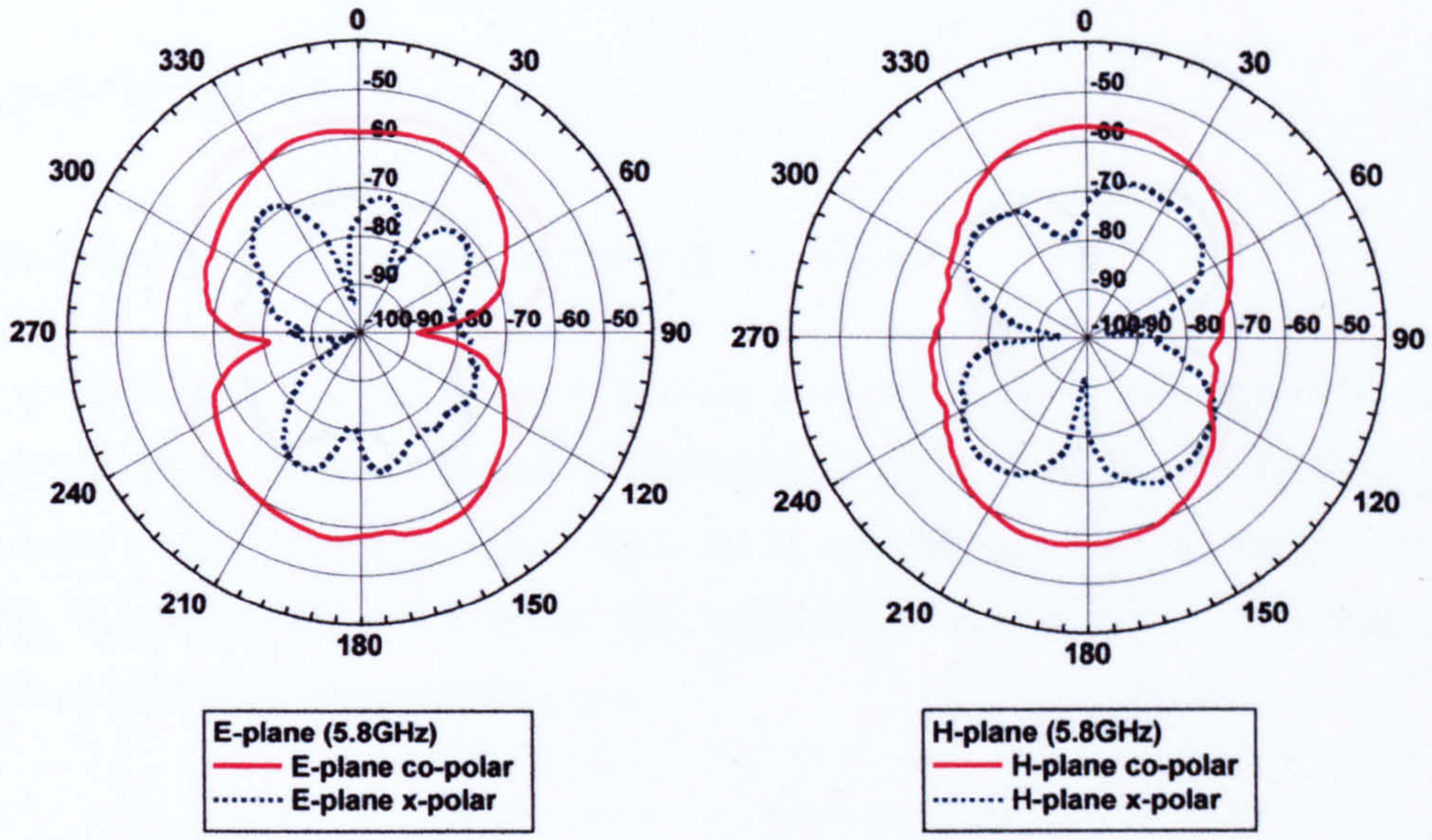

Figure C.1 Radiation patterns for the single layer CPW leather antenna at 2.45GHz, 5.2GHz and 5.8GHz

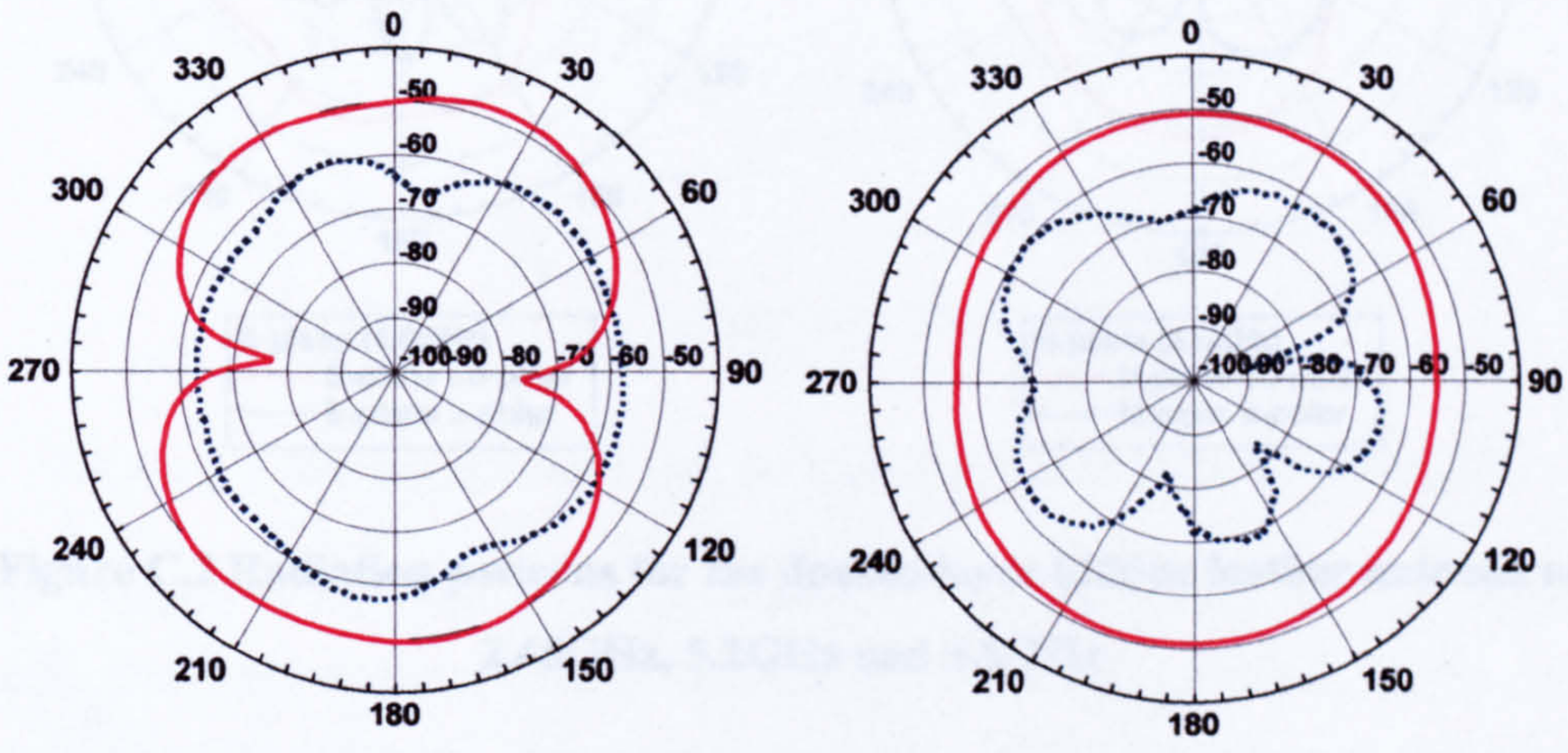

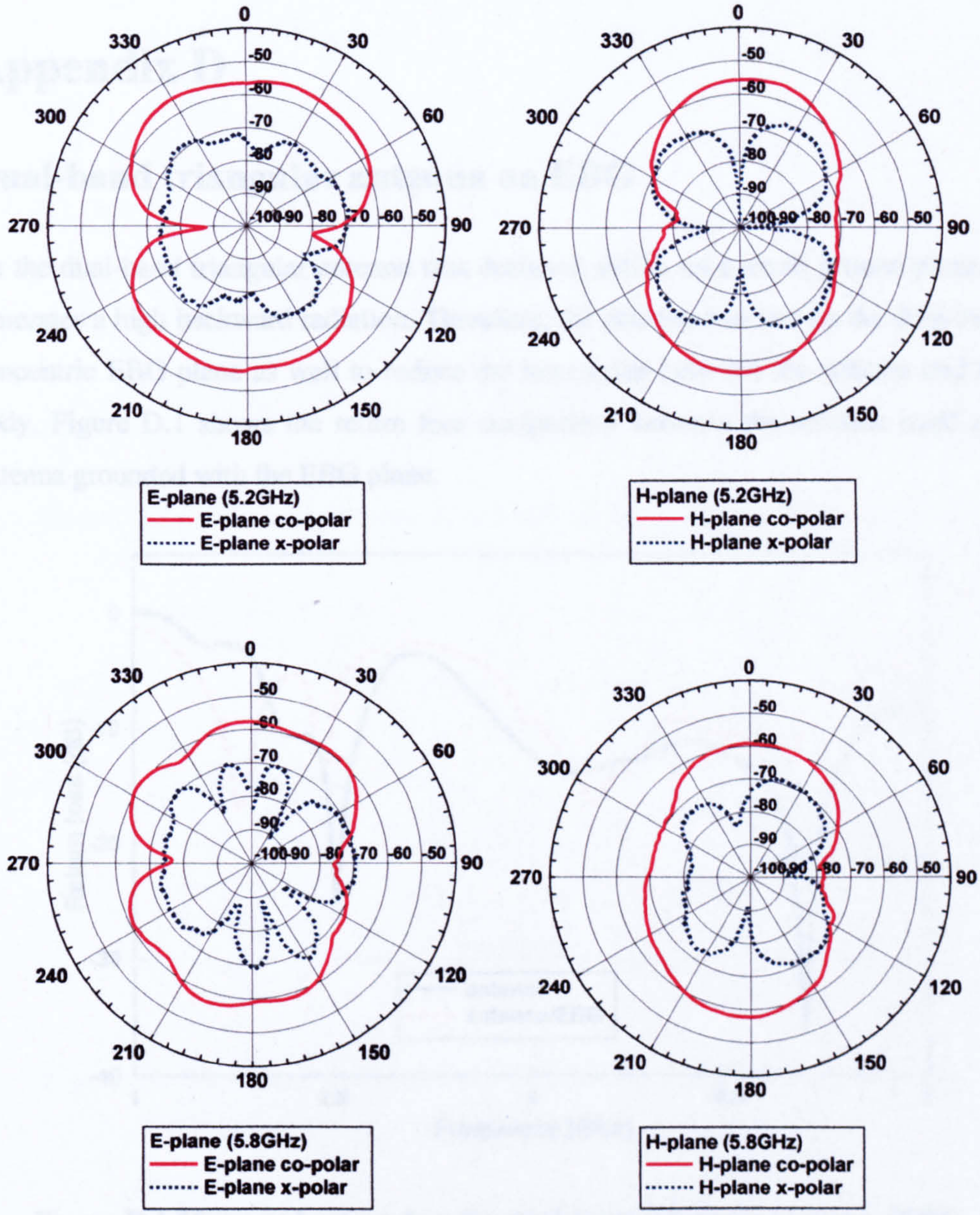

Figure C.2 Radiation patterns for the double-layer hidden leather antenna at 2.45GHz, 5.2GHz and 5.8GHz

Appendix D

Dual-band triangular antenna on EBG

As the dual-band triangular antenna was designed sitting on a small ground plane, it generates a high backward radiation. Therefore, the antenna was test on the dual-band concentric EBG plane as well to reduce the interaction between the antenna and the body. Figure D.1 shows the return loss comparison between the antenna itself and antenna grounded with the EBG plane.

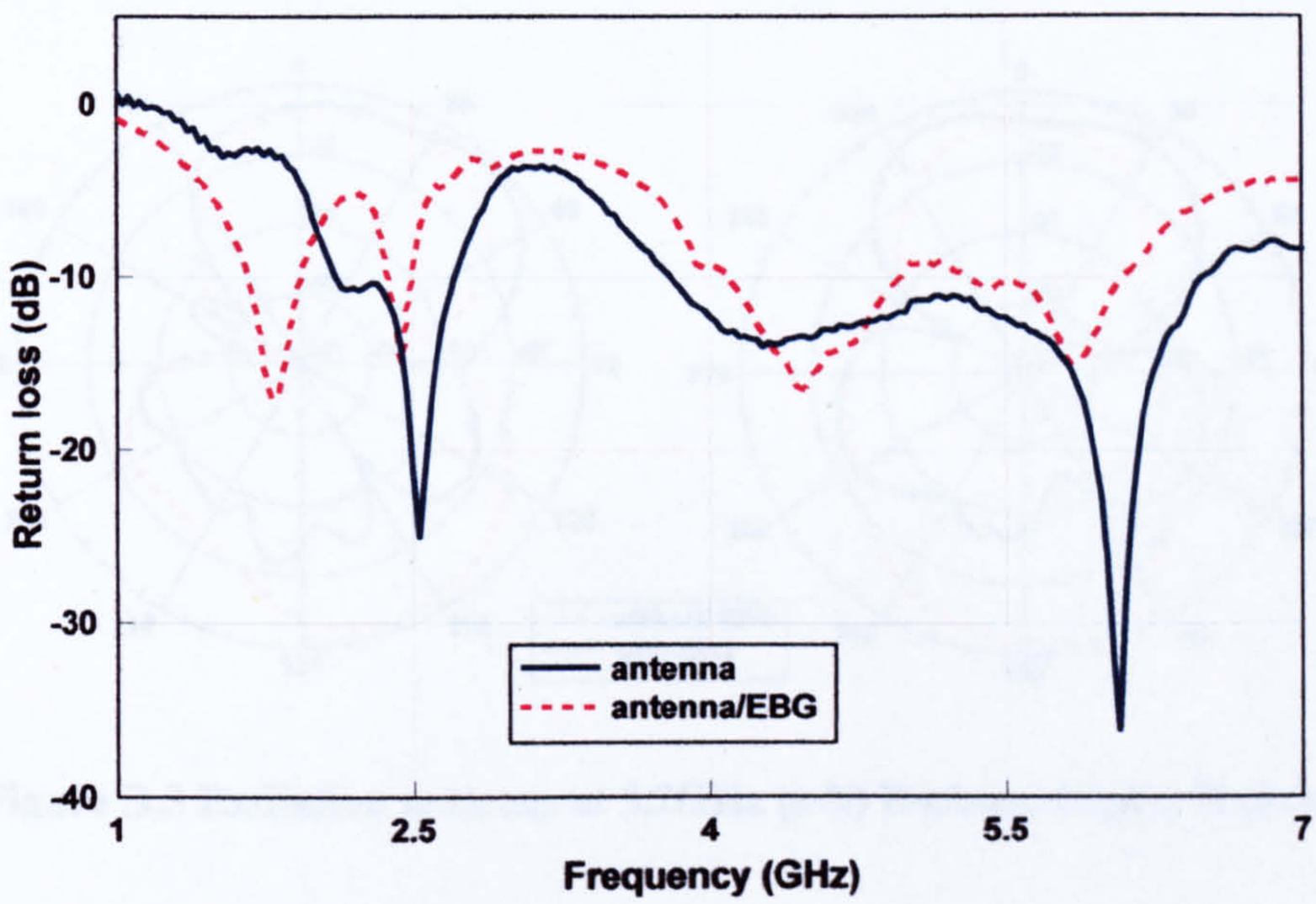

Figure D.1 Measured return loss for dual-band triangular antenna/EBG

The presence of the EBG ground has narrowed the bandwidth for both resonant bands. The EBG antenna covers the band of 2.36GHz to 2.48GH at the lower frequency band, which has a bandwidth about 5%. At the higher frequency band, the EBG antenna near covers the frequency range of 4.12GHz to 6.08GHz, which has a wide bandwidth more than 20%.

The radiation patterns of the EBG triangular antenna were measured in the anechoic chamber at 2.45GHz, 5.2GHz and 5.8GHz respectively. The E-plane and H-plane patterns at these frequencies are plotted in Figure D.2, D.3 and D.4 correspondingly.

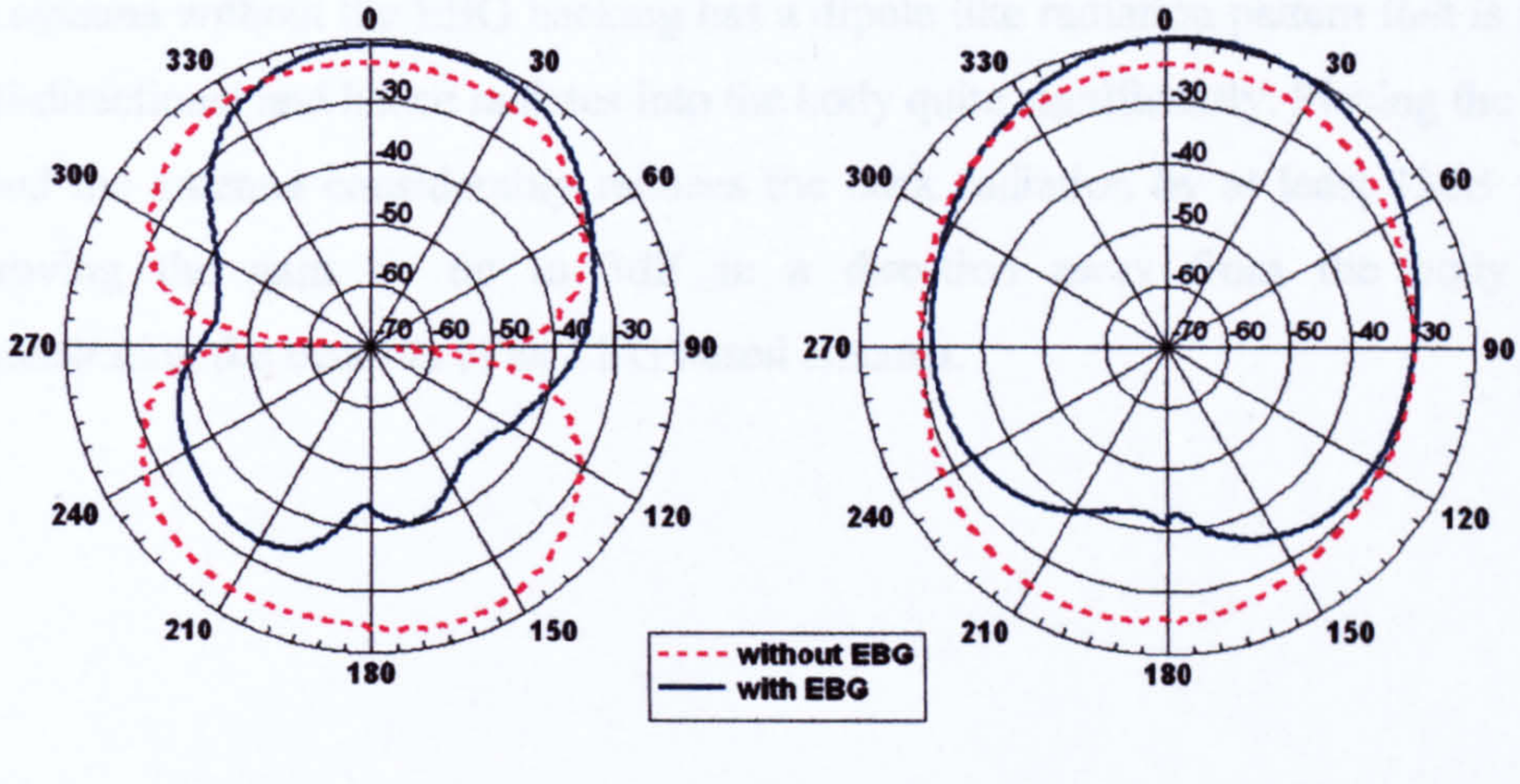

Figure D.2 Radiation patterns at 2.45GHz (left) E-plane, (right) H-plane

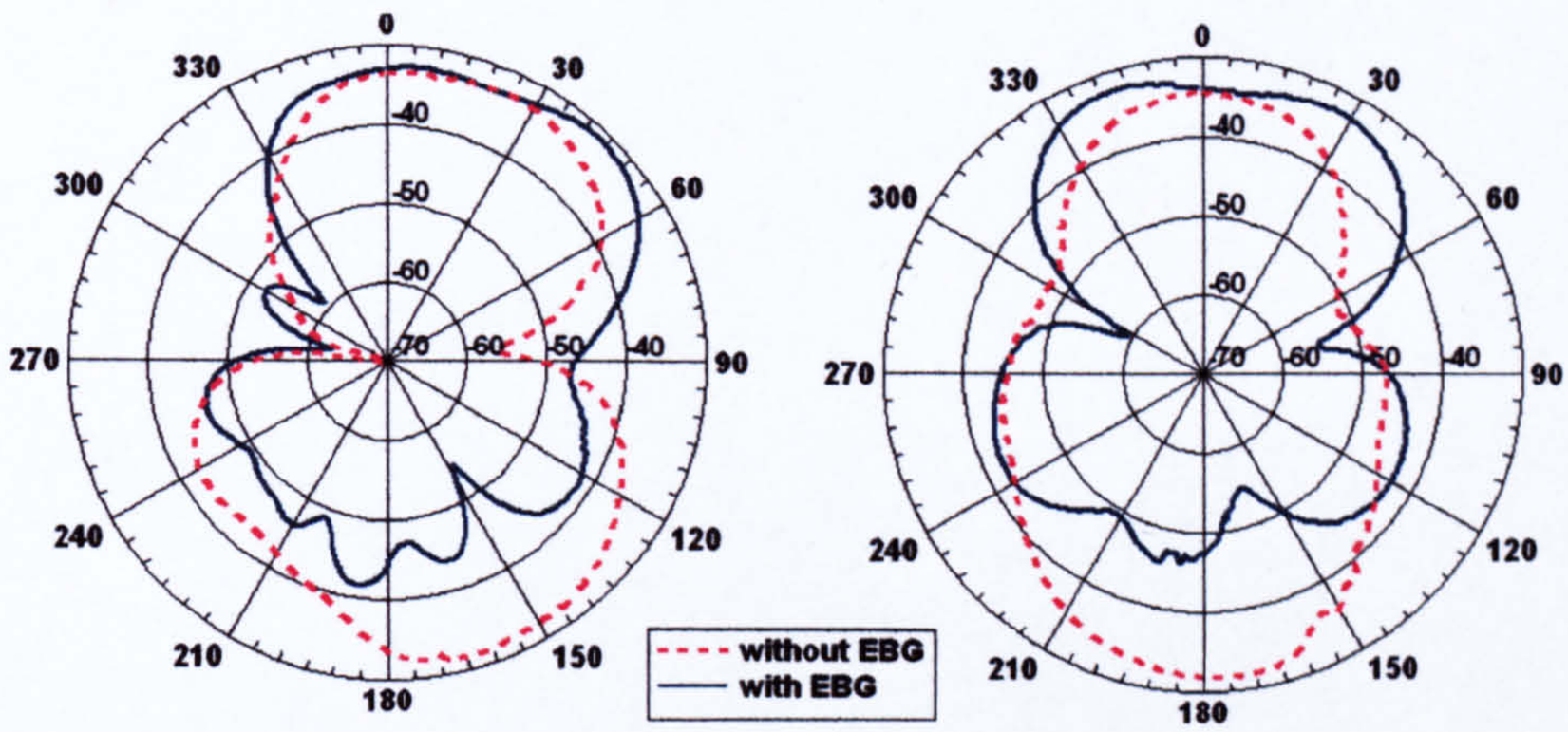

Figure D.3 Radiation patterns at 5.2GHz (left) E-plane, (right) H-plane

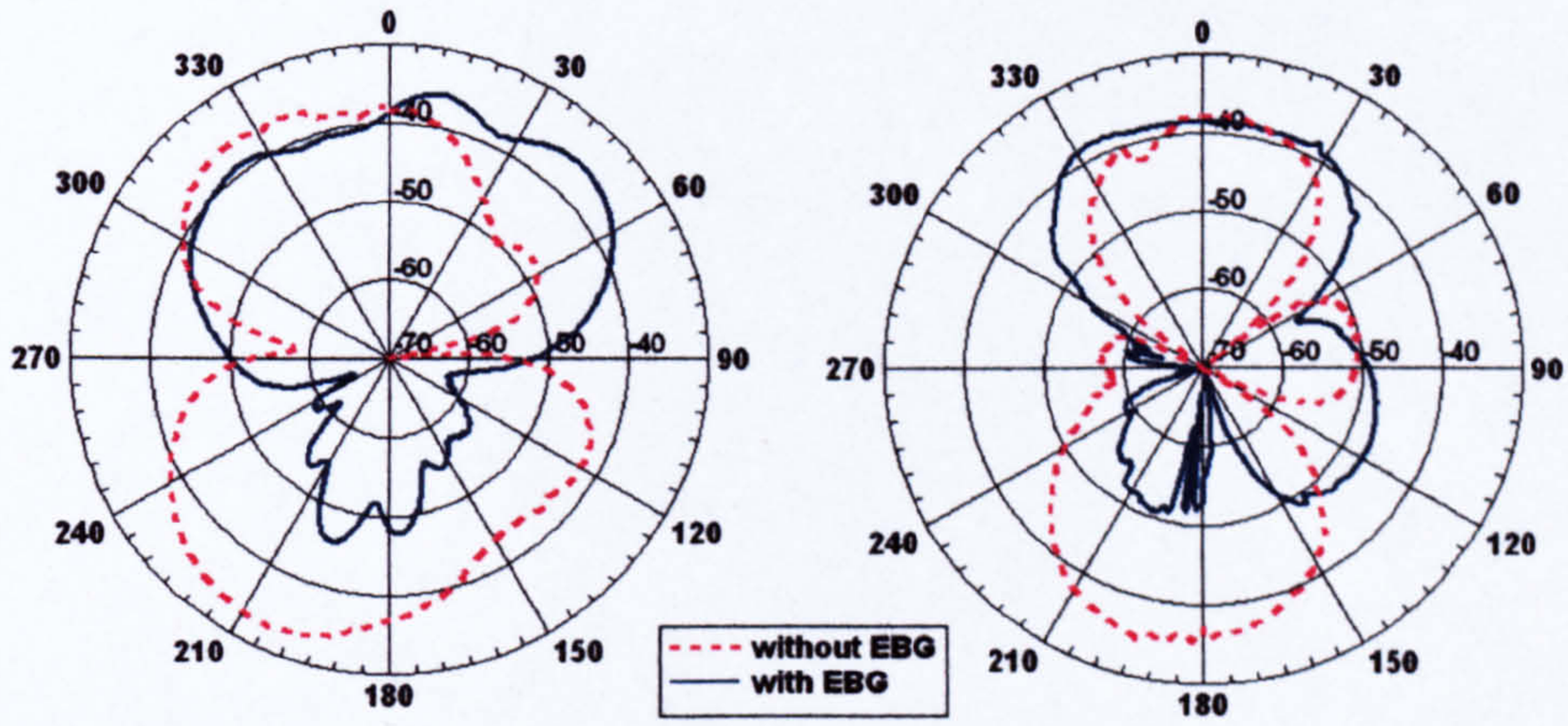

Figure D.4 Radiation patterns at 5.8GHz (left) E-plane, (right) H-plane

The antenna without the EBG backing has a dipole like radiation pattern that is fairly omni-directional and hence radiates into the body quite significantly. Placing the BEG behind the antenna considerably reduces the back radiation by at least 13dB while improving the gain by up to 3dB in a direction away from the body thus demonstrating the benefits of an EBG based antenna.